



저작자표시-비영리-변경금지 2.0 대한민국

이용자는 아래의 조건을 따르는 경우에 한하여 자유롭게

- 이 저작물을 복제, 배포, 전송, 전시, 공연 및 방송할 수 있습니다.

다음과 같은 조건을 따라야 합니다:



저작자표시. 귀하는 원저작자를 표시하여야 합니다.



비영리. 귀하는 이 저작물을 영리 목적으로 이용할 수 없습니다.



변경금지. 귀하는 이 저작물을 개작, 변형 또는 가공할 수 없습니다.

- 귀하는, 이 저작물의 재이용이나 배포의 경우, 이 저작물에 적용된 이용허락조건을 명확하게 나타내어야 합니다.
- 저작권자로부터 별도의 허가를 받으면 이러한 조건들은 적용되지 않습니다.

저작권법에 따른 이용자의 권리는 위의 내용에 의하여 영향을 받지 않습니다.

이것은 [이용허락규약\(Legal Code\)](#)을 이해하기 쉽게 요약한 것입니다.

[Disclaimer](#)

공학박사학위논문

**Flexure and Fatigue Behavior of RC  
Beam under the Combined Effect of  
Freeze-thaw Cycles and Seawater**

동결융해 및 해수의 복합열화를 고려한  
RC 보 정적 및 피로 거동

2023 년 8 월

서울대학교 대학원

건설환경공학부

안 준 용

# **Flexure and Fatigue Behavior of RC Beam under the Combined Effect of Freeze-thaw Cycles and Seawater**

동결융해 및 해수의 복합열화를 고려한  
RC 보 정적 및 피로 거동

지도 교수 조 재 열

이 논문을 공학박사 학위논문으로 제출함  
2023 년 7 월

서울대학교 대학원  
건설환경공학부  
안 준 용

안준용의 공학박사 학위논문을 인준함  
2023 년 7 월

위 원 장 \_\_\_\_\_ (인)

부위원장 \_\_\_\_\_ (인)

위 원 \_\_\_\_\_ (인)

위 원 \_\_\_\_\_ (인)

위 원 \_\_\_\_\_ (인)

## ABSTRACT

# **Flexure and Fatigue Behavior of RC Beam under the Combined Effect of Freeze-thaw Cycles and Seawater**

An, JunLong

Department of Civil & Environmental Engineering

The Graduate School

Seoul National University

Concrete infrastructures constructed in the Arctic regions are susceptible to numerous environmental damages, including freeze-thaw cycles, seawater, and external loads. Previous studies showed that freeze-thaw cycles and seawater will exacerbate the deterioration, however, most of the studies considered the damages independently due to the limited testing conditions. The current design codes specify minimum requirement of concrete properties in accordance with exposure categories and classes in order to ensure the performance under the aggressive environment. To ensure the performance of concrete structures during their service life and the design's reliability, investigations based on experimental and analytical studies are imperative.

The objective of this study was to investigate the effect of concrete strength on the flexure and fatigue behavior of RC beams. Subsequently, the flexure and fatigue behavior of RC beams exposed to combined effect of freeze-

thaw cycles and seawater was investigated. The following procedures were performed to conduct the experimental studies.

At first, a comparative analysis was conducted on previous studies related to the freeze-thaw cycles, seawater, and external loads with the background of cold region construction.

Next, the current design codes were summarized which include exposure categories based on damage factors and the corresponding minimum requirement of concrete property. The minimum compressive strength of concrete specified in design codes was applied to investigate the effect of concrete strength. In the light of the limitations of previous studies, experimental schemes at the structural level were developed.

Flexure and fatigue test were conducted according to the design code requirements and the limitations from previous studies. Total 12 RC beams were fabricated to experimentally investigate the effect of concrete strength, freeze-thaw cycles, and seawater. Measurement schemes considering temperature effect were established prior to the structural test since electronic measuring sensors have a specific allowable operation temperature range. The structural behavior including ultimate load, fatigue life, deflection, strain of rebar, and cracking behavior were measured under various temperature conditions. The experimental results demonstrated that normal strength concrete had greater deterioration under freeze-thaw cycles and seawater exposure. Freeze-thaw cycles and seawater decreased the material properties of concrete and structural behavior of RC beams, and the combined effect of freeze-thaw cycles and seawater accelerated the deterioration of RC beams.

Conversely, the specimen with high concrete strength (60 MPa) exhibited superior performance compared to the specimen with normal concrete strength. Analytical studies incorporating finite element analysis, section analysis, and regression analysis were conducted for the behavior that were difficult to obtain from experiments.

Freeze-thaw resistance increased as concrete strength increased, however, concrete strength at higher than 60 MPa is not recommended in cold region construction. To better evaluate the capacity of concrete structures under the effect of freeze-thaw cycles and seawater exposure, both static and fatigue tests were recommended to be conducted. To account for actual environmental conditions, the effect of freeze-thaw cycles and seawater should be simultaneously considered in experimental studies. Lastly, the definition of low temperature in design codes was recommended to be defined based on the target temperature of structures.

**Keywords:** Cold region, Concrete structures, Freeze-thaw cycles, Seawater exposure, Combined effect, Concrete strength, Flexure behavior, Fatigue behavior

**Student Number:** 2016-28243

# TABLE OF CONTENTS

<b>LIST OF TABLES</b> .....	<b>x</b>
<b>LIST OF FIGURES</b> .....	<b>xi</b>
<b>NOTATIONS</b> .....	<b>xxii</b>
<b>I. Introduction</b> .....	<b>1</b>
1.1. Research Background .....	1
1.2. Objectives and Scope .....	3
1.3. Organization .....	5
<b>II. Literature Review</b> .....	<b>7</b>
2.1. Introduction .....	7
2.2. Deterioration of RC Structures .....	8
2.2.1. Introduction .....	8
2.2.2. Chemical Deterioration .....	8
2.2.3. Physical Deterioration .....	12
2.2.3.1 <i>External load</i> .....	12
2.2.3.2 <i>Freeze-thaw cycles</i> .....	16
2.2.4. Combined Effect of Multi-damages .....	22

2.3. Design Codes for Durability .....	30
2.3.1. Introduction.....	30
2.3.1. Provisions Based on Exposure Class .....	30
2.4. Concluding Remarks .....	34
<b>III. Experimental Program .....</b>	<b>36</b>
3.1. Introduction.....	36
3.2. Test Program.....	37
3.2.1. Test Variables.....	37
3.2.2. Dimension of Specimens.....	42
3.3. Material Tests.....	43
3.3.1. Concrete.....	43
3.3.2. Reinforcing Steel Bars .....	46
3.4. Fabrication of Specimens .....	48
3.4.1. Reinforcement .....	48
3.4.2. Placement of Concrete .....	50
3.5. Seawater Saturation .....	51
3.6. Freeze-thaw Cycles.....	54
3.7. Loading Protocol.....	57
3.8. Test Setup .....	61
3.9. Instrumentation.....	64
3.9.1. ERSGs and Thermocouple.....	65
3.9.2. LVDTs.....	67
3.9.3. Clip-on Displacement Transducer .....	68



3.10. Validity of Thermal Data .....	70
3.11. Concluding Remarks.....	77
<b>IV. Experimental Results and Discussion .....</b>	<b>78</b>
4.1. Material Properties of Concrete.....	78
4.2. Temperature of RC Beams .....	81
4.3. Static Flexural Test of RC Beams .....	83
4.3.1. Effect of Concrete Strength.....	83
4.3.1.1 <i>Failure mode</i> .....	83
4.3.1.2 <i>Central deflection</i> .....	85
4.3.1.3 <i>Strain of reinforcing bars</i> .....	87
4.3.1.4 <i>Estimation of shrinkage strain</i> .....	91
4.3.1.5 <i>Summary</i> .....	100
4.3.2. Effect of Freeze-thaw Cycles and Seawater .....	102
4.3.2.1 <i>Failure mode</i> .....	102
4.3.2.2 <i>Crack width</i> .....	104
4.3.2.3 <i>Central deflection</i> .....	107
4.3.2.4 <i>Strain of reinforcing bars</i> .....	113
4.3.2.5 <i>Summary</i> .....	117
4.4. Fatigue Flexural Test of RC Beams .....	118
4.4.1. Validity of Fatigue Design .....	118
4.4.1.1 <i>Designed stress range</i> .....	118
4.4.1.2 <i>Static loading before fatigue test</i> .....	120

4.4.2. Effect of Concrete Strength	122
4.4.2.1 Failure mode	122
4.4.2.2 Crack width	125
4.4.2.3 Central deflection	129
4.4.2.4 Strain of reinforcing bars	135
4.3.2.5 Summary	142
4.4.3. Effect of Freeze-thaw Cycles and Seawater	143
4.4.3.1 Failure mode	143
4.4.3.2 Crack width	145
4.4.3.3 Central deflection	151
4.4.3.4 Strain of reinforcing bars	156
4.3.3.5 Summary	160
4.5. Overall Comparison of Static and Fatigue Behavior	161
4.6. Concluding Remarks	163
<b>V. Analytical Study</b>	<b>165</b>
5.1. Introduction	165
5.2. Analytical Study on Static Behavior	167
5.2.1 Geometry Model	167
5.2.2 Material Model	167
5.2.2.1 Concrete	167
5.2.2.2 Reinforcement	170
5.2.2.3 Steel plate	170

5.2.3 Boundary Conditions	171
5.2.4 Analysis Results	171
5.2.4.1 Central deflection	171
5.2.4.2 Strain of reinforcing bars	173
5.2.4.3 Crack width	175
5.2.5 Prediction of Crack Width	177
5.2.5.1 Crack propagation	177
5.2.5.2 Crack width	180
5.3. Analytical Study on Fatigue Behavior	183
5.3.1 Fatigue Analysis of RC beams	183
5.3.2 Modified Prediction Model	186
5.4. Concluding Remarks	189
<b>VI. Conclusion</b>	<b>191</b>
6.1. Effect of Concrete Strength	192
6.2. Effect of Freeze-thaw Cycles and Seawater	194
6.3. Recommendations Considering Combined Effect	196
6.4. Further Study	198
<b>References</b>	<b>199</b>
<b>Appendix A</b>	<b>214</b>
<b>Appendix B</b>	<b>218</b>

**Appendix C ..... 226**

**국문초록 ..... 233**

## LIST OF TABLES

Table 2.1 Composition of seawater (Alexander, 2016) .....	10
Table 2.2 Phase alteration in cementitious material (Alexander, 2016) .....	11
Table 2.3 Details of fatigue tests in previous studies .....	15
Table 2.4 Stress range in design codes .....	16
Table 2.5 Material properties of concrete under freeze-thaw cycles .....	19
Table 2.6 Test methods for freeze-thaw cycles of concrete .....	21
Table 2.7 Structural behavior of RC component under combined damage ....	29
Table 2.8 Clause for concrete structures by exposure class .....	32
Table 3.1 Test program .....	41
Table 3.2 Mix proportion of concrete .....	44
Table 3.3 Compression tests result of concrete cylinder .....	45
Table 3.4 Tension tests result of reinforcing steel bars .....	47
Table 3.5 Thermal properties of concrete in FEA .....	73
Table 4.1 Estimation of shrinkage strain of RC beams .....	100
Table 4.2 Strength of RC beams .....	111
Table 4.3 Comparison of static behavior of RC beams .....	112
Table 4.4 Comparison of cracking load before fatigue loading .....	121
Table 4.5 Primary feature of static and fatigue tests .....	162
Table 4.6 Comparative analysis of predicted stress range .....	185

# LIST OF FIGURES

Figure 2.1 The main attack of concrete structures exposed to marine environment (Wang et al., 2022).....	8
Figure 2.2 Chloride-induced corrosion of steel (Hansson, 2011).....	12
Figure 2.3 S-N curve of reinforcing bars (Lee et al., 2018).....	14
Figure 2.4 Mechanism in freeze-thaw cycles: (a) Expansion during freeze-thaw cycles; (b) Contraction during freeze-thaw cycles (Sicat et al. 2013) .....	17
Figure 2.5 Representation of salt rise, evaporation, and crystallization in concrete (Wang et al. 2022).....	23
Figure 2.6 Representation of salt frost damage: (a) at freezing temperatures; (b) at low temperatures; (c) At thawing temperatures (Wang et al. 2021) .....	24
Figure 2.7 Deterioration of ITZ: (a) the control; (b) under fatigue load; (c) under combined action of freeze-thaw cycles and fatigue (Yang et al. 2018).....	27
Figure 3.1 Designation of reinforced concrete beams.....	38
Figure 3.2 Flow chart of experiment.....	39
Figure 3.3 Configuration of RC beams .....	42
Figure 3.4 Compression test of concrete cylinder.....	45
Figure 3.5 Uniaxial tension test of reinforcing steel bars.....	46
Figure 3.6 Stress-strain curve of reinforcing bars: (a) D22-SD400 (30MPa Beam); (b) D22-SD400 (60MPa Beam); (c) D19-SD400; (d) D10-SD400.....	48
Figure 3.7 Installation of strain gauges and thermocouple .....	49
Figure 3.8 Reinforcement on the support of beams: (a) Steel plate; (b) Steel plate in RC beams .....	50

Figure 3.9 Fabrication of RC beams and concrete cylinders .....	51
Figure 3.10 Seawater saturation of RC beams .....	52
Figure 3.11 Weighting of seawater-immersed RC beams .....	52
Figure 3.12 Weight change of seawater-saturated of RC beams: (a) 30MPa beams; (b) 60MPa beams .....	53
Figure 3.13 Temperature in freeze-thaw cycles: (a) ASTM C666/C666M; (b) CEN/TS 12390-9.....	55
Figure 3.14 Preliminary test results of freeze-thaw cycles based on FEA: (a) 30 MPa RC beam; (b) 60 MPa RC beam .....	56
Figure 3.15 Estimate of service load as a function of experimental capacity	57
Figure 3.16 Load protocol of fatigue test: (a) Stress range in load-deflection curve; (b) Constant sinusoidal mode .....	60
Figure 3.17 Grid work on the surface of RC beams.....	61
Figure 3.18 Test setup of RC beams at room temperature .....	62
Figure 3.19 Schematic test setup for freeze-thaw cycles test of RC beams: (a) Front view; (b) Side view.....	63
Figure 3.20 Actual test setup of RC beams in freeze-thaw cycles .....	64
Figure 3.21 Designation of the ERSGs .....	66
Figure 3.22 Location of ERSGs and thermocouple .....	67
Figure 3.23 Constant Temperature Chamber for LVDTs .....	68
Figure 3.24 Crack gauge at bottom of RC beam.....	69
Figure 3.25 Temperature of 30 MPa companion specimen: (a) Seawater- saturated; (b) Air-cured .....	70
Figure 3.26 Temperature of 60 MPa companion specimen: (a) Seawater- saturated; (b) Air-cured .....	71
Figure 3.27 Modeling of specimen in FEA: (a) Companion specimen; (b) Geometric model.....	71
Figure 3.28 Temperature input in FEA: (a) 30 MPa companion specimen; (b) 60 MPa companion specimen .....	72

Figure 3.29 Thermal strain of rebar: (a) FLA type strain gauge (30 MPa RC beam); (b) CFLA type strain gauge (60 MPa RC beam).....	74
Figure 3.30 Derivation of SCFT: (a) FLA type strain gauge (30 MPa RC beam); (b) CFLA type strain gauge (60 MPa RC beam).....	74
Figure 3.31 Temperature of 30 MPa companion specimen by FEA: (a) Seawater-saturated; (b) Air-cured.....	75
Figure 3.32 Temperature of 60 MPa companion specimen by FEA: (a) Seawater-saturated; (b) Air-cured.....	75
Figure 3.33 Thermal strain of 30 MPa companion specimen by FEA: (a) Seawater-saturated; (b) Air-cured.....	76
Figure 3.34 Thermal strain of 60 MPa companion specimen by FEA: (a) Seawater-saturated; (b) Air-cured.....	76
Figure 4.1 Material properties of 30 MPa concrete: (a) Effect of freeze-thaw cycles; (b) Effect of freeze-thaw cycles & seawater; (c) Effect of curing method under freeze-thaw cycles.....	79
Figure 4.2 Material properties of 60 MPa concrete: (a) Effect of freeze-thaw cycles; (b) Effect of freeze-thaw cycles & seawater; (c) Effect of curing method under freeze-thaw cycles.....	80
Figure 4.3 Temperature of 30 MPa RC beams: (a) Seawater-saturated; (b) Air-cured.....	81
Figure 4.4 Temperature of 60 MPa RC beams: (a) Seawater-saturated; (b) Air-cured.....	82
Figure 4.5 Failure of RC beams at room temperature: (a) SRTA60; (b)SRTA30 .....	83
Figure 4.6 Failure of air-cured RC beams under freeze-thaw cycles: (a) ScTA60; (b)ScTA30 .....	84
Figure 4.7 Failure mode of seawater-saturated RC beams under freeze-thaw cycles: (a) ScTS60; (b)ScTS30 .....	85
Figure 4.8 Load-deflection relation at room temperature .....	86



Figure 4.9 Load-deflection relation after freeze-thaw cycles with air-cured condition.....	87
Figure 4.10 Load-deflection relation after freeze-thaw cycles with seawater-saturated condition .....	87
Figure 4.11 Load-tensile strain relation at room temperature .....	88
Figure 4.12 Load-tensile strain relation after freeze-thaw cycles with air-cured condition.....	89
Figure 4.13 Load-tensile strain relation after freeze-thaw cycles with seawater-saturated condition .....	89
Figure 4.14 Load-compressive strain relation at room temperature.....	90
Figure 4.15 Load-compressive strain relation after freeze-thaw cycles with air-cured condition .....	90
Figure 4.16 Load-compressive strain relation after freeze-thaw cycles with seawater-saturated condition .....	91
Figure 4.17 Concrete stress-strain fitting curve; (a) Thorenfeldt model-based curve; (b) Hognestad parabolic-based curve .....	91
Figure 4.18 Stress-strain curve of reinforcing bars; (a)Tensile rebar; (b) Compressive rebar.....	92
Figure 4.19 Load-deflection relation by preliminary analysis .....	93
Figure 4.20 Analysis results of SRTA30; (a) Load-deflection relation; (b) Load-strain relation .....	94
Figure 4.21 Analysis results of ScTA30; (a) Load-deflection relation; (b) Load-strain relation .....	94
Figure 4.22 Analysis results of ScTS30; (a) Load-deflection relation; (b) Load-strain relation .....	95
Figure 4.23 Analysis results of SRTA60; (a) Load-deflection relation; (b) Load-strain relation .....	95
Figure 4.24 Analysis results of ScTA60; (a) Load-deflection relation; (b) Load-strain relation .....	96

Figure 4.25 Analysis results of ScTS60; (a) Load-deflection relation; (b) Load-strain relation .....	96
Figure 4.26 Estimated shrinkage strain of SRTA30; (a) With consideration of tension stiffening; (b) Without consideration of tension stiffening	97
Figure 4.27 Estimated shrinkage strain of ScTA30; (a) With consideration of tension stiffening; (b) Without consideration of tension stiffening	97
Figure 4.28 Estimated shrinkage strain of ScTS30; (a) With consideration of tension stiffening; (b) Without consideration of tension stiffening	98
Figure 4.29 Estimated shrinkage strain of SRTA60; (a) With consideration of tension stiffening; (b) Without consideration of tension stiffening	98
Figure 4.30 Estimated shrinkage strain of ScTA60; (a) With consideration of tension stiffening; (b) Without consideration of tension stiffening	99
Figure 4.31 Estimated shrinkage strain of ScTS60; (a) With consideration of tension stiffening; (b) Without consideration of tension stiffening	99
Figure 4.32 Failure of 30 MPa concrete RC beams: (a) SRTA30; (b)ScTA30; (c) ScTS30.....	103
Figure 4.33 Failure of 60 MPa concrete RC beams: (a) SRTA60; (b)ScTA60; (c) ScTS60.....	104
Figure 4.34 Position of crack gauges in 60 MPa RC beams: (a) SRTA60; (b)ScTA60; (c) ScTS60 .....	105
Figure 4.35 Comparison of flexural crack width of 60 MPa RC beams .....	106
Figure 4.36 Comparison of shear crack width of 60 MPa RC beams .....	107
Figure 4.37 Load-deflection relationship of 30 MPa RC beams.....	108
Figure 4.38 Load-deflection relationship of 60 MPa RC beams.....	109
Figure 4.39 Load-deflection relationship of 30 MPa RC beams at early stage .....	110
Figure 4.40 Load-deflection relationship of 60 MPa RC beams at early stage .....	110
Figure 4.41 Load-strain relationship of 30 MPa RC beams.....	113

Figure 4.42 Load-strain relationship of 60 MPa RC beams.....	114
Figure 4.43 Load-strain relationship of 30 MPa RC beams at early stage....	114
Figure 4.44 Load-strain relationship of 60 MPa RC beams at early stage....	115
Figure 4.45 Deflection-tensile strain relationship of 30 MPa RC beams.....	115
Figure 4.46 Deflection-tensile strain relationship of 60 MPa RC beams.....	116
Figure 4.47 Load-compressive strain relationship of 30 MPa RC beams.....	116
Figure 4.48 Load-compressive strain relationship of 60 MPa RC beams.....	117
Figure 4.49 Stress range in load-deflection relationship: (a) 30 MPa RC beam; (b) 60 MPa RC beam.....	118
Figure 4.50 Stress range in load-strain relationship: (a) 30 MPa RC beam; (b) 60 MPa RC beam .....	119
Figure 4.51 Stress range in stress-strain curve of rebar: (a) Rebar in 30 MPa RC beam; (b) Rebar in 60 MPa RC beam.....	120
Figure 4.52 Load-deflection relationship in static tests: (a) 30 MPa RC beams; (b) 60 MPa RC beams .....	120
Figure 4.53 Load-N relationship: (a) FRTA30; (b) FRTA60.....	122
Figure 4.54 Load-N relationship: (a) FcTA30; (b) FcTA60.....	122
Figure 4.55 Load-N relationship: (a) FcTS30; (b) FcTS60.....	123
Figure 4.56 Failure of RC beams at room temperature: (a) FRTA60; (b) FRTA30 .....	124
Figure 4.57 Failure of air-cured RC beams under freeze-thaw cycles: (a) FcTA60; (b) FcTA30 .....	124
Figure 4.58 Failure mode of seawater-saturated RC beams under freeze-thaw cycles: (a) FcTS60; (b) FcTS30 .....	125
Figure 4.59 Position of crack gauges in RC beams: (a) FRTA30; (b)FcTA30; (c) FcTS30; (d) FRTA60; (e) FcTA60; (f) FcTS60 .....	126
Figure 4.60 Crack width range at room temperature: (a) FRTA30; (b) FRTA60 .....	127

Figure 4.61 Crack width range under freeze-thaw cycles with air-cured condition: (a) FcTA30; (b) FcTA60 .....	128
Figure 4.62 Crack width range under freeze-thaw cycles with seawater- saturated condition: (a) FcTS30; (b) FcTS60.....	129
Figure 4.63 Central deflection at room temperature: (a) Deflection-N relation; (b) Increasing ratio-N relation.....	130
Figure 4.64 Central deflection under freeze-thaw cycles with air-cured condition: (a) Deflection-N relation; (b) Increasing ratio-N relation .....	131
Figure 4.65 Central deflection under freeze-thaw cycles with seawater- saturated condition: (a) Deflection-N relation; (b) Increasing ratio-N relation.....	132
Figure 4.66 Central deflection of simply supported beam .....	132
Figure 4.67 Flexural stiffness at room temperature: (a) Stiffness-N relation; (b) Increasing ratio-N relation.....	133
Figure 4.68 Flexural stiffness under freeze-thaw cycles with air-cured condition: (a) Stiffness-N relation; (b) Increasing ratio-N relation .....	134
Figure 4.69 Flexural stiffness under freeze-thaw cycles with seawater- saturated condition: (a) Stiffness-N relation; (b) Increasing ratio-N relation.....	135
Figure 4.70 Tensile strain at room temperature: (a) Strain-N relation; (b) Increasing ratio-N relation .....	136
Figure 4.71 Tensile strain under freeze-thaw cycles with air-cured condition: (a) Strain-N relation; (b) Increasing ratio-N relation .....	137
Figure 4.72 Tensile strain under freeze-thaw cycles with seawater-saturated condition: (a) Strain-N relation; (b) Increasing ratio-N relation ..	138
Figure 4.73 Strain range at room temperature.....	139
Figure 4.74 Strain range under freeze-thaw cycles with air-cured condition	139

Figure 4.75 Strain range under freeze-thaw cycles with seawater-saturated condition.....	139
Figure 4.76 Compressive strain at room temperature .....	140
Figure 4.77 Compressive strain under freeze-thaw cycles with air-cured condition.....	141
Figure 4.78 Compressive strain under freeze-thaw cycles with seawater-saturated condition .....	142
Figure 4.79 Failure of 30 MPa concrete RC beams: (a) FRTA30; (b)FcTA30; (c) FcTS30.....	144
Figure 4.80 Failure of 60 MPa concrete RC beams: (a) FRTA60; (b)FcTA60; (c) FcTS60.....	144
Figure 4.81 Position of crack gauges in 30 MPa RC beams: (a) FRTA30; (b)FcTA30; (c) FcTS30 .....	145
Figure 4.82 Crack width range of 30 MPa RC beams: (a) FRTA30; (b) FcTA30; (c) FcTS30.....	147
Figure 4.83 Position of crack gauges in 60 MPa RC beams: (a) FRTA60; (b)FcTA60; (c) FcTS60 .....	148
Figure 4.84 Flexural crack width range of 60 MPa RC beams: (a) FRTA60; (b) FcTA60; (c) FcTS60 .....	149
Figure 4.85 Shear crack width range of 60 MPa RC beams: (a) FRTA60; (b) FcTA60; (c) FcTS60.....	150
Figure 4.86 Central deflection of 30 MPa RC beams: (a) Deflection-N relation; (b) Deflection range-N relation.....	152
Figure 4.87 Central deflection of 60 MPa RC beams: (a) Deflection-N relation; (b) Deflection range-N relation.....	152
Figure 4.88 Central deflection increasing ratio of 30 MPa RC beams.....	153
Figure 4.89 Central deflection increasing ratio of 60 MPa RC beams.....	154
Figure 4.90 Flexural stiffness of 30 MPa RC beams: (a) Stiffness-N relation; (b) Stiffness increasing ratio-N relation .....	154

Figure 4.91 Flexural stiffness of 60 MPa RC beams: (a) Stiffness-N relation; (b) Stiffness increasing ratio-N relation .....	155
Figure 4.92 Tensile strain of 30 MPa RC beams: (a) Strain-N relation; (b) Strain range-N relation .....	156
Figure 4.93 Tensile strain of 60 MPa RC beams: (a) Strain-N relation; (b) Strain range-N relation .....	157
Figure 4.94 Tensile strain increasing ratio of 30 MPa RC beams .....	158
Figure 4.95 Tensile strain increasing ratio of 30 MPa RC beams .....	158
Figure 4.96 Compressive strain of 30 MPa RC beams .....	159
Figure 4.97 Compressive strain of 60 MPa RC beams .....	160
Figure 5.1 Geometry model of RC beam in finite element analysis .....	167
Figure 5.2 Thorenfeldt compression curve.....	168
Figure 5.3 Stress-strain curve of concrete in FEA .....	169
Figure 5.4 Plasticity model for reinforcement: (a) Material tests result; (b) Von mises plasticity model .....	170
Figure 5.5 Load-deflection relation of 30 MPa beam in FEA: (a) SRTA30; (b) ScTA30; (c) ScTS30.....	172
Figure 5.6 Load-deflection relation of 60 MPa beam in FEA: (a) SRTA60; (b) ScTA60; (c) ScTS60.....	173
Figure 5.7 Load-strain relation of 30 MPa beam in FEA: (a) SRTA30; (b) ScTA30; (c) ScTS30; (d) Position of strain gauges.....	174
Figure 5.8 Load-strain relation of 60 MPa beam in FEA: (a) SRTA60; (b) ScTA60; (c) ScTS60; (d) Position of strain gauges.....	175
Figure 5.9 Load-crack width relation of 60 MPa beam in FEA: (a) SRTA60; (b) ScTA60; (c) ScTS60 .....	176
Figure 5.10 Crack width contour of 30 MPa beam in FEA: (a) SRTA30; (b) ScTA30; (c) ScTS30.....	178
Figure 5.11 Crack contour of 60 MPa beam in FEA: (a) SRTA60; (b) ScTA60; (c) ScTS60.....	179

Figure 5.12 Crack width of 30 MPa beam in FEA.....	180
Figure 5.13 Comparison of load-crack width relation: (a) At room temperature; (b) Under freeze-thaw cycles with air-cured condition; (c) Under freeze-thaw cycles with seawater-saturation condition	182
Figure 5.14 Characteristic fatigue strength curves for steel (CEB-FIP, 2010) .....	183
Figure 5.15 Fatigue life analysis of RC beams .....	184
Figure 5.16 Modified prediction model of RC beams.....	187
Figure 5.17 Difference of predicted stress range of RC beams.....	188
Figure A.1 Stress-strain curve for concrete cylinder of RC beams: (a) SRTA30; (b) ScTA30; (c) ScTS30 .....	215
Figure A.2 Stress-strain curve for concrete cylinder of RC beams: (a) SRTA60; (b) ScTA60; (c) ScTS60 .....	216
Figure A.3 Stress-strain curve for concrete cylinder of RC beams: (a) FRTA60; (b) FcTA60; (c) FcTS60 .....	217
Figure B.1 Load-deflection curve of 30 MPa RC beams: (a) SRTA30; (b) ScTA30; (c) ScTS30.....	219
Figure B.2 Load-tensile strain curve of 30 MPa RC beams: (a) SRTA30; (b) ScTA30; (c) ScTS30.....	220
Figure B.3 Load-compressive strain curve of 30 MPa RC beams: (a) SRTA30; (b) ScTA30; (c) ScTS30 .....	221
Figure B.4 Load-deflection curve of 60 MPa RC beams: (a) SRTA60; (b) ScTA60; (c) ScTS60.....	222
Figure B.5 Load-tensile strain curve of 60 MPa RC beams: (a) SRTA60; (b) ScTA60; (c) ScTS60.....	223
Figure B.6 Load-compressive strain curve of 60 MPa RC beams: (a) SRTA60; (b) ScTA60; (c) ScTS60 .....	224
Figure B.7 Load-crack width curve of 60 MPa RC beams: (a) SRTA60; (b) ScTA60; (c) ScTS60.....	225

Figure C.1 Deflection-N curve of 30 MPa RC beams: (a) FRTA30; (b) FcTA30; (c) FcTS30.....	227
Figure C.2 Tensile strain-N curve of 30 MPa RC beams: (a) FRTA30; (b) FcTA30; (c) FcTS30.....	228
Figure C.3 Compressive strain-N curve of 30 MPa RC beams: (a) FRTA30; (b) FcTA30; (c) FcTS30 .....	229
Figure C.4 Deflection-N curve of 60 MPa RC beams: (a) FRTA60; (b) FcTA60; (c) FcTS60.....	230
Figure C.5 Tensile strain-N curve of 60 MPa RC beams: (a) FRTA60; (b) FcTA60; (c) FcTS60.....	231
Figure C.6 Compressive strain-N curve of 60 MPa RC beams: (a) FRTA60; (b) FcTA60; (c) FcTS60 .....	232



# NOTATIONS

Symbol	Definition and description
$A_c$	= Area of concrete section RC beam
$A_{st}$	= Nominal cross-sectional area of reinforcement
$M_{cr}$	= Cracking moment
$M_d$	= Flexural strength with design strengths of materials
$M_n$	= Nominal flexural strength
$P_{max}$	= Maximum load
$b$	= Width of RC beam
$d$	= Effective depth of RC beam
$f_c$	= Actual compressive strength of concrete from tests
$f_{ck}$	= Specified compressive strength of concrete
$f_y$	= Specified yield strength for non-prestressed reinforcement
$f_r$	= Modulus of rupture
$h$	= Depth of RC beam
$s$	= Spacing of stirrups
$\phi$	= Strength reduction factor
$\rho$	= Reinforcement ratio for flexural reinforcement
$N$	= Fatigue life
$\Delta\sigma$	= Stress range

# **I. Introduction**

## **1.1. Research Background**

Currently, the demand for natural resources has constantly been increasing due to the population increase. It has been assessed that by approximate 30% of the world's undiscovered gas and 13% of the oil might be found in the Arctic circle (Gautier et al., 2009). However, the Arctic region presented a rather harsh temperature environment that is approximately in the range of -60~40°C. In such a temperature condition, material properties of concrete may be altered subjected to repeated freeze-thaw cycles. Concrete structures such as offshore structure, bridge, wharves, and pavement are significantly vulnerable especially when in a saturated state. Water in concrete capillary pores expands upon freezing stage, and crack will occur if the expanding pressure exceeds tensile strength of cement paste.

Except for the harsh temperature environment, chloride attack and external load have also been inevitable consideration in design of concrete structures. Concrete pavement, bridge decks as well as concrete in a splash zone suffer combined effect of freeze-thaw cycles and chloride attack. In general, chloride ions deteriorate the concrete structures by corrosion of the reinforcing bars, and the corrosion will be accelerated when the concrete structures subjected to freeze-thaw cycles. Chloride ions will be easier to reach reinforcing bars with the support of cracked cement paste.

Concrete structures will further be deteriorated in case there are external loads, for instance, static and fatigue from environment ((Li et al., 2011; Waagaard, 1977). To ensure the usability of concrete structures under multi-damage condition, the experimental studies may need to be conducted. Through the experimental results, both material properties and structural behavior of RC element may need to be investigated considering the combined effect of multi-damage.

## 1.2. Objectives and Scope

In this study, the objective of this study was to investigate the flexure and fatigue behavior of RC beam exposed to combined effect of freeze-thaw cycles and seawater. For the objectives mentioned above, the following scope of the study were presented.

First, the previous studies that were related to the RC beam behavior under freeze-thaw cycles, chloride attack, and external load were analyzed. From the literature review, the primary limitations of studies have been captured. In addition, the current design codes were comparatively analyzed in which the clauses for durability showed differences. With the bases, the necessity of experimental studies into structural behavior of RC element under multi-damage was proposed, and requirements from design codes were referred.

With the basis of literature review and analysis of current design codes, structural tests were conducted which took combined effect of damage account. The most severe temperature condition of the Arctic region was simulated in freeze-thaw cycles test. Chloride attack was simulated by artificial saltwater in the laboratory test. Finally, flexure and fatigue load were conducted combined with freeze-thaw cycles and seawater. Through the experimental results, the structural behavior of reinforced concrete beam under the combined damage was presented.

Considering that experiments were not able to reflect all of the structural behavior, extra analytical study including finite element analysis and verification of fatigue life were carried out. The influence of concrete strength,

freeze-thaw cycles, seawater on the structural behavior of RC beam were further verified and investigated. Based on the experimental and analytical results, recommendations on cold region construction considering combined effect were proposed.

### **1.3. Organization**

Chapter 1 presents an introduction in terms of entire framework of thesis in which the general research background, scope, objectives were illustrated.

Chapter 2 shows the review of the previous studies on behavior of RC beams regarding freeze-thaw cycles, seawater, and applied load. Moreover, design of concrete structures in current design codes with respect to exposure classes have been reviewed. From the reviewal, limitations in previous studies were captured.

Chapter 3 exhibits the experimental program including freeze-thaw cycles, seawater, and applied load. Total 12 reinforced concrete beams were fabricated and tested in flexure and fatigue tests. To evaluate the freeze-thaw damage, RC beams were categorized into seawater-saturation condition and air-cured condition in freeze-thaw cycles. The procedure to achieve seawater saturation state and the loading scheme of fatigue test that was derived based on static test was illustrated. It should be noted that most of the measuring tool such as strain gauge, linear variable differential transducers (LVDTs) have been prescribed its allowable operation temperature. Therefore, measuring schemes at low temperature was briefly introduced.

In Chapter 4, the effect of concrete strength, freeze-thaw cycles, seawater exposure was discussed. The failure mode and crack propagations were firstly discussed, then followed by the thermal analysis in which the validity of the temperature input was demonstrated. In static test, load, deflection, strain of rebar, and crack width of the RC beams (only for 60MPa RC beam) were

discussed. Moreover, section analysis was adopted to further analyze the strain attributed to the shrinkage. For the case of fatigue test, results regarding fatigue life, deflection, flexural stiffness, strain of rebar, stress range and crack width of RC beams were analyzed.

The analytical study was discussed in Chapter 5 in order to further verify the test results and predict the behavior that cannot obtain form the tests. At first, the validity of the finite element model was verified by means of comparing the analytical results and test results. Then verifications and predictions on structural behavior was conducted considering the concrete strength that were adopted in this study. Furthermore, the fatigue analysis based on existing models were conducted to verify the test results, and a modified prediction model of S-N relation was proposed and compared.

Chapter 6 summarized above-mentioned study and presented conclusions, including effect of concrete strength, freeze-thaw cycles, and seawater. Finally, recommendations regarding design of concrete structures in cold regions was proposed.

Appendix A presented the material test data that were not shown in the chapter. Appendix B and C included the detailed experimental data from the RC beam tests.

## **II. Literature Review**

### **2.1. Introduction**

Durability of concrete structures is crucial from the perspective of design, especially exposed to aggressive environment where various damage factors shall be under consideration. In general, concrete structures exposed to both physical and chemical deterioration. To enhance the durability, experimental studies with various additives and external protection have been widely applied. Design codes specify required properties of concrete in accordance with exposure categories and classes.

Chapter 2.2 reviewed the previous studies relevant to the physical and chemical deterioration of the concrete. The mechanism of freeze-thaw cycles chloride attack based on previous studies as well as its limitations were discussed.

Then, current design codes related to the durability design of concrete structures have been compared in Chapter 2.3. Based on the comparison, further experimental verifications can be established.



## 2.2. Deterioration of RC Structures

### 2.2.1. Introduction

This chapter illustrates the general deteriorations that have been divided into physical and chemical factors. Besides, the combined effect of multi-damages based on previous studies have been presented.

### 2.2.2. Chemical Deterioration

Concrete structures in marine environment subjected to seawater corrosion where the chloride attack will occur. It has commonly been known that seawater contains various chemical composition, and sodium and chloride ions present the dominant concentration.

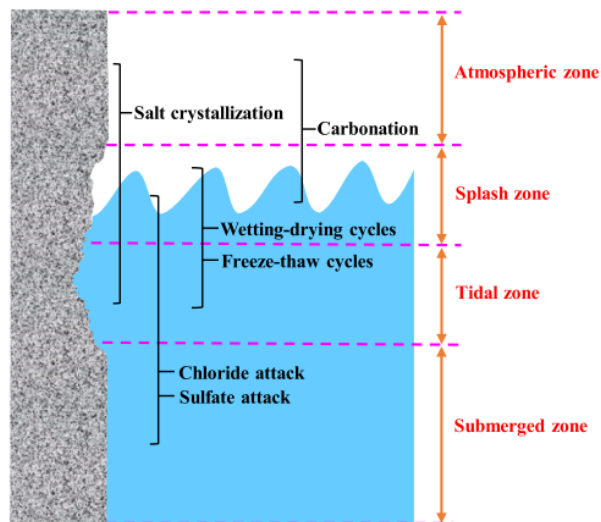


Figure 2.1 The main attack of concrete structures exposed to marine environment (Wang et al., 2022)

Concrete in the marine environment suffers from multiple damages such as freeze-thaw cycles, chemical attack of seawater, carbonization, wetting-drying cycles as shown in Figure 2.1. In cold regions, the deterioration caused by freeze-thaw cycles will be exacerbated exposed to marine environment. Moreover, concrete structures in marine environment will also suffer from combined effect of multiple damages.

Table 2.1 shows the detailed composition of the seawater in the world where the average concentration of sodium chloride is reported as approximate 3.5% by mass. In marine environment, concrete can be deteriorated by the chemical reaction which lead to several phase alteration.

The first phase alteration has been reported as the formation of gypsum and brucite due to the reaction of seawater with calcium hydroxide. Furthermore, aragonite will be deposited on the surface of the concrete which is caused by CO<sub>2</sub>-dissovled seawater (Alexander, 2016).

Another phase alteration can be attributed to the leaching of cement hydration products. Friedel's salt (2CaO·Al<sub>2</sub>O<sub>3</sub>·CaCl<sub>2</sub>·10H<sub>2</sub>O) will be formed when the chloride ions react with calcium aluminate (C<sub>3</sub>A) and monosulphoaluminate (AFm)(Birnin-Yauri et al., 1998). The mechanism of the crystallization of Friedel's salt has been reported as absorption and anion exchange, and the detailed process has been shown in Eq. (2.1) (Suryavanshi et al., 1996).

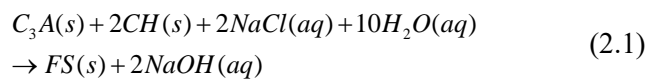


Table 2.1 Composition of seawater (Alexander, 2016)

Major ions	Concentration (g/l)					
	Mediterranean Sea	North Sea	Atlantic Ocean	Baltic Sea	Arabian Gulf	Red Sea
Na <sup>+</sup>	12.40	12.20	11.10	2.19	2.70	11.35
Mg <sup>2+</sup>	1.50	1.110	1.21	0.26	2.30	1.87
Cl <sup>-</sup>	21.27	16.55	20.00	3.96	36.9	22.66
SO <sub>3</sub> <sup>-</sup>	2.60	2.22	2.18	0.58	5.12	3.05
TDS*	38.80	33.06	35.37	7.11	66.65	40.96

\*Total dissolved solids

The ettringite and Friedel's salt distributed differently, for instance, Friedel's salt can be found in the inner zones while the ettringite usually exist on the surface of the concrete. Except for the Friedel's salt and ettringite, another common alteration of phase has been reported as the decalcification of calcium silicate hydrate (CSH) and conversion to noncementitious M-S-H (Alexander, 2016). However, the diffusion of Cl<sup>-</sup> has been indicated to be faster than Mg<sup>2+</sup>, and the decalcification of C-S-H has been accelerated in a high concentration of chloride solutions such as seawater (Kurdowski, 2004).

Table 2.2 summarized the common phase change of the concrete in chloride solutions. Only three common phase alteration have been listed in

which the chemical reactions of concrete with seawater can be properly reflected.

Table 2.2 Phase alteration in cementitious material (Alexander, 2016)

Original phases	Altered phases
Calcium hydroxide	Gypsum Brucite Aragonite
Calcium aluminate hydrate and AFM	Friedel's salt Ettringite
Calcium silicate hydrate (CSH)	Decalcified CSH Magnesium silicate hydrate (MSH) Thaumasite

It has been reported that chloride-induced deterioration of concrete structures consume significant resources (Bremner et al., 2001). Deterioration of concrete usually result in corrosion of steel at which the corrosive ions will ingress. Figure 2.2 shows the schematic representation of chloride-induced corrosion of steel in concrete. The corrosion of steel is an electrochemical process, the passive film (FeO·OH) form on the surface of steel that mitigate the corrosion. Generally, the passive film stably protect steel in concrete where the pH greater than 13. Several conditions such as the drop of pH lower than 1 or the chloride ions with high concentration will break the passive film which initiate the corrosion of steel. Concrete in marine environment or bridge decks with deicing salt usually subjected to high concentration of chloride ions, and

the ingress of chloride ions will be accelerated when concrete cracked by external environment.

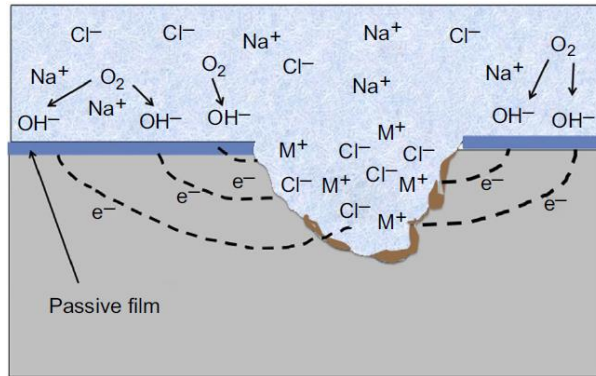


Figure 2.2 Chloride-induced corrosion of steel (Hansson, 2011)

Chloride-induced deterioration by deicing salts have been widely studied (Shi et al., 2010, 2013; Muthumani et al., 2014). However, previous studies indicated that deterioration by chloride ions usually combined with other damage factors such as external load and freeze-thaw cycles (Andrade et al., 2002; Jiang and Yuan, 2013; Söylev and Richardson, 2008).

### 2.2.3. Physical Deterioration

#### 2.2.3.1 External load

Concrete structures such as offshore structures and bridge decks not only subjected to chemical deterioration but also severe physical actions. The repeated wave load in marine environment and vehicle load on bridge accumulate the fatigue damage of concrete structures. In offshore structure towers, the stress conditions basically presented axial with no flexural moment. However, a flexural gradient has been presented in areas of local stress

concentrations (Waagaard, 1977). For the case of bridge, over millions of cars and trucks have been reported to cross the Canada-United States border in 2011 (Mirzazadeh et al, 2017).

Concrete under cyclic loading may present microcracks that possibly in a different orientation, and eventually reach failure even if the exerted load is lower than its compressive strength. The capillary pore structure of concrete will be damaged under the action of fatigue loading. It is specified that fatigue strength of concrete for  $10^7$  cycles of compression, tension or flexure is approximate 55% of its static strength (ACI 215R-74, 1997). In general, fatigue stress is usually resisted by reinforcing bars after cracking of concrete in a flexural reinforced concrete component.

Plenty much of fatigue tests with reinforcing bars have been carried out since 20<sup>th</sup> century, and it turns out that the fatigue strength of reinforcing bars is affected by its geometric and physical properties. Also, previous studies show that fatigue strength of reinforcing bars are influenced by average stress, grade, and loading (Heffernan and Erki, 2004; Moss, 1982). By measuring the strain, internal as well as surface microcrack, the mechanism of fatigue fractures has been properly investigated. The progressive microcrack on the surface of the specimen has been detected before the occurrence of failure. To achieve the failure in reinforced concrete component, the concept of fatigue limit has been proposed. Fatigue limit indicates a stress range below which the specimen will not reach failure within an infinite number of loading cycles. Fatigue failure usually divided into low cycle fatigue and high cycle fatigue as shown in Figure 2.3 (Lee et al., 2018). Offshore structures, bridge decks, and other common

concrete structures can be regarded as in the range of high cycle fatigue in which the stress range is below the yield strength of reinforcing bars. Nevertheless, concrete structures subjected to the action of earthquake shall be classified as low cycle fatigue failure where the stress range will be larger than yield strength of reinforcing bars. In general, the number of fatigue cycles corresponding to fatigue limit has been taken as 200 million.

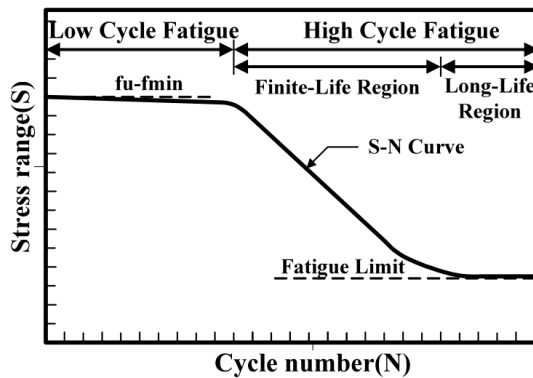


Figure 2.3 S-N curve of reinforcing bars (Lee et al., 2018)

Typically, fatigue life is determined by the stress range and frequency applied on testing specimen. To investigate structural behavior under fatigue loading, fatigue tests with different stress range (load range) and loading frequency were carried out in previous studies, as shown in Table 2.3. It shows the details of the fatigue test in previous studies from which the applied stress range and frequency have been presented. Small-scale reinforced concrete beam or prestressed beam have been used to conduct the fatigue tests, and the load range is applied by the ratio of ultimate strength in static tests. The loading frequency have been shown in the range of 1~10Hz with force control mode. Fatigue test is an accelerated test method in the laboratory, therefore, selection

of proper frequency that is able to simulate the actual loading condition has been significantly important. Fatigue design is usually conducted based on material tests, however, it has been reported that the fatigue behavior varies along with the composite behavior between concrete and steel, and failure mode would change by reinforcement ratio (Byun, 1997). Besides, bond strength would influence the fatigue behavior of RC member (Papakonstantinou, 2001; Mirzazadeh, 2017), therefore, not only material tests but also at structural level may need to be considered in fatigue design.

Table 2.3 Details of fatigue tests in previous studies

	Beam, mm	Load range (stress range)	Frequency (MPa)	Loading mode
Helgason et al. (1976)	155×258×2,632	(145MPa)	4, 8	-
Barnes and Mays (1999)	130×230×2,300	0.053~0.53P <sub>u</sub>	1	-
Papakonstantinou et al. (2001)	152×152×1,231	0.045~0.85P <sub>u</sub>	2	Force control
		0.045~0.52P <sub>u</sub>	3	
Xie et al. (2012)	100×200× 1,850	0.06~0.6P <sub>u</sub>	10	
Loo et al. (2012)	88×75× 1,500	0.22~0.75P <sub>u</sub>	1.5	-
		0.17~0.69P <sub>u</sub>		
	175×350×3,000	0.15~0.49P <sub>u</sub>		
	350×700×6,000	0.19~0.61P <sub>u</sub>		
Parvez and Foster (2015)	100×200× 1,200	0.22~0.78P <sub>u</sub>	3	Force control
	300×180×3,000	0.21~0.74P <sub>u</sub>	1.5	
Mirzazadeh et al. (2017)	200×400×4,000	0.25~0.75P <sub>u</sub>	1	
Choo et al. (2018)	200×200×2,175	0~0.85P <sub>y</sub>	1	
Banjara and Ramanjaneyulu (2020)	150×200× 1,800	0.2~ (0.65, 0.75, 0.85) P <sub>u</sub>	4	Force control

Current design codes specified the stress range above which fatigue damage shall be considered in concrete structures. Table 2.4 summarized the



stress range prescribed in current design codes. It can be roughly deduced that fatigue damage shall be considered when the stress range in concrete structures surpass 150MPa. However, the specified stress range in design codes are mostly based on material(rebar) test, therefore, the actual fatigue behavior in concrete structures can be differ. Previous investigations indicate that loading frequency between 1Hz and 15Hz have little effect on the fatigue life (ACI 215R-74, 1997; Murdock, 1965). For a higher stress range, the effect of loading frequency has also been observed where the effect of creep needs to be taken into consideration (AWAD and Hilsdorf, 1971).

Table 2.4 Stress range in design codes

Design codes	Stress range (MPa)	Notes
KDS 14 20 00 (2021)	>150	For $f_y \geq 400\text{MPa}$
ACI 215R-74 (1997)	>138	
Eurocode 2 (2004)	>150	For $N \geq 2 \times 10^6$

\*  $f_y$ : yield strength of rebar; N: number of fatigue cycles

### 2.2.3.2 Freeze-thaw cycles

In cold regions, frost damage has been regarded as one of the most severe factors that deteriorate the concrete structures. Water in capillary pores freeze at low temperature which result in an expansion of volume by approximate 9% (Neville, 1995). Figure 2.4 exhibited mechanism of frost damage in freeze-thaw cycles. At low temperature, freezing initiate in the larger pores due to the greater surface tension of the frozen pore water in the capillary pores. The expansion caused by frozen water generate the hydraulic pressure, leading to the movement of unfrozen water from small/gel pores into larger pores. The

hydraulic pressure is determined by several factors such as type of cement past, degree of saturation of pore structure, freezing rate, and distance among near pore (Detwiler et al., 1989). Once the expansion pressure exceeds the tensile strength of the cement paste at low temperature, internal cracking occurs. However, the hydraulic pressure sometimes is not the only source to cause inter damage due to the smaller magnitude of pressure. Pressure from the accumulation of the frozen water in capillary pores may contribute the energy for damage. During the thawing stage, pore water flows into microcracks that have been caused by expansion pressure, and further expansion in capillary pores and microcracks is initiated. In this manner, the internal damage is accumulated with repeated freeze-thaw cycles.

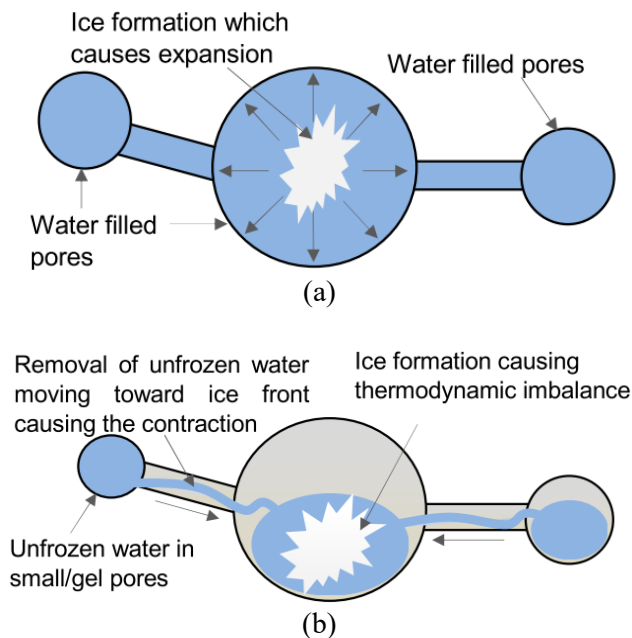


Figure 2.4 Mechanism in freeze-thaw cycles: (a) Expansion during freeze-thaw cycles; (b) Contraction during freeze-thaw cycles (Sicat et al. 2013)

It should be noted that not all the pore water freezes at low temperature since the freezing point of pore water is also related to the surface tension of frozen water especially in smaller gel pores. To experimentally evaluate the frost damage, the freezing point of pore water shall first be investigated. The ice formation process in concrete pores through conductivity of concrete have been experimentally investigated from which indicate that majority of the pore solution in concrete freeze above  $-10^{\circ}\text{C}$  (Cai and Liu, 1998). Likewise, the test related to the ice content at different temperature have been conducted. Test results indicate that frost damage primarily occur in the range of  $-10^{\circ}\text{C}$  to  $-50^{\circ}\text{C}$  (Johannesson, 2010). Electrical conductivity test has been carried out in order to evaluate the ice content of mortar. It has been demonstrated that the freezing point of pore solution is about  $-7^{\circ}\text{C}$ , and a model to estimate the ice content by applying electrical measurements has been proposed (Wang et al., 2016). For most concrete and cement paste, the major part of the pore water freeze at temperature down to  $-20^{\circ}\text{C}$ . Only negligible amounts of ice formation is possible below  $-55^{\circ}\text{C}$ . (Sereda and Litvan, 1980). At temperature down to  $-78^{\circ}\text{C}$ , gel pores are reported to freeze, however, it is too small to initiate the frost damage.

Material properties of concrete deteriorate under freeze-thaw cycles mainly by expansion pressure of frozen water. Under the environment of chloride ions such as marine environment and the bridge deck or road slab with de-icing agent, the frost damage is more severe. The frost damage is highly depending on its degree of saturation and the pore structures. Concrete seldom suffers from frost damage in a dry-out condition at which no expansion pressure by frozen water occur. It is also essential to reduce the porosity by lowering the

water cement ratio of fresh concrete which substantially increase the compressive strength of concrete. Previous studies have primarily focus on saturation and porosity of concrete in order to mitigate the frost damage of concrete. Additives such as air-entraining agent and other composite have been applied to increase the frost resistance of concrete. It has been experimentally reported that relative dynamic modulus of elasticity (RDME) and strength of concrete decrease during freeze-thaw cycles as shown in Table 2.5. The degree of saturation has also been found to increase the damage, and deterioration presented dramatic difference under the seawater-saturated condition.

Table 2.5 Material properties of concrete under freeze-thaw cycles

	No. FTC	Dimension (mm)	Material properties		Note
			$f_c'$	RDME	
Cao et al. (2015)	125	100×100×100	$f_c'$ (40MPa)	38% ↓	-
			RDME	97% ↓	
Shang and Song (2006)	75	100×100×400	$f_c'$ (30MPa)	37% ↓	Water-saturated
			RDME	58% ↓	
Zhang et al. (2020)	32	100×100×400	$f_c'$ (30MPa)	22% ↓	-
			RDME	22% ↓	
Diao et al. (2012)	300	100×100×100	$f_c'$ (50MPa)	13% ↓	Seawater-saturated
Shang et al. (2009)	400	100×100×100	$f_c'$ (30MPa)	53% ↓	Air-entrained
		100×100×400	RDME	23% ↓	
Amini and Tehrani (2011)	28	Ø50×L100	$f_c'$ (25MPa)	8% ↓	Plain water
				27% ↓	Seawater

\* FTC: freeze-thaw cycles; RDME: relative dynamic modulus elasticity

Most of the studies have paid much attention to the material properties of concrete under freeze-thaw cycles, only few studies have been carried out investigating the effect of freeze-thaw cycles on structural behavior of reinforced concrete member. The ultimate load of structural behavior of reinforced concrete (RC) beam showed 13% decrease. Also, the greater durability of high strength concrete under freeze-thaw cycles has been verified. (Cao et al., 2015). RC beam exhibited only 7.4% and 1.0% decrease of yield and ultimate strength under the combined action of 300 cycles of freeze-thaw and seawater corrosion from which the minor effect on load carrying capacity can be demonstrated. However, ductility of RC beam decreases by approximate 15% during combined damage (Diao et al., 2012b). In a similar manner, the yield and ultimate load of RC beam under 80 cycles of freeze-thaw test present an 4% and 13% decrease (Duan et al., 2017). For the case of alternative action of 300 cycles of freeze-thaw and seawater corrosion, the yield and ultimate load showed an decrease of 10% and 15% compared to the beam at air-cured condition (Liu et al., 2015). In short, load carrying capacity such as yield and ultimate load under freeze-thaw cycles showed decreasing trend, and damage increase with the presence of seawater.

Except for the decreasing effect on yield load, ultimate load as well as ductility, freeze-thaw cycles also deteriorate bond strength of RC member. A linear decrease of bond strength between concrete and reinforcing bars under freeze-thaw cycles has been reported (Ji et al. 2008). Pull-out tests subjected to freeze-thaw cycles have been conducted in previous studies. Tests results indicate that freeze-thaw-induced degradation of concrete not only result in decrease of bond behavior but also reduction of tension-stiffening effect

(Petersen et al. 2007). Deterioration of bond strength of RC member have been experimentally verified by the variation of tensile strain. In tensile strain-deflection relation of RC beam, deflection have been presented greater value at the same tensile strain in which the deterioration of bond strength is possibly the main reason. (Jang et al. 2009). Moreover, the decreased the bond strength also affect ultimate load of RC beam (Cao et al. 2015).

The standard test methods of freeze-thaw cycles such as ASTM, CEN/TS CIF-Test have been published. Table 2.6 presents the details of the standard test methods prescribed in documents mentioned above.

Table 2.6 Test methods for freeze-thaw cycles of concrete

	ASTM C666/C666M (2015)	CEN/TS 12390-9 (2006)			CIF-Test (2004)
		Slab-Test	Cube-Test	CF-/CDF- Test	
Specimen, mm	75~125 (width, depth, diameter) 275~405 (length)	150×150×50	100×100×100	150×140×50	150×110×70
Temperature Range, °C (environ.)	-18~4	-18~24(upp.) -22~16(low.)	-13~22(upp.) -17~18(low.)	-20~20	-20~20
Duration of each FTC, h	2.5~6.25 (min)	24	24	12	12
Cycles	300	56	56	14(CDF) 28(CF)	-
Recommended acceptance criteria	RDME<60%	Scaling<1000 g/m <sup>2</sup>	Scaling<3% by weight	Scaling<1500 g/m <sup>2</sup>	RDME<80%

\* FTC: freeze-thaw cycles; RDME: relative dynamic modulus elasticity

Temperature history, specimen preparation, and acceptance criteria that is to evaluate the performance of concrete have been specified. However, there are no test method regarding freeze-thaw cycles at structural level have been established. Researchers conduct freeze-thaw cycles test based on material test method or on their own discretion. Feasible testing schemes, in accordance with frost damage of concrete, for freeze-thaw cycles shall therefore be properly established.

#### **2.2.4. Combined Effect of Multi-damages**

Concrete structures in cold regions suffers from combined damage factors throughout the year, and that has been accepted as the primary loss of durability (Scherer, 2004). The deterioration of concrete structures initiates from the pore structures at micro level, then further affect the material and structural behavior. Previous studies show that crystallization of saltwater has been regarded as a damage factor in concrete structures (Thaulow and Sahu, 2004). Figure 2.5 exhibits the schematic representation of concrete in marine environment in which salt crystallization, evaporation of moisture, and capillary absorption have been presented. Salt crystallization on the surface of concrete is usually the primary cause of pressure, and further damage the microstructure of concrete. The actual mechanism of deterioration, that is by crystallization pressure, is initiated through the ingress of dissolved salt in concrete pores. Moreover, the evaporation of moisture and repeated wetting-drying cycles increase the saturation of saltwater.

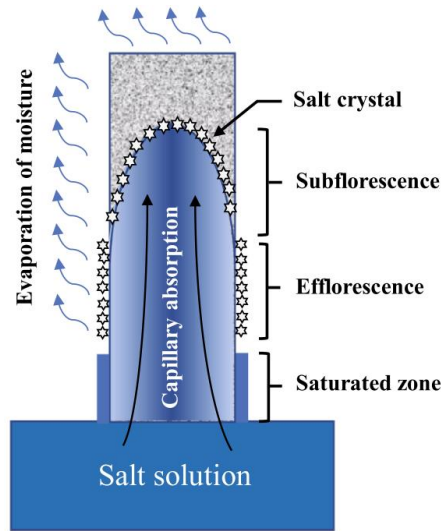


Figure 2.5 Representation of salt rise, evaporation, and crystallization in concrete (Wang et al. 2022)

Previous studies have been largely focusing on the durability of concrete structures from the perspective of single damage factor. Deterioration considering multiple mechanism have been started to investigate since last two decades (Wang et al. 2022). The durability of concrete under freeze-thaw cycles and chloride ions have been experimentally studied in previous studies, and model for chloride ions diffusion have also been developed (Hao et al. 2018; Li et al. 2016). In addition, studies that are related to the effect of combined effect of freeze-thaw cycles, chloride attack, sulphate attack, and carbonation have been widely conducted (Chai et al. 2018; Liu et al. 2018; Xiao et al. 2019). Under the combined action of freeze-thaw cycles, the damage caused by crystallization pressure increase since chloride ions are pushed into larger size of pores in which the sodium chloride starts to precipitate as temperature decrease (Sun et al. 2020).



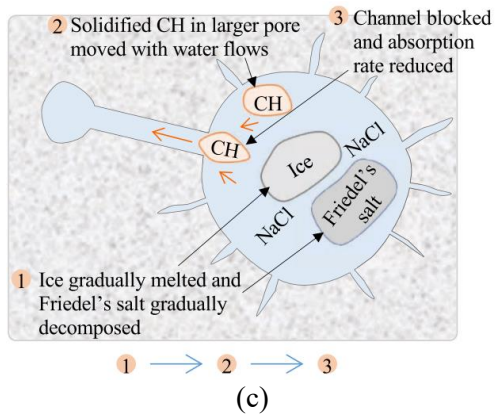
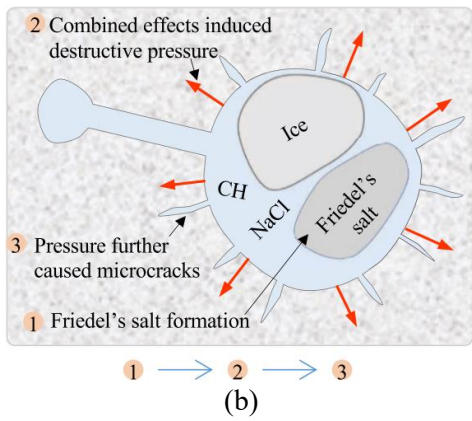
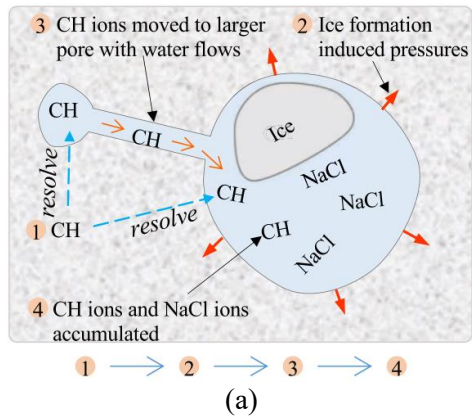


Figure 2.6 Representation of salt frost damage: (a) at freezing temperatures; (b) at low temperatures; (c) At thawing temperatures (Wang et al. 2021)

The internal damage of concrete in cold regions is possibly attributed to the crystallization pressure and ice expansion stress. Figure 2.6 present the detailed deterioration mechanism of concrete under combined effect of chloride ions and low temperatures (Wang et al. 2021). At freezing temperature, the calcium hydroxide (CH) resolve in the solution, and ice will form in the larger pores at which the hydraulic pressure, crystallization pressure as well as frost heaving pressure. The solution in smaller pores flow into the larger pore due to the chemical potential difference, and CH ions that are mixed with pore solution will ingress into the larger pores at the same time. The expansive products Friedel's salt will form in the larger pores as the amount of CH ions and sodium chloride ions increase. Finally, microcracks will form in the concrete matrix due to the expansive pressure caused by salt crystallization and ice formation. When the temperature increase, ice and Friedel's salt in the larger pores start to gradually decompose. However, CH ions are hardly able to flow out of larger pores and resume its original solution even though the chemical difference exist at thawing stage. The solidified CH ions could even block the channel that connect the smaller pores and lager pores, and further reduction of absorption rate could occur. A volume expansion has been reported due to the crystallization of Friedel's salt (Qiao et al. 2018), and the expansion could results in further increase of crack width under external load (Wu et al. 2020). At thawing stage of freeze-thaw cycles, sodium chloride could precipitate to form crystals which could produce tensile hoop stress (Flatt, 2002).

It has been demonstrated that pores and microcracks have been detected after penetration of chloride ions and freeze-thaw cycles. Therefore, the combined action of freeze-thaw cycles and chloride ions are more severe than

its single action (Bogas et al. 2016). In general, interface transition zone (ITZ) has smaller tensile strength where cracks initially occur. Under the combined effect of freeze-thaw cycles and chloride ions, ITZ become more vulnerable due to the greater porosity compared to the undamaged state (Hao et al. 2018).

Except for the effect of freeze-thaw cycles and chloride ions ingress, external load such as vehicle on bridge deck as well as environmental load on offshore structures cannot be ignored. Previous studies indicate that the deterioration of concrete member increase under the combined action of flexural loading, freeze-thaw cycle, and chloride ions (Mu et al. 2002; Zhao et al. 2021). In addition to the static load, the combined effect of fatigue load and freeze-thaw cycles has also been mentioned (Li et al. 2011). As mentioned, ITZ is a weak zone in cement paste which is first destroyed when the concrete subjected to external load. Under the combined damage of freeze-thaw cycles and external load, microcrack that have been caused by freeze-thaw cycles initiate from the pores. Then microcracks further develop along with the ITZ, which can be regarded as a bridging effect between concrete pores and ITZ. The irrecoverable strain initiated under the action of external load that result in greater crack width, and finally the more serious deterioration is accumulated (Li et al. 2019).

The damage accumulation under the combined effect of freeze-thaw cycles and fatigue load has been verified through acoustic emission (Qiao et al. 2015). Microcracks initiate and propagate fast as the cycles of freeze-thaw increase, and redistribution of pore solution occur during thawing stage. Pore solution flow into microcracks which incubate for next frost damage. Pores and

microcrack expand again as temperature decrease, and further internal damage are accumulated. What should be noted is that the direction of the microcrack is relatively different at low temperature compared with that of at room temperature (Li et al. 2019). Generally, cracks at room temperature usually firstly occur at the bottom of specimen under the action of external load and further propagate along with ITZ. On the contrary, large amount of strain energy is accumulated at low temperature prior to the occurrence of cracks. When strain energy release by the occurrence of cracks, the direction of cracks is relatively determined.

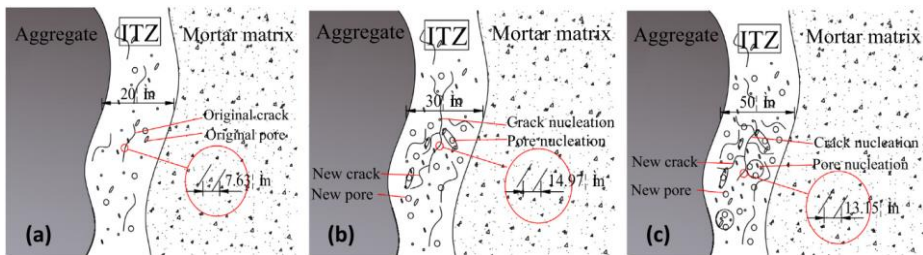


Figure 2.7 Deterioration of ITZ: (a) the control; (b) under fatigue load; (c) under combined action of freeze-thaw cycles and fatigue (Yang et al. 2018)

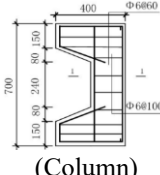
Under the combined action of freeze-thaw cycles and fatigue load, the width of ITZ has been reported to increase (Yang et al., 2018). Figure 2.7 reveals the deterioration mechanism of the ITZ under the various actions. ITZ under the fatigue loading shows greater crack width compared to the control matrix. In addition to the increased crack width, new microcracks and pores can be observed under the action of fatigue loading. For the case of matrix under combined actions of freeze-thaw cycles and fatigue load, mortar matrix presents more severe deterioration. It can be explained by repeated expansion

and contraction under the action of freeze-thaw cycles accelerate the stress increase. Large amounts of new pores and microcracks are generated as the stress in ITZ randomly increase. Through the freeze-thaw cycles test combined with sustained load, the vulnerability of ITZ in porous material has been highlighted. Microcracks in ITZ propagate fast and finally affect the permeability of the porous material (Kosior-Kazberuk and Berkowski, 2017).

Most of the previous studies have been conducted at material level, only few studies have focused on the structural level. Table 2.7 shows the combined effect of multiple damages on the structural behavior of RC component. Limited test data indicate that reinforced concrete component under combined action of freeze-thaw cycles, chloride ions, and external load exhibit the most serious deterioration. It can be referred that the deterioration increases as the stress ratio and freeze-thaw cycles increase. Furthermore, deterioration highly depends on the grade of concrete since magnitude of porosity directly influence the frost resistance of the concrete. Beam with concrete strength greater than 60MPa shows relatively steady change in flexural strength. However, structural behavior with high strength concrete beam has been scarcely conducted.

However, only one type of concrete strength has been applied in the most of tests and the combined effect of multiple damages hardly achieved due to the limitation of test equipment. Damage factors should be simulated in accordance with actual conditions of concrete structures. Damage factors in cold regions generally simultaneously influence the durability of concrete structures. To ensure the durability and usability of concrete structures in cold regions, current design codes need also to be comparatively analyzed.

Table 2.7 Structural behavior of RC component under combined damage

	Specimen (mm)	$f_c$ (MPa)	Damage factors	$P_u$
Sun et al. (1999)	40×40×160 (Beam)	40	FTC (20)	33% ↓
			FTC (20) Sustained load	46% ↓
		60	FTC (60)	25% ↓
			FTC (60) Sustained load	25% ↓
		80	FTC (500)	14% ↓
			FTC (500) Sustained load	15% ↓
Bo et al. (2011)	100×150×700 (Beam)	33	FTC (400) Corrosive solution	5% ↓
			FTC (400) Corrosive solution Sustained load	29% ↓
Diao et al. (2012)	 (Column)	46	FTC (300) Seawater	12% ↓
			FTC (300) Seawater Sustained load	27% ↓
Liu et al. (2015)	100×150×800 (Beam)	42	FTC (300) Seawater	7% ↓
			FTC (300) Seawater Fatigue load	23% ↓
Duan et al. (2017)	150×250×2,000 (Beam)	37	FTC (80)	13% ↓
			FTC (80) Sustained load	28% ↓

\* FTC (No): freeze-thaw cycles (No. of cycles);  $P_u$ : flexural strength

## **2.3. Design Codes for Durability**

### **2.3.1. Introduction**

Large amount of studies has been focused on the durability of concrete structures with the background of cold regions. The importance of combined effect of multiple damage have been emphasized. Experimental studies shall be reflected in practical application, and design codes are the basic access. Therefore, the provisions in current design codes in terms of durability of concrete structures need to be comparatively analyzed.

This chapter illustrated the provisions in various design codes. Design codes from South Korea (KDS 14 20 00: 2021), European countries (NS+NA,2014; Eurocode 2; DS2426; DIN 1045-2: 2008-08), USA (ACI 318-19), Canada (CSA A23.1: 2004), and Oceania countries (NZS 3101-1, 2006; AS 3600-2001) were included. Comparison regarding exposure class, exposed structures were firstly listed, then the corresponding minimum requirement for air content and specified compressive strength of concrete were compared.

### **2.3.1. Provisions Based on Exposure Class**

Table 2.8 presents the clause for concrete structures in accordance with exposure class. Exposed class can be classified into categories where the structures only subjected to freeze-thaw cycles or combined effect of freeze-thaw cycles and chloride ions attack. Correspondingly, design codes prescribed the minimum requirement for air content and specified compressive strength of concrete in order to achieve the designed durability.

The issues whether combined effect of multiple damage shall be considered has not been clearly specified in design codes. Furthermore, the minimum specified compressive strength of concrete was prescribed as 30MPa which is close the requirement in normal construction. As mentioned in previous studies, concrete under the combined action of multiple damage, the deterioration can be accelerated. The similar provisions were also found in design codes such as Eurocode 2 (2004), ACI 318-19 (2019), and AS 3600-2001 (2001). To achieve the durability during its service life, the minimum requirement in design codes for the condition of cold regions possibly need to be experimentally analyzed.



Table 2.8 Clause for concrete structures by exposure class

Design Codes	Class	Condition	Category	Min. requirement	
				Air Content (%)	$f_{ck}$ (MPa)
KDS 14 20 00 (2021)	EF3	동결에 노출되는 물보라 지역(비말대) 및 간만에에 위치한 해양 콘크리트	FTC	6.0	30
ACI 318-19 (2019)	F3	Concrete exposed to FTC with frequent exposure to water and exposure to deicing chemicals	FTC	4.5~7.5	35
Eurocode 2 (2004)	C1	RC exposed to chloride with or without FTC (Bridge decks, parking decks, ramps, marine structures)	FTC; Seawater spray; Salt water pools	5~8	35
CSA A23.3 (2014)	XF4	Road and bridge deck, splash zone of marine structures and other concrete surface	FTC; De-icing agent; Seawater	4	35
	XS3	Tidal, splash and spray zones (Parts of marine structures)	Chloride from seawater	-	35
	XF3	High water saturation with de-icing agents or seawater	FTC	4	30

Design Codes	Class	Condition	Category	Min. requirement	
				Air Content (%)	$f_{ck}$ (MPa)
DS 2426 - EN 206-1 (2011)	XF4	Road and bridge deck, splash zone of marine structures and concrete surface	FTC; De-icing agent; Seawater	.45	40
DIN 1045-2 (2014)		Marine structures in the tidal zone		-	30
GOST 31384 (2017)		Marine structures		4	35
NZS 3101-1 (2006)	C	Tidal, splash and spray zones	Seawater	4~8% (10mm aggr.) 3~6% ( $\geq 20$ mm aggr.)	30 (50 year) 25 (25~49 year)
AS 3600-2001 (2001)	C	In tidal or splash zones	Seawater	-	32

## 2.4. Concluding Remarks

Chapter 2 comparatively analyzed the previous studies as well as the current design codes. Previous studies present the historical research related to the durability that contain the effect of freeze-thaw cycles, chloride ions, and external load. Based on the results from previous studies, design codes with respect to durability of concrete in aggressive environment have been referred.

The mechanism of deterioration by freeze-thaw cycles, chloride ions, and external load was firstly illustrated. Experimental results indicate that damage factors considering actual condition of construction shall be simulated. However, most of the studies did not fully consider the combined effect of damage due to the limitation of testing conditions, and only material levels of experiment were widely carried out. With the support of experimental facilities in which the actual environment of cold regions can be properly simulated, the prediction results from material tests may further be verified at structural level. Generally, the fatigue behavior was estimated based on the rebar tests since reinforcing bars mainly resist the cyclic load. Nevertheless, structural behavior which considered the composite behavior between concrete and steel has been seldom conducted. At structural level, failure mode could change with respect to reinforcing ratio (Byun, 1997), and bonding force could influence the fatigue behavior of RC member (Papakonstantinou, 2001; Mirzazadeh, 2017). Therefore, the effect of freeze-thaw cycles and seawater on the structural behavior need to be simultaneously investigated.

Design codes from various countries were compared. The minimum requirement of concrete strength and air content was specified for the purpose of expected performance. Previous studies (Liu, 2016; Zhang 2019) mentioned that combined effect of freeze-thaw cycles and seawater increase the deterioration, and beam with high strength concrete will increase the freeze-thaw resistance (Sun, 1999). To investigate the structural behavior of RC member using normal strength concrete (NSC) and high strength concrete (HSC), the minimum specified concrete strength was adopted from KDS 14 20 00: 2021. Herein, the performance by using the minimum specified concrete strength in design code can be comparatively investigated.

## **III. Experimental Program**

### **3.1. Introduction**

Most of experimental studies with respect to freeze-thaw cycles, chloride ions attack has been conducted at material level. At structural level, static and fatigue tests at room temperature have been widely found in literature. However, the experimental studies regarding structural behavior of reinforced concrete members under the combined action of freeze-thaw cycles, chloride ions, and external load has been seldom carried out (Diao et al, 2011; Diao et al. 2012; Liu et al, 2015).

In this chapter, experiments considering the combined effect of freeze-thaw cycles, chloride ions, and external are conducted with reinforced concrete (RC) beams. The annual temperature environment of the Arctic region was experimentally simulated where concrete structures suffer from repeated freeze-thaw cycles. Chloride ions attack are simulated by the artificially mixed seawater, which contains 3.5% of sodium chloride by mass (Alexander, 2006). To fully achieve the frost damage caused by freeze-thaw cycles, beams that are subjected to freeze-thaw cycles immersed in seawater until there is no weight change occur. The concrete cylinders were manufactured from the same batch of concrete that was used to investigate the material properties. The external load is divided into static and fatigue mode. The flexural static behavior of RC beams has been initially investigated, then the fatigue tests have been conducted based on static tests. Tests results have been analyzed with respect to static and fatigue behavior RC beam, and its material properties are concluded.

## **3.2. Test Program**

### **3.2.1. Test Variables**

Test variables based on literature review and analysis of design codes were determined.

First, concrete strength was selected in order to assess the effect of concrete strength which referred the minimum specified compressive strength of concrete in design code (KDS 14 20 00: 2021, 2021). As a design aids, the effect of high strength concrete on structural behavior of reinforced concrete (RC) component under the combined multiple damage was expected to be investigated. Next, the loading methods that simulate the service load was selected. In general, concrete structures in cold region are under the action of static and fatigue load. Fatigue load such as wave load to offshore structures and vehicle load on bridge deck would accumulate the damage during its service life, and it accelerate the damage caused by freeze-thaw cycles and chloride ions attack. The magnitude of fatigue load and frequency varies in practice condition, and thus the service load state has been simulated the investigate the fatigue behavior. Additionally, the temperature condition of RC beam, including room temperature and freeze-thaw cycles were defined. Room temperature (20 °C) was planned to assess the effect of freeze-thaw cycles. The temperature of freeze-thaw cycles was determined in accordance with the most severe temperature range in the Arctic region. It has been experimentally demonstrated that concrete had more severe freeze-thaw damage with seawater condition. Therefore, the beam curing method before freeze-thaw cycles which

divided into air-cured and seawater-saturated condition was planned, deducing the effect of seawater exposure on the material properties and structural behavior.

The designation of specimen was determined based on test variables, as shown in Figure 3.1. The designation of RC beam was classified as the sequence of loading mode, temperature condition, beam curing method before freeze-thaw cycles, and compressive strength of concrete.

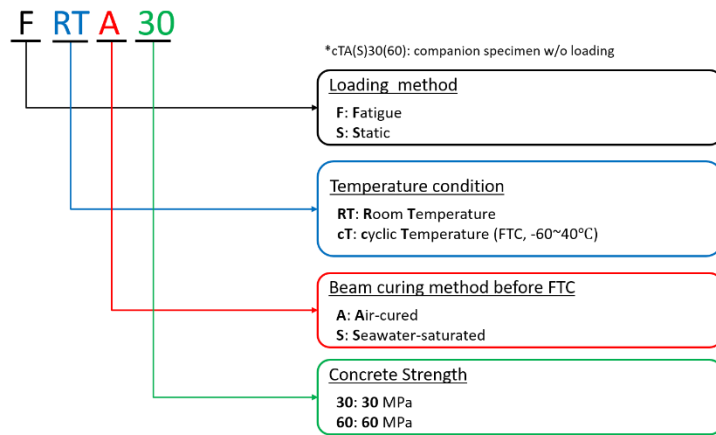


Figure 3.1 Designation of reinforced concrete beams

On the basis of designation, Table 3.1 exhibited the test program of this study. A total 12 reinforced concrete beams were used in this study, and the corresponding test procedure was depicted as shown in Figure 3.2. Part of RC beams, which were expected to suffer from freeze-thaw cycles with seawater-saturated state, were immersed in artificially mixed seawater. The weight of RC beams was measured prior to immerse in seawater by which the increase of weight in seawater can be measured. Measurement of weight was conducted

with interval of approximate 7 days. RC beams were regarded as saturation state when there was no weight change. When RC beams reach seawater-saturated state, the experiments were launched in order to maintain a close curing age. Material tests of concrete and reinforcing steel bars were also conducted. It should be noted that material properties of concrete were measured along with each beam tests since freeze-thaw cycles and seawater may alter the properties of concrete.

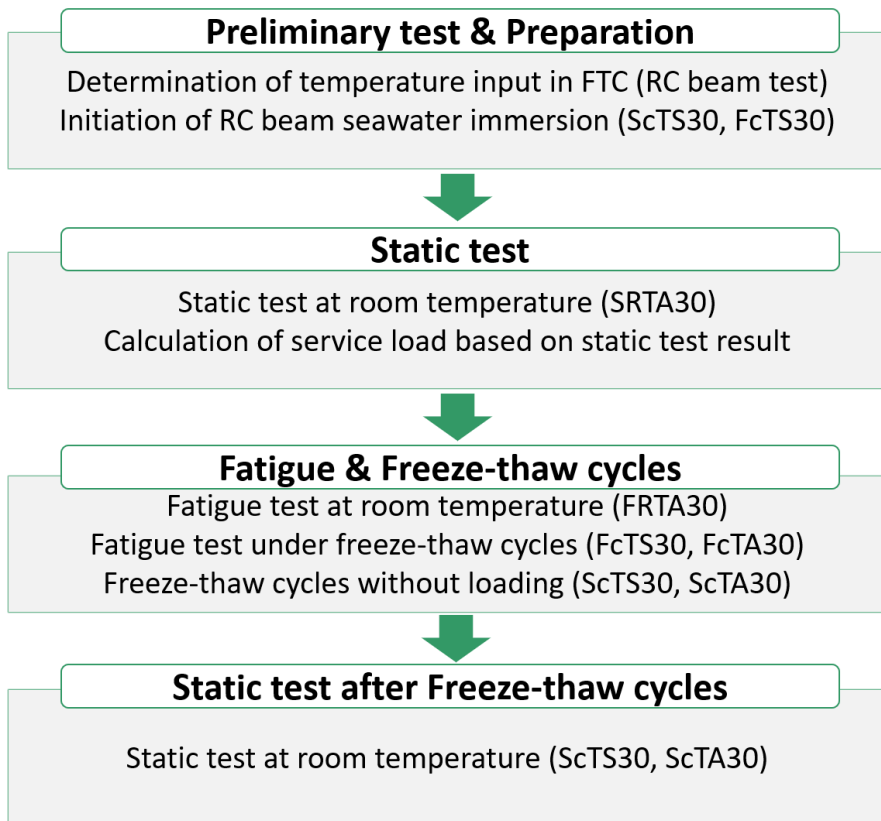


Figure 3.2 Flow chart of experiment



Experiments had been conducted in Extreme Temperature Chamber constructed in Seoul National University which permit simultaneous action of loading and temperature implementation in the range of -60~60°C. The flexural static test of RC beam with normal strength concrete (NSC: 30MPa) was first carried out, and then the fatigue history of RC beam was derived that simulate the service load state. The stress range and frequency were determined to fail the RC beams with the manner of rupture of tensile reinforcing bars. Temperature history of freeze-thaw cycles were determined based on finite element analysis and RC beam tests. The thermal properties of concrete and reinforcing bars from previous studies were adopted (Asadi et al, 2018; Shafigh et al, 2018), and finally verified by further trial and error method through finite element analysis and actual beam tests. With the fatigue history and temperature history determined, fatigue test of RC beams under combined effect of freeze-thaw cycles and seawater saturation were conducted. Moreover, the scaled RC beams with a length of 500 mm were fabricated to measure the temperature strain. Considering the loss of water during freeze-thaw cycles, the seawater-saturated beams were wrapped by plastic films prior to freeze-thaw cycles test. At the same time, RC beams that were designed to investigate the flexural static behavior subjected to freeze-thaw cycles were put aside the fatigue test beam. For instance, FcTS30 and ScTS30 were under the same freeze-thaw cycles. In this way, from the flexural static test and flexural fatigue test at room temperature to the beams subjected combined actions were carried out. For the RC beams with high strength concrete, identical tests were conducted which was to verify the effect of high strength concrete on structural behavior under combined effect of freeze-thaw cycles and seawater exposure.

Table 3.1 Test program

ID	$f_{ck}$ (MPa)	Loading method	Temperature condition (°C)	Loading condition	
				Beam curing before FTC	Testing temperature (°C)
SRTA30	30	Static	20	Air-cured	20°C
ScTA30			-60~40 (FTC)	Air-cured	
ScTS30				Seawater-saturated	
FRTA30		Fatigue	20	Air-cured	-60~40°C (FTC)
FcTA30			-60~40 (FTC)	Air-cured	
FcTS30				Seawater-saturated	
SRTA60	60	Static	20	Air-cured	20°C
ScTA60			-60~40 (FTC)	Air-cured	
ScTS60				Seawater-saturated	
FRTA60		Fatigue	20	Air-cured	-60~40°C (FTC)
FcTA60			-60~40 (FTC)	Air-cured	
FcTS60				Seawater-saturated	

\* FTC: freeze-thaw cycles

### 3.2.2. Dimension of Specimens

RC beams were designed to ensure tension-controlled failure. Considering the largest-possible beam length to be tested in the Extreme Temperature Chamber, the length was modified to 3,800 mm. At structural level, the freeze-thaw cycles are hard to comply with the standard test method which was established based on material tests. Additionally, the coordination between cyclic load and freeze-thaw cycles were considered during which RC beams can be suffered certain cycles of freeze-thaw damage. The cross-section of RC beams was remained 200 × 400 mm considering the efficient temperature transmission. The spacing of stirrup was determined with 100 mm in order to avoid shear failure, and it satisfied the fundamental requirement in design code which less than half of effect depth of RC beam. Concrete cover of RC beam was 50mm which follows the durability requirement in accordance with exposure class (EF4) in design code (KDS 14 20 00: 2021, 2021). Figure 3.3 shows the modified configuration of RC beam which has dimension of 200×400×3,800mm. The specified compressive strength of 30MPa and 60MPa were applied in fabrication of specimen, and SD400 grade deformed steel bars with diameter of 22mm (D22), 19mm (D19), 10mm (D10) were respectively used as tension, compression, and shear reinforcement.

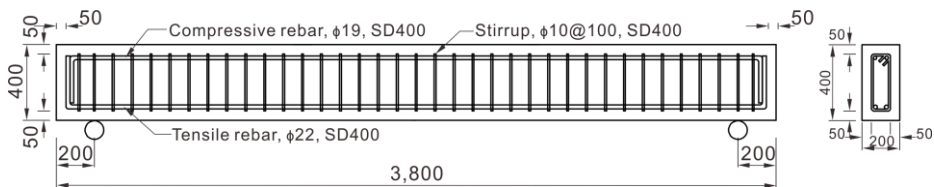


Figure 3.3 Configuration of RC beams

### **3.3. Material Tests**

#### **3.3.1. Concrete**

Two types of reinforced concrete beams were fabricated. The specified compressive strength of concrete is 30MPa and 60MPa, respectively. The 30MPa concrete denoted the minimum specified compressive strength of concrete in design code (KDS 14 20 00: 2021, 2021), which may not enough to resist combined effect of multiple damage during service life. It has been noted that 300 cycles of freeze-thaw have been taken as the criterion for frost resistance in standard test method (ASTM C666/C666M, 2015; KS F 2456, 2013). Previous studies showed that high strength concrete showed greater freeze-thaw resistance, and 60MPa concrete did not fail until 500 cycles of freeze-thaw cycle (Sun et al. 1999). Therefore, RC beams with 60MPa concrete strength were fabricated in order to verify the effect of high strength concrete on structural behavior under the combined effect of freeze-thaw cycles and seawater.

Table 3.2 showed the mix proportion of concrete. Type I Portland cement was used in mix and the maximum aggregate size of 25mm was applied. 30MPa and 60MPa strength concrete presented water cement ratio of 0.29 and 0.24, respectively. The average slump of 30MPa and 60MPa concrete were respectively measured as 180mm and 120mm. Concrete cylinders with dimension of 150×300mm were placed and air cured on site with the same condition with RC beams. For the case of the seawater saturation specimen, the

cylinders were immersed in seawater with RC beams. The compression tests were conducted in accordance with standard test method (ASTM C39, 2014).

Table 3.2 Mix proportion of concrete

$f_{ck}$ (MPa)	Unit weight (kg/m <sup>3</sup> )					
	Water	Cement	Fine aggregate	Coarse aggregate	Admixture	Air content (%)
30	115	395	812	981	2.77	4.2
60	160	660	727	929	7.26	3.6

The Universal Testing Machine (UTM) in Seoul National University was applied in compression test as shown in Figure 3.4. Test results were shown in Table 3.3 and elastic modulus were determined by the slope of a line drawn from a stress of zero to 0.45 times compressive strength of concrete using stress-strain curve (ACI 318-19, 2019).



Figure 3.4 Compression test of concrete cylinder

The average compressive strength of concrete was shown as 37MPa and 59MPa for normal strength (30 MPa) and high strength (60 MPa) concrete. The displacement of concrete with respect to load were measured by Linear Variable Differential Transducers (LVDTs). Then the strains were calculated in the range of Bernoulli region (B-region) in which the discontinuity region (D-region) can be taken out of consideration.

Table 3.3 Compression tests result of concrete cylinder

Class	$f_{ck}$ (MPa)	$t$ (days)	$f_{cm}$ (MPa)	$E_c$ (MPa)
NSC	30	111	37	21,246
HSC	60	155	59	23,131

\* NSC: Normal Strength Concrete; HSC: High Strength Concrete

### 3.2.2. Reinforcing Steel Bars

In total three types reinforcing steel bars were adopted in fabrication of RC beams. The material properties of each type of reinforcing steel bars were measured in accordance with standard test method (ASTM 370-18, 2019). The standard products of SD400 grade deformed reinforcing steel bars with diameter of 22mm (D22), 19mm (D19), and 10mm (D10) were selected.

Three specimens of each type were used in uniaxial tension test as shown in Figure 3.5. Tension tests were carried out using UTM at Seoul National University, and Video Extensometer machine was applied in measurement of strain with respect to tensile load. The rate of loading was determined based on standard test method which was 1mm/min. Tension tests were conducted until rupture of reinforcing bars, and results were shown in Table 3.4 and Figure 3.6.

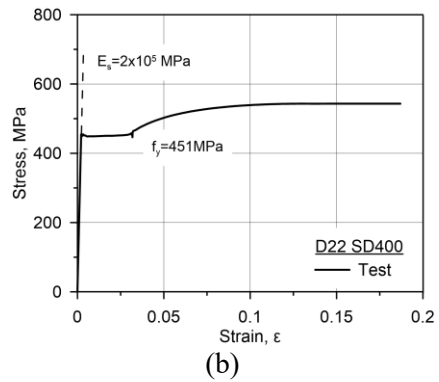
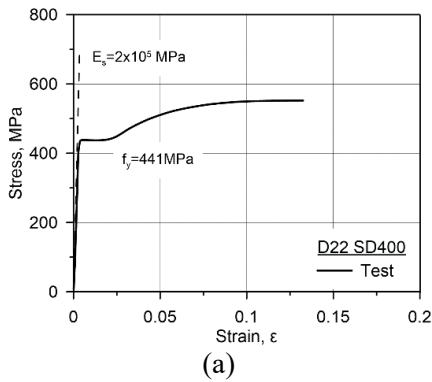


Figure 3.5 Uniaxial tension test of reinforcing steel bars

Tests result indicated that reinforcing bars exceeded the designed yield strength which was derived by the 0.2% offset method. It should be noted that the D22 reinforcing bars for 30MPa and 60MPa RC beams were from the two different batches which showed approximate 2% difference in terms of yield strength.

Table 3.4 Tension tests result of reinforcing steel bars

Diameter	$\epsilon_y$	$f_y$ (MPa)	$\epsilon_{sh}$ ( $\times 10^{-3}$ )	$\epsilon_u$ ( $\times 10^{-3}$ )	$f_u$ (MPa)	$E_s$ (MPa)
D22 (30MPa Beam)	0.0022	441	0.0233	-	536	200,000
D22 (60MPa Beam)	0.0023	451	0.0314	0.2175	545	200,000
D19	0.0023	453	0.0216	0.1267	588	200,000
D10	0.0024	478	0.0264	0.1065	636	200,000





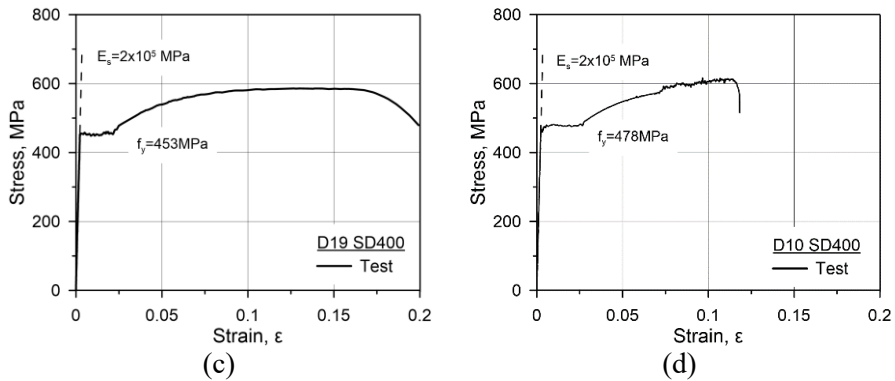


Figure 3.6 Stress-strain curve of reinforcing bars: (a) D22-SD400 (30MPa Beam); (b) D22-SD400 (60MPa Beam); (c) D19-SD400; (d) D10-SD400

### 3.4. Fabrication of Specimens

Reinforced concrete beams for the effect of combined damage were fabricated. The following procedures were conducted to achieve the fabrication of specimens.

1. Assembly of reinforcing steel bars
2. Attachment of strain gauge and thermocouple
3. Placement of reinforced concrete beams

#### 3.4.1. Reinforcement

A total two types of assembly of reinforcing bars were carried out which differ in the length of RC beams but with identical cross-section. Herein, the name of companion beam was designated in order to distinguish the specimen. Reinforcing bars under the combined action of freeze-thaw cycle and fatigue

tests generate a certain magnitude of strain, however, the strain caused by mechanical or temperature would be hardly distinguished. Therefore, the specimen that was only subjected to temperature effect shall be measured. Considering that temperature transmit mainly through the cross-section and less effect on length of RC beam, the companion beams with a length of 500mm were fabricated based on prediction by finite element analysis.

Reinforcement was firstly assembled before install strain gauges and thermocouple. Figure 3.7 showed the installation of strain gauge attachment and thermocouple. In total two types of strain gauges were used due to the allowable temperature of strain gauge. The strain gauge that were usually used at room temperature cannot be directly applied to measure the strain at low temperature. For the cases of beams under combined action of freeze-thaw cycles and applied load, the strain gauges that was designed to counteract major part of temperature effect at low temperature were used.



Figure 3.7 Installation of strain gauges and thermocouple

### 3.4.2. Placement of Concrete

Placement of concrete were carried out after assembly of reinforcing bars and installation of measuring sensors. Concrete at support of RC beams are vulnerable under the repeated cycles of loading at which the horizontal displacement possibly occurs by the local abrasion. Therefore, steel plate that was welded with shear stud were installed on the support position of RC beams prior to the placement of concrete in order to prevent the local failure or abrasion during fatigue tests.



Figure 3.8 Reinforcement on the support of beams: (a) Steel plate; (b) Steel plate in RC beams

Concrete cylinders with dimension of  $\text{Ø}150 \times 300$  mm was fabricated from the same batch of concrete. Considering the material properties subjected to freeze-thaw cycles, eight concrete cylinders were fabricated for each beam that were designed for freeze-thaw cycles. Fabricated concrete cylinders were cured with the same condition of RC beams which demolded after 24 hours. Beams and concrete cylinders were under air-cured condition until tests or seawater immersion.



Figure 3.9 Fabrication of RC beams and concrete cylinders

### 3.5. Seawater Saturation

Part of the fabricated RC beams, which were designed to suffer freeze-thaw cycles at seawater-saturated condition, had been immersed in artificially mixed salt water. The saltwater simulates the average NaCl concentration of seawater that is 3.5g/L by mass (Alexander, 2006). Except for the RC beams, the concrete cylinders from the same batch of concrete had been immersed in seawater. RC beams with 30 MPa and 60 MPa concrete strength were immersed at different curing age due to the testing conditions that were 28 days and 141 days, respectively.



Figure 3.10 Seawater saturation of RC beams

Immersed RC beams and concrete cylinders were periodically (by approximate a week) weighted in order to monitor the change of mass. Figure 3.11 shows the actual weighting of RC beams by scale with a division value of 200 g. The weighting of RC beams had been conducted until there was no significant weight change.



Figure 3.11 Weighting of seawater-immersed RC beams

Figure 3.12 exhibited the change of weight of RC beams during the entire immersed time. By approximate 60 days, the seawater-immersed RC beams presented constant weight with respect to time during which the saturated state had been achieved. 30 MPa RC beams and 60 MPa RC beams presented increased weight of 1.17% (8.8 kg) and 0.50% (3.9 kg), respectively. The difference can be explained by the smaller porosity of higher strength concrete, which restrain the ingress of seawater into concrete pores. With a greater saturation state, the 30 MPa concrete beams were estimated greater freeze-thaw damage compared to the 60 MPa concrete beams.

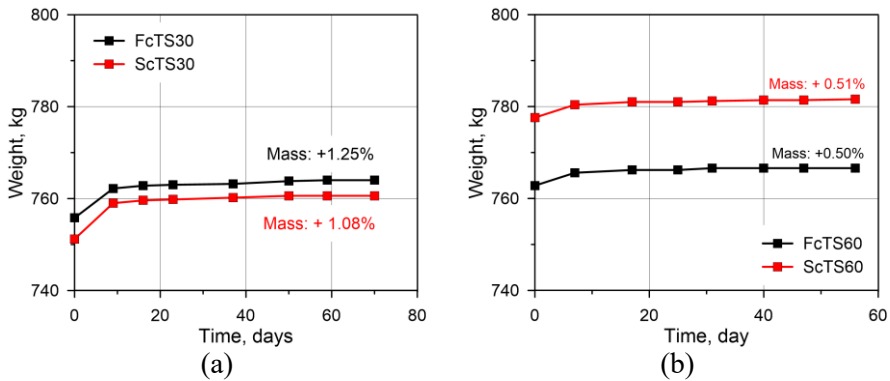


Figure 3.12 Weight change of seawater-saturated of RC beams: (a) 30MPa beams; (b) 60MPa beams

### 3.6. Freeze-thaw Cycles

In general, the number of freeze-thaw cycles varies with respect to different regions, therefore, it is difficult to quantitatively simulate the actual conditions. Freeze-thaw resistance was usually evaluated based on accelerated test in laboratory which determine the properties of concrete after freeze-thaw cycles. Freeze-thaw cycles test were carried out based on standard test method such as ASTM C666 and CEN/TS 12390-9. However, the standard test methods are limited at material level, there are no standard freeze-thaw cycles test method at structural level. In previous studies, freeze-thaw cycles test at structural level mostly conducted based on standard test method with a small-scale component. Therefore, a feasible scheme of freeze-thaw cycles test need to be build up based on standard test method and mechanism of frost damage.

The external temperature input of freeze-thaw cycles test simulates the most severe temperature range in the Arctic regions that is  $-60 \sim 40$  °C. The standard test method ASTM C666/C666M and CEN/TS 12390-9 respectively specified the target temperature of specimen as  $-18 \sim 4$  °C and  $-15 \sim 20$  °C. It indirectly provides the information of temperature range that are able to cause freeze-thaw damage. ASTM C666/C666M shows a rapid test method whereas CEN/TS 12390-9 consider the change of temperature in 24 hours.

At structural level, both ASTM C666/C666M and CEN/TS 12390-9 cannot be directly applied since the target temperature of specimen would hardly achieve due to the larger size of specimen. It was noted that for the most

of specimens the major part of ice formation occurs in the range down to  $-20$  °C (Sereda and Litvan, 1980).

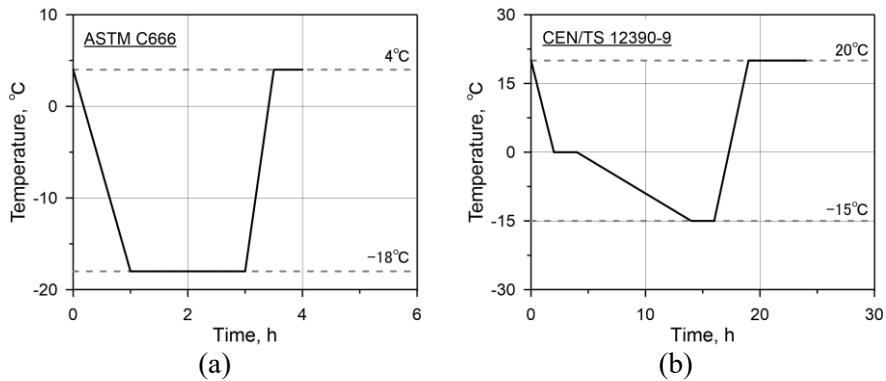


Figure 3.13 Temperature in freeze-thaw cycles: (a) ASTM C666/C666M; (b) CEN/TS 12390-9

In the light of the standard test method and previous study, for an efficient freeze-thaw cycles test, the target temperature of specimen has been determined as  $-20$  °C. The thawing temperature of specimen has been defined as  $20$  °C that was referred from CEN/TS 12390-9. Preliminary freeze-thaw cycles tests were conducted with the basis of finite element analysis. Then, three freeze-thaw cycles for each temperature type were implemented to ensure the constant temperature change. It should be mentioned that the temperature history of freeze-thaw cycles does not directly simulate the actual condition of cold regions since the number of freeze-thaw cycles vary with respect to different regions. Freeze-thaw cycles in this study reflected the qualitative indication of durability of RC element which is similar to the ASTM C666/C666M and CEN/TS 12090-9 at material level. Additionally, the temperature history considered the frequency of fatigue cyclic loading that were designed to



simultaneously exert on RC beams. The early fatigue failure possibly occurs if the temperature history of freeze-thaw cycles were too long, and the freeze-thaw damage would be hard to be reflected.

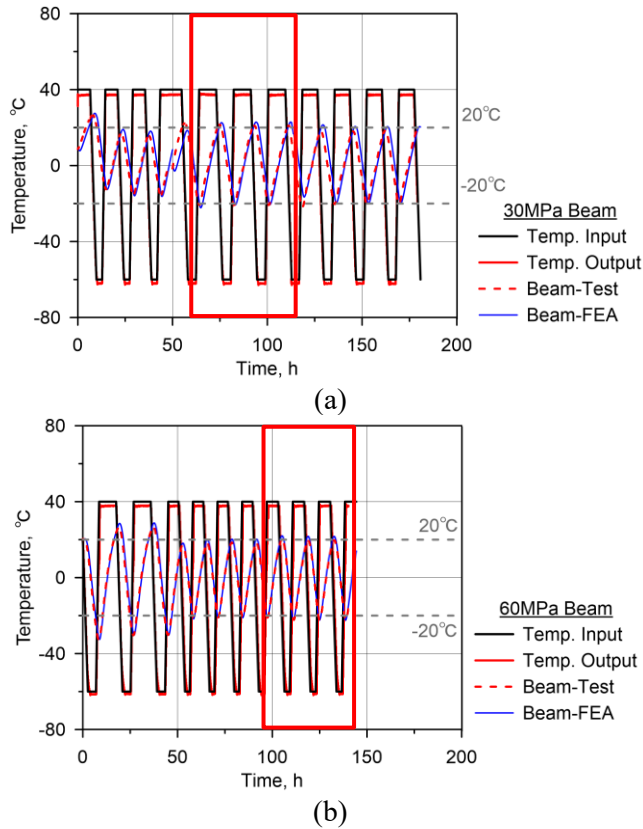


Figure 3.14 Preliminary test results of freeze-thaw cycles based on FEA: (a) 30 MPa RC beam; (b) 60 MPa RC beam

The preliminary test results indicated that the target temperature in RC beam repeated in the range of  $-20 \sim 20$  °C as shown in Figure 3.14. The identical temperature was input in other RC beams which had the same

specified concrete strength. Besides, concrete cylinders were included in the freeze-thaw environment with RC beams.

### 3.7. Loading Protocol

Static flexural tests were conducted under displacement control with a loading rate of 2 mm/min. The ultimate strength of RC beams was evaluated at room and after freeze-thaw cycles.

The service load state was simulated in fatigue tests. Magnitude of service load was referred from previous study (Birrcher, 2009), which derived magnitude of service load based on the load factor in design codes (AASHTO, 2020). Load case considered dead load ( $\approx 25\%$  of service load) and live load ( $\approx 75\%$  of service load) by a certain portion. Besides, the ratio of nominal flexural strength and experimental value were included to derive service load. Finally, the magnitude of service load was expressed as a function of experimental capacity as given in Figure 3.15.

$\phi$ Nominal Capacity $\approx \eta$ Service Load	
$\frac{\phi}{\eta}$	$\approx \frac{\text{Service Load}}{\text{Nominal Capacity}}$
<b>Assumptions:</b>	
1). Load Case: 1.25DL + 1.75LL	} $\eta = 1.4$
2). DL = 75% of Service Load LL = 25% of Service Load	
3). Nominal = 2/3 Experimental	
$2/3 \frac{0.70}{1.4} = 0.33$	$\approx \frac{\text{Service Loads}}{\text{Experimental Capacity}}$
$\phi$ = strength reduction factor, 0.70 $\eta$ = load factor DL = dead load LL = live load	

Figure 3.15 Estimate of service load as a function of experimental capacity

With the same procedure mentioned above, the magnitude of service load of RC beam was derived. The difference in this study is the strength reduction factor ( $\phi$ ), which is 0.9 for flexural component in design code (ACI 318-19). In accordance with the design code (ACI 318-19), the following assumptions are made in which the  $\eta$  equals 1.3.

1. Strength in KDS 14 20 00: 1.2DL+1.6LL.
2. DL: 25% of service load; LL: 75% of live load.

The experimental capacity was obtained from the static flexural test at room temperature. Lastly, the magnitude of service load of RC beam was calculated as  $0.56 P_u$ , which defined as the upper load of fatigue load. Generally, the service load is utilized to evaluate the serviceability performance of RC member, the ratio of nominal flexural strength and experimental result is appropriate. RC beams for fatigue tests were all applied service load as upper load of fatigue load.

$$\frac{160 \cdot 0.9}{197 \cdot 1.3} = 0.56 \approx \frac{\text{Service Loads}}{\text{Experimental Capacity}}$$

The lower load of fatigue load was determined considering fatigue limit and testing conditions. In general, fatigue limit is determined based on 2 million cycles of fatigue load. Previous studies proposed equations for estimating the fatigue limit of reinforcing bars. When the fatigue cycles equal 2 million cycles, fatigue limit can be calculated as following. It can be deduced that the minimum stress range shall be greater than 152 MPa in order to achieve the fatigue failure which was estimated a rupture of tensile rebar.

$$N = 2 \times 10^6 \text{ cycles}$$

$$\Delta\sigma = (7.825 - \log N)100 = 121 \text{ MPa (Byun et al. 1997)} \quad (3.1)$$

$$\Delta\sigma = (6.696 - \log N)/0.0055 = 152 \text{ MPa (Helgason et al. 1976)} \quad (3.2)$$

It can be deduced that the minimum stress range of reinforcing bars shall be greater than 152 MPa in order to achieve the fatigue failure which was estimated as rupture of tensile rebar. Considering a smooth loading cycles by UTM, of zero load need to be avoided. Magnitude of 10% of yield strength of tensile rebar, that the corresponding load was approximate  $0.14 P_u$ , was selected as lower load of fatigue load in which the major range of the service load can be covered.

RC beams were applied a sinusoidal loading pattern with a maximum frequency of 2 Hz. This was selected since previous studies reported that beams under fatigue load at frequencies greater than 2 Hz were unable to fully recover from the previous state (Barnes and Mays, 1999). Therefore, frequency of 2 Hz was applied for the fatigue tests at room temperature and 1 Hz for the fatigue tests combined with freeze-thaw cycles. Frequency of 1Hz at freeze-thaw cycles environment considered the early failure by fatigue loading during which the freeze-thaw damage would be reduced. The natural frequency of RC beam was calculated considering the resonance during fatigue tests, as shown in Equation 3.3~3.4. It showed a greater value compared to loading frequency, implying that resonance would not occur under cyclic loading.

$$k = \frac{48EI}{a(3L^2 - 4a^2)} \quad (3.3)$$

$$\omega_n = \sqrt{\frac{k}{m}} = \sqrt{\frac{48EI}{ma(3L^2 - 4a^2)}} = 5.67 \quad (3.4)$$

Figure 3.16 exhibited the loading protocol of the fatigue test where the stress range in load-deflection curve and constant sinusoidal mode were presented. This loading protocol was derived based on the experimental result and nominal flexural strength of 30 MPa RC beam. The identical loading protocol was applied on 60 MPa RC beam for the purpose of investigating the effect of concrete strength on structural behavior of RC beam.

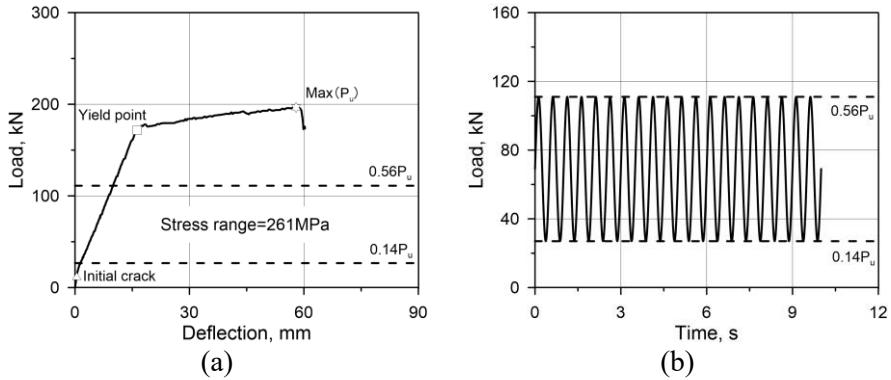


Figure 3.16 Load protocol of fatigue test: (a) Stress range in load-deflection curve; (b) Constant sinusoidal mode

### 3.8. Test Setup

The RC beams, including concrete cylinders, were transported from the factory to the Extreme Performance Test Center constructed in Seoul National University. To better observe the crack propagation during loading, grid work on the surface of RC beams was carried out. RC beams were weighted at its initial state. Then, part of the RC beams was immersed in artificially mixed seawater, and rest of them were cured in atmospheric condition. Grid work was performed on the both sides of the RC beams in order to capture the more accurate crack behavior.

The static flexural test was firstly conducted in the Extreme Temperature Chamber. Extreme Temperature Chamber was assembled with 50 Ton UTM and temperature control system (-60 ~ 60 °C) in which simultaneous action of temperature input and loading were available. Therefore, the combined effect of freeze-thaw cycles, seawater, and applied load can be achieved.



Figure 3.17 Grid work on the surface of RC beams

The static flexural test and fatigue test were conducted using four-point bending setup with a loading span of 3,400 mm and a constant moment zone of 1,000 mm as shown in Figure 3.18. Besides, two steel plates were placed at loading point for the purpose of preventing local failure of concrete on the compression zone.

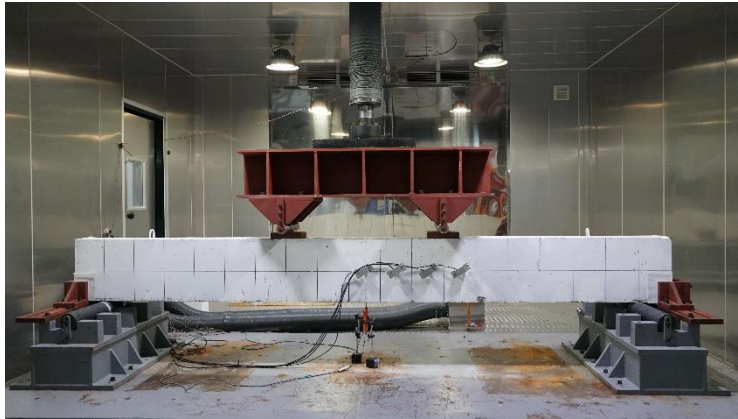


Figure 3.18 Test setup of RC beams at room temperature

Roller and hinge conditions were applied as boundary conditions of tested RC beams. Lateral-constrained jigs were mounted on the support for the purpose of preventing lateral displacement of beams during fatigue test. In addition, Teflon sheets were attached on the surface of RC beams and lateral-constrained jigs. This was to minimize the friction between RC beams and jigs during the fatigue test, which generate repeated movement RC beams in longitudinal direction. Room temperature tests were conducted under the constant temperature condition of 20 °C in order to eliminate the effect of temperature change on the structural behavior.

Fatigue tests combined freeze-thaw cycles were planned with the same setup with that of at room temperature. RC beams that were designed to evaluate the effect of freeze-thaw cycles were placed next to the fatigue tested beams in Extreme Temperature Chamber. Figure 3.19 exhibited the schematic setup of freeze-thaw cycles test. RC beam subjected to combined action of freeze-thaw cycles and fatigue loading was placed right below the UTM whereas the beam only subjected to freeze-thaw cycles was placed in front of fatigue beam. In this way, static flexural tests were conducted after freeze-thaw cycles.

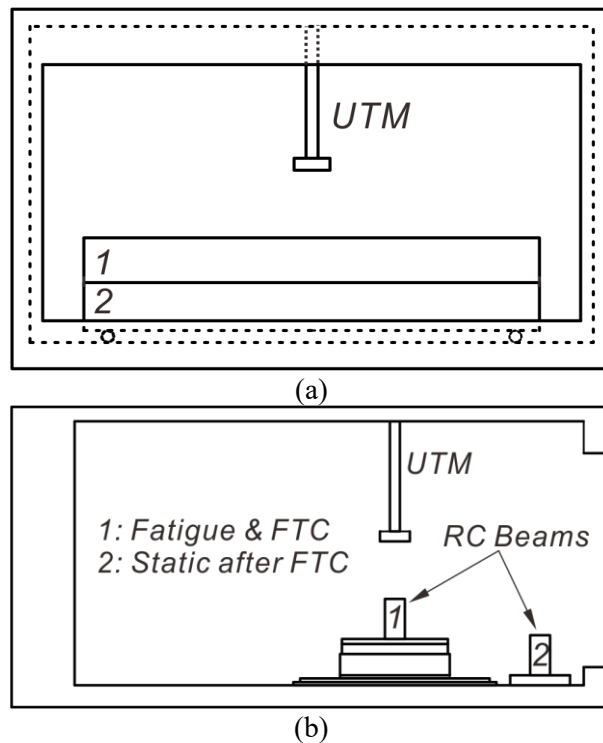


Figure 3.19 Schematic test setup for freeze-thaw cycles test of RC beams: (a) Front view; (b) Side view



Fatigue tests were conducted until the rupture of tensile rebar while the beams were loaded to flexural failure in static flexural tests. It should be noted that the saturation of RC beams was considered during the freeze-thaw cycles. Figure 3.20 showed the actual test setup of RC beams. Beams with saturated condition were wrapped with plastic films in order to prevent the water loss during the thawing phase in freeze-thaw cycles.



Figure 3.20 Actual test setup of RC beams in freeze-thaw cycles

### 3.9. Instrumentation

Strain gauge, thermocouple, and displacement transducer were used to measure the testing data. In total eight strain gauges were used to measure the strain of reinforcing bars. Eight strain gauges were evenly distributed to compressive and tensile rebar in the constant moment zone. Thermocouples were mounted inside of RC beams to monitor the temperature change under freeze-thaw cycles. In addition, two types of displacement transducer were applied to measure the deflection of RC beams and crack width. Load in UTM

and displacement of the stroke were measured through the internal load cell and displacement transducer. The displacement was compared between LVDTs and from that of stroke.

### **3.9.1. ERSGs and Thermocouple**

Specification of 5 mm Electric Resistance Strain Gauges (ERSGs) were respectively attached on the compressive and tensile rebars. Figure 3.21 showed the detailed designation of strain gauges. Since tested specimens were tension-controlled RC beams, therefore, strain gauges in the constant moment zone were attached for both compressive and tensile rebar as shown in Figure 3.22. Considering the effect of temperature on the measurement, strain gauges that are available at low temperature were used in the freeze-thaw cycles in which the fatigue load were companioned. In general, the allowable temperature of strain gauges that are used at room temperature is down to  $-10\text{ }^{\circ}\text{C}$ . Lead wire are also easily affected by temperature change which finally result in disorder of the testing data. Therefore, the effect of low temperature on the strain gauges shall be considered especially under the combined action of freeze-thaw cycles and fatigue load.

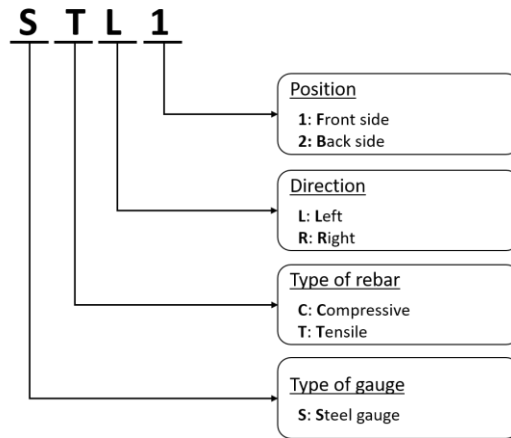
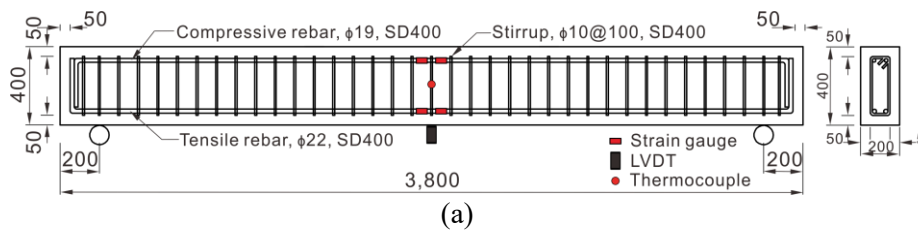


Figure 3.21 Designation of the ERSGs

Thermocouple was primarily mounted inside of RC beams prior to the placement of concrete in order to monitor the temperature flow during freezing-thawing cycles. Freeze-thaw cycles test were usually conducted in accordance with standard test method. However, the standard test methods are only available at material level, therefore, the actual temperature flow in RC beams need to be monitored. Temperature of RC beams was monitored in the center point at which the entire temperature can be ensured to reach target temperature.



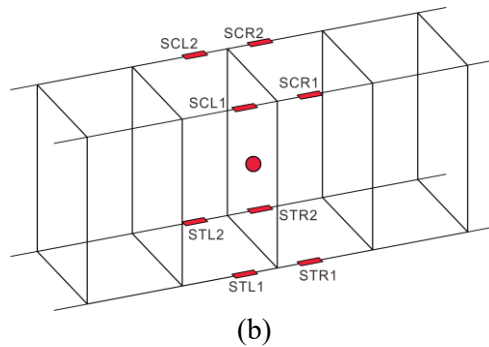


Figure 3.22 Location of ERSGs and thermocouple

### 3.9.2. LVDTs

Linear Variables Differential Transducer (LVDT) with 50 mm and 100 mm stroke were used to measure the central deflection of RC beams. Specially designed Constant Temperature Chamber was applied in the measurement of deflection under the combined action of freeze-thaw cycles and fatigue load. Similar to the strain gauge, as an electric resistance type, the LVDT also has its allowable operation temperature that is by approximate  $-10\text{ }^{\circ}\text{C}$ . In freeze-thaw cycles test, temperature vary from  $-60$  to  $40\text{ }^{\circ}\text{C}$  during which LVDT possibly not be able work. Therefore, Constant Temperature Chamber was designed to ensure the temperature maintain constant in which LVDT placed. During the freeze-thaw cycles, temperature in the chamber will maintain constant through the ventilation system constructed outside of Extreme Temperature Chamber. Considering the temperature effect on the stroke of LVDT, white bars made from quartz were connected through the hole in the chamber. In the preliminary test, Constant Temperature Chamber performed well by maintaining the designated temperature even in the temperature of  $-60\text{ }^{\circ}\text{C}$  which demonstrated the feasibility of the measurement of deflection during freeze-thaw cycles.

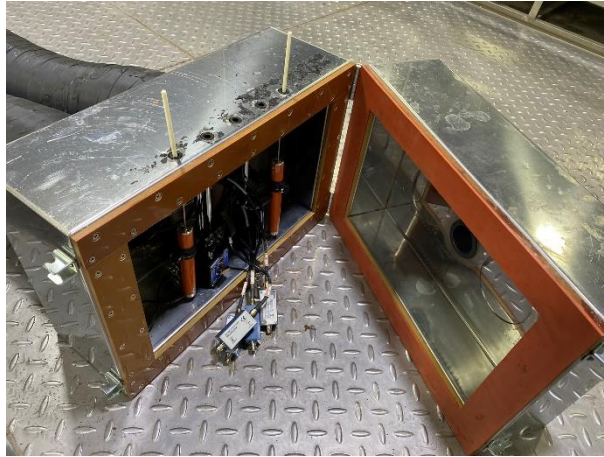


Figure 3.23 Constant Temperature Chamber for LVDTs

### 3.9.3. Clip-on Displacement Transducer

Clip-on displacement transducer, for the measurement of crack width, were mounted in static flexural tests and fatigue tests. In static flexural tests, only 60 MPa RC beam were mounted at its 90% of service load. The crack width of 30 MPa RC beams were not able to be measured due to the testing conditions. Two cycles of static loading were initially conducted prior to the fatigue tests in the range of fatigue load range. After two cycles of static loading, in total ten Clip-on Displacement Transducers were mounted at bottom of RC beams. Both flexural and shear crack width were considered on which transducers were mounted. To better attach the transducer jig, the surface of concrete was polished by electric grind, then cleaned up with alcohol pad. Lastly, jigs were mounted with CN which is a glue with powerful stickiness. Figure 3.24 showed crack gauge that were mounted at bottom of RC beams. Crack width was measured during entire fatigue tests, and crack width range in the range of fatigue load range were comparatively analyzed.



Figure 3.24 Crack gauge at bottom of RC beam

As all the measuring tools finished mounting, tests commenced under the designed rate of loading. Dynamic data logger and static data logger were applied in the tests. In static tests, data acquisition carried out with sampling rate of 1 Hz. Considering the reliability of test results, sampling rate of 200 Hz with interval of 500, 1,000 seconds was applied in fatigue tests. The interval of data sampling was adjusted from 1,000 second to 500 second at the final phase of fatigue tests. The adjustment of interval was to better capture the behavior near the failure.

### 3.10. Validity of Thermal Data

Following the instrumentation of RC beam, the validity of thermal data was verified based finite element analysis. Figure 3.25 and Figure 3.26 presented the temperature of 30 MPa and 60 MPa companion specimens under freeze-thaw cycles. The temperature of companion specimens was measured with the purpose of checking the temperature of RC beams without loading. It turned out that temperature of 30 MPa and 60 MPa companion specimens reached the target temperature of  $-20\sim 20$  °C. The validity of thermal data was then verified through analytical study. Finite element analysis was adopted to verify the testing data. Herein, target temperature and thermal stain of rebar were verified which indicate the damage of RC specimen caused by freeze-thaw cycles. Two types of companion specimen, which differ in concrete strength, was applied in the analysis.

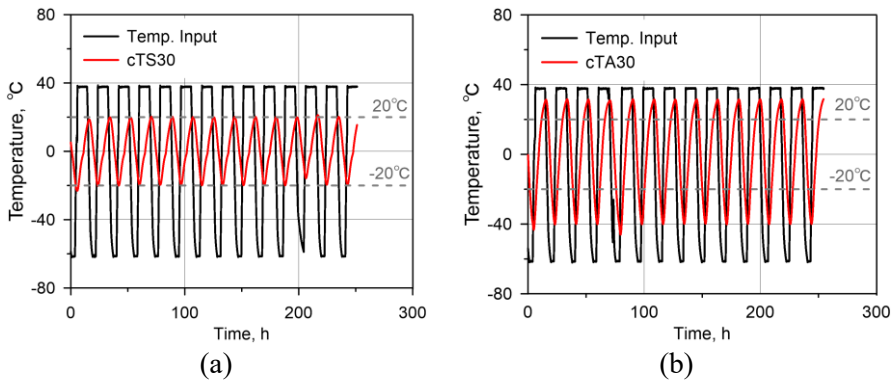


Figure 3.25 Temperature of 30 MPa companion specimen: (a) Seawater-saturated; (b) Air-cured

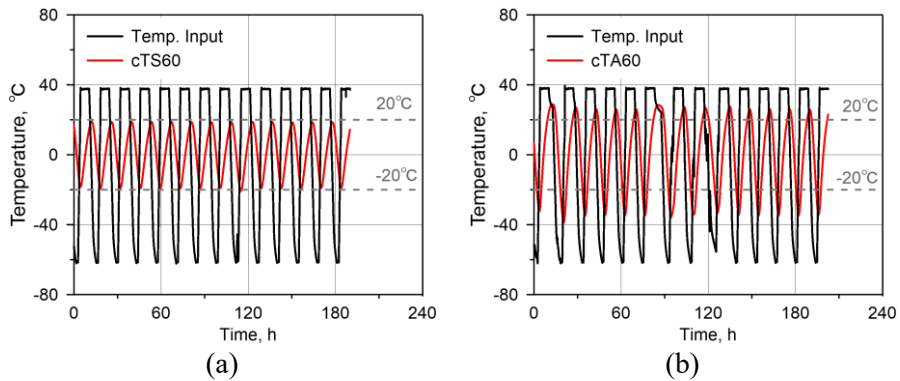


Figure 3.26 Temperature of 60 MPa companion specimen: (a) Seawater-saturated; (b) Air-cured

Geometric model was built up based on the actual dimension of companion specimen as shown in Figure 3.27. Hinge and roller were selected as boundary condition for the convergence in thermal analysis. Temperature input that is identical to the actual test was adopted as given in Figure 3.28. Only five cycles of freeze-thaw cycles were considered during which the same temperature will repeat in the rest of cycles.

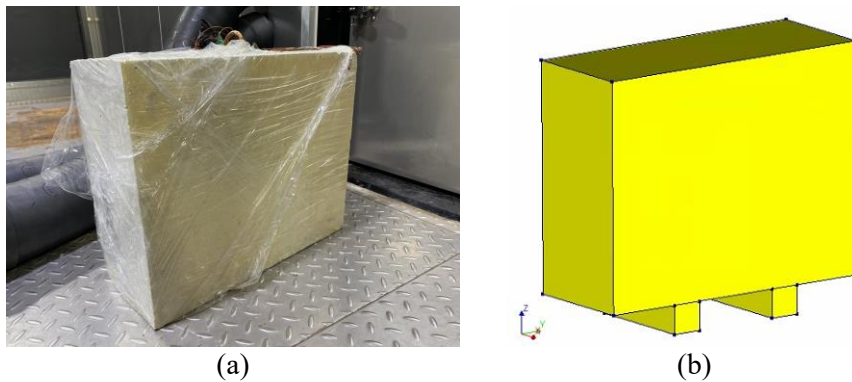


Figure 3.27 Modeling of specimen in FEA: (a) Companion specimen; (b) Geometric model



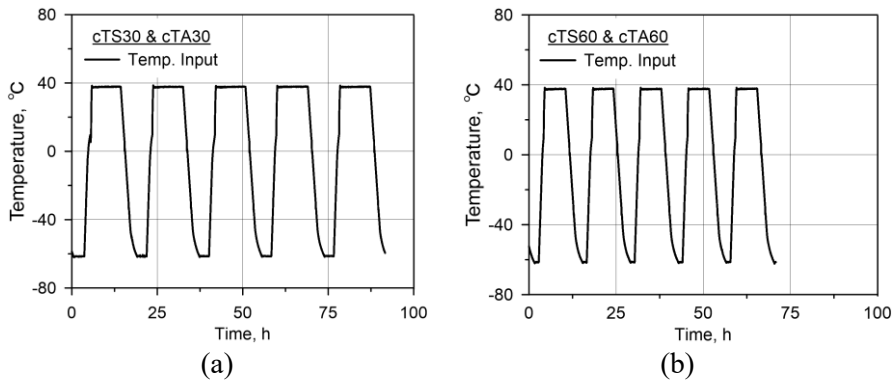


Figure 3.28 Temperature input in FEA: (a) 30 MPa companion specimen; (b) 60 MPa companion specimen

Thermal properties of concrete and reinforcement were selected in accordance with the previous studies. It has been reported that conductivity of concrete generally ranges from 0.14 to 3.85 (Asadi et al. 2018). The range of specific heat capacity lies in 0.64 to 1.05 (Shafiqh et al. 2018). The above-mentioned thermal properties were adjusted based on the test results since the properties of concrete may differ by its heterogeneity. Table 3.5 presented the final thermal properties of concrete that were applied in FEA. For the cases of specific heat capacity greater than the value reported in previous studies, it can be caused by the saturation of the seawater in which the specific heat capacity of seawater is known as  $3.993 \text{ kJ}/(\text{kg} \cdot ^\circ\text{C})$ . Because the 30 MPa concrete have larger porosity compared to the 60 MPa concrete, the similar value for specific heat capacity could be possible. The strain of pure rebar was measured during the freeze-thaw cycles tests which was to simulate the thermal expansion behavior during freeze-thaw cycles.

Table 3.5 Thermal properties of concrete in FEA

Diameter	Conductivity $W / (m \cdot ^\circ C)$	Specific heat capacity $kJ / (kg \cdot ^\circ C)$	Coefficient of thermal expansion
cTA30	0.27	1.03	Based on testing data
cTS30	0.68	3.92	
cTA60	0.38	1.25	
cTS60	0.78	3.52	

Figure 3.29 showed the strain of rebar with respect to temperature which stand for the actual strain variation of rebar during freeze-thaw cycle. In general, the thermal output is obtained when the temperature of specimen become uniform, and then the coefficient of thermal expansion (CTE) can be calculated. However, during the actual freeze-thaw cycles, the temperature of specimen would change before having a uniform temperature due to the varying temperature. Therefore, the conventional CTE of steel that is known as by approximately  $1.0 \times 10^{-5}$  would be different from that of actual value during freeze-thaw cycles. To simulate the thermal expansion behavior during freeze-thaw cycles, the “Strain Correction Factor for Temperature change (SCFT)” was introduced. SCFT was derived with the similar procedure of calculating CTE, which was the ratio of strain change and temperature change. Considering the similarity of properties of concrete and steel, the identical CTE of concrete and rebar was assumed due to the limitation of testing condition. Figure 3.30 presented the derived SCFT which may present negative value due to the difference in type of strain gauges.

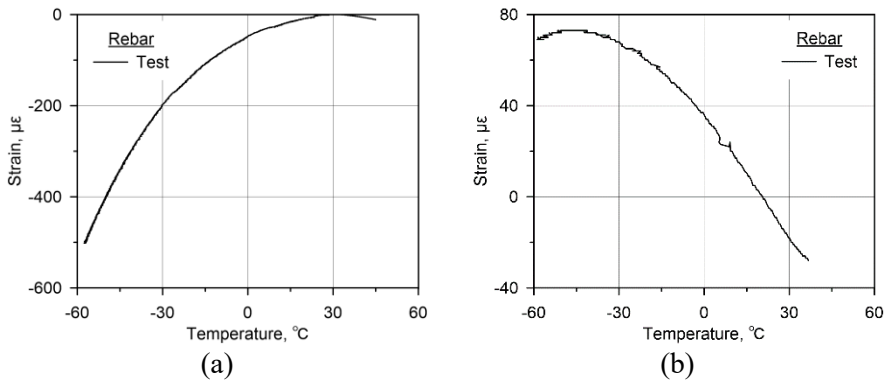


Figure 3.29 Thermal strain of rebar: (a) FLA type strain gauge (30 MPa RC beam); (b) CFLA type strain gauge (60 MPa RC beam)

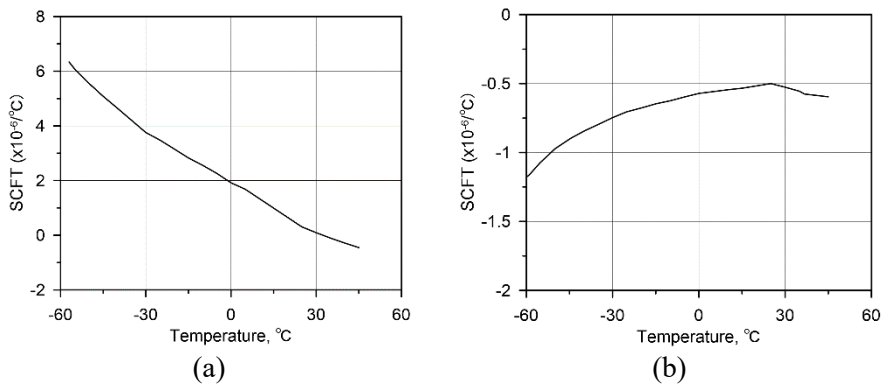


Figure 3.30 Derivation of SCFT: (a) FLA type strain gauge (30 MPa RC beam); (b) CFLA type strain gauge (60 MPa RC beam)

FEA was conducted with the mesh size of 50 mm which showed greater efficiency in mesh tests. Iterative method of Quasi-Newton was applied and convergence norm of energy, displacement and force with the tolerance of 0.01 was adopted in the analysis. Analysis results indicated that the temperature of companion specimen was well predicted by FEA by approximate 2 °C difference as shown in Figure 3.31 and Figure 3.32.

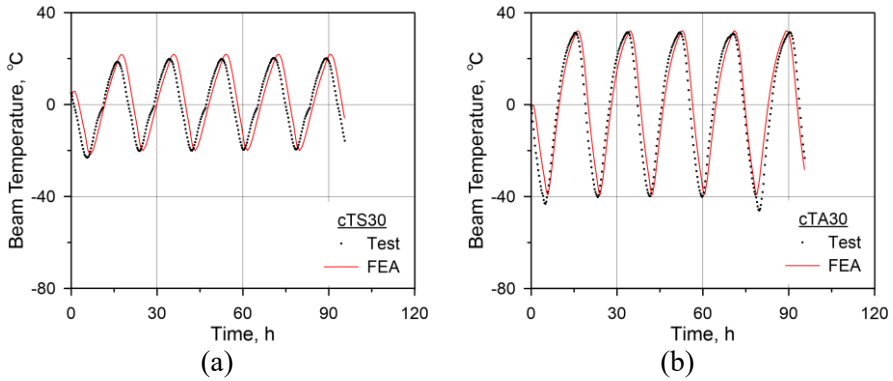


Figure 3.31 Temperature of 30 MPa companion specimen by FEA: (a) Seawater-saturated; (b) Air-cured

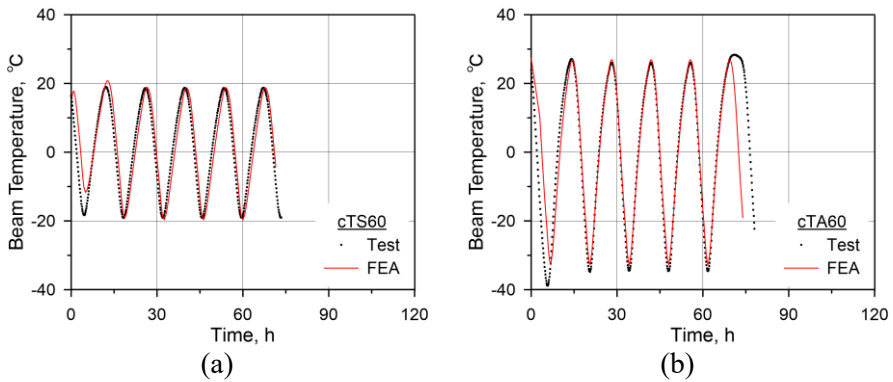


Figure 3.32 Temperature of 60 MPa companion specimen by FEA: (a) Seawater-saturated; (b) Air-cured

Thermal strain predicted by FEA was in a good agreement compared to the test results as given in Figure 3.33 and Figure 3.34. The difference of FEA and test results was possibly caused by the sensitivity of the strain tested in freeze-thaw cycles. Through the FEA analysis, the validity of thermal data tested under freeze-thaw cycles was verified and thus appropriate to be further analyzed.

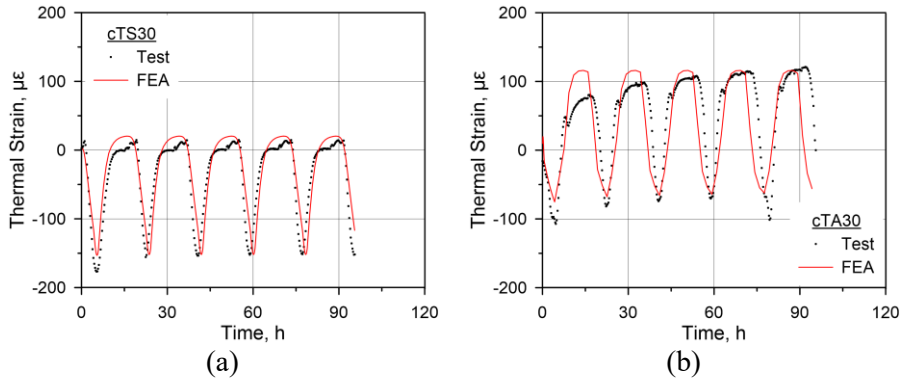


Figure 3.33 Thermal strain of 30 MPa companion specimen by FEA: (a) Seawater-saturated; (b) Air-cured

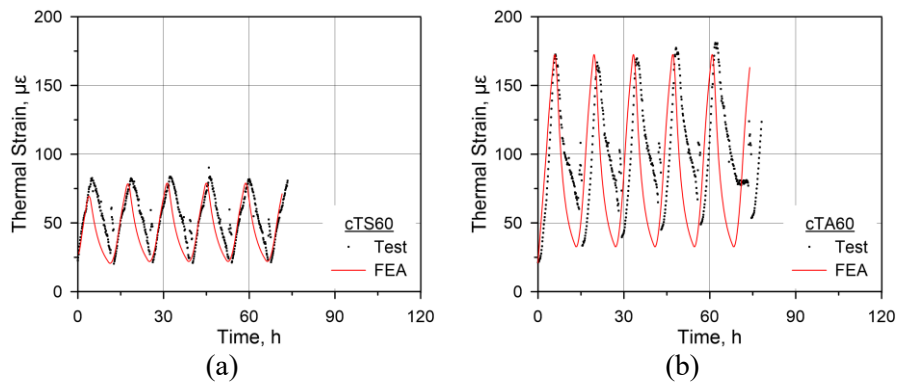


Figure 3.34 Thermal strain of 60 MPa companion specimen by FEA: (a) Seawater-saturated; (b) Air-cured

### **3.11. Concluding Remarks**

In this chapter, the experimental programs and validity of thermal data were introduced. The design of specimen based on test variables and testing condition were initially carried out. Then, the process of specimen fabrication and curing method were revealed where the seawater saturation was included. Temperature for freeze-thaw cycles and loading protocol for static and fatigue tests were derived based on previous studies and standard test methods. Finally, the test setup accompanied with instrumentations were detailly illustrated. Considering its complexity of entire test program, specially designed instruments such as temperature-related tools were applied in the tests.

The validity of thermal data from freeze-thaw cycles were further verified through finite element analysis. FEA well predict the temperature and thermal strain of rebar which verify the validity of testing data during freeze-thaw cycles.

## **IV. Experimental Results and Discussion**

### **4.1. Material Properties of Concrete**

Material properties of concrete and reinforcing bars were experimentally investigated along with the structural tests. The stress-strain curve of the concrete subjected to freeze-thaw cycle and seawater were shown in Figure 4.1. It revealed that the elastic modulus and compressive strength of 30 MPa concrete respectively decreased by approximate 12% and 5% under freeze-thaw cycles. Under the saturation state, elastic modulus and compressive strength of concrete further decreased under freeze-thaw cycles that were 41% and 26%, respectively. It can be deduced that concrete under combined effect of freeze-thaw cycles and seawater had more severe deterioration.

The peak strain of ScTA30 showed 25% greater value compared to SRTA30, which can be caused by the shrinkage during air-cured condition. However, the peak strain of ScTS30 exhibited almost the same value in comparison to SRTA30, signifying the reduced shrinkage due to the sufficient water supply during seawater immersion. This behavior was also detected in 60 MPa concrete in which the ScTA60 presented by approximately 1.9% compared to SRTA60. Except for the expansion stress by frozen pore water, the expansive stress by formation of Friedel's salt in concrete pore would also cause internal damage.

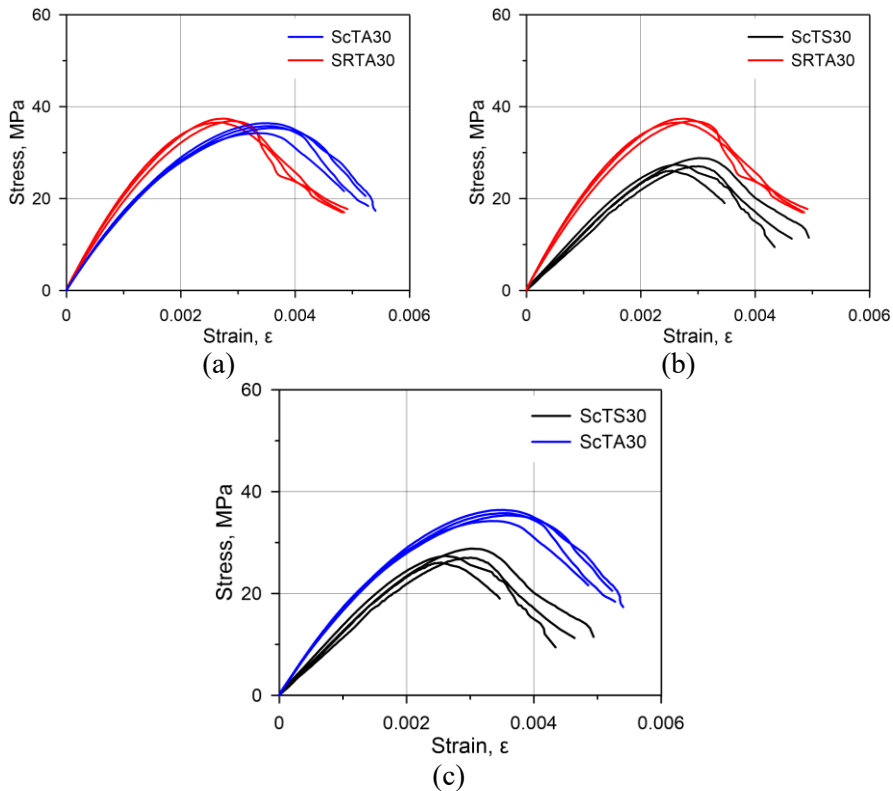


Figure 4.1 Material properties of 30 MPa concrete: (a) Effect of freeze-thaw cycles; (b) Effect of freeze-thaw cycles & seawater; (c) Effect of curing method under freeze-thaw cycles

For the case of 60 MPa strength concrete, it showed rather greater resistance towards freeze-thaw cycles and seawater as given in Figure 4.2. Elastic modulus and compressive strength of concrete did not exhibit much difference subjected to freeze-thaw cycles. A slight decrease of 6% and 5% in terms of elastic modulus and compressive strength can be found under the action of freeze-thaw cycles. In contrast to the 30 MPa concrete, 60 MPa concrete showed an increased property by seawater.



The increase under the action of seawater could be attributed to the continued hydration of concrete since the curing of concrete at immersion was 141 days. Besides, the amount of Friedel's salt formed in concrete pore could have been relatively small due to the greater porosity.

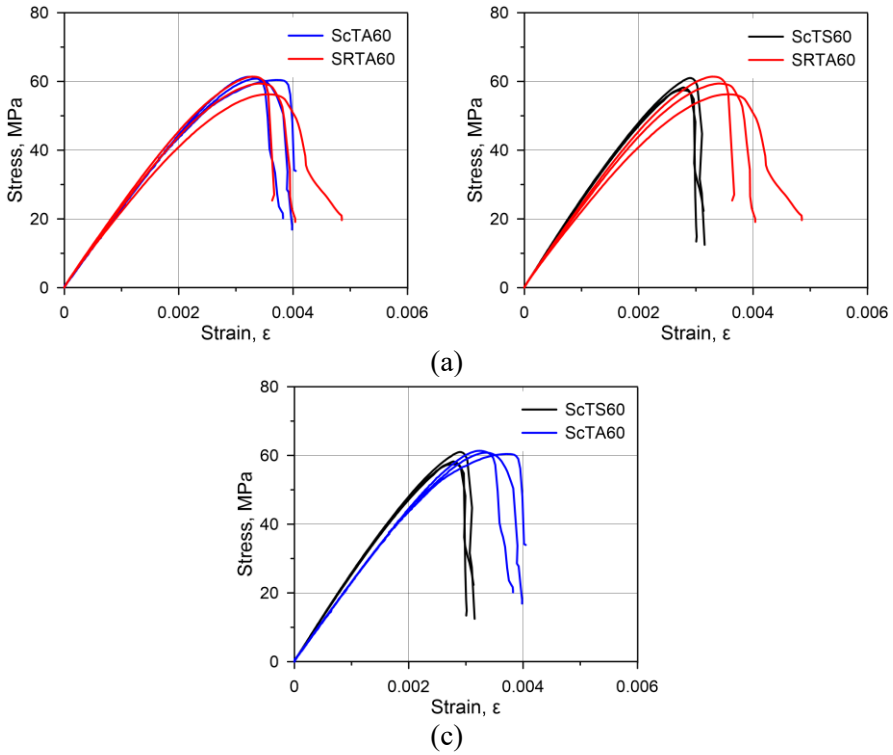


Figure 4.2 Material properties of 60 MPa concrete: (a) Effect of freeze-thaw cycles; (b) Effect of freeze-thaw cycles & seawater; (c) Effect of curing method under freeze-thaw cycles

## 4.2. Temperature of RC Beams

The temperature of RC beams under freeze-thaw cycles were measured which indicated the range of  $-24 \sim 22$  °C and  $-37 \sim 28$  °C respectively for the 30 MPa beam of seawater-saturated and air-cured. It has been reported that the major part of the ice formation during cooling took place in the range down to  $-20$  °C (Sereda and Litvan, 1980). Therefore, the freeze-thaw damage under two types of temperature range could be similar.

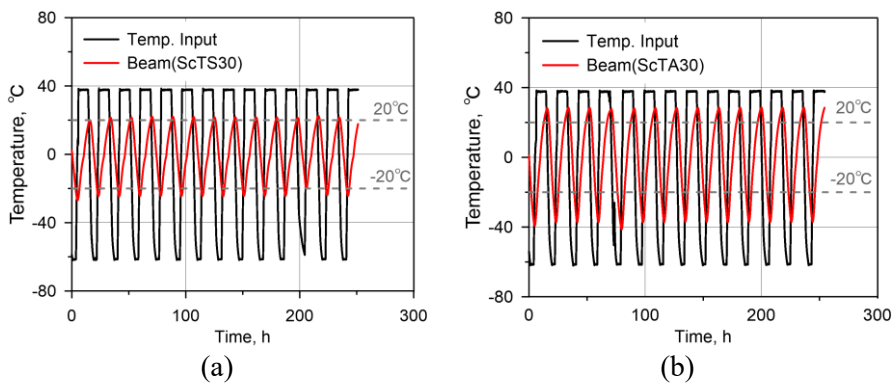


Figure 4.3 Temperature of 30 MPa RC beams: (a) Seawater-saturated; (b) Air-cured

Figure 4.4 showed the temperature of 60 MPa RC beams during freeze-thaw cycles. It also presented the similar temperature range which were  $-24 \sim 19$  °C and  $-30 \sim 24$  °C respectively for seawater-saturated and air-cured beam.

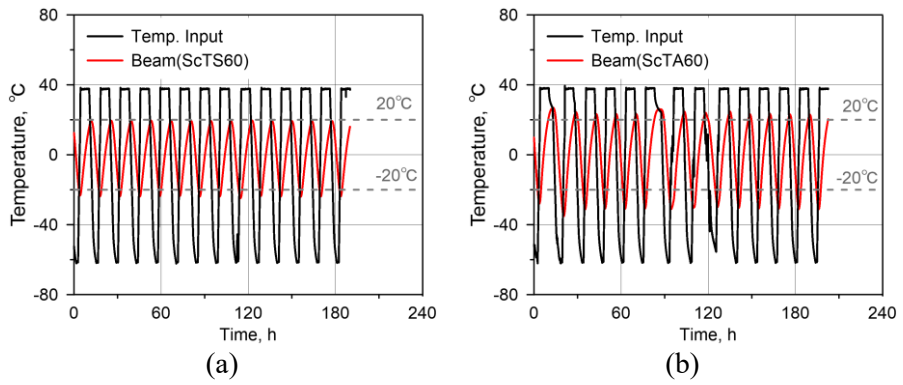


Figure 4.4 Temperature of 60 MPa RC beams: (a) Seawater-saturated; (b) Air-cured

## 4.3. Static Flexural Test of RC Beams

### 4.3.1. Effect of Concrete Strength

#### 4.3.1.1 Failure mode

RC beams were loaded to failure at room temperature after freeze-thaw cycles. It all failed with the mode of crushing of concrete at compression zone.

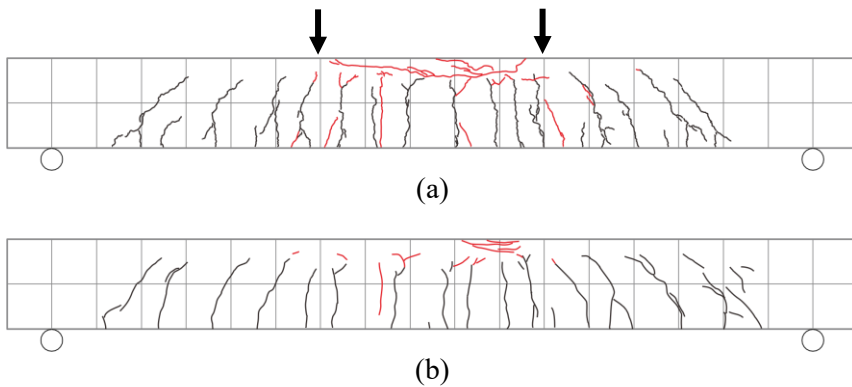


Figure 4.5 Failure of RC beams at room temperature: (a) SRTA60; (b) SRTA30

The failure of RC beam that had not been subjected to freeze-thaw cycles was shown in Figure 4.5. Beam with 60 MPa concrete strength showed relatively smaller spacing of cracks and higher crack propagation towards compression zone. The smaller spacing of cracks was possibly caused by the increased bond strength in which the more effective stress transfer would occur.

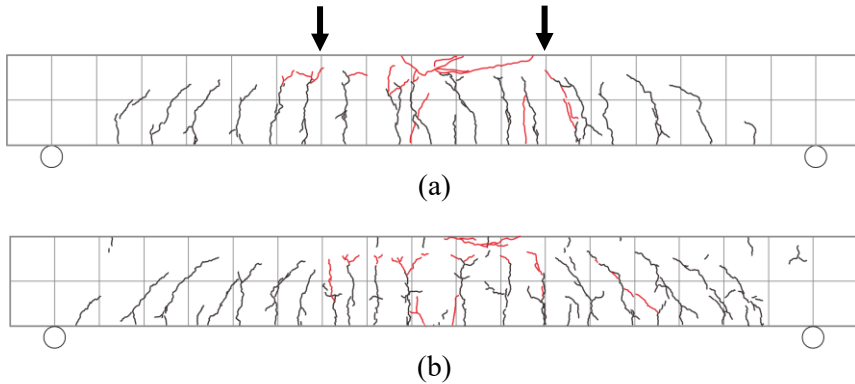
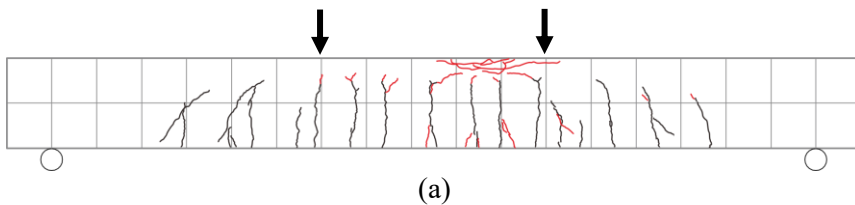


Figure 4.6 Failure of air-cured RC beams under freeze-thaw cycles: (a) ScTA60; (b)ScTA30

Considering thermal effect, there were more cracks in 30 MPa RC beam which occurred during freeze-thaw cycles as given in Figure 4.6. Thermal cracks both in tension and compression zone of RC beam were observed. As the load increased, some of thermal cracks further propagated along with structural cracks. However, such thermal cracks were not found in 60 MPa RC beam which was possibly contributed by its higher freeze-thaw resistance due to the smaller concrete porosity of higher strength concrete. Finally, 30 MPa RC beam subjected to freeze-thaw cycles presented more complex cracks distribution at failure.



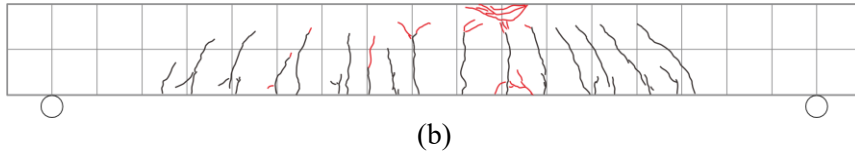


Figure 4.7 Failure mode of seawater-saturated RC beams under freeze-thaw cycles: (a) ScTS60; (b)ScTS30

At seawater-saturated state, RC beams with different concrete strength did not show much difference except the higher crack propagation in 60 MPa RC beam as shown in Figure 4.7. As the loading increased, the 60 MPa beam showed relatively brittle behavior of crack propagation by the characteristics of high strength concrete. RC beams failed by crushing of concrete with a similar position in compression zone.

#### 4.3.1.2 Central deflection

Central deflection of RC beam with two LVDT, which were symmetrically settled under RC beam, was measured as the load increased. The averaged value of deflection was adopted provided that there was eccentric loading occur. Figure 4.8~4.10 depicted the comparison of load-deflection curve with difference of concrete strength. RC beams went through three working stage under difference temperature conditions. At stage I, applied load increased linearly as deflection increased which finally meet the first crack. RC beams with 60 MPa concrete exhibited averagely 56% higher cracking load. However, the deflection at cracking load did not show much difference that was less than 0.1 mm. After first crack, RC beams behaved linearly until yield of tensile rebar. More cracks were observed at constant moment zone that had been propagated from the bottom of RC beams. RC beams with 60 MPa concrete revealed

greater flexural stiffness contributed to its greater elastic modulus concrete. Because 60 MPa concrete beam had greater flexural stiffness, the central deflection during working stage II showed smaller value.

RC beams presented gradual increase of applied load as the central deflection increased. Finally, RC beams failed with the manner of crushing of concrete and 60 MPa concrete beam showed approximate 7% greater ultimate load. Besides, the ultimate deflection of 60 MPa beam had averagely 16% greater value at room temperature. Under freeze-thaw cycles and seawater-saturated condition, the increased value respectively showed 20% and 47%. In this manner, the 60 MPa concrete beams had 43% larger ductility compared to the 30 MPa concrete beams. Herein, the ductility was calculated as deflection ductility which was the ratio of the ultimate deflection to the yield deflection of RC beams.

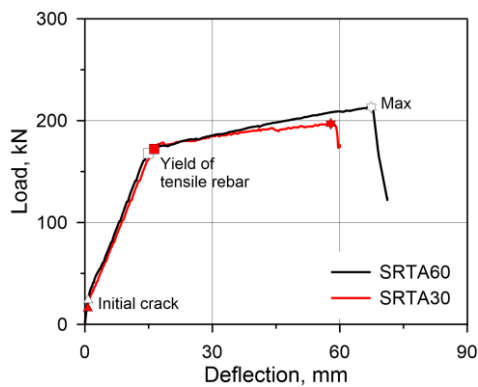


Figure 4.8 Load-deflection relation at room temperature

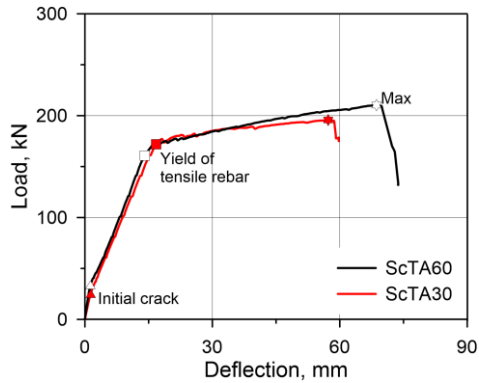


Figure 4.9 Load-deflection relation after freeze-thaw cycles with air-cured condition

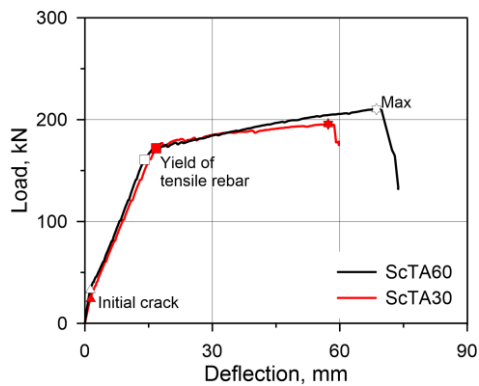


Figure 4.10 Load-deflection relation after freeze-thaw cycles with seawater-saturated condition

#### 4.3.1.3 Strain of reinforcing bars

Strain of tensile and compressive reinforcing bars were analyzed that were embedded in RC beams. Figure 4.11~4.13 presented variation of tensile strain with respect to increased loading under different temperature conditions. Tensile strain linearly increased in elastic stage, and it showed decreased gradient from which the loss of tension stiffening effect could have occurred.



The loss of tension stiffening effect can be found greater in 60 MPa concrete beams that could be caused by higher bond strength. Stress transfer through bond strength inside of RC beam would be more effective in higher strength concrete. Therefore, the more severe stress concentration would occur as the concrete strength increased.

Generally, 30 MPa RC beams should have shown greater value by its smaller elastic modulus. However, RC beams with 30 MPa concrete exhibited smaller tensile strain which had contrast behavior with that of central deflection. This behavior occurred in all specimens no matter there were freeze-thaw cycles or seawater. Considering the characteristic of normal strength and high strength concrete, it could be explained by the greater shrinkage strain of higher strength concrete. It has been reported that high strength concrete showed greater shrinkage, especially in terms of autogenous shrinkage (Mehta and Monteiro, 2014). Further analysis shall be conducted in order to verify the greater strain in 60 MPa concrete beams were caused by shrinkage.

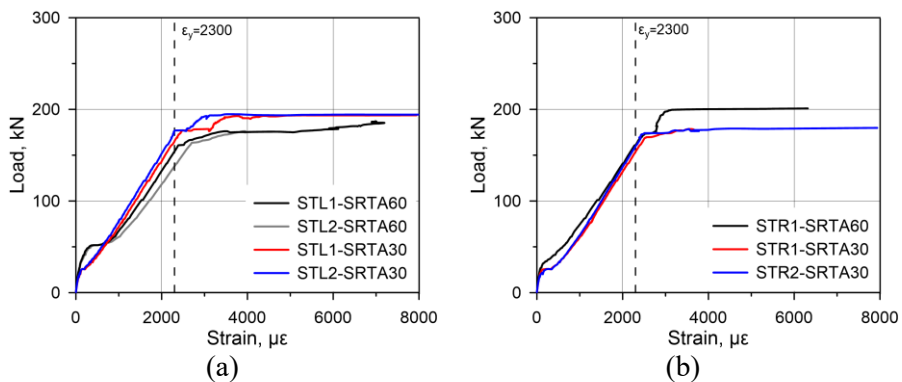


Figure 4.11 Load-tensile strain relation at room temperature

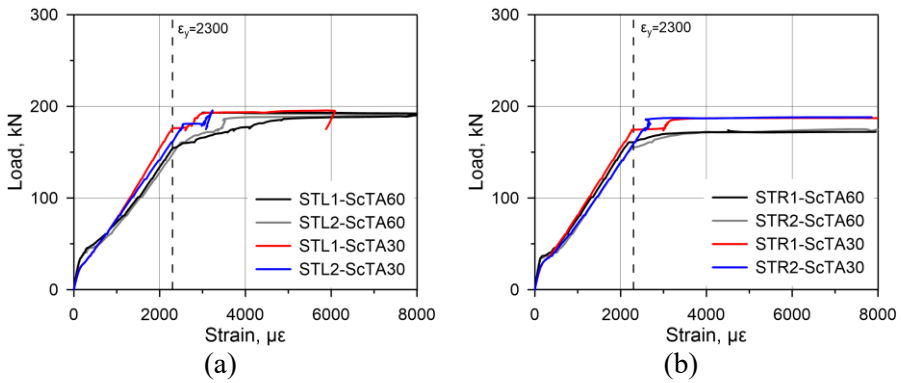


Figure 4.12 Load-tensile strain relation after freeze-thaw cycles with air-cured condition

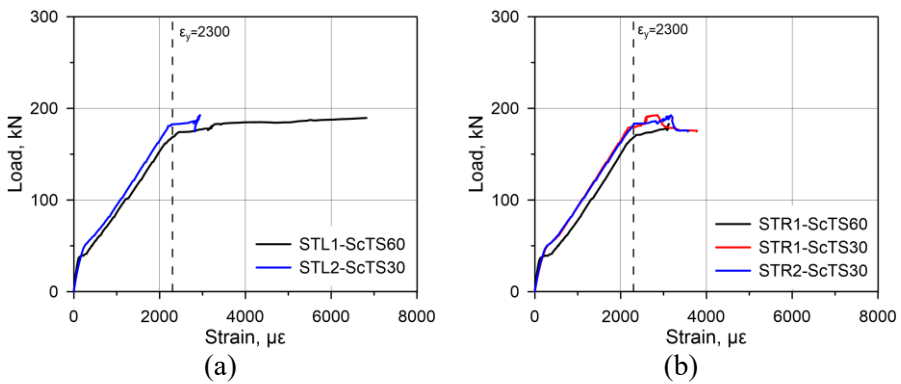


Figure 4.13 Load-tensile strain relation after freeze-thaw cycles with seawater-saturated condition

Compressive strain of reinforcing bars as well showed similar behavior corresponding to the tensile strain. Figure 4.14~4.16 exhibited compressive strain of reinforcing bars of RC beams under different temperature conditions. Some of strain gauges were damaged during fabrication of specimen from which the strain could not be measured. Based on the provided testing data, RC beams with 30 MPa concrete showed greater compressive strain as load

increased. It can be deduced that the concrete in compression zone may have been in a compressed state due to the greater shrinkage. This behavior would be more severe in higher strength concrete which indirectly distributed smaller stress on compressive reinforcing bars. The smaller compressive strain of 60 MPa RC beams was presented in all specimens no matter there were freeze-thaw cycles or seawater.

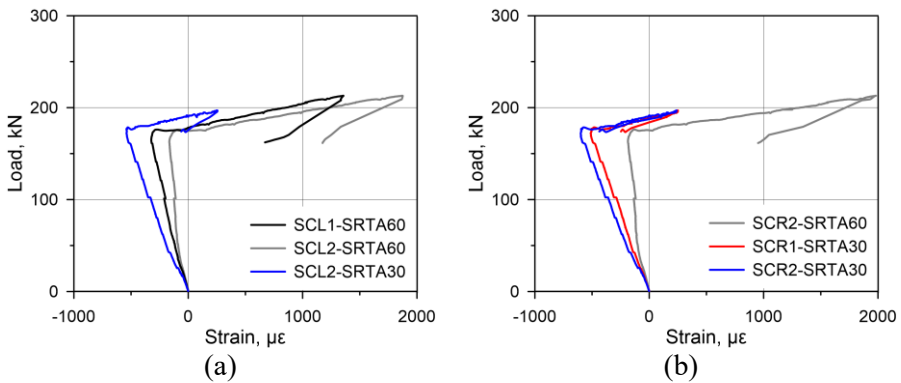


Figure 4.14 Load-compressive strain relation at room temperature

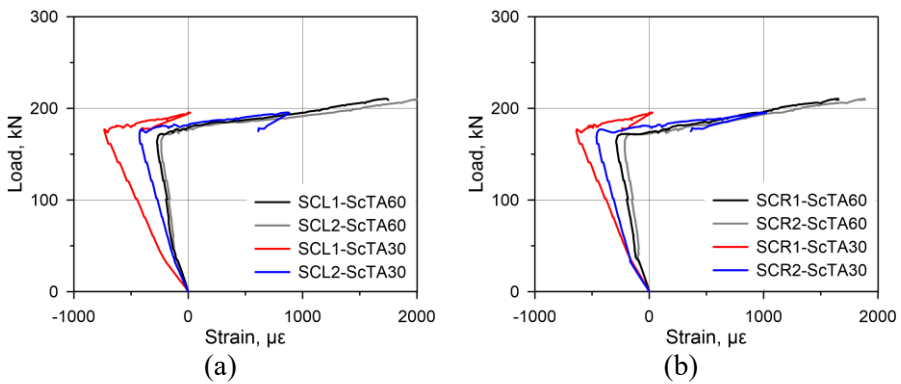


Figure 4.15 Load-compressive strain relation after freeze-thaw cycles with air-cured condition

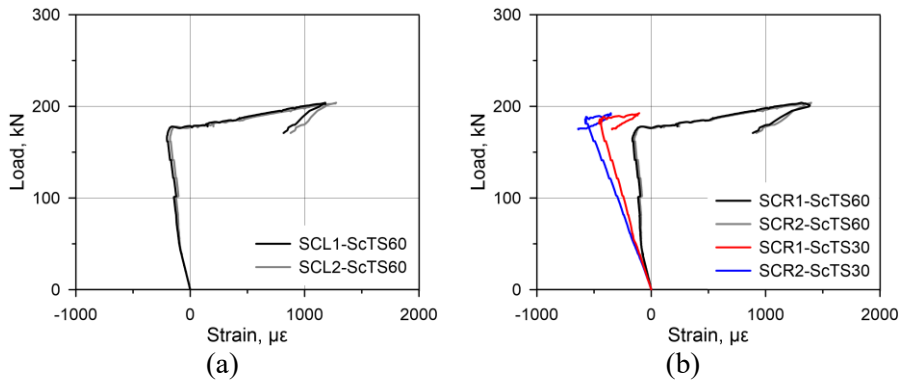


Figure 4.16 Load-compressive strain relation after freeze-thaw cycles with seawater-saturated condition

#### 4.3.1.4 Estimation of shrinkage strain

Section analysis based on material testing data was conducted to verify the shrinkage strain of RC beams. Considering the heterogeneity of concrete, stress-strain curve of concrete adopted fitting model in which Hognestad parabolic and Thorenfeldt were adopted as compressive based curve as shown in Figure 4.17.

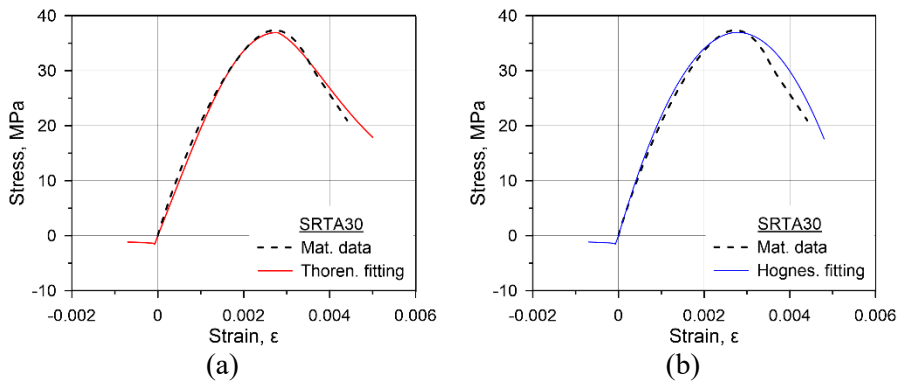


Figure 4.17 Concrete stress-strain fitting curve; (a) Thorenfeldt model-based curve; (b) Hognestad parabolic-based curve

The peak stress and peak strain from concrete compression test were applied in above mentioned existing model. Tension stiffening model from (Vecchio, 1982; Vecchio and Collins, 1986) were adopted as shown in Equation 4.1~4.2.  $f_1, f_t, \varepsilon_1$  respectively represented the pre

$$f_1 = \frac{f_t}{1 + \sqrt{200\varepsilon_1}} \quad (\text{Vecchio \& Collins 1982}) \quad (4.1)$$

$$f_1 = \frac{f_t}{1 + \sqrt{500\varepsilon_1}} \quad (\text{Kirschner \& Collins 1986}) \quad (4.2)$$

Where  $f_1$  =principal average concrete tensile stress;  $f_t$ = cracking strength;  $\varepsilon_1$ =principal tensile strain.

The material testing data of reinforcing bars were applied in the section analysis.

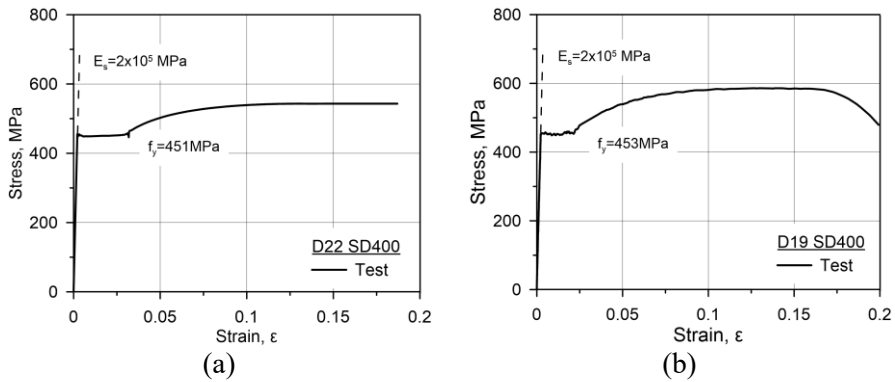


Figure 4.18 Stress-strain curve of reinforcing bars; (a)Tensile rebar; (b) Compressive rebar

The preliminary section analysis in terms of room temperature test was carried out in order that the material model would be valid in following analysis. To better evaluate the shrinkage strain, structural behavior to the range of yield load was analyzed. Analysis results showed that load-deflection relation was well predicted by section analysis and results by two tension stiffening model did not show much difference as given in Figure 4.19. Therefore, the Vecchio (1982) model was adopted to reflect tension stiffening effect based on Hognestad Parabolic compressive base curve.

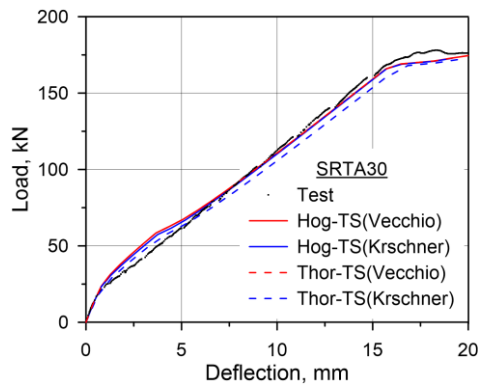


Figure 4.19 Load-deflection relation by preliminary analysis

Concrete stress-strain relation without consideration of tension stiffening effect was also applied. This was to reflect the range of shrinkage as well as for the consistent results in comparisons. Herein, only tensile strength of concrete was applied in tensile behavior in which the tension stiffening effect was not considered.

Figure 4.20~4.23 exhibited analysis results of 30 MPa concrete RC beams which reflected load-deflection and load-strain behavior. Shrinkage strain were

estimated by means of shifting the analysis results to the test results. Estimation of strain was based on yield point of RC beam at which the analysis results and test results would approximately overlap. The final shrinkage strain of RC beams was compared in terms of the range of shrinkage based whether the tension stiffening effect was considered.

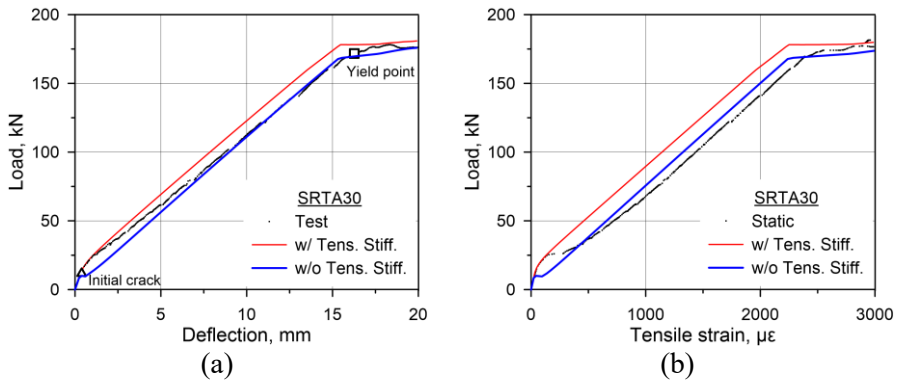


Figure 4.20 Analysis results of SRTA30; (a) Load-deflection relation; (b) Load-strain relation

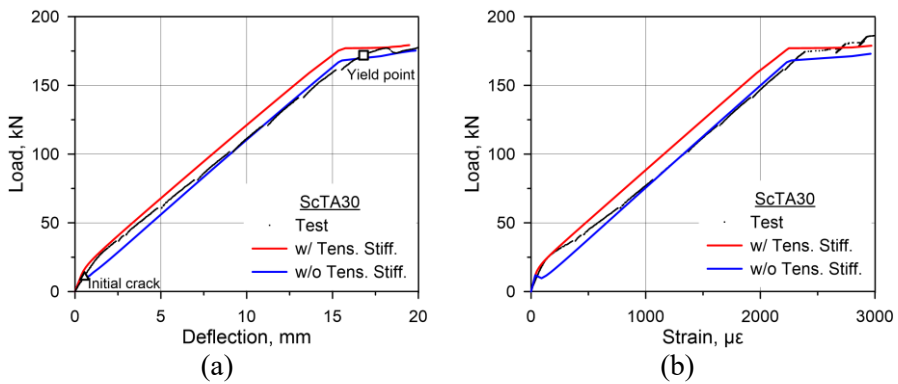


Figure 4.21 Analysis results of ScTA30; (a) Load-deflection relation; (b) Load-strain relation

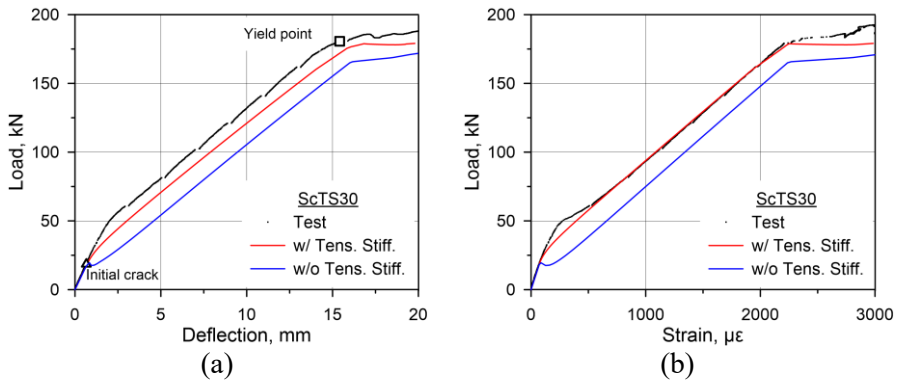


Figure 4.22 Analysis results of ScTS30; (a) Load-deflection relation; (b) Load-strain relation

With the similar procedure, sectional analysis with respect to 60 MPa concrete RC beams were conducted. Figure 4.23~4.25 presented the analysis results in terms of load-deflection and load-strain relation. It can be deduced that 60 MPa RC beams had larger range of shrinkage based on analysis results. This could be attributed to the greater shrinkage strain.

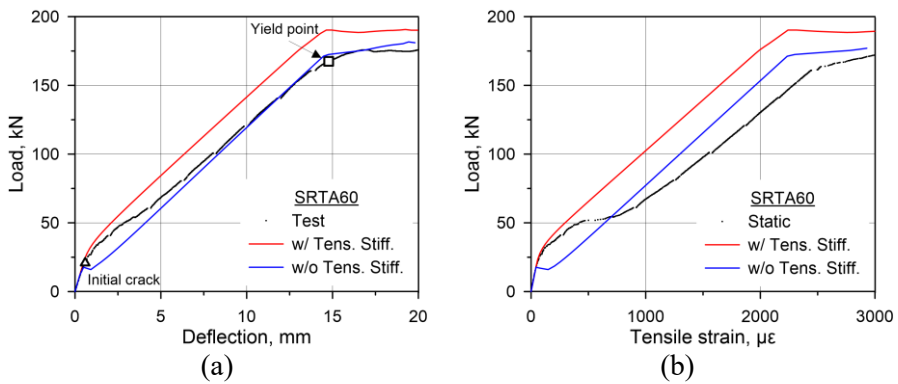


Figure 4.23 Analysis results of SRTA60; (a) Load-deflection relation; (b) Load-strain relation



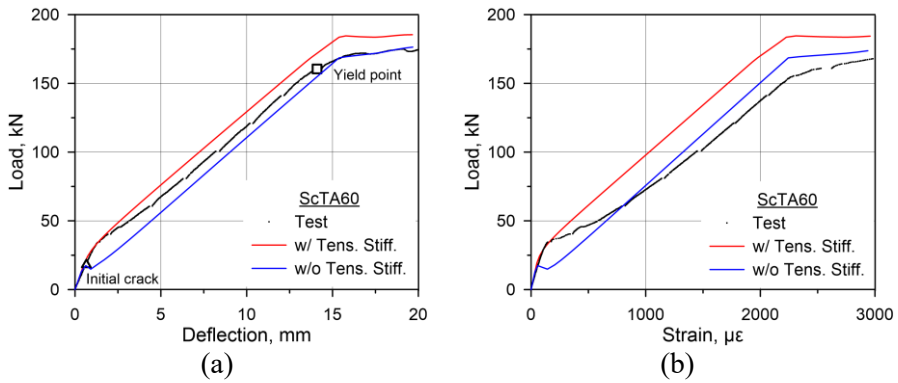


Figure 4.24 Analysis results of ScTA60; (a) Load-deflection relation; (b) Load-strain relation

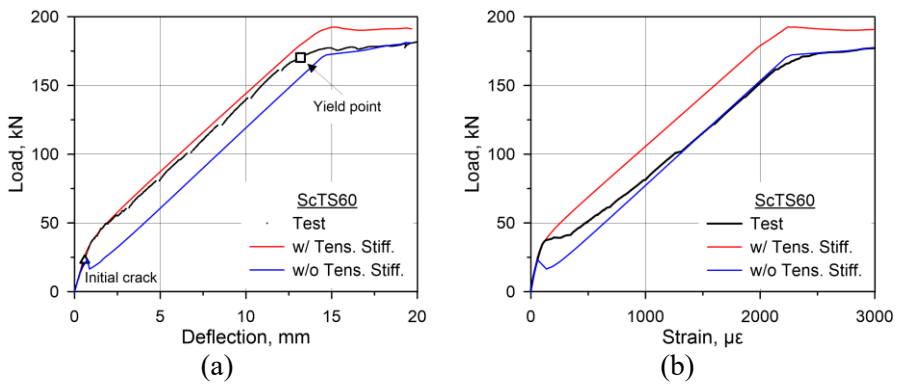


Figure 4.25 Analysis results of ScTS60; (a) Load-deflection relation; (b) Load-strain relation

To specifically evaluate the shrinkage of strain of RC beams for which different strength of concrete applied, the finally estimation of shrinkage strain were compared as given in Figure 4.26~4.31.

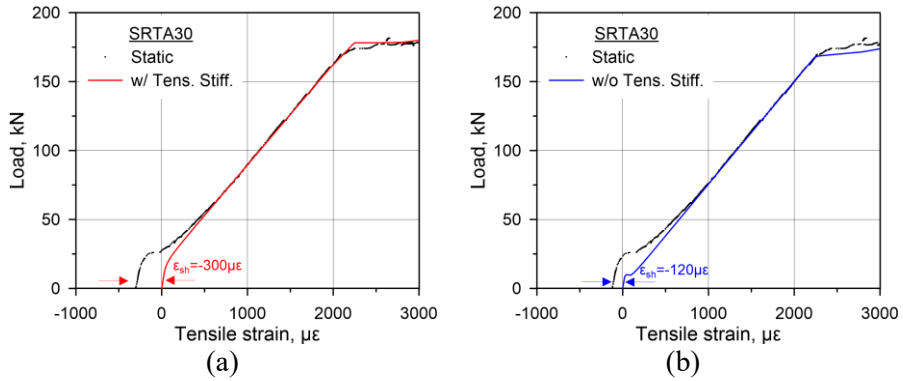


Figure 4.26 Estimated shrinkage strain of SRTA30; (a) With consideration of tension stiffening; (b) Without consideration of tension stiffening

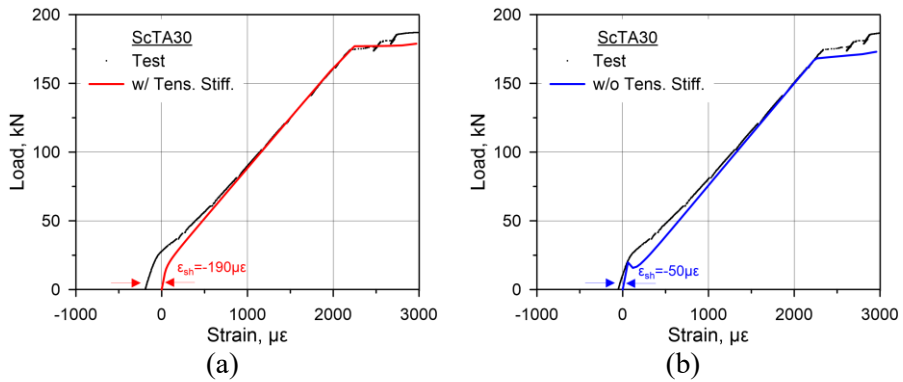


Figure 4.27 Estimated shrinkage strain of ScTA30; (a) With consideration of tension stiffening; (b) Without consideration of tension stiffening

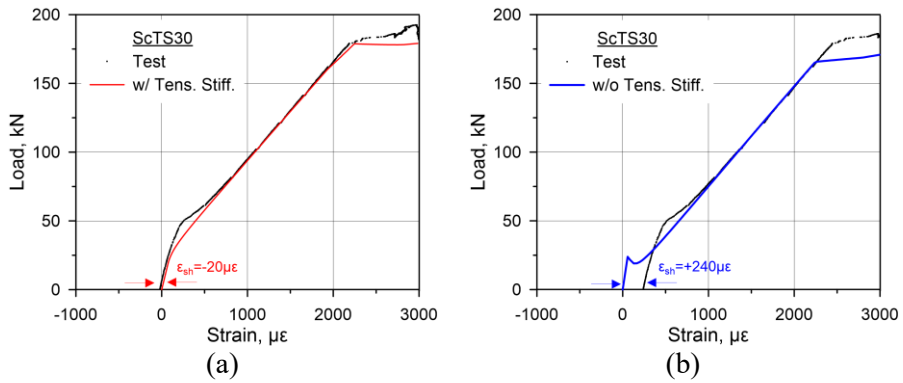


Figure 4.28 Estimated shrinkage strain of ScTS30; (a) With consideration of tension stiffening; (b) Without consideration of tension stiffening

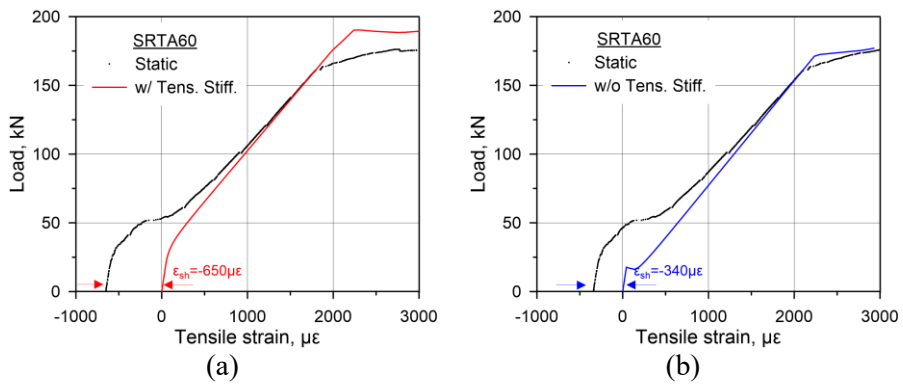


Figure 4.29 Estimated shrinkage strain of SRTA60; (a) With consideration of tension stiffening; (b) Without consideration of tension stiffening

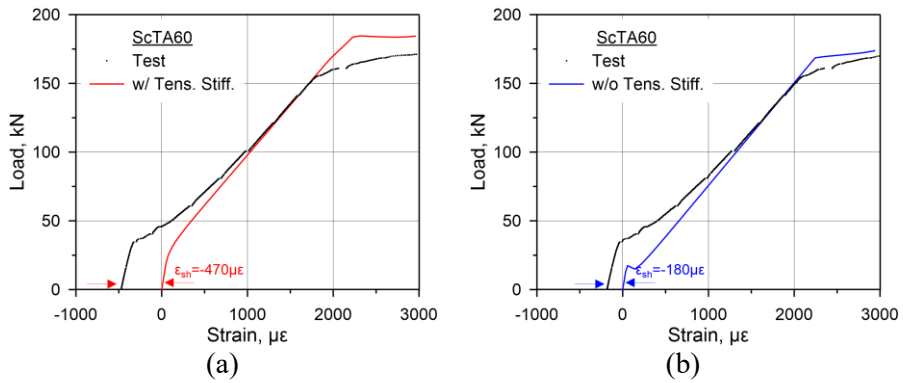


Figure 4.30 Estimated shrinkage strain of ScTA60; (a) With consideration of tension stiffening; (b) Without consideration of tension stiffening

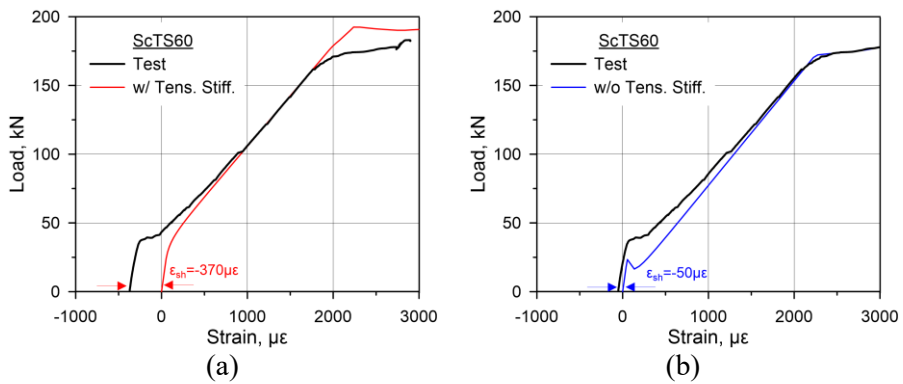


Figure 4.31 Estimated shrinkage strain of ScTS60; (a) With consideration of tension stiffening; (b) Without consideration of tension stiffening

The estimated shrinkage strain was summarized to evaluate the effect of concrete strength on RC beams. Table 4.1 exhibited the estimated shrinkage strain of RC beams. RC beams with 60 MPa concrete showed greater shrinkage strain no matter the tension stiffening effect was considered. These results were consistent with the greater shrinkage strain mentioned in previous studies. Therefore, the greater strain in 60 MPa concrete RC beams could be attributed

to the larger shrinkage of high strength concrete. In addition to the greater shrinkage strain in high strength concrete, effect of freeze-thaw cycles and seawater can be found. Compared to the specimen at room temperature, RC beams subjected to freeze-thaw cycle presented smaller strain. RC beams that had been immersed in seawater had further decreased strain which can be caused by mitigation of shrinkage during immersion. For further analysis for the effect of freeze-thaw cycles and seawater, the testing data in terms of different temperature conditions and beam curing method shall be comparatively analyzed.

Table 4.1 Estimation of shrinkage strain of RC beams

	Shrinkage strain of RC beam ( $\mu\epsilon$ )					
	SRTA30	ScTA30	ScTS30	SRTA60	ScTA60	ScTS60
w/ tension stiffening	-300	-190	-20	-650	-470	-370
w/o tension stiffening	-120	-50	0	-340	-180	-50

#### 4.3.1.5 Summary

In this Chapter, the effect of concrete strength on the flexure and fatigue behavior was illustrated. The normal strength concrete (30 MPa) and high strength concrete (60 MPa) was used to investigate both material properties and structural behavior. Six RC beams failed by the crushing of concrete at compression zone and concrete strength did not affect the failure mode. RC beams with 60 MPa concrete strength showed better performance compared to 30 MPa RC beams. 60 MPa RC beams showed by approximately 56% larger

cracking load and 7% larger ultimate load in comparison to 30 RC beams. Under the combined effect of freeze-thaw cycles and seawater, material properties of 30 MPa concrete exhibited by approximately 26% of reduction in compressive strength whereas 60 MPa concrete had negligible reduction under freeze-thaw cycles. The strain of tensile rebar was measured by electric resistance strain gauge, and 60 MPa RC beams showed greater rebar strain. This was possibly attributed by the greater autogenous shrinkage of high strength concrete which was verified based on section analysis. Additionally, 30 MPa RC beams revealed averagely 44% smaller ductility compared to 60 MPa RC beams. This can be caused by the early crushing of concrete at compression zone due to the smaller concrete strength and more deterioration by freeze-thaw cycles.

## **4.3.2. Effect of Freeze-thaw Cycles and Seawater**

### *4.3.2.1 Failure mode*

Figure 3.32 illustrated the failure of reinforced normal strength concrete beams, which exhibited crushing of the concrete in compression zone at the point of failure. Three RC beams were all tested at room temperature, in which ScTA30 and ScTS30 were loaded to failure after freeze-thaw cycles.

Compared to SRTA30, there were numerous thermal cracks can be observed in ScTA30. Thermal cracks occurred during freeze-thaw cycles, which were attributed to the repeated expansion and contraction of concrete. In addition, those thermal cracks in RC beam further propagated along with structural cracks, leading to more severe deterioration of RC beam. Thermal cracks in tension and compression zone may account for the larger strain in tensile and compressive strain of reinforcing bars.

In contrast to SRTA30 and ScTA30, no visible thermal cracks were found in ScTS30 after freeze-thaw cycles. As the loading increased, fewer structural cracks were detected in ScTS30, that can be contributed to the formation of Friedel's salt crystallization of NaCl in concrete pores. The Friedel's salt was reported to generate volume expansion in concrete pores, resulting in further deterioration of concrete (Qiao et al. 2018). But at initial stage, the formation of Friedel's salt can make concrete pores denser (Zhang and Wu, 2019), which may contribute to the reduction of cracks on the surface of RC beam.

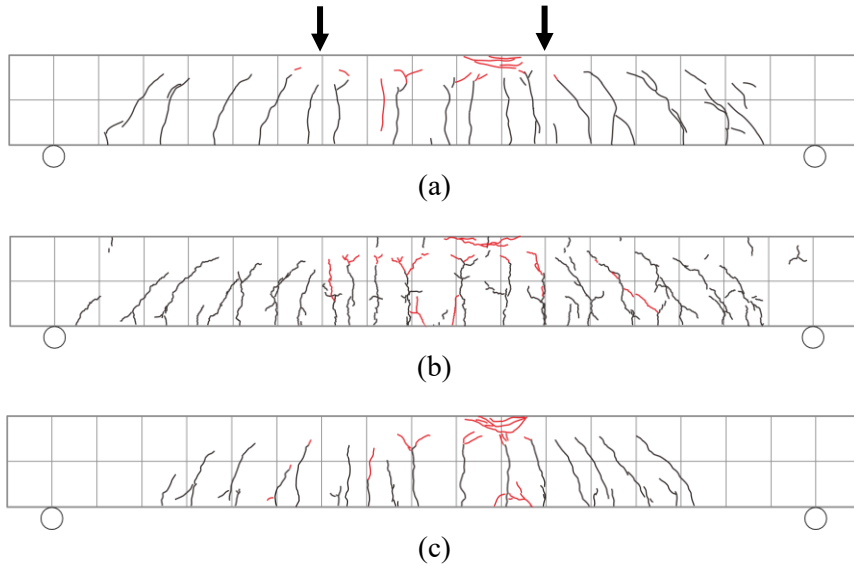


Figure 4.32 Failure of 30 MPa concrete RC beams: (a) SRTA30; (b) ScTA30; (c) ScTS30

Effect of freeze-thaw cycles and seawater on failure of reinforced high strength concrete beams were depicted in Figure 4.33. Using high strength concrete, cracks in RC beams showed less difference after freeze-thaw cycles. This was due to the greater durability of high strength concrete by its smaller porosity. The smaller porosity curtailed expansion stress caused by freezing of pore water in concrete.

RC beam that were immersed in seawater presented reduced cracks pattern. There were no thermal cracks observed after freeze-thaw cycles. It was similar to the behavior in ScTS30, indicating that seawater may reduce the cracks by formation of crystallization in concrete pores. However, compared to SRTA60, ScTS60 did not show much difference as difference between SRTA30 and



ScTS30. This can be attributed to the fewer absorption of high strength concrete during immersion of seawater, in which less effect from chloride crystallization.

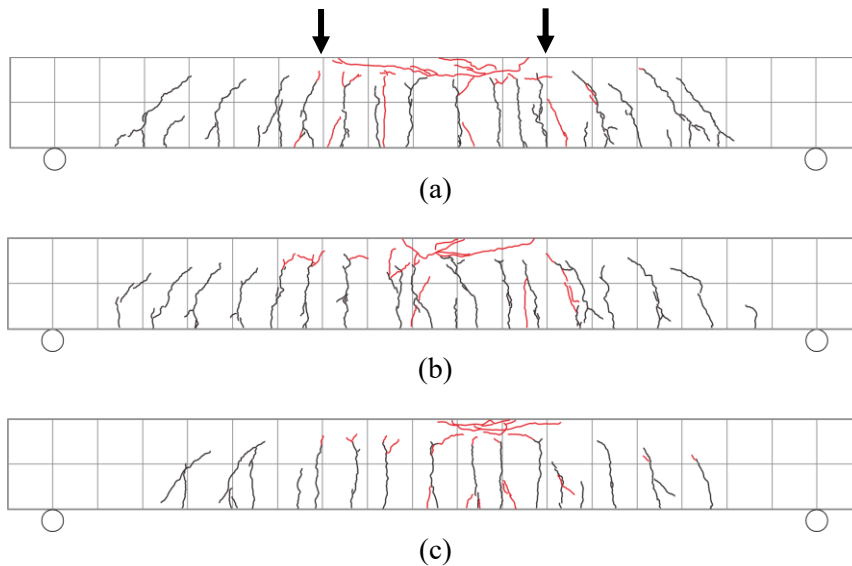


Figure 4.33 Failure of 60 MPa concrete RC beams: (a) SRTA60; (b)ScTA60; (c) ScTS60

#### 4.3.2.2 Crack width

Following the failure mode and crack propagation of RC beams, the crack width along with increased loading was analyzed. Only crack width of 60 MPa concrete RC beams were measured in the static tests due to the testing conditions. The crack width of 30 MPa concrete RC beams need to be estimated based on analytical study.

Crack gauges were mounted after loading to the service load, and unloading to the original state, then reloading to measure the crack width. Figure 4.34 depicted the position of the crack gauge, at which the crack width

was measured. Flexural and shear cracks were evenly measured, however, not all the cracks were able to be measured due to the limited number of crack gauges. Herein, the designation of crack gauge consisted of type of cracks and position crack. “F” and “S” in the designation of crack gauges respectively represented the flexural cracks and shear cracks. Notation “Cr” represented cracks, while “L” and “R” indicated left and right sides with the benchmark on the centerline of RC beams. Basically, four flexural crack width and three shear cracks in each side were measured in order that both flexural and shear behavior can be captured.

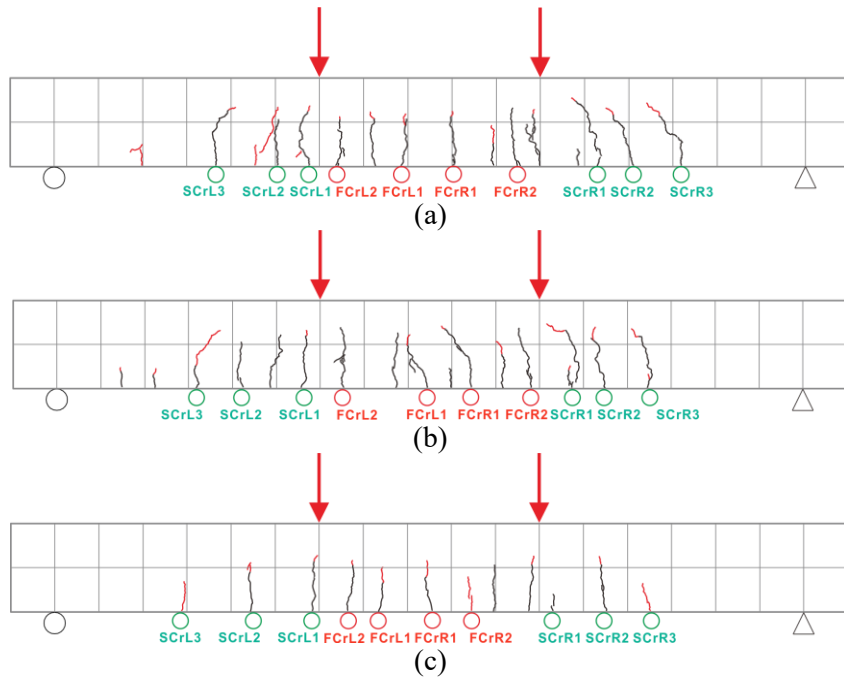


Figure 4.34 Position of crack gauges in 60 MPa RC beams: (a) SRTA60;  
(b)ScTA60; (c) ScTS60

The results of flexural crack width and shear crack width were compared among three RC beams as shown in Figure 4.35~4.36. Only the maximum crack width was comparatively analyzed, for better evaluation of effect of freeze-thaw cycles and seawater. Crack width of ScTA60 that was subjected to freeze-thaw cycles, did not show much difference, compared to the beam SRTA60. This can be attributed to the greater durability of high strength concrete under freeze-thaw cycles, or crack width rarely affected by freeze-thaw cycle at structural level.

Among the comparisons, ScTS60 that was saturated by seawater exhibited the largest crack width, indicating the increasing effect of seawater. Generally, the crystallization Friedel's salt was reported to produce expansion stress in capillary pores, resulting in cracks in cement paste (Qiao et al. 2018). Moreover, the NaCl crystallization in concrete pores could generate tensile hoop stress, which may increase the crack width (Wu et al. 2020). Additionally, reduced number of cracks may lead to increase of crack width at the same load, suggesting the more severe condition under aggressive environment.

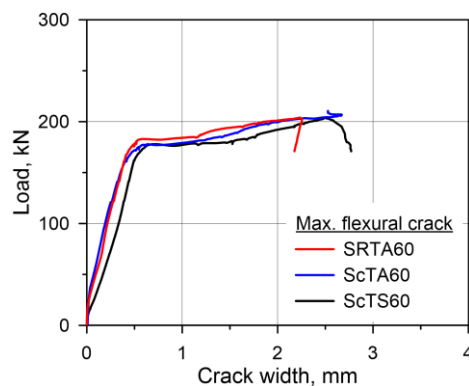


Figure 4.35 Comparison of flexural crack width of 60 MPa RC beams

Shear cracks were found to be merely affected by freeze-thaw cycles and seawater in comparison to flexural crack width. This was due to the fact that RC beams test basically aimed to evaluate the flexural behavior, therefore, the shear behavior was inhibited by sufficient shear reinforcement.

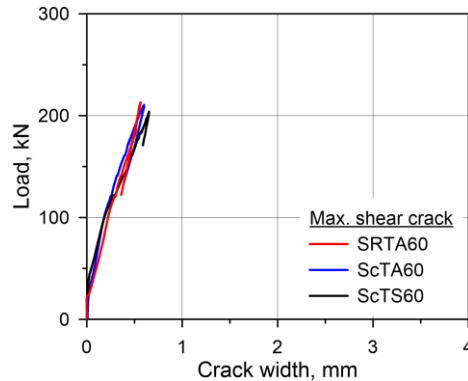


Figure 4.36 Comparison of shear crack width of 60 MPa RC beams

#### 4.3.2.3 Central deflection

The validity of RC beam design and testing data were verified through the comparison of between theoretical and experimental results. Table 4.2 showed the strength of RC beams, including cracking load, yield load, and ultimate load. The experimental results showed averagely 15% greater value compared to the designed flexural strength that was calculated based on material tested results, indicating a feasible design of RC beams. However, the cracking load by experiment showed relatively smaller value than designed value. This may be caused by heterogeneity of concrete and sensitivity of strain gauge, at which the cracking load was determined based on load-strain curve. Generally, the cracking load will be determined when the first crack occur, however, the change of stiffness based on deflection and strain can be differ due to the

sensitivity of the sensor. Strain gauges provide more sensitive signal which will be further used to determine the load at cracking moment.

Both 30 MPa and 60 MPa RC beam showed a similar result in comparison between experimental and designed strength. However, the cracking load had no consistency among comparison, which was possibly due to the effect of Friedel's salt in concrete pores. In designed strength, the effect of chloride crystallization cannot be reflected, leading to an inconsistent result.

After validation of testing data, the structural behavior of RC beams in terms of central deflection was firstly analyzed. Figure 4.37 ~ 4.38 depicted the load-deflection behavior of 30 MPa and 60 MPa RC beams. The testing values were detailed in Table 4.3. Testing results indicated that freeze-thaw cycles had a decreasing effect on load carrying capacities, but the decreasing ratio was minimal which were less than 10%. This result occurred both on 30 MPa and 60 MPa RC beams, showing that structural behavior was hardly affected by single action of freeze-thaw cycles.

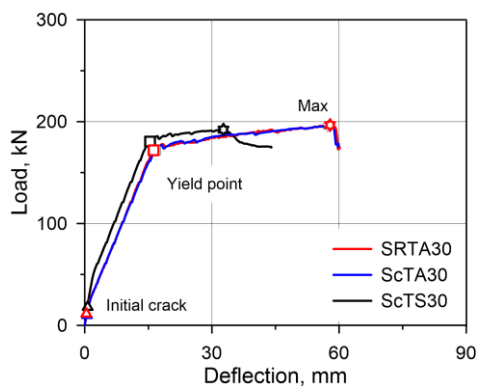


Figure 4.37 Load-deflection relationship of 30 MPa RC beams

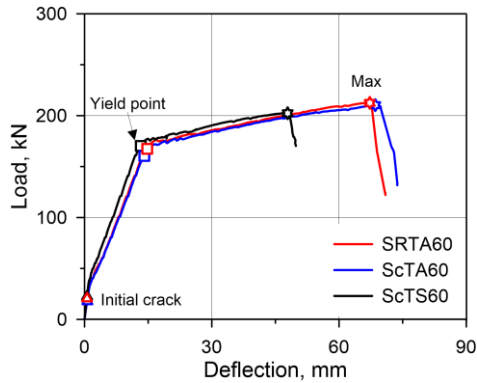


Figure 4.38 Load-deflection relationship of 60 MPa RC beams

Compared to the RC beams at room temperature and after freeze-thaw cycles, seawater-saturated RC beam after freeze-thaw cycles showed further decrease in terms of ultimate load. Seawater primarily affected cracking load of RC beam, which behavior showed both in 30 MPa and 60 MPa beams. By approximately 54% and 9% increase were found respectively in 30 MPa and 60 MPa RC beams. The increasing effect may be caused by the formation of Friedel's salt, which will make microstructure denser (Zhang and Wu, 2019). Besides, further hydration of concrete during seawater immersion could have progressed. This mechanism also accounted for the reduced crack propagation of seawater-saturated RC beams. Except for the increased cracking load, seawater decreased ductility by approximately 41% and 19% for 30 MPa and 60 MPa RC beams, respectively. The effect of seawater in high strength concrete beam was smaller due to the smaller porosity of the concrete.

To further analyze the effect of freeze-thaw cycles and seawater on RC beams, the behavior in early stage of loading was compared as shown in Figure 4.39~4.40. Herein, the behavior of before and after first crack can be found. At

early stage of loading, ScTA30, the air-cured RC beam subjected to freeze-thaw cycles presented smaller flexural stiffness, demonstrating the decreasing effect of freeze-thaw cycles on RC beam. The decrease may have been caused by the deteriorated concrete properties during freeze-thaw cycles during which the microcracks propagated. In contrast to ScTA30, ScTS30 that was subjected to the same freeze-thaw cycles revealed less decrease, which can be contributed to the effect of chloride crystallization. A similar behavior was also found in 60 MPa RC beam, but less decrease due to the greater durability of concrete.

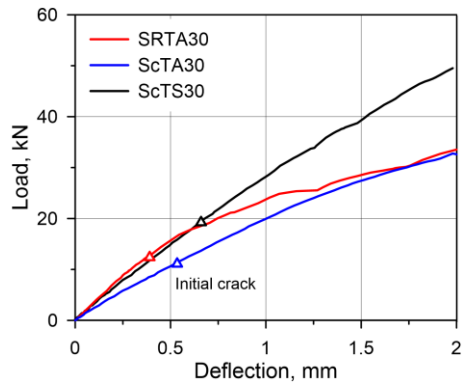


Figure 4.39 Load-deflection relationship of 30 MPa RC beams at early stage

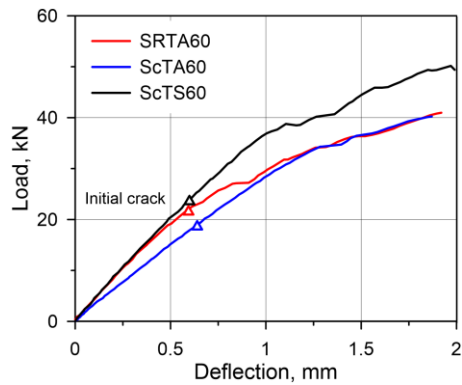


Figure 4.40 Load-deflection relationship of 60 MPa RC beams at early stage

Table 4.2 Strength of RC beams

Beam ID	Concrete		Theoretical (kN)		Experimental (kN)			Comparison	
	Age	$f_{cm}$ (MPa)	$P_{cr,T}$ (1)	$P_{u,T}$ (2)	$P_{cr,E}$ (3)	$P_{y,E}$ (4)	$P_{u,E}$ (5)	(3)/ (1)	(5)/ (2)
SRTA30	111	37	34	172	13	172	197	0.41	1.15
ScTA30	213	35	33	171	11	172	195	0.33	1.14
ScTS30	195	453	29	166	19	181	192	0.66	1.16
SRTA60	151	59	42	184	22	168	213	0.52	1.16
ScTA60	218	58	42	184	19	164	210	0.43	1.14
ScTS60	216	59	42	184	24	168	204	0.47	1.11



Table 4.3 Comparison of static behavior of RC beams

Beam ID	$P_{cr}$	$P_y$	$P_u$	$\frac{P_{cr}}{P_{cr,SRTA30/60}}$	$\frac{P_y}{P_{y,SRTA30/60}}$	$\frac{P_u}{P_{u,SRTA30/60}}$	$\delta_{cr}$	$\delta_y$	$\delta_u$	$\mu_\delta$	$\frac{\delta_{cr}}{\delta_{cr,SRTA30/60}}$	$\frac{\delta_y}{\delta_{y,SRTA30/60}}$	$\frac{\delta_u}{\delta_{u,SRTA30/60}}$	$\frac{\mu_\delta}{\mu_{\delta,SRTA30/60}}$
SRTA30	13	172	197	1	1	1	0.4	16.3	57.9	3.55	1	1	1	1
ScTA30	11	172	195	0.90	1	0.99	0.5	16.8	57.3	3.41	1.38	1.03	0.99	0.96
ScTS30	19	181	192	1.54	1.05	0.97	0.7	15.5	32.3	2.08	1.69	0.92	0.56	0.59
SRTA60	22	168	213	1	1	1	0.6	14.9	67.4	4.52	1	1	1	1
ScTA60	19	164	210	0.87	0.98	0.99	0.6	14.6	68.6	4.70	1	0.98	1.02	1.04
ScTS60	24	168	204	1.09	1.00	0.96	0.6	12.8	47.4	3.70	1	0.86	0.70	0.81

#### 4.3.2.4 Strain of reinforcing bars

Tensile strain with respect to increased loading was depicted in Figure 4.41 for the 30 MPa RC beams. Tensile strain of ScTA30 decreased after freeze-thaw cycle at the same level, indicating that there should be deterioration in interface of concrete and reinforcing bars. It has been reported that the bond strength of RC member will be degraded under freeze-thaw cycles (Cao et al. 2015; Petersen et al. 2007). Less deformation of reinforcing bars will occur as the bond strength decrease, further leading to a smaller tensile strain of RC beams. RC beam after sweater saturation condition presented decreased tensile strain due to the greater flexural stiffness. The shrinkage of RC beam was mitigated during seawater immersion, and increased cracking load by formation of chloride crystallization presented decreased tensile strain. The same behavior was also detected in 60 MPa RC beams, however, the difference was less than 30 MPa RC beams because of the greater durability.

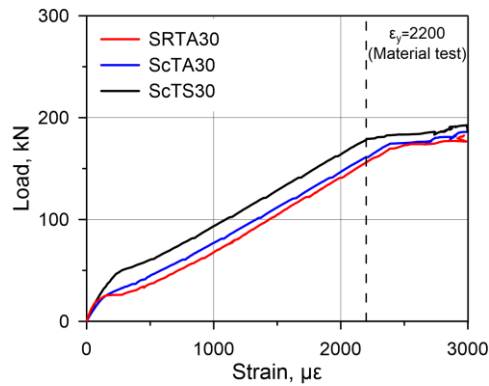


Figure 4.41 Load-strain relationship of 30 MPa RC beams

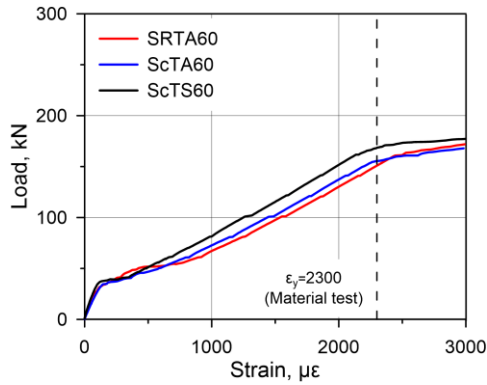


Figure 4.42 Load-strain relationship of 60 MPa RC beams

Tensile strain at early stage, during which behavior before and after cracking load was detailed in Figure 4.43~4.44. Tensile strain increased after freeze-thaw cycles at the same level, indicating the reduction of flexural stiffness. No significant change of tensile strain can be found in seawater-saturated RC beams, which was due to the denser microstructure of concrete capillary pores. Similarly, 60 MPa RC beams had relatively smaller variations as the comparison shown in load-deflection relationship.

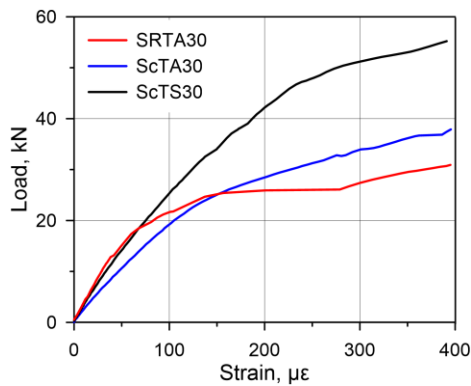


Figure 4.43 Load-strain relationship of 30 MPa RC beams at early stage

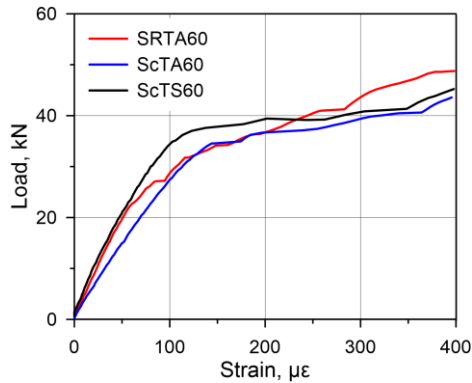


Figure 4.44 Load-strain relationship of 60 MPa RC beams at early stage

To further analyze the effect of freeze-thaw cycles and seawater, the deflection-tensile strain relationships were depicted as illustrated in Figure 4.45~4.46. Tensile strain up to yield strain was depicted since strain had an irregular signal output by the large deformation after yielding. RC beams subjected to freeze-thaw cycles, the greater deflection was presented at the same strain level. This was primarily due to the loss of bond strength during freeze-thaw cycles (Jang et al. 2009). RC beams with 60 MPa concrete also exhibited the same behavior, and seawater-saturated beams had less variations.

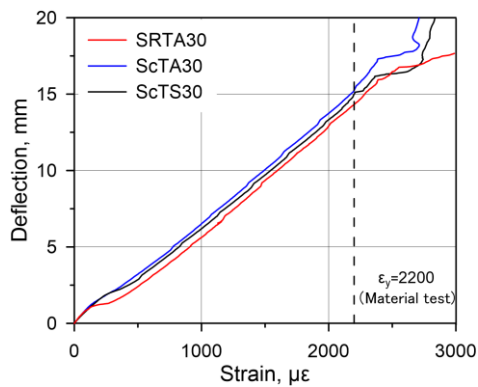


Figure 4.45 Deflection-tensile strain relationship of 30 MPa RC beams

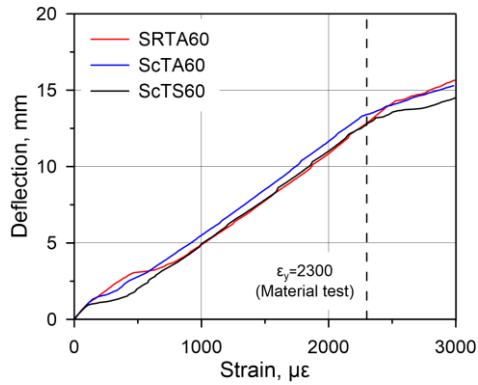


Figure 4.46 Deflection-tensile strain relationship of 60 MPa RC beams

The compressive strains exhibited a minor increasing effect after freeze-thaw cycles. This phenomenon could be attributed to the propagation microcracks of concrete under the repeated freeze-thaw cycles. As a result, the compressive stress of reinforcing bars in compression zone of RC beams could be increased. Corresponding to the decreased tensile strain, the compressive strain also showed smaller values. The mitigation of shrinkage and contribution of chloride crystallization at early stage reduce the cracks. Therefore, less reduction of strain in seawater-saturated RC beams can be found.

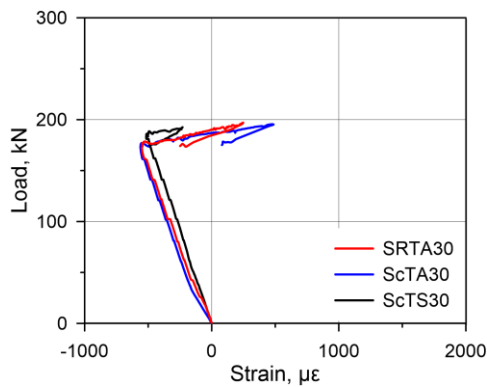


Figure 4.47 Load-compressive strain relationship of 30 MPa RC beams

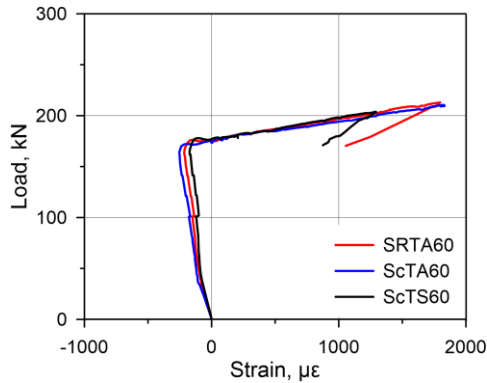


Figure 4.48 Load-compressive strain relationship of 60 MPa RC beams

#### 4.3.2.5 Summary

The effect of freeze-thaw cycles and seawater on the flexure and fatigue behavior was presented in this Chapter. Freeze-thaw cycles showed minor decreasing effect on the load carrying capacity which was less than 10%. This may be due to the limited number of freeze-thaw cycles. Test results indicated that freeze-thaw cycles and seawater decreased compressive strength and elastic modulus of concrete at material level. At structural level, there were thermal cracks formed on the surface of 30 MPa RC beams, signifying the freeze-thaw damage by repeated expansion and contraction of concrete pores. Furthermore, freeze-thaw cycles decreased the cracking load, ultimate load of RC beams. Similarly, seawater showed decreasing effect on ultimate load and ductility of RC beams. It should be noted that seawater increased the cracking load of RC beams which can be attributed to the formation of Friedel's salt in concrete pores, which made concrete pore structure denser (Zhang, 2019). Denser concrete pore structures on the beam surface possibly reduced the number of cracks, then increased crack width of RC beams.

## 4.4. Fatigue Flexural Test of RC Beams

### 4.4.1. Validity of Fatigue Design

#### 4.4.1.1 Designed stress range

The designed stress range (tension rebar) was verified based on static RC beam test and tensile test of rebar prior to the fatigue tests. Figure 4.49 depicted the stress range in load-deflection relationship, in which the designed stress range for fatigue tests were 261 MPa and 232 MPa, respectively for the 30 MPa RC beams and 60 MPa RC beams. It should be noted that the stress range was derived based on the static test of 30 MPa RC beam, which was to investigate the effect of freeze-thaw cycles and seawater at the same load level.

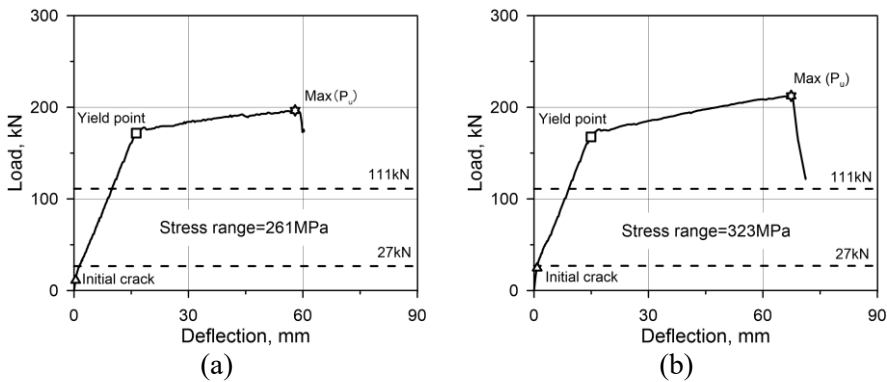


Figure 4.49 Stress range in load-deflection relationship: (a) 30 MPa RC beam;  
(b) 60 MPa RC beam

The minimum load of cyclic load was higher than the cracking load of 30 MPa RC beam at room temperature, however, smaller than 60 MPa RC beam. Therefore, the smaller tensile strain in 60 MPa RC beam was presented at

minimum load level, leading to a larger stress range in 60 MPa RC beam since the strain at maximum load of cyclic load was resemble. The stress range in load-tensile strain relationship were detailed in Figure 4.50.

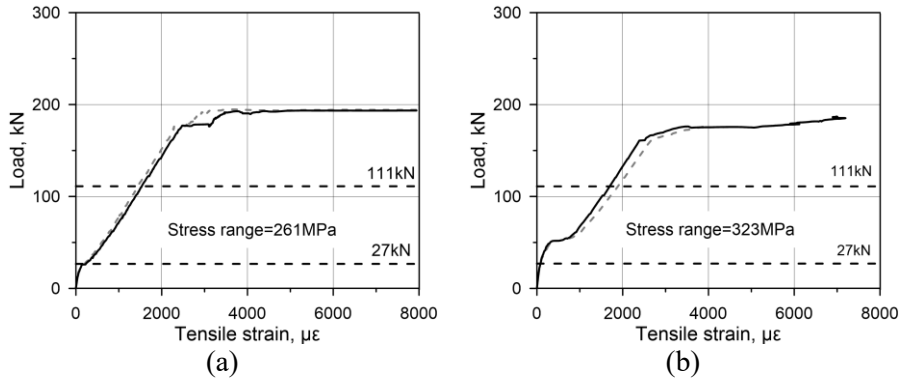


Figure 4.50 Stress range in load-strain relationship: (a) 30 MPa RC beam; (b) 60 MPa RC beam

To verify the designed stress range, stress range at material level was compared. The stress at the same strain level from RC beam tests were checked, and the difference was less than 5%, demonstrating the validity of the designed stress range. After verifying the validity of the designed stress range, the fatigue tests were initiated.



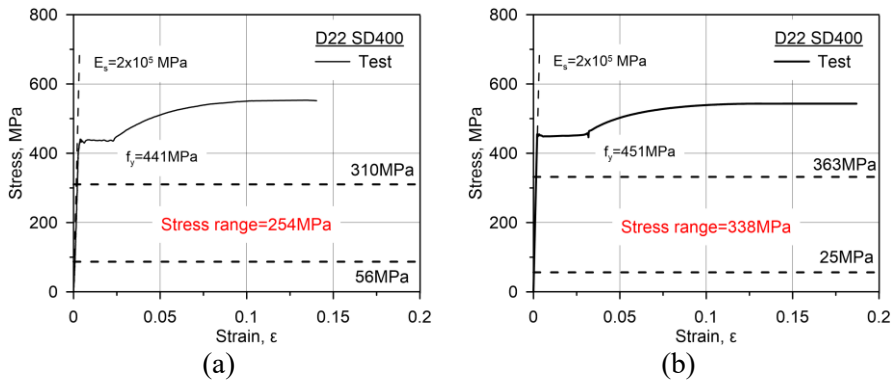


Figure 4.51 Stress range in stress-strain curve of rebar: (a) Rebar in 30 MPa RC beam; (b) Rebar in 60 MPa RC beam

#### 4.4.1.2 Static loading before fatigue test

Two cycles of static tests in the range of fatigue load were conducted in order to check if the applied stress range was well input, and examined the capacity of testing facilities at cyclic loading mode. The deflection range of RC beams showed similar results that were tested before fatigue loading and freeze-thaw cycles as shown in Figure 4.52.

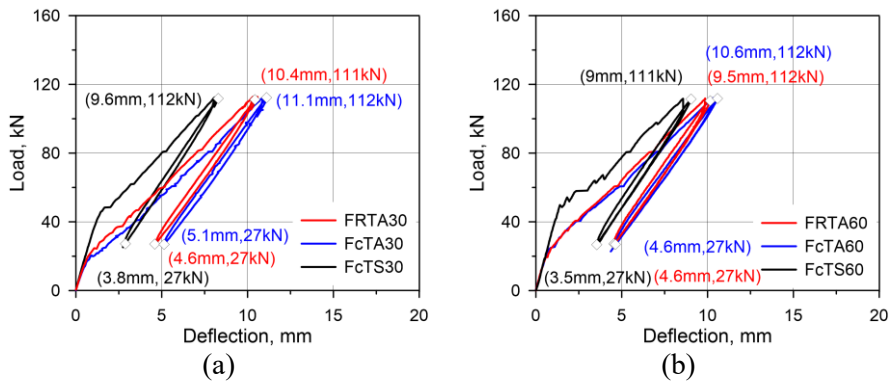


Figure 4.52 Load-deflection relationship in static tests: (a) 30 MPa RC beams; (b) 60 MPa RC beams

The cracking load of FcTS30, which was saturated by seawater, presented an increase compared to FRTA30. It can be deduced that the reason of increase in cracking load was by seawater immersion, compared to the results in static tests. The formation of Friedel's salt and further hydration by sufficient water supply may have contributed the better performance of concrete. RC beam with 60 MPa concrete showed relatively smaller variation after seawater immersion by its smaller porosity. Table 4.3 illustrated the comparison of cracking load in two cycles static tests where the effect of seawater was detailed.

Table 4.4 Comparison of cracking load before fatigue loading

Beam ID	Theoretical (kN)	Experimental (kN)	Comparison
	$P_{cr,T}$ (1)	$P_{cr,E}$ (2)	(2)/ (1)
FRTA30	20	14	0.70
FcTA30	20	13	0.65
FcTS30	18	24	<b>1.33</b>
FRTA60	24	19	0.79
FcTA60	24	19	0.79
FcTS60	26	24	<b>0.92</b>

## 4.4.2. Effect of Concrete Strength

### 4.4.2.1 Failure mode

RC beams under cyclic loading basically failed by rupture of tensile rebar. The input of cyclic loading was examined until failure of RC beams as shown in Figure 4.53~4.54. Under different temperature conditions, designed cyclic load was well applied in RC beams. Applied load up to the failure of RC beams was presented, and 60 MPa beams averagely had shorter fatigue life.

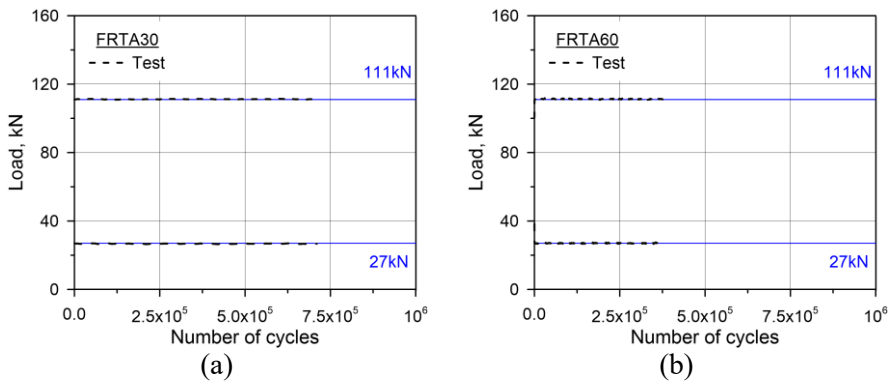


Figure 4.53 Load-N relationship: (a) FRTA30; (b) FRTA60

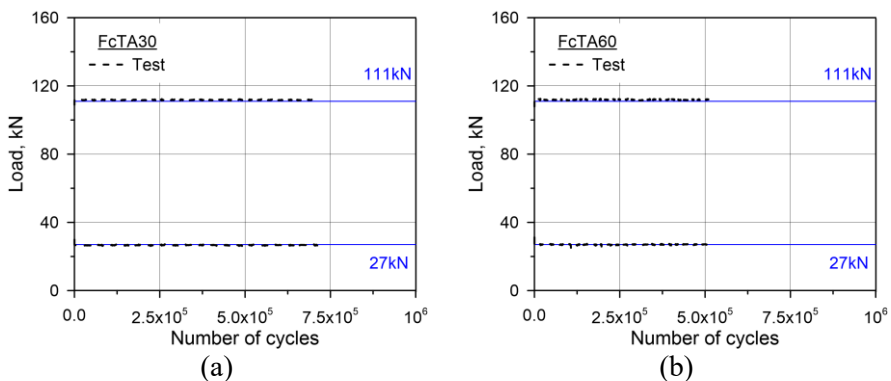


Figure 4.54 Load-N relationship: (a) FcTA30; (b) FcTA60

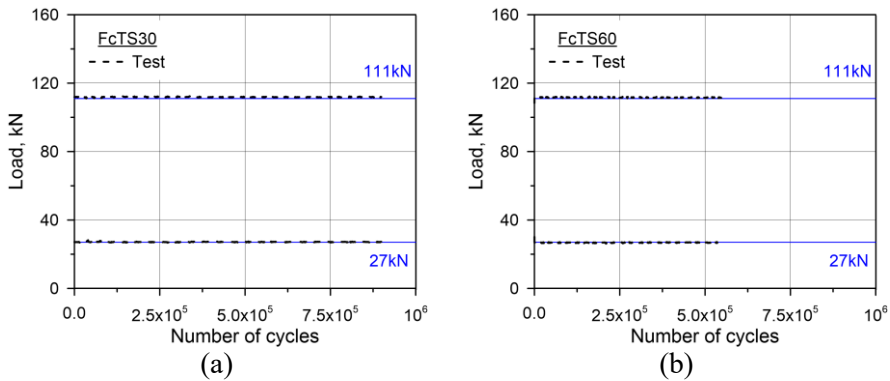
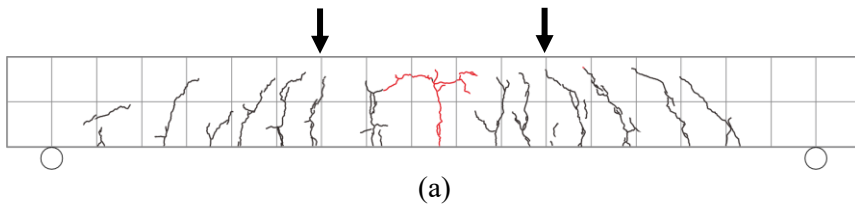


Figure 4.55 Load-N relationship: (a) FcTS30; (b) FcTS60

Failure mode at room temperature showed less difference except the higher neutral axis of 60 MPa RC beam. However, the fatigue life of 60 MPa RC beam exhibited shorter fatigue life which may be attributed to the increased bond strength and greater shrinkage of concrete.

In general, bond strength increases along with the concrete strength, indicating more effective stress transmission through bond force. The effective stress transmission will result in stress concentration that leads to internal cracks in RC beams. In this way, the spacing of cracks width will be shorter in high strength concrete RC beams, leading to a faster loss of tension stiffening as the number of cyclic load increase (Yun et al. 1998). This behavior was more apparent under freeze-thaw cycles as shown in Figure 4.57.



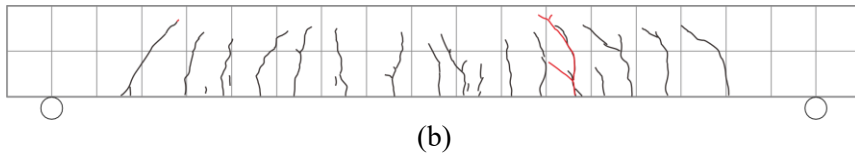


Figure 4.56 Failure of RC beams at room temperature: (a) FRTA60; (b) FRTA30

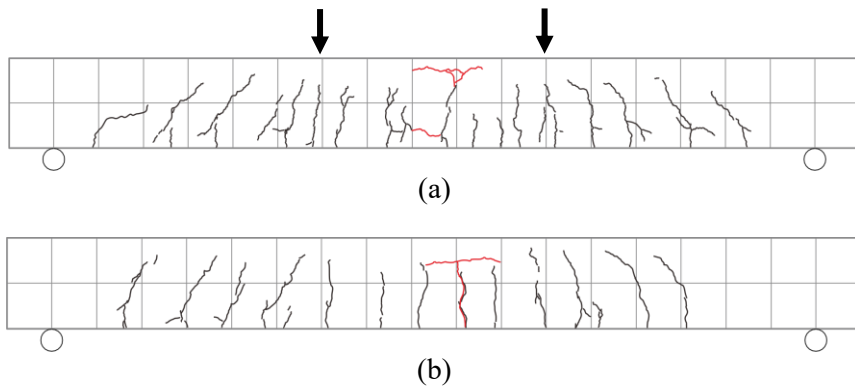


Figure 4.57 Failure of air-cured RC beams under freeze-thaw cycles: (a) FcTA60; (b) FcTA30

RC beams under freeze-thaw cycle with seawater-saturated condition showed relatively fewer cracks. 60 MPa RC beam had larger spacing of cracks under cyclic load due to the greater bond strength, leading to the shorter fatigue life. RC beams with 30 MPa concrete revealed the wider range of crack propagation at failure that could be caused by the more severe deterioration of normal strength concrete. Under the effect of freeze-thaw cycles and seawater saturation, 30 MPa concrete showed greater deterioration in terms of concrete strength and elastic modulus, whereas the 60 MPa concrete was rarely affected by freeze-thaw cycles and seawater-saturation.

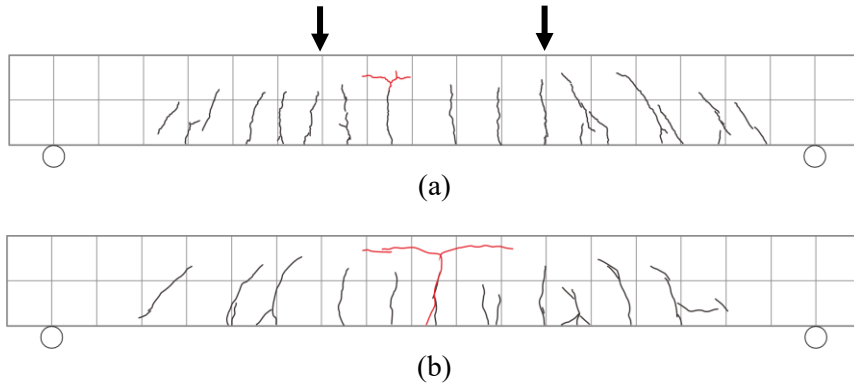


Figure 4.58 Failure mode of seawater-saturated RC beams under freeze-thaw cycles: (a) FcTS60; (b) FcTS30

#### 4.4.2.2 Crack width

Crack width of RC beams were measured by crack gauge, which were mounted after two cycles static tests. For the case of 30 MPa RC beams, only flexural cracks in pure bending zone were measured due to the testing conditions as depicted in Figure 4.59. Herein, notation “Cr” represented the term “Crack”, while sequential numbers were serial number of crack gauges. In 60 MPa RC beams, both flexural and shear cracks were able to be measured, and notation of “F” and “S” respectively stood for the “Flexural” and “Shear” based on its position. To classify the position of crack gauge in a RC beams, “L” and “R” were adopted to represent the “Left” and “Right” side with the benchmark of centerline in 60 MPa RC beams. It should be noted that, extra cracks occurred and propagated as the number of cyclic loading increased, but majority of cracks propagated in less than 20,000 cycles. The red box in RC beams denoted the cracking point where the failure occurred with rupture of tensile rebar.

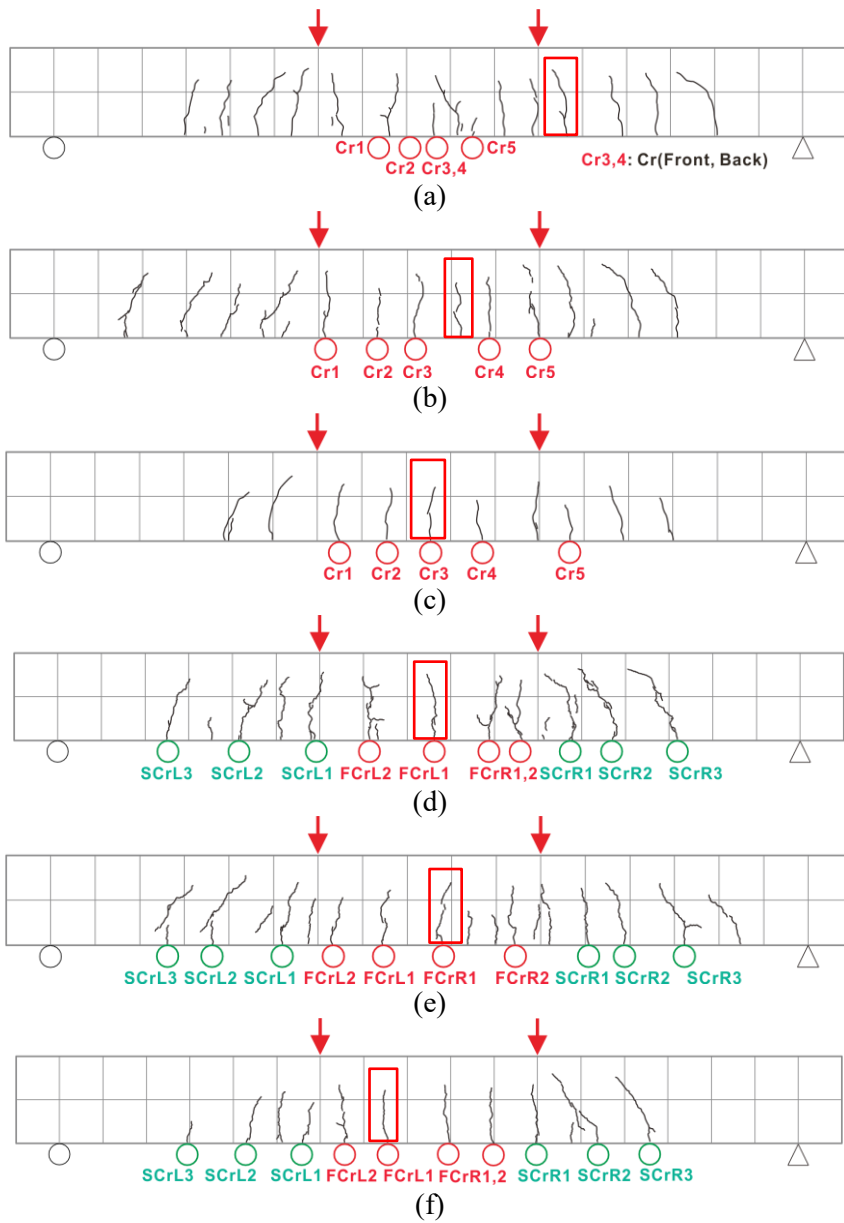


Figure 4.59 Position of crack gauges in RC beams: (a) FRTA30; (b) FcTA30; (c) FcTS30; (d) FRTA60; (e) FcTA60; (f) FcTS60

Crack width of RC beams were measured until failure of RC beams as shown in Figure 4.60~4.62. The results were presented in the form of crack width range in the fatigue load range since the initial crack width was different after two cycles static tests.

At room temperature, concrete strength merely affected the crack width with the increased number of cyclic loading. It should be noted that the crack width of “FCrL2” accidentally measured two adjacent cracks, at which another crack was found within the range of crack gauge. Without consideration of accidentally measured cracks, the general cracks width range were found to be similar, implying the minor effect of concrete strength at room temperature.

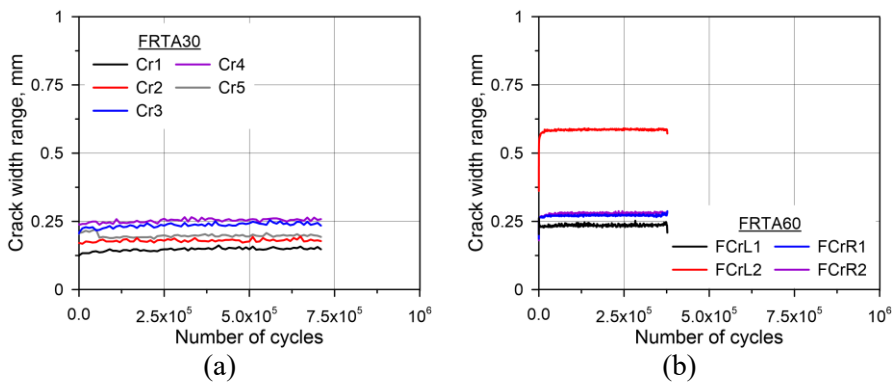


Figure 4.60 Crack width range at room temperature: (a) FRTA30; (b) FRTA60

Under freeze-thaw cycles with air-cured condition of RC beam, crack width range of 60 MPa RC beam was by approximately 0.2~0.4 mm, while 30 MPa RC beam had range of 0.13~0.29. Analyzing the crack width and its exact position of failure point, it can be found that the crack width development of failure point was successfully measured. However, the failure point was not



able to be detected which may result in the difference in entire comparison. It was estimated that the crack width range of FcTA30 can be larger if the crack width in failure point was measured.

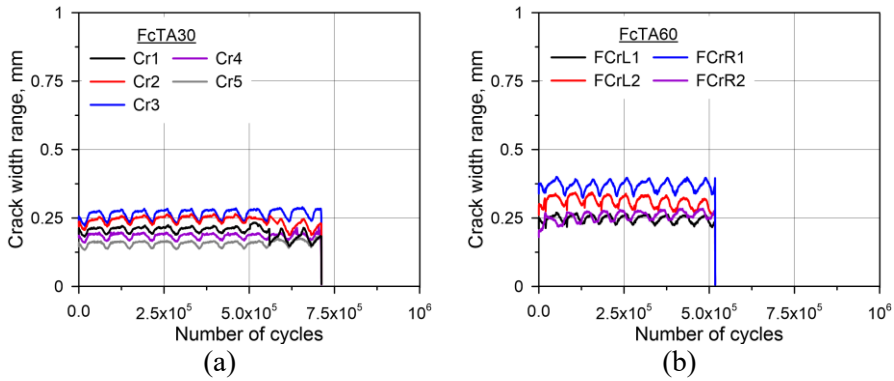


Figure 4.61 Crack width range under freeze-thaw cycles with air-cured condition: (a) FcTA30; (b) FcTA60

Crack width exhibited larger difference when RC beams were saturated by seawater as shown in Figure 4.62. The greater increasing effect of seawater on crack width of 30 MPa RC beam can be found, which was due to the vulnerability to seawater ingress. The range crack width in 30 MPa RC beam showed larger value that was in 0.12~0.51mm, while in 60 MPa RC beam it ranged in 0.24~0.5 mm. 30 MPa concrete has larger porosity compared to 60 MPa concrete in which more seawater will be filled during immersion. In addition, 30 MPa concrete will be subjected to more severe free-thaw damage attributed to the higher water content in concrete pores. For the case of 60 MPa RC beam, reduced porosity and connectivity of high strength concrete will curtail the ice-growth (Liu and Hansen, 2016), signifying a reduced deterioration by freeze-thaw cycles.

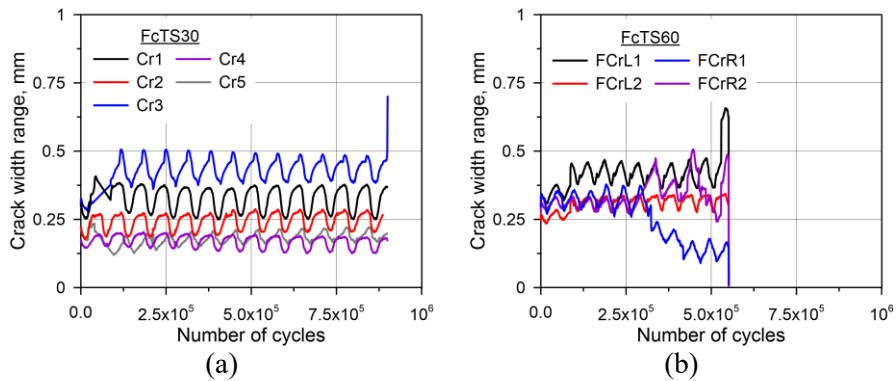


Figure 4.62 Crack width range under freeze-thaw cycles with seawater-saturated condition: (a) FcTS30; (b) FcTS60

#### 4.4.2.3 Central deflection

Central deflection of RC beams at different temperature conditions were measured in order to evaluate the deformation of RC beams. At room temperature, RC beams showed less difference by concrete strength, as shown in Figure 4.63. The increasing ratio of deflection of 60 MPa and 30 MPa RC beams presented little difference that were 29% and 22%, respectively. It should be noted that the increasing ratio was defined as the ratio of deflection at the cycles of loading to the initial deflection, which indicated the damage accumulation velocity. In the following analysis, including deflection and strain response of rebar, damage accumulation was evaluated with the support of increasing ratio.

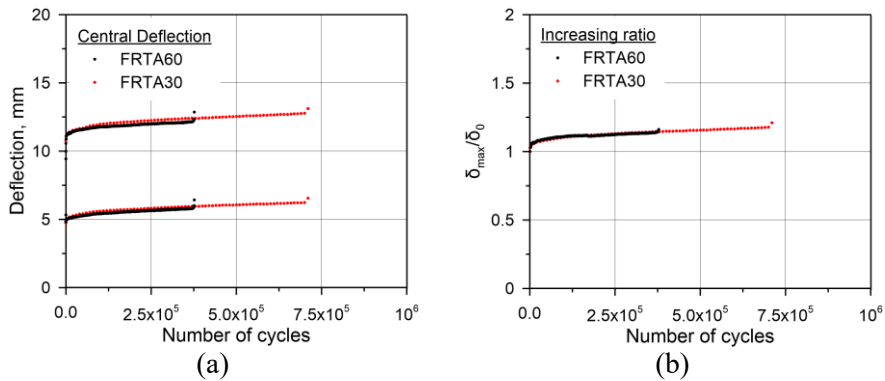


Figure 4.63 Central deflection at room temperature: (a) Deflection-N relation;  
(b) Increasing ratio-N relation

Under freeze-thaw cycles, deflection of RC beams presented periodical change which was caused by the cyclic temperature change, during which the capacity of RC beams was periodically changed. It can be found that the FcTA30 presented larger fluctuation under freeze-thaw cycles, implying the vulnerability of reinforced normal strength concrete beams. Moreover, FcTA30 had greater increasing ratio of deflection under freeze-thaw cycles, signifying the faster damage accumulation. Compared to FcTA30, FcTA60 that was reinforced with high strength concrete showed relatively smaller fluctuation under freeze-thaw cycles. The increasing ratio deflection of FcTA60 exhibited by approximately 20%, while FcTA30 had by up to 44%. During the freeze-thaw cycles, 30 MPa concrete beams will have more internal damage due to the expansion and contraction of pore water, and melted pore water can flow into cracks, further resulting in freeze-thaw damage. This phenomenon was reduced by the smaller porosity of 60 MPa concrete.

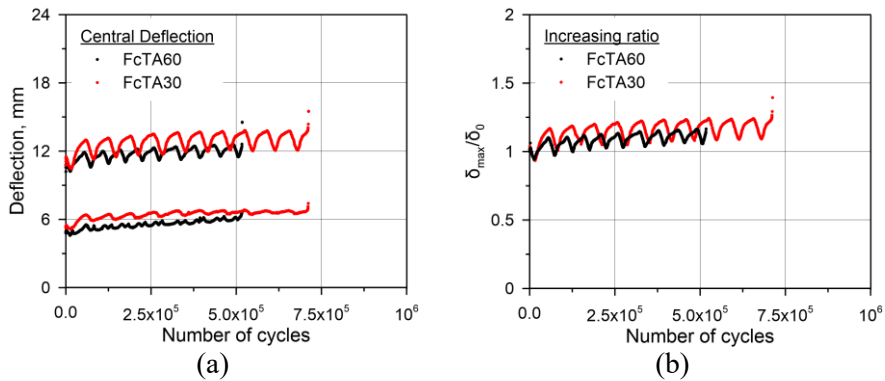


Figure 4.64 Central deflection under freeze-thaw cycles with air-cured condition: (a) Deflection-N relation; (b) Increasing ratio-N relation

With seawater-saturated condition, RC beams showed larger difference of deflection between normal and high strength concrete. Similar to the behavior with air-cured condition, seawater-saturated RC beams also had periodical fluctuation under freeze-thaw cycles. However, FcTS30 that was reinforced with 30 MPa concrete had greater deflection compared to the FcTS60 as illustrated in Figure 6.65. Except for the larger deflection of FcTS30, the increasing ratio of FcTS30 showed by approximately 74% whereas FcTS60 only had 28%. As mentioned in air-cured conditions, freeze-thaw cycles had more effect on normal strength concrete beam. Furthermore, the expansive product generated during immersion of seawater can also affect the behavior of RC beam. Generally, the expansive product will fill in the pores and generate micro-crack, and further ingress into the micro-cracks, promoting the degradation of concrete (Chen et al. 2017). Deterioration of FcTS60 was smaller that was attributed to the fewer absorption of seawater during immersion, and corresponding damage was reduced under freeze-thaw cycles.

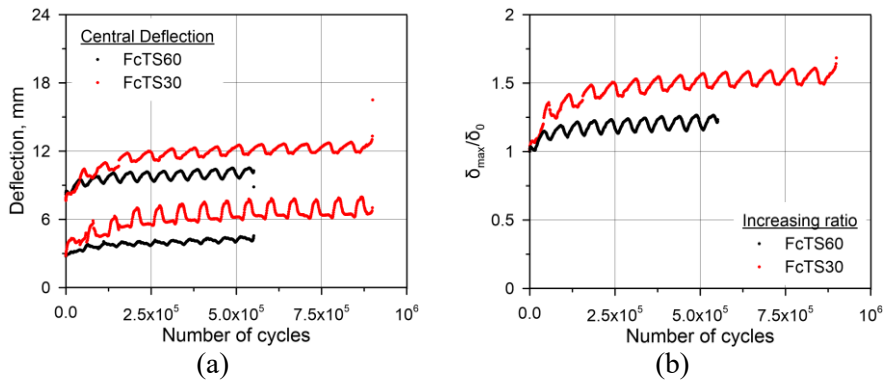


Figure 4.65 Central deflection under freeze-thaw cycles with seawater-saturated condition: (a) Deflection-N relation; (b) Increasing ratio-N relation

A simply supported RC beam having shear span  $a$ , was depicted in Figure 4.66. With the basis of central deflection, the flexural stiffness of RC beam was derived as the Equation 4.4.

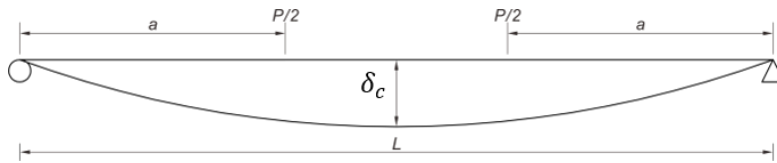


Figure 4.66 Central deflection of simply supported beam

Central deflection of RC beam can be expressed as Equation 4.3

$$\delta_c = \frac{Pa}{48EI} (3L^2 - 4a^2) \quad (4.3)$$

In this study, shear span length  $a=1.2 L/3.4$  gives

$$EI = 0.0184 \frac{PL^3}{\delta_c} \quad (4.4)$$

Similar to the development of central deflection, flexural stiffness showed less variation at room temperature, and increasing ratio of FRTA30 and FRTA60 respectively showed 17% and 19% with respect to number of cyclic loading. It can be deduced that flexural stiffness was merely influenced by concrete strength at room temperature.

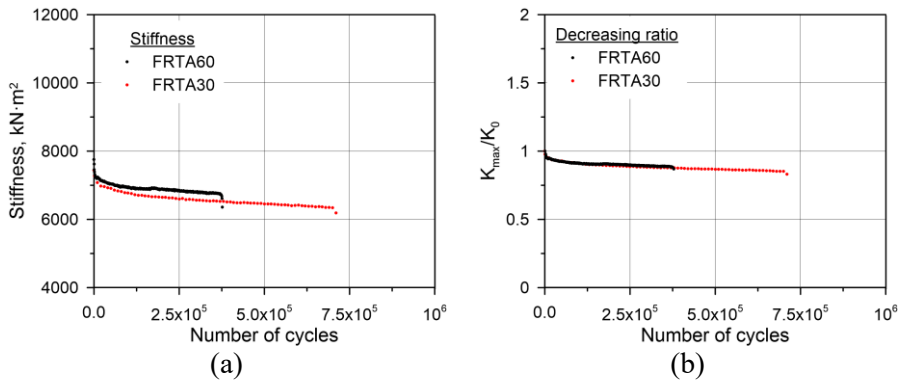


Figure 4.67 Flexural stiffness at room temperature: (a) Stiffness-N relation;  
(b) Increasing ratio-N relation

Under freeze-thaw cycles with air-cured condition, flexural stiffness varied with different concrete strength as given in Figure 4.68. Flexural stiffness under freeze-thaw cycle basically presented a decrease with respect to number of cyclic loading. FcTA30 exhibited smaller stiffness compared to FcTA60 along with cyclic loading since 60 MPa concrete has greater elastic modulus of concrete. The increasing ratio of FcTA30 and FcTA60 had greater difference compared to the RC beams at room temperature which were 22% and 12%, respectively, indicating the faster damage accumulation in FcTA30. The flexural stiffness is primarily determined by elastic modulus of concrete under freeze-thaw cycles, for the reinforcing bars are rarely deteriorated. The

deterioration of concrete properties directly results in the reduction of flexural stiffness, and normal strength concrete are more vulnerable to freeze-thaw cycles. Therefore, the deterioration of flexural stiffness was in FcTA30 compared to FcTA60.

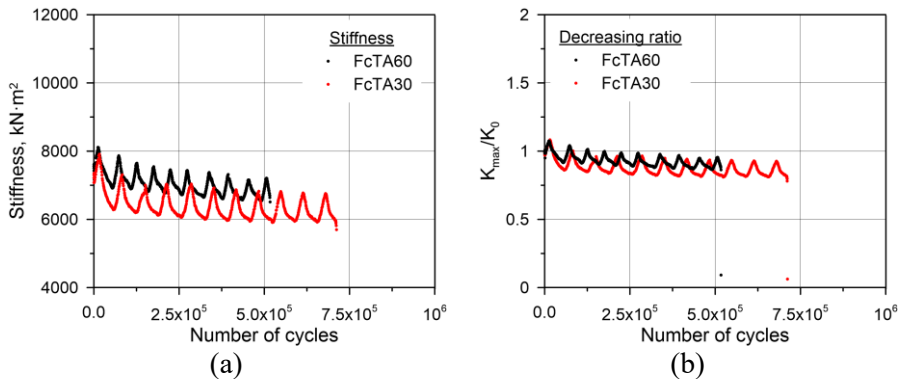


Figure 4.68 Flexural stiffness under freeze-thaw cycles with air-cured condition: (a) Stiffness-N relation; (b) Increasing ratio-N relation

Considering the seawater saturation under freeze-thaw cycles, RC beams behaved similarly compared to the air-cured condition as shown in Figure 4.69. What stood out in the seawater-saturated condition was the larger difference by difference concrete strength. Freeze-thaw cycle affected flexural stiffness by means of propagating internal damage, during which the material properties of concrete decreased. With the participation of seawater, the internal damage can be more serious attributed to the higher water content in concrete pores. Moreover, the expansive products can generate extra micro-crack, leading to further deterioration of concrete. In this manner, FcTS30 that was reinforced with normal strength concrete suffered more severe deterioration under freeze-thaw cycles, showing a greater degradation of flexural stiffness. The increasing

ratio of flexural stiffness demonstrated 42% in FcTS30 whereas only 20% presented in FcTS60.

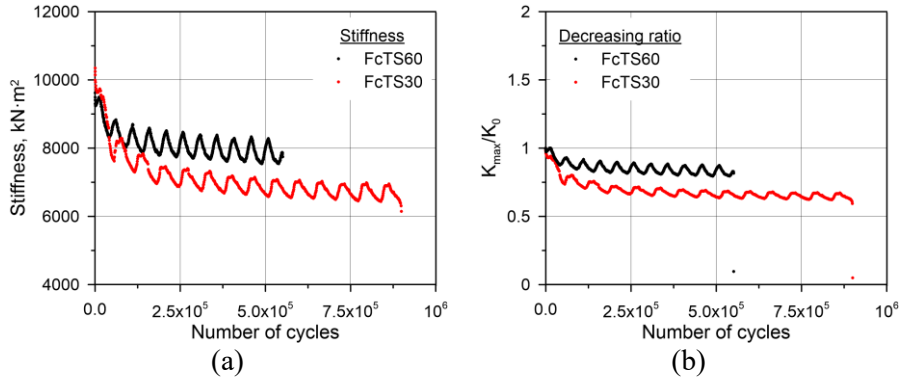


Figure 4.69 Flexural stiffness under freeze-thaw cycles with seawater-saturated condition: (a) Stiffness-N relation; (b) Increasing ratio-N relation

#### 4.4.2.4 Strain of reinforcing bars

Tensile strain of RC beams was measured in order to measure the accumulated damage under cyclic loading. Figure 7.70 exhibited the tensile strain with respect to number of cyclic loading at room temperature. It should be noted that limited strain data were detected attributed to the damage of strain gauges during fatigue tests. Therefore, the comparison in the range of measured strain data was conducted. It has been reported that the strain of reinforcing bars usually has rapid increase in less than 5% of fatigue life, and by approximately 95% of stable damage stage during which deflection and strain remains relatively constant (Charalambidi et al. 2016; Xie et al. 2012), indicating a relatively constant stress range. These findings indicated that the limited data in this study can be used to analyze the fatigue behavior since the strain gauges detected data up to the range of stable stage.



Along with the number of cyclic loadings, FRTA30 that was reinforced with normal strength concrete showed relatively smaller tensile strain compared to FRTA60. As analyzed in static tests, this result can be caused by the greater shrinkage of high strength concrete, especially in autogenous shrinkage. Nevertheless, the damage accumulation which was presented in the form of increasing ratio, exhibited 9.4% in FRTA30 while 3.6% in FRTA60. It demonstrated little difference in damage accumulation by different concrete strength at room temperature.

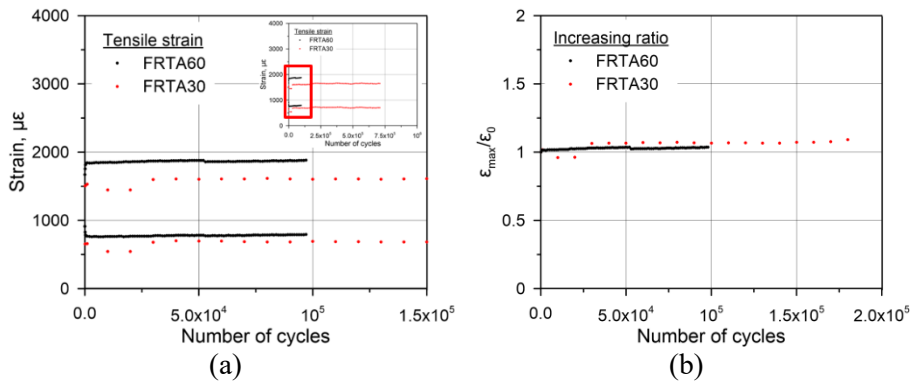


Figure 4.70 Tensile strain at room temperature: (a) Strain-N relation; (b) Increasing ratio-N relation

A similar phenomenon was also found under freeze-thaw cycles with air-cured condition, signifying a little effect of freeze-thaw cycle on deformation of reinforcing bars. Likewise, compared to the FcTA60, FcTA30 had little difference in increasing ratio of tensile strain, indicating a minor effect of concrete strength on tensile strain under freeze-thaw cycles.

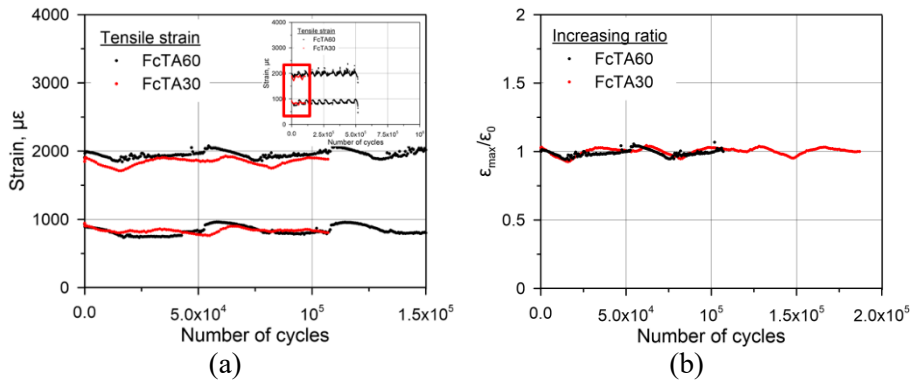


Figure 4.71 Tensile strain under freeze-thaw cycles with air-cured condition:

(a) Strain-N relation; (b) Increasing ratio-N relation

With the consideration of seawater saturation under freeze-thaw cycles, FcTS30 had smaller tensile strain compared to FcTS60 along with cyclic loadings. This result can be caused by the greater shrinkage of high strength concrete as analyzed in static test results. However, the accelerated damage accumulation on FcTS30 can be found in comparison to FcTS60, which was 15% and 6%, respectively. Accelerated damage can be attributed to the greater deterioration of the 30 MPa concrete, in which the both effect of freeze-thaw cycles and seawater were implemented on RC beam.

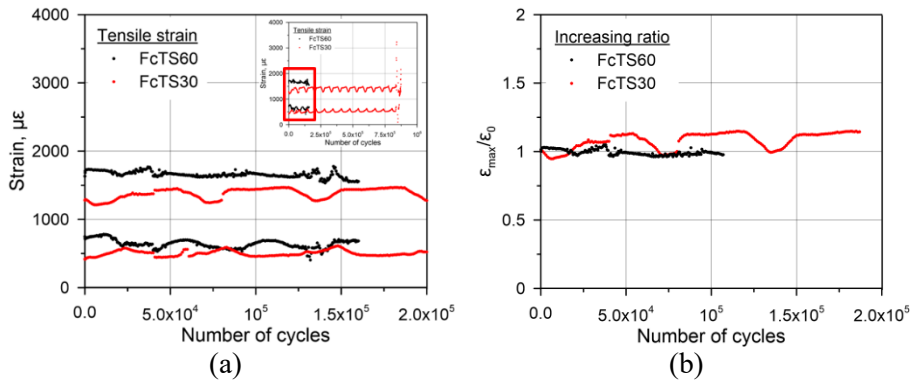


Figure 4.72 Tensile strain under freeze-thaw cycles with seawater-saturated condition: (a) Strain-N relation; (b) Increasing ratio-N relation

Following the behavior in tensile strain, the strain range by cyclic loadings was comparatively analyzed as shown Figure 4.73~4.75. RC beams with 60 MPa concrete showed relatively greater strain range in comparison to 30 MPa RC beam, which was approximately 12% by average. The greater strain range of 60 MPa RC beam can be attributed to the greater bond strength. Under the cyclic load, the bond between concrete and steel would be destroyed in a certain range which was assumed as “effective range of bond loss”. As the concrete strength increased, the effective range of bond loss would be reduced contributed to the greater bond strength. The strain range can be regarded as the ratio of crack width to the range of effective range of bond loss. Therefore, the strain range would increase as the effective range of bond loss decrease, resulting in the increase of strain range. RC beams under larger strain range, an earlier rupture of tensile rebar will occur as the number of cyclic load increased.

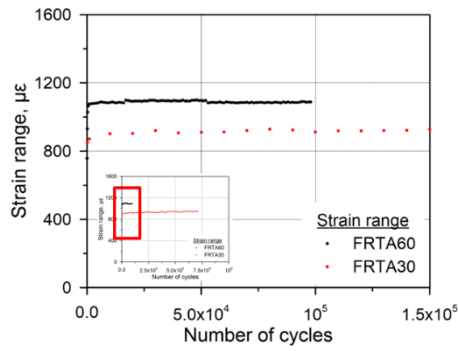


Figure 4.73 Strain range at room temperature

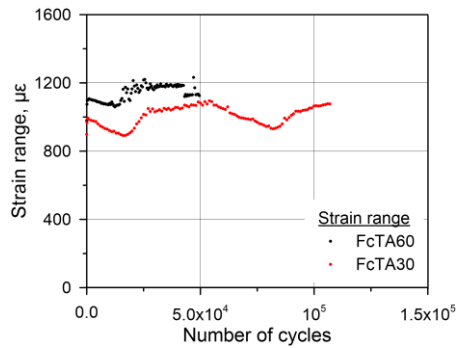


Figure 4.74 Strain range under freeze-thaw cycles with air-cured condition

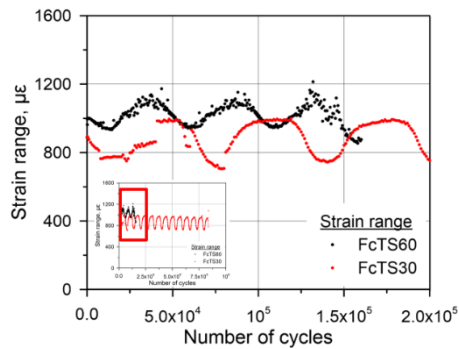


Figure 4.75 Strain range under freeze-thaw cycles with seawater-saturated condition

In compression strain of reinforcing bars, RC beams with 30 MPa concrete showed greater value at room temperature. Compressive strain of FRTA30 increased as the cyclic loading increased, but a decreasing trend was found in FRTA60. This was due to the neutral axis shifted towards compression zone of RC beam and finally surpass the compressive rebar, hence, the compressive rebar behaved in a tensile manner.

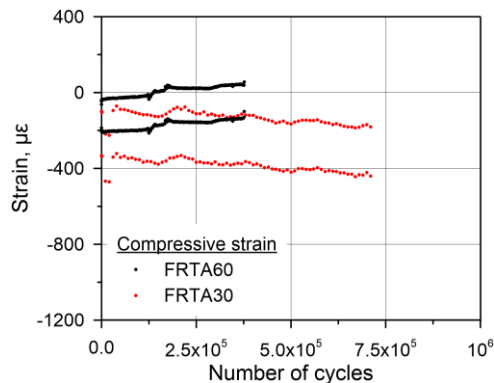


Figure 4.76 Compressive strain at room temperature

Generally, the greater tensile strain will result in greater compressive strain in accordance with the force equilibrium. Under the freeze-thaw cycles with air-cured condition, FcTA60 was expected to present larger compressive strain due to its corresponding larger tensile strain that was caused by greater shrinkage. However, FcTA30 showed slight larger compressive strain as the number of cyclic loading increased as shown in Figure 4.77. At the material level, both concrete strength and elastic modulus decreased under freeze-thaw cycles, and this phenomenon may cause greater stress distribution on compression rebar. Due to the larger deterioration of 30 MPa concrete, FcTA30 possibly exhibited greater compressive strain that it was expected. Additionally,

the greater shrinkage of 60 MPa RC beam lead to a contract state, resulting in smaller compressive strain.

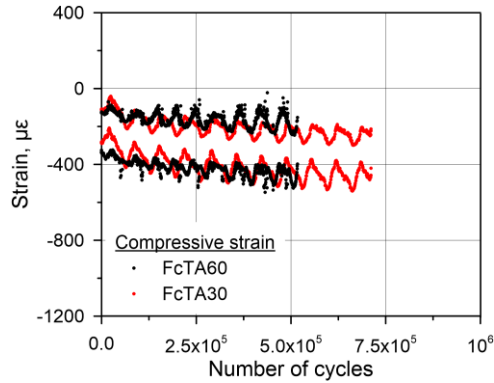


Figure 4.77 Compressive strain under freeze-thaw cycles with air-cured condition

A similar behavior can also be found in seawater-saturated condition under freeze-thaw cycles as given in Figure 4.88. The shrinkage of FcTS30 and FcTS60 was reduced by sufficient water supply during seawater immersion. In concrete material tests, both concrete strength and elastic modulus decreased under freeze-thaw cycles with seawater-saturated condition, leading to a larger stress distribution in compression bar of RC beam. Besides, the greater shrinkage of 60 MPa concrete resulted in a contract state of RC beam, signifying a smaller compressive strain compared to FcTS30. The behavior in compressive strain indicated that 30 MPa RC beam had smaller freeze-thaw and seawater resistance in comparison to the RC beam with 60 MPa concrete.

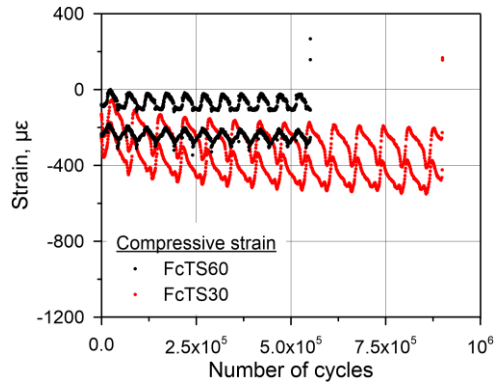


Figure 4.78 Compressive strain under freeze-thaw cycles with seawater-saturated condition

#### 4.3.2.5 Summary

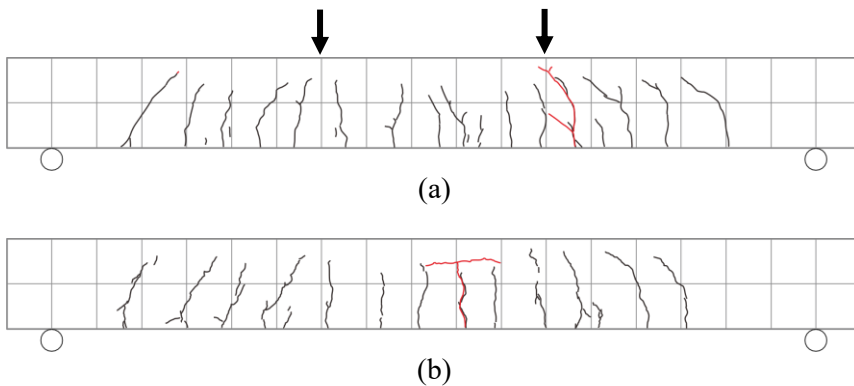
The effect of concrete strength on the fatigue behavior was investigated and all RC beams failed by the rupture of tensile rebar. It should be mentioned that the fatigue life of 60 MPa RC beams averaged shorter than 30 MPa RC beams by approximately 38%. This can be attributed to the increased bond strength, leading to the small range of bond loss under fatigue load and finally increased the strain range of tensile rebar at same crack width.

Except for the fatigue life, RC beams with 30 MPa concrete had relatively greater deterioration compared to 60 MPa RC beams, including larger deflection and smaller flexural stiffness as cyclic load increased. Besides, the deflection and tensile strain increasing ratio, which reflected the damage accumulation, presented 46% and 9% greater value in 30 MPa RC beams compared to 60 MPa RC beams. Similar to the damage accumulation, the range of crack width demonstrated a larger value in 30 MPa, implying the potential degradation under combined effect of freeze-thaw cycles and seawater.

### 4.4.3. Effect of Freeze-thaw Cycles and Seawater

#### 4.4.3.1 Failure mode

RC beams at different temperature conditions failed by rupture of tensile rebar, and position of failure was marked with red line as shown in Figure 4.79. Under freeze-thaw cycles, fatigue life of FcTA30 increased due to the freezing stage of freeze-thaw cycles, during which the capacity of RC beams can be increased. With seawater-saturated state, the fatigue life of FcTS30 further increased which can be caused by smaller stress range. The reduced number of cracks in FcTS30 can be observed that was also detected in static tests. During period of seawater immersion, the cracking load increased, which was greater than the cracking load of RC beam, and hence the stress range of tensile rebar can be reduced. Besides, the shrinkage of RC beam can be reduced by sufficient water supply. However, under freeze-thaw cycles with participation of seawater, FcTS30 presented a wider propagation of cracks at compression zone that was possibly attributed to the more severe deterioration of concrete. Therefore, FcTS30 exhibited longer fatigue life, but a more severe failure mode.





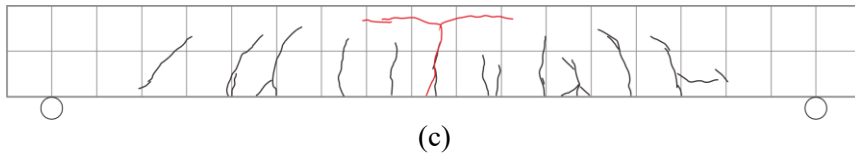


Figure 4.79 Failure of 30 MPa concrete RC beams: (a) FRTA30; (b)FcTA30;  
(c) FcTS30

RC beams with 60 MPa concrete exhibited a similar behavior compared to 30 MPa RC beams including failure mode. The fatigue life of RC beam increased under freeze-thaw cycles, and seawater saturation further extended the fatigue life. Less difference of crack propagation can be found between FRTA60 and FcTA60 by the greater freeze-thaw resistance of high strength concrete, but still recued cracks by seawater can be observed.

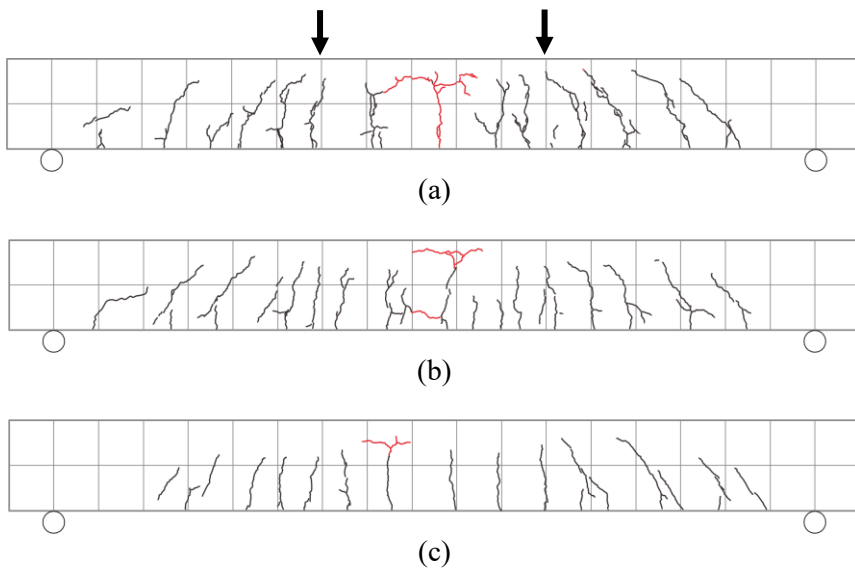


Figure 4.80 Failure of 60 MPa concrete RC beams: (a) FRTA60; (b)FcTA60;  
(c) FcTS60

#### 4.4.3.2 Crack width

The crack width of RC beams was comparatively analyzed since freeze-thaw cycles and seawater primarily influence the structural behavior of RC beams through affecting the properties of concrete. The position of crack gauges was depicted in Figure 4.81, the detailed designation of crack gauges was illustrated in chapter 4.3.2.2. The failure spot at which rupture of tensile rebar occurred was marked with red box, which was almost located moment zone.

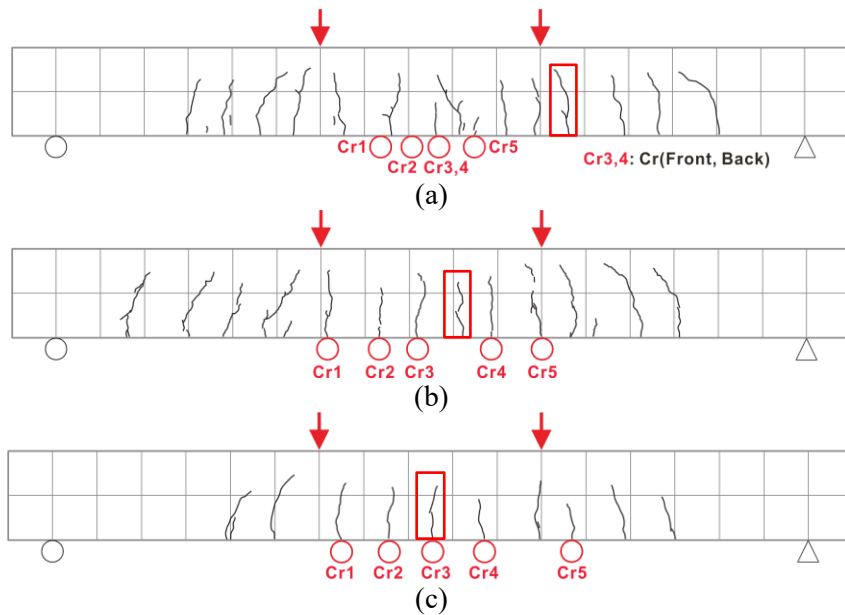


Figure 4.81 Position of crack gauges in 30 MPa RC beams: (a) FRTA30; (b) FcTA30; (c) FcTS30

The crack width range of 30 MPa RC beams were compared as given in Figure 4.82. The temperature during freeze-thaw cycles was depicted, in which the variation of RC beam capacity along with temperature can be found. Crack width of FcAT30 showed less difference compared to FRTA30 which were 0.12~0.26 mm and 0.13~0.29 mm, respectively, implying a little effect of freeze-thaw cycles on crack width. Concrete strength and elastic modulus decreased under freeze-thaw cycles, however, there was no significant variation of crack width under the single effect of temperature cycles. It should be noted that the crack width at failure spot was not measured since the exact the spot of failure cannot be predicted. Therefore, crack width at failure spot may have presented a larger value, at which the increasing effect of freeze-thaw cycles can be found.

FcTS30 that was saturated with seawater showed relatively greater crack width compared to FRTA30 and FcTA30. It showed approximate crack width range of 0.13~0.51 mm, which was two times greater than that of FRTA30. This can be caused by the immersion of seawater, during which the formation of Friedel's salt occurred in concrete pores, leading to the reduced number of cracks. The reduced cracks would result in increased crack width at the same load. Moreover, the crack width of RC beams with 30 MPa concrete showed less variation under freeze-thaw cycles, however, it increased after saturation of seawater, demonstrating an increasing effect of seawater through formation of chloride crystallization in concrete pores.

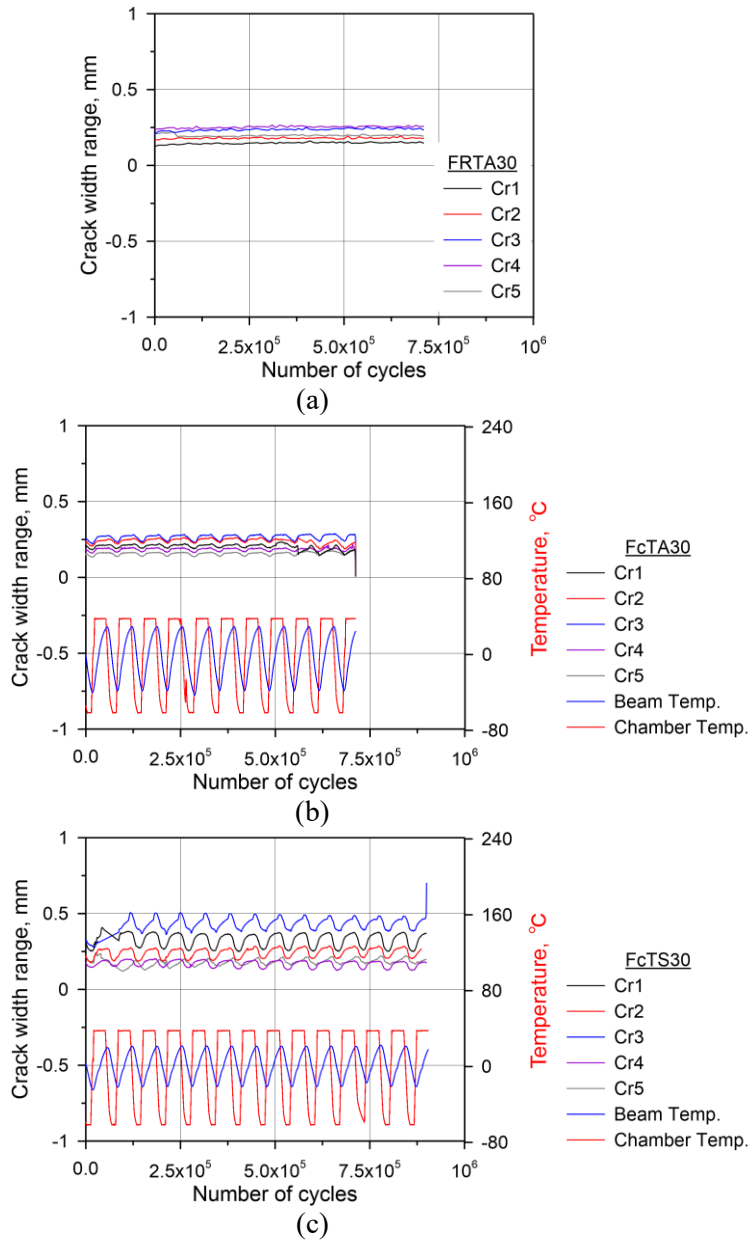


Figure 4.82 Crack width range of 30 MPa RC beams: (a) FRTA30; (b) FcTA30; (c) FcTS30

Similarly, the position of crack gauge in 60 RC beams was depicted as shown in Figure 4.83. It concluded both flexural and shear cracks, and crack gauges were evenly distributed in each sides of shear zone.

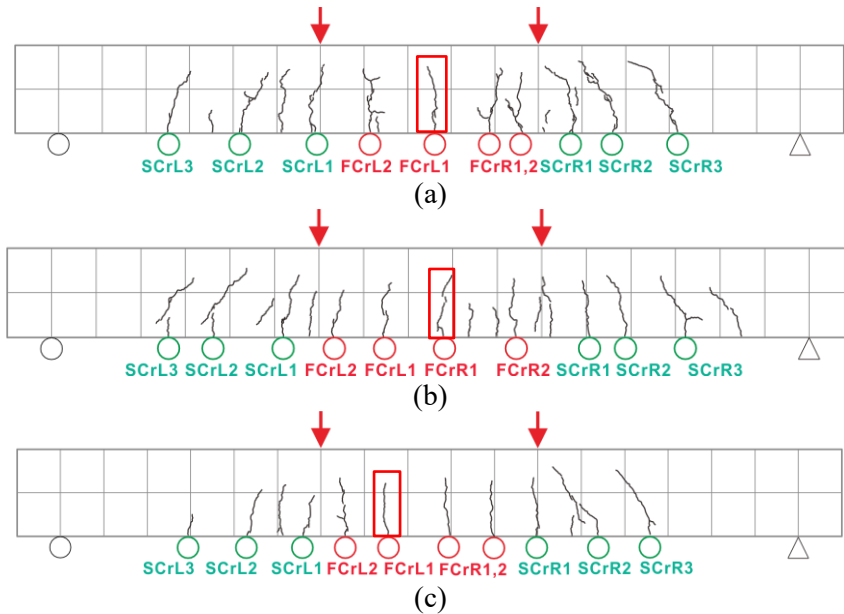


Figure 4.83 Position of crack gauges in 60 MPa RC beams: (a) FRTA60; (b) FcTA60; (c) FcTS60

Figure 4.84~4.85 illustrated the crack width range of 60 RC beams under different temperature conditions. Both flexural and shear crack width showed a similar behavior with 30 MPa RC beams. It exhibited less variation under the effect of freeze-thaw cycles, however, an increasing effect of seawater can be observed in FcTS60. Compared to 30 MPa RC beams, the increasing rate was relatively smaller contributed to the denser pore structures, signifying a little effect of freeze-thaw cycles and seawater on 60 MPa RC beam.

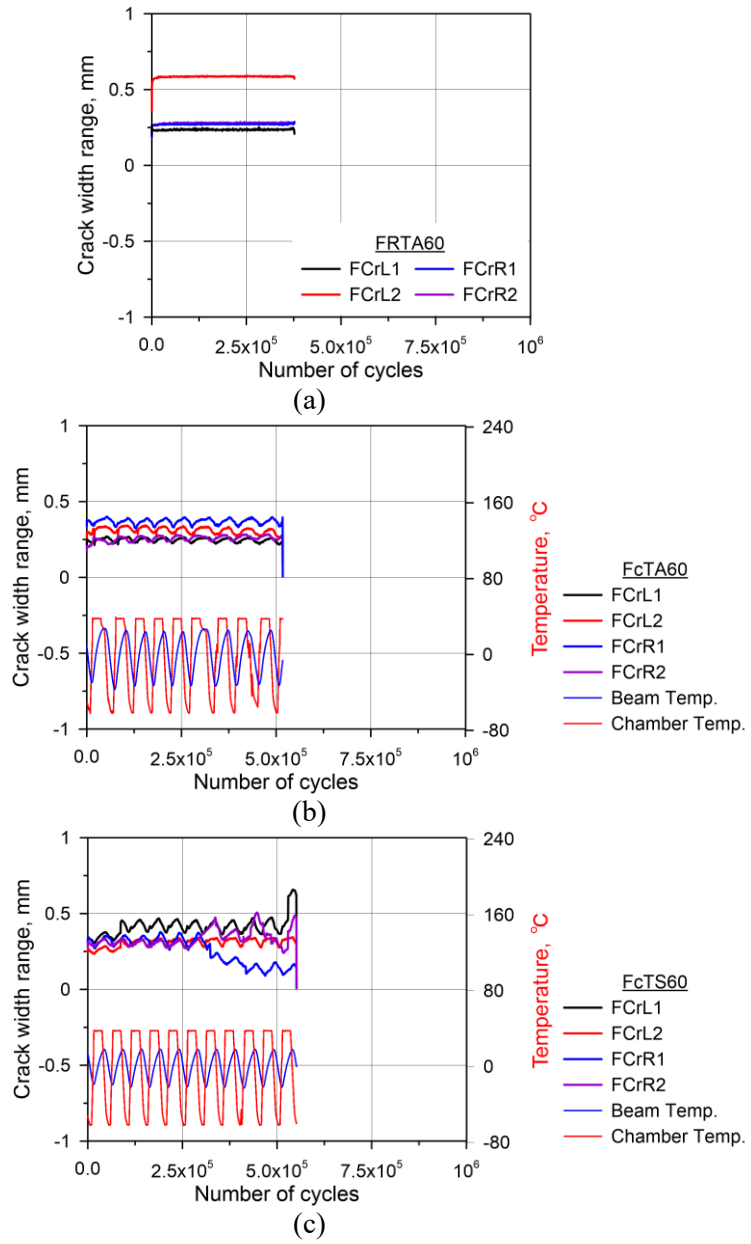


Figure 4.84 Flexural crack width range of 60 MPa RC beams: (a) FRTA60; (b) FcTA60; (c) FcTS60

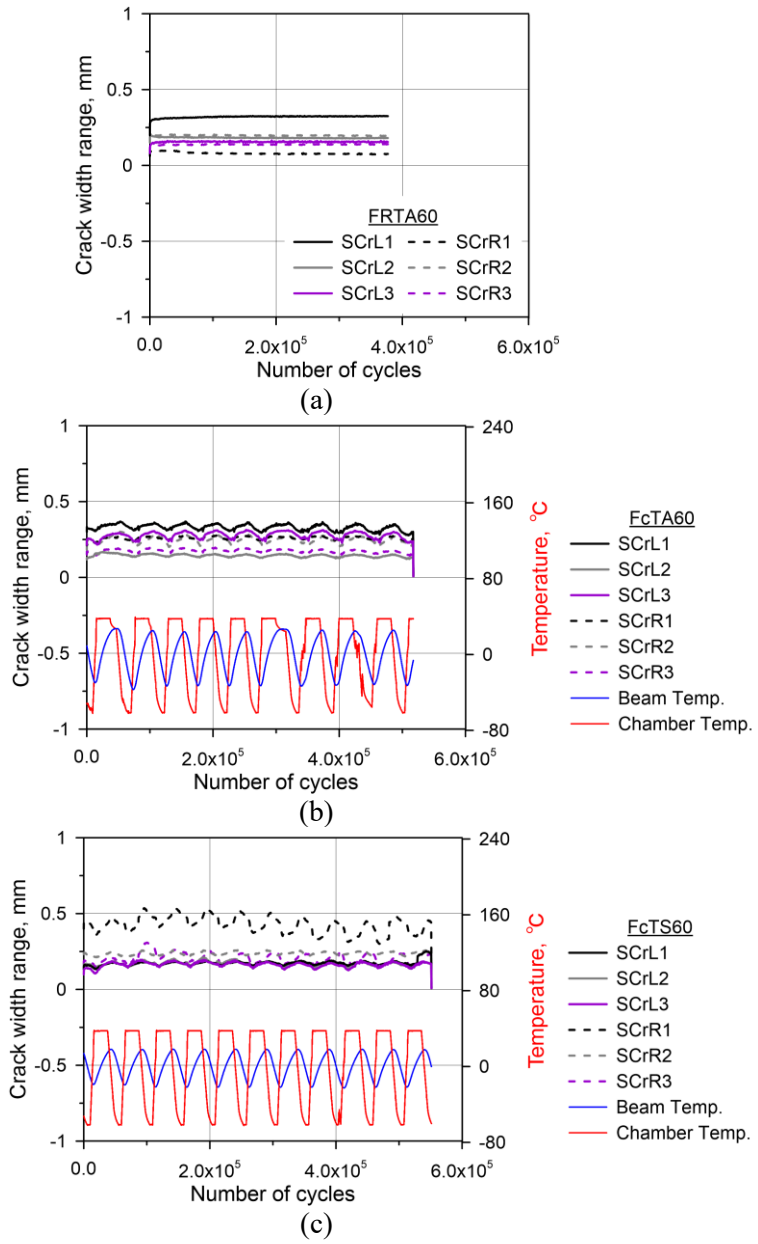


Figure 4.85 Shear crack width range of 60 MPa RC beams: (a) FRTA60; (b) FcTA60; (c) FcTS60

#### 4.4.3.3 Central deflection

Central deflection of RC beams including deflection range was analyzed in order to evaluate the deformation capacity as shown in Figure 4.86. Central deflection increased along with the number of cyclic loading. FcTA30 that was subjected to freeze-thaw cycles with air-cured condition presented an increased deflection, compared to FRTA30. Generally, the deflection of FcTA30 should be equal to FRTA30 when they were at room temperature, and thus the deflection will be different only under low temperature. However, it was shown that the 30 MPa concrete under freeze-thaw cycles decreased, therefore, the entire capacity of RC FcTA30 can be decreased which further lead to increase of deflection. In contrast to FcTA30, FcTS30 exhibited a smaller deflection at initial stage, even though subjected to freeze-thaw cycles. This was possibly attributed to the formation of chloride crystallization, which made micro structure denser (Zhang and Wu, 2019). The chloride crystallization not only making microstructure denser but also generating micro-cracks. At low stress, the connected pores and microcracks in concrete are compacted (Yuan et al. 2020). A similar behavior was also exhibited in 60 MPa RC beams as shown in Figure 4.87. However, less effect of freeze-thaw cycles and seawater can be found, implying a greater durability by the smaller porosity of 60 MPa concrete.

Deflection range of 30 MPa showed the largest fluctuation in FcTS30 due to the higher water content. At room temperature, the deflection range was similar to FRTA30, but decreased at low temperature contributed to the frozen pore water. This behavior was smaller in 60 MPa RC beams as shown in Figure 4.87, in which the absorbed seawater was less than 30 MPa RC beams.



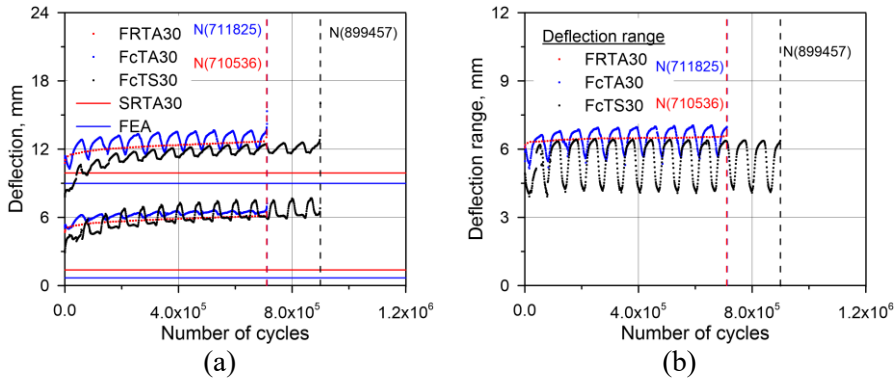


Figure 4.86 Central deflection of 30 MPa RC beams: (a) Deflection-N relation; (b) Deflection range-N relation

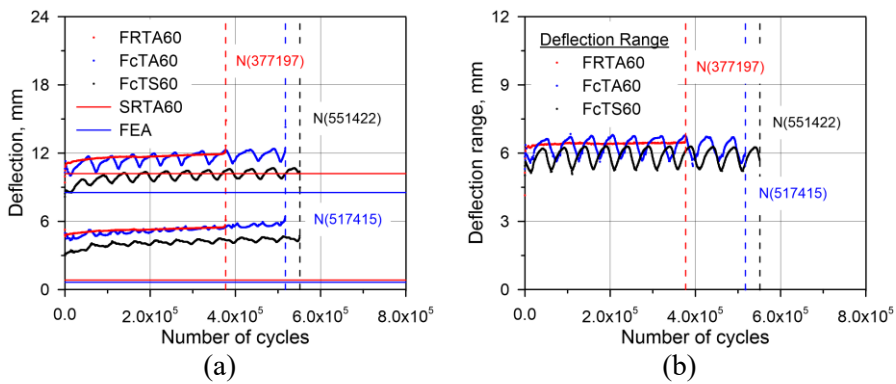


Figure 4.87 Central deflection of 60 MPa RC beams: (a) Deflection-N relation; (b) Deflection range-N relation

Central deflection increasing ratio of RC beams were compared as shown in Figure 4.88~4.89. This was indicated by the ratio of deflection at certain number of loading cycles to the initial deflection. In 30 MPa RC beams, FcTA30 showed greater increasing ratio as the cyclic loading increased, signifying an accelerated damage accumulation under freeze-thaw cycles. At low stress level, the connected pores and microcracks that was generated by formation of

expansive products were compacted, leading to a smaller central deflection. As the loading cycles increased, the compacted effect was overcompensated, leading to the increase of microcracks (Bao and Wang, 2017; Lim et al. 2000). Therefore, with the support of expansion stress of the chloride crystals FcTS30 showed the greatest increasing ratio of central deflection, which was up to 68% while FRTA30 and FcTA30 presented 21% and 39%, respectively.

In 60 MPa RC beams, FcTS60 that was saturated by seawater also showed the greatest increasing ratio of 26%, but a smaller difference compared to FRTA60 and FcTA60 that were 21% and 17%, respectively. The greater durability of 60 MPa concrete may account for the less difference among three RC beams. At material level, 60 MPa concrete showed less variation under freeze-thaw cycles and seawater saturation, leading to a less variation of performance at structural level.

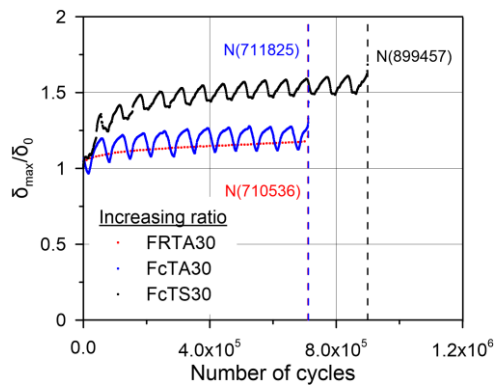


Figure 4.88 Central deflection increasing ratio of 30 MPa RC beams

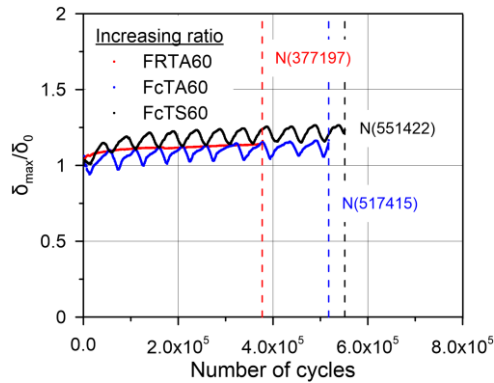


Figure 4.89 Central deflection increasing ratio of 60 MPa RC beams

The flexural stiffness of RC beams including decreasing ratio with respect to number of cyclic loadings was analyzed as depicted in Figure 4.90~4.91. Flexural stiffness of showed the smallest value in FcTS30, compared to FRTA30 and FcTA30, which was due to the formation of chloride crystals in concrete pore. Under the effect of freeze-thaw cycles and seawater, FcTS30 showed the greatest decreasing ratio of stiffness which was 41%, whereas FRTA30 and FcTA30 respectively had 17% and 22%.

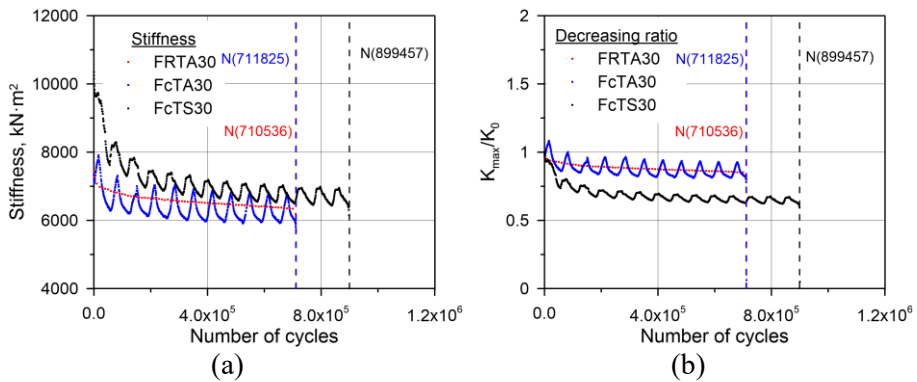


Figure 4.90 Flexural stiffness of 30 MPa RC beams: (a) Stiffness-N relation;  
(b) Stiffness increasing ratio-N relation

The decreasing ratio of flexural stiffness showed similar value among RC beams with 60 MPa concrete. Only a slightly higher increasing ratio was found in FcTS60 that was by approximately 21%, while 17% and 14% was calculated in FRTA60 and FcTA60, respectively. It can be concluded that freeze-thaw cycles had little effect on flexural stiffness, especially on 60 MPa RC beams. Under the combined effect of freeze-thaw cycles and seawater, damage accumulation was faster attributed to the formation of chloride crystals in concrete pores. Compared to 30 MPa RC beams, RC beams with 60 MPa concrete showed less variation under freeze-thaw cycles and seawater.

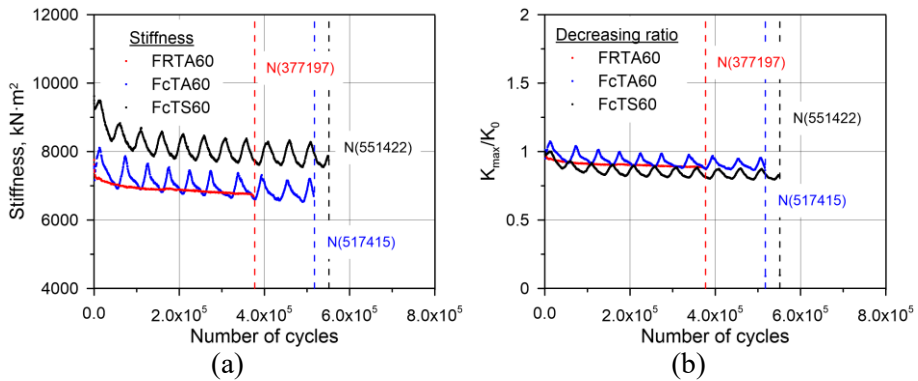


Figure 4.91 Flexural stiffness of 60 MPa RC beams: (a) Stiffness-N relation;  
(b) Stiffness increasing ratio-N relation

#### 4.4.3.4 Strain of reinforcing bars

Tensile strain of reinforcing bars along with number of cyclic loading was compared as given in Figure 4.92~4.93. The strain range was then calculated based on measured tensile strain. Limited strain data were obtained due to the damage of strain gauges. However, there were more than 10% of the strain data were measured, and thus still available to be comparatively analyzed as illustrated in chapter 4.4.2.4.

From the measured data it can be found that FcTA30 presented larger tensile strain that was possibly attributed to the shrinkage of concrete. During the immersion in seawater, the shrinkage of RC beam recued, resulting in decreased of strain in FcTS30. Furthermore, decreased deflection by seawater directly decreased the deformation of tensile reinforcing bars. FcTS30 showed larger variation in strain range due to the repeated change of RC beam capacity under freeze-thaw cycles. The enhancing effect of low temperature during freeze-thaw cycle can account for the increased fatigue life of RC beams.

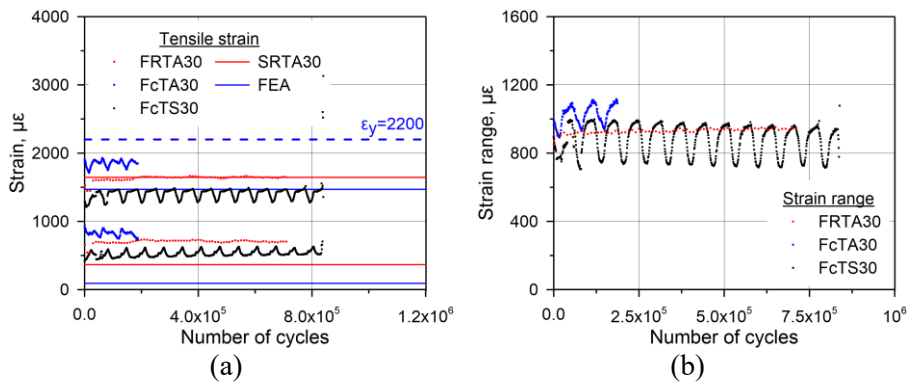


Figure 4.92 Tensile strain of 30 MPa RC beams: (a) Strain-N relation; (b)

Strain range-N relation

A similar fatigue behavior can be observed in 60 MPa RC beams in which the air-cured FcTA60 presented the largest tensile strain, implying the effect of shrinkage on tensile strain. With seawater-saturated condition, FcTS60 had a smaller tensile strain, compared to FRTA60 and FcTA60, signifying the mitigation of shrinkage during immersion. The effect of seawater was less than in 30 MPa RC beams based on the fluctuation of stress range under freeze-thaw cycles.

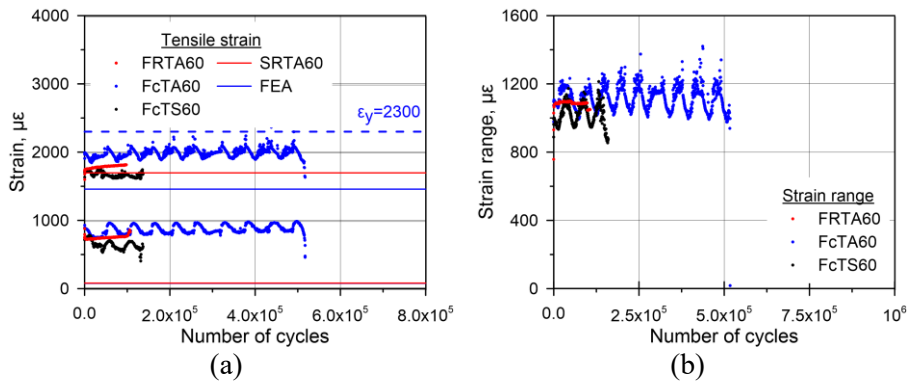


Figure 4.93 Tensile strain of 60 MPa RC beams: (a) Strain-N relation; (b) Strain range-N relation

Except for the tensile strain and strain range, the tensile increasing ratio that was to evaluate the velocity of damage accumulation was compared as shown in Figure 4.94. FcTA30 showed by 4% increasing ratio, which was smaller than FRTA30 with 9%, demonstrating little or adverse effect of freeze-thaw cycles under air-cured condition. It can be found that FcTS30 showed the greatest increasing ratio by approximately 15%, implying the accelerated damage accumulation under combined effect of freeze-thaw cycles and seawater.

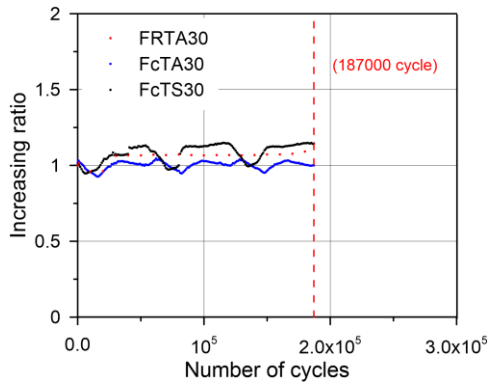


Figure 4.94 Tensile strain increasing ratio of 30 MPa RC beams

In the case of RC beams with 60 MPa concrete, less variations can be found among comparisons as given in Figure 4.95. Compared to FRTA60 with increasing ratio of 4%, FcTA60 presented a similar increasing ratio of 7%. FcTS60 had an increasing ratio of 6% under the freeze-thaw cycles and seawater resistance, demonstrating the greater durability of 60 MPa concrete. The greater freeze-thaw and seawater resistance was contributed to the smaller porosity of concrete.

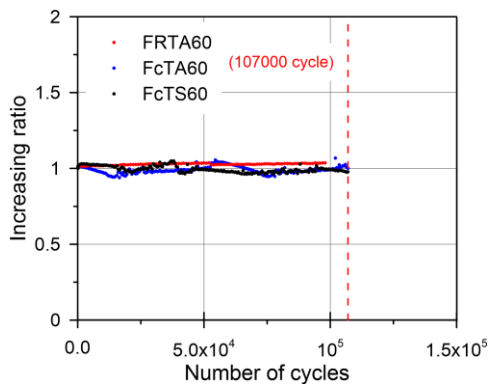


Figure 4.95 Tensile strain increasing ratio of 60 MPa RC beams

Following the tensile strain, the corresponding compressive strain of RC beams with 30 MPa concrete was compared as shown in Figure 4.96. Increased compressive strain was found in FcTA30 and FcTS30, which can be caused by the degraded concrete properties. As the concrete strength decreased, the stress distribution in compression rebar will increase, reflecting an increased compressive strain. Considering the beam curing method, air-cured FcTA30 had a slightly larger compressive strain, which can be caused by the larger tensile strain based on force equilibrium.

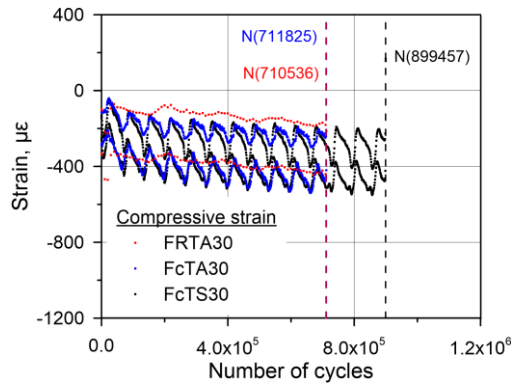


Figure 4.96 Compressive strain of 30 MPa RC beams

RC beams with 60 MPa concrete showed a larger difference among three specimens as given in Figure 4.97. At first, the neutral axis of FRTA60 was found to surpass the compression rebar, and therefore the compression rebar behaved in a tensile manner. Under freeze-thaw cycles, the increased tensile strain of FcTA60 directly resulted in the larger compressive strain in accordance with force equilibrium in cross-section of RC beam. The compressive strain of FcTS60 presented a relatively smaller value since the shrinkage of RC beam reduced during seawater immersion.



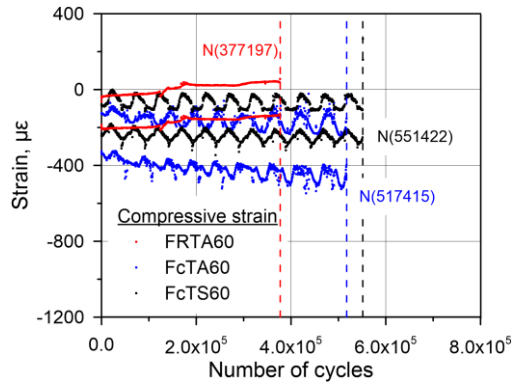


Figure 4.97 Compressive strain of 60 MPa RC beams

#### 4.3.3.5 Summary

Test results implied that the freeze-thaw cycles increased fatigue life of RC beams which can be primarily occurred by increased the capacity of RC beam during freezing stage of freeze-thaw cycles. It turned out that seawater increased the crack width under freeze-thaw cycles possibly due to the reduced number of cracks. The reduced number of cracks may result in greater crack width at the same load. This behavior was also detected in 60 MPa RC beams, however, the difference was relatively small because of the smaller porosity of high strength concrete. Seawater was found to decrease the deflection of RC beams which can be caused by the denser microstructure of concrete and less shrinkage of RC beam by seawater immersion. Furthermore, seawater accelerated the damage accumulation under freeze-thaw cycles which was demonstrated by the greater deflection and tensile strain increasing ratio. Additionally, seawater decreased strain range which was possibly by the reduced cracks, leading to the decreased rebar stress.

## **4.5. Overall Comparison of Static and Fatigue Behavior**

Two types of structural tests were conducted, which were categorized into flexure and fatigue tests. The objectives of two types of structural tests were to investigate the structural behavior under combined effect of freeze-thaw cycles, seawater, and applied load. Herein, the necessity of two types structural tests were analyzed based on experimental and analytical results.

The primary feature of static and fatigue tests was detailed as shown in Table 4.5. In static tests, the primary structural behavior such as ultimate strength, ultimate deflection, ultimate strain, and crack width was experimentally investigated. The structural behavior in static tests focus on the ultimate capacity of RC beam, indicating the limit under extreme conditions. Referring the fatigue behavior, it was mainly concentrated on the above-mentioned structural behavior with respect to number of cyclic loadings, showing the damage accumulation process along with time.

With the basis of experimental results, the main limitation of static test was that the structural behavior under repeated loading cannot be estimated. Considering the actual conditions, most of the RC structures behaved within the limit of ultimate strength, and cyclic response at service load was the most common state. The fatigue tests in which the reliable fatigue life prediction is available. Moreover, the fatigue behavior at structural level can be investigated. Therefore, both static and fatigue tests needed to be considered in design for better understanding of RC beam under aggressive environment.

Table 4.5 Primary feature of static and fatigue tests

Beam ID	Structural behavior of RC beams				Note
	Load	Deflection	Strain	Crack width	
Static	Ultimate strength	Ultimate deflection Ductility	Ultimate strain	Crack width	Evaluation of ultimate capacity
Fatigue	Fatigue life	Deflection-N	Strain-N Stress range	Crack width-N	Fatigue life prediction under repeated loading

## 4.6. Concluding Remarks

In this chapter the experimental results of flexure and fatigue tests were illustrated for the purpose of investigating the effect of concrete strength, freeze-thaw cycles, and seawater. The primary experimental results were exhibited as follows.

Under combined effect of freeze-thaw cycles and seawater, there were 41% and 26% reduction of concrete strength and elastic modulus in 30 MPa concrete. In 60 MPa concrete, only 5% and 6% deterioration of concrete strength and elastic modulus was observed. At structural level, RC beams all failed by the crushing of concrete at compression zone and concrete strength did not affect the failure mode. 60 MPa RC beams exhibited 56% and 7% larger cracking load and ultimate load, respectively. The tensile rebar strain of 60 MPa RC beams showed greater value than 30 MPa RC beams. This was possibly attributed by the greater autogenous shrinkage of high strength concrete which was verified based on section analysis. Besides, 30 MPa RC beams revealed 44% smaller ductility compared to the 60 MPa RC beams, and this behavior was exacerbated under the combined effect of freeze-thaw cycles and seawater, implying the more deterioration of 30 MPa specimen.

RC beams with 30 MPa concrete had 46% and 9% greater increasing ratio than 60 MPa RC beams in terms of central deflection and tensile strain, respectively. Moreover, the range of crack width was greater in 30 MPa RC beams under combined effect of freeze-thaw cycles and seawater, indicating the smaller resistance of 30 MPa concrete RC beam under aggressive condition.

However, 60 MPa RC beams showed shorter fatigue life than 30 MPa RC beams, which can be attributed to the increased bond strength. Increased bond strength of RC beam can further reduce the range of bond loss, and finally increased strain range.

In static tests, freeze-thaw cycles decreased the cracking load and ultimate strength of RC beams. Moreover, previous studies referred that freeze-thaw cycles could decrease the bond strength of RC beams (Peterson, 2007; Jang, 2009; Cao, 2015), leading to a smaller strain at the same load level. Under the combined effect of freeze-thaw cycles and seawater, ultimate load and ductility of RC beam further decreased. It should be noted that the cracking load of RC beam increased that was possibly due to the formation of chloride crystals in concrete pores, resulting in the denser microstructure. Then the denser microstructure possibly reduced the number of cracks, leading to the increase of crack width at the same load.

In fatigue tests, fatigue life increased under freeze-thaw cycles contributed to the improved capacity of RC beam in freezing stage of freeze-thaw cycles. Seawater increased the crack width under freeze-thaw cycles possibly due to the reduced number of cracks, resulting in the greater crack width at the same load. Seawater decreased the deflection of RC beams which can be caused by the denser microstructure of concrete and reduced shrinkage during seawater immersion. Tensile strain decreased after immersion of seawater possibly caused by the reduction of shrinkage. Furthermore, the damage accumulation was accelerated under the combined effect of freeze-thaw cycles and seawater.

## **V. Analytical Study**

### **5.1. Introduction**

Flexure and fatigue tests were conducted to investigate the combined effect of freeze-thaw cycles, seawater, and applied load on structural behavior of RC beams in Chapter 4. It was concluded that freeze-thaw cycles decreased the material properties of concrete and structural behavior of RC beams. The performance of concrete and RC beam further decreased under the combined effect of freeze-thaw cycles, seawater. In this Chapter, analytical studies on flexure tests were conducted to predict the crack width of 30 MPa RC beams, and the effect of concrete strength on crack width was presented. Moreover, the analytical studies on fatigue tests was carried out which verified the fatigue life of RC beams based on existing models.

In flexure tests, the crack width of RC beams which was a primary index to evaluate the structural behavior. However, the crack width of RC beams with 30 MPa concrete was not able to be measured in flexure tests due to the insufficient testing apparatus. Furthermore, the cracks on RC beams were randomly propagated and thus was hard to quantitatively measure and analyze. Therefore, considering the limited testing conditions and random distribution of cracks, the crack width of RC beams under monotonic loading need to be predicted.

The fatigue life of RC beams was predicted based on existing prediction model by which the validity of test results was verified. The differences

between predicted and experimental results were analyzed from the formulation of existing models. Most of current prediction models were formulated in accordance with rebar tests in which the effect of bond between concrete and steel cannot be properly considered. Considering the difference between material and structural tests, the modified prediction model for fatigue life on the basis of existing model was proposed.

## 5.2. Analytical Study on Static Behavior

### 5.2.1 Geometry Model

Six RC beams were simulated with 3-Dimensional model. The analyses were conducted with the same dimension of RC beams in DIANA commercial programs as presented in Figure 5.1. The steel plate on the loading point and support was modeled to better simulate the experiment. Concrete members and steel plates were modeled with eight-node solid elements, and reinforcement was embedded in concrete member to achieve composite action under monotonic loading.

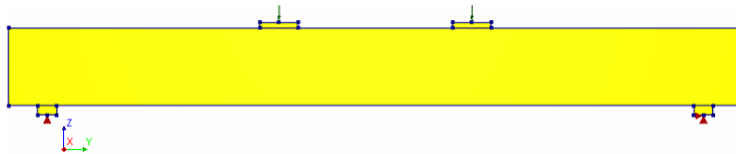


Figure 5.1 Geometry model of RC beam in finite element analysis

### 5.2.2 Material Model

#### 5.2.2.1 Concrete

As a heterogeneous material, cracks in RC beams were hard to predicted in advance, and therefore the smeared cracking was adopted considering the unpredictable crack propagation of RC beams. Total strain-based model was used for a stable analysis of 3-Dimensional RC beams.

Compressive behavior of concrete applied the testing data obtained from concrete cylinder compression tests. Besides, Thorenfeldt model, as given in



Equation 5.1~5.2, fit with material testing results that were compressive strength and peak strain of concrete. In general, the compressive tests of concrete cylinder vary among repeated tests due to the heterogeneity of concrete, and thus the existing models reflected with averaged material results was used.

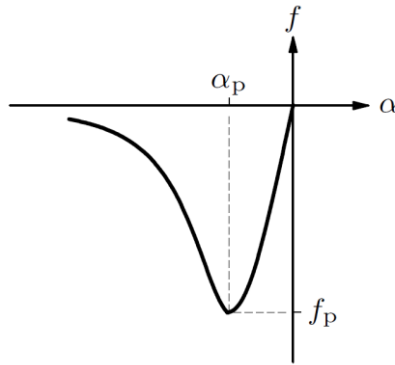


Figure 5.2 Thorenfeldt compression curve

$$f = -f_p \frac{\alpha}{\alpha_p} \left( \frac{n}{n - \left( 1 - \left( \frac{\alpha}{\alpha_p} \right)^{nk} \right)} \right) \quad (5.1)$$

Herein, the  $n$  and  $k$  were respectively

$$n = 0.80 + \frac{f_{cc}}{17}; \quad k = \begin{cases} 1 & , \text{ if } \alpha_p < \alpha < 0 \\ 0.67 + \frac{f_{cc}}{62} & , \text{ if } \alpha \leq \alpha_p \end{cases} \quad (5.2)$$

The tensile behavior was modeled with linear-crack energy model in which the Mode-I fracture energy was considered. The tensile strength of concrete was calculated based on existing model (Chen, 2007), as given in Equation 5.3, since the tensile tests were not able to be conducted. This equation was derived based simply supported beam tests, and valid for a monotonically loaded beam.

$$f_{ct} = 0.26\sqrt{f_c} \quad (5.3)$$

The representative stress-strain curve based on Thorenfeldt model and linear-crack energy was established, as depicted in Figure 5.3. From the stress-strain curve, it can be concluded that the fitting curve showed close value with testing results.

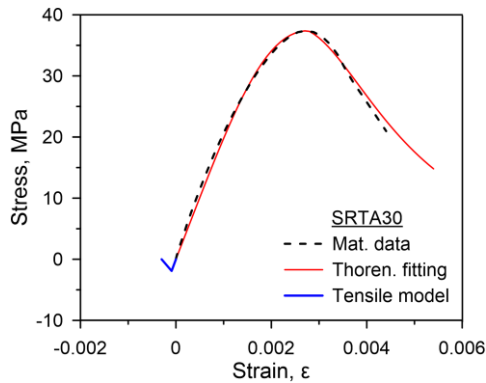


Figure 5.3 Stress-strain curve of concrete in FEA

### 5.2.2.2 Reinforcement

The discrete reinforcement element was used in FE model which was to verify the rebar strain at each component. Embedded reinforcement was applied in order to fully achieve the composite behavior with concrete in RC beams. Moreover, the material tests data were reflected in Von mises plasticity model, incorporating the hardening behavior in elastoplastic material model, as shown in Figure 5.4.

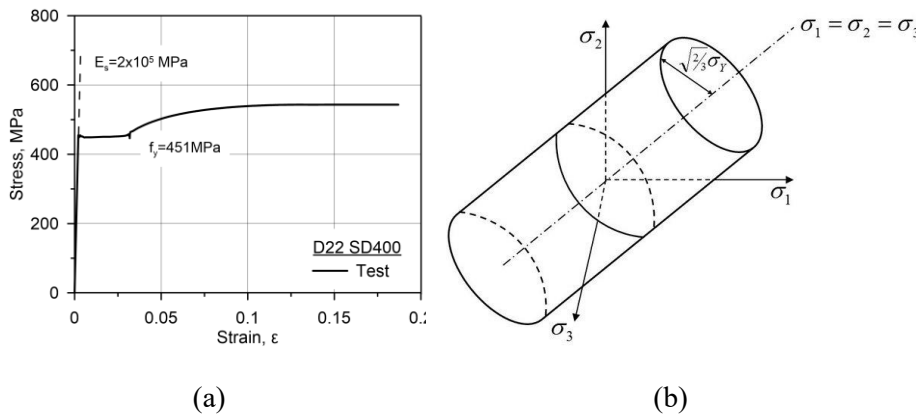


Figure 5.4 Plasticity model for reinforcement: (a) Material tests result; (b) Von mises plasticity model

### 5.2.2.3 Steel plate

The incremental load was applied on the steel plates which were modeled as linear elastic with elastic modulus of 200,000 MPa. This was to prevent the local failure of concrete in compression zone. Considering the vertical compressive force from loading, the properties of interface was out of consideration in the FE analysis.

### **5.2.3 Boundary Conditions**

Boundary conditions were simulated based on experiments that were roller and hinge in two supports. This was achieved by constraining the two support in vertical displacement and allowing horizontal freedom in roller support. Steel plate with 50 mm width was modeled in support, which was to minimize fixed moment force on supports but to ensure the local failure under exerted loading.

### **5.2.4 Analysis Results**

#### *5.2.4.1 Central deflection*

The central deflection of 30 MPa RC beams was verified as shown in Figure 5.5. FEA results were in a good agreement with experimental results with 10% difference in yield and ultimate load. Compressive behavior by material tests and Thorenfeldt fitting model showed close prediction, implying the feasibility of the fitting model in further analysis. With the consideration of seawater saturation, the stiffness predicted by FEA exhibited smaller value compared to experimental results. This can be caused by the different amounts of expansive products in concrete pores at material and structural level. Concrete cylinders were saturated in the same seawater with RC beams, but the ratio of weight increase was estimated to be different based on weight change. Therefore, the effect of seawater on concrete cylinders and RC beams can be differ, leading to the difference in stiffness prediction.

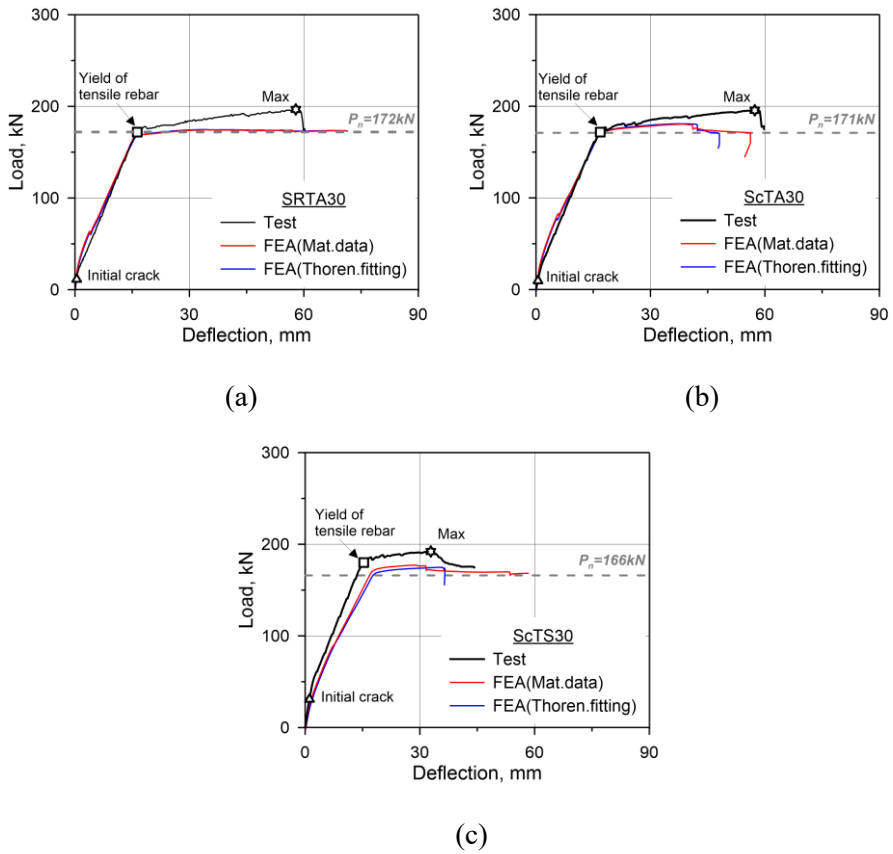


Figure 5.5 Load-deflection relation of 30 MPa beam in FEA: (a) SR TA30; (b) Sc TA30; (c) Sc TS30

In 60 MPa RC beams, FEA well predicted the experimental results as given in Figure 5.6. There was smaller prediction of stiffness in SR TA60 and Sc TA60, which can be attributed the shrinkage of RC beams during air-cured condition. This phenomenon was not found in Sc TS60 since the shrinkage can be mitigated by adequate water supply during seawater immersion. There was less variation of material properties of 60 MPa concrete under freeze-thaw cycles and seawater which accounted for the close prediction in Sc TS60.

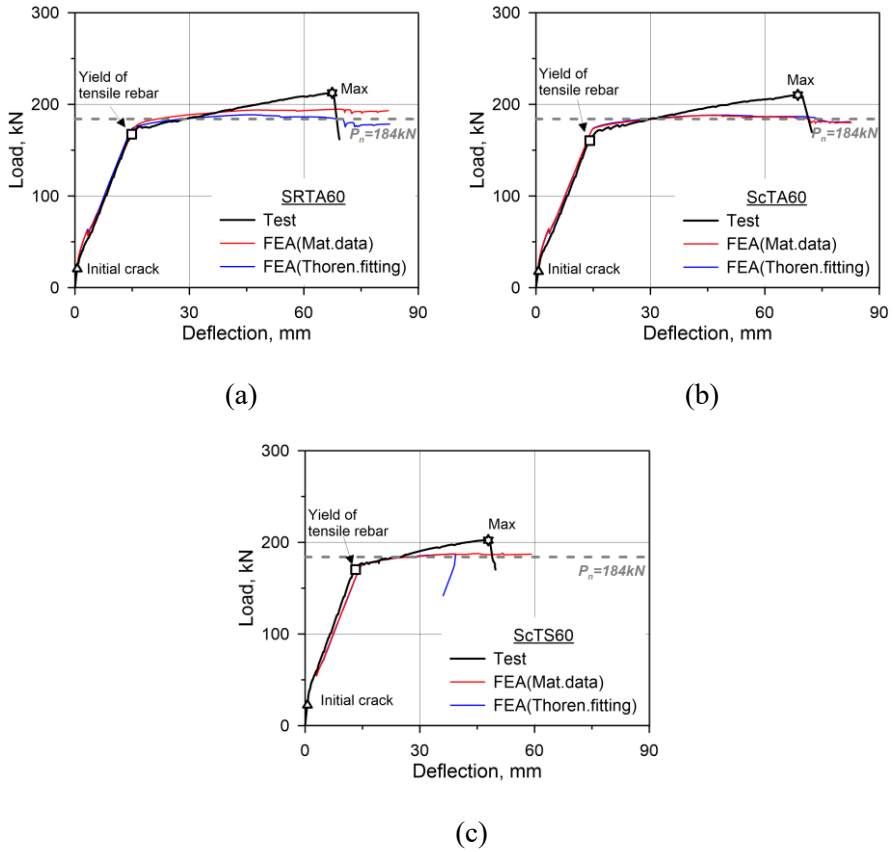


Figure 5.6 Load-deflection relation of 60 MPa beam in FEA: (a) SRTA60; (b) ScTA60; (c) ScTS60

#### 5.2.4.2 Strain of reinforcing bars

The strain of reinforcing bars was then verified by comparing to the experimental results, as depicted in Figure 5.7. FEA results predicted smaller tensile strain at initial stage, which was possibly attributed to the shrinkage. It showed opposite behavior in ScTS30 where the FEA had smaller strain compared to test results. During the seawater immersion, the shrinkage would be reduced and degree of reduction in material and structural level can be differ.

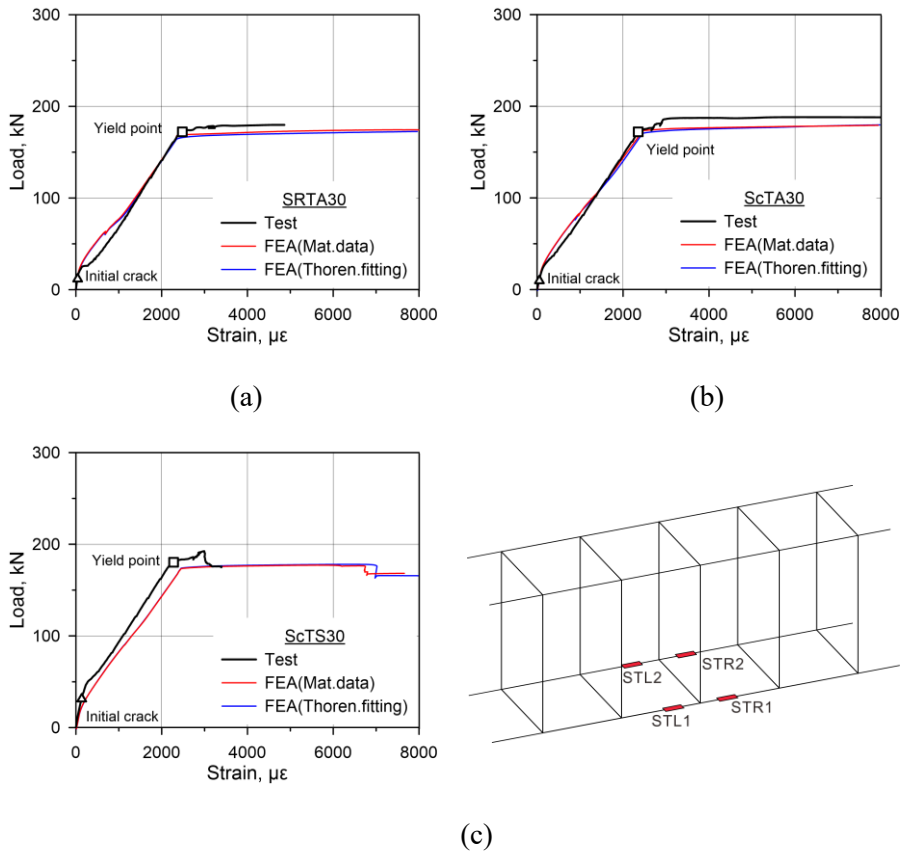


Figure 5.7 Load-strain relation of 30 MPa beam in FEA: (a) SRTA30; (b) ScTA30; (c) ScTS30; (d) Position of strain gauges

In 60 MPa RC beams, the smaller strain of reinforcing bars at the same load level were predicted by FEA, as shown in Figure 5.8. The smaller strain of SRTA60 and ScTA60 was possibly attributed to the shrinkage strain during air-cured condition but ScTS60 did not present the behavior. This can be due to the mitigated shrinkage of ScTS60 by sufficient water supply during immersion.

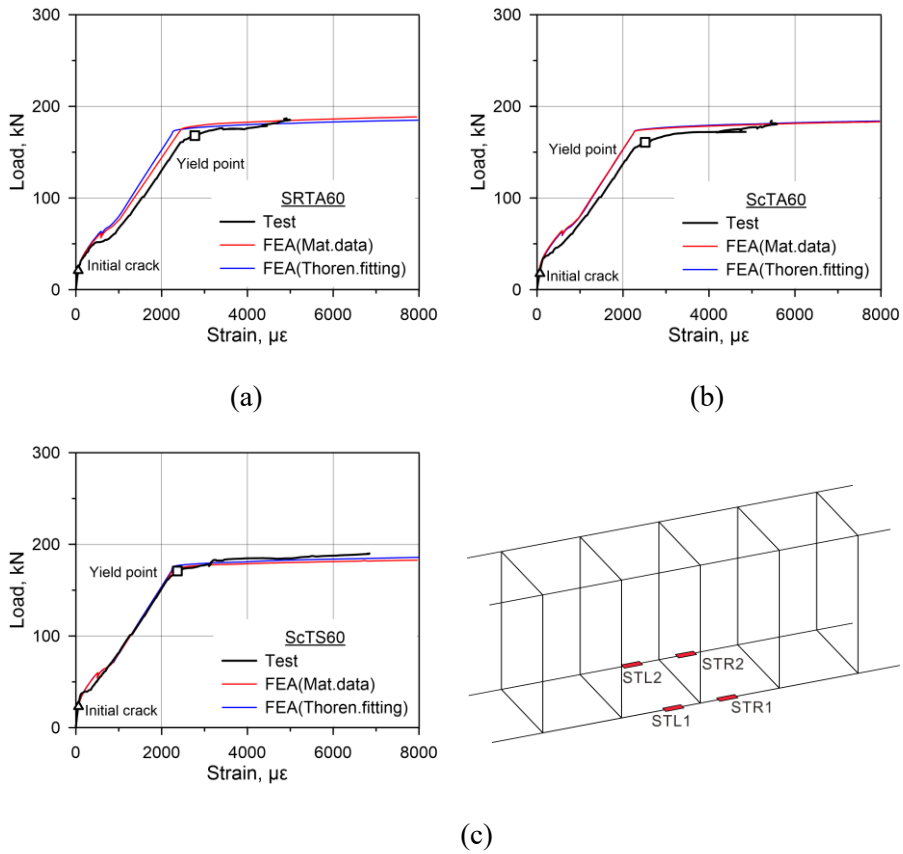


Figure 5.8 Load-strain relation of 60 MPa beam in FEA: (a) SRTA60; (b) ScTA60; (c) ScTS60; (d) Position of strain gauges

#### 5.2.4.3 Crack width

The crack width of 60 MPa RC beams were measured from experiments and predicted based on FEA. Figure 5.9 showed the variation of crack width along with incremental loading. Crack widths were measured in reloading stage, during which the cracking behavior was not able to be captured again, resulting in the discrepancy at initial loading stage. The maximum crack width of RC beams was compared for the purpose of evaluating the most severe condition.



Also, the maximum crack width from FEA was extracted in comparison to experimental results. FEA results showed that the crack width was well predicted to experimental results. Through the comparison between prediction and test results, the validity of FE model can be verified and it may be used to predict the behavior that was not able to obtain from the test.

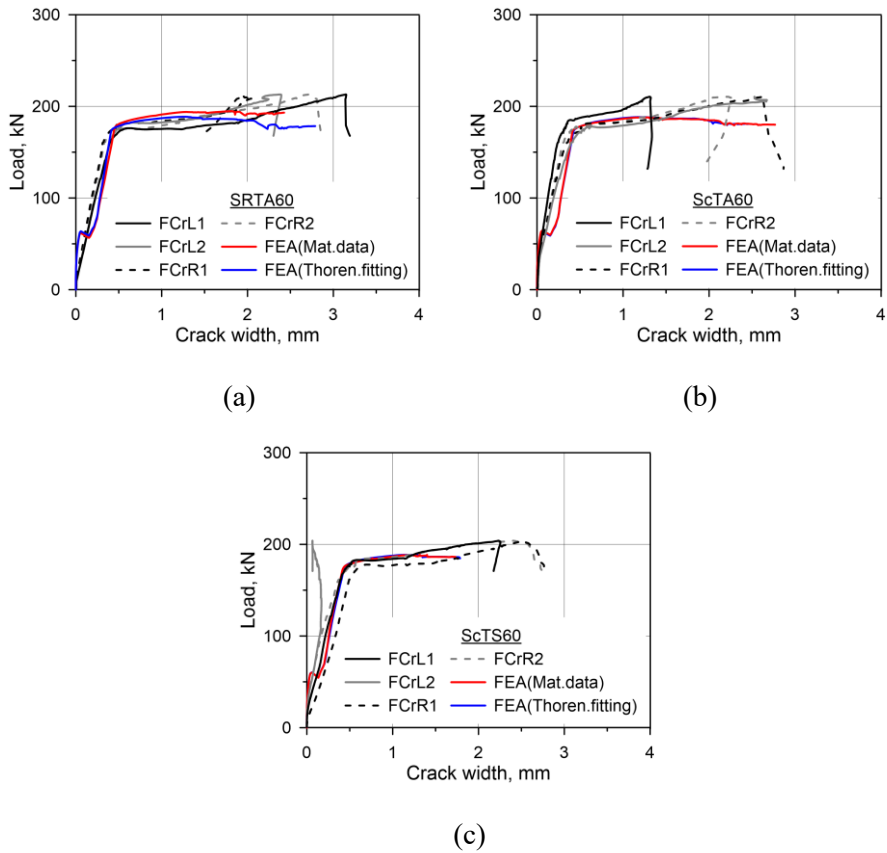


Figure 5.9 Load-crack width relation of 60 MPa beam in FEA: (a) SRTA60; (b) ScTA60; (c) ScTS60

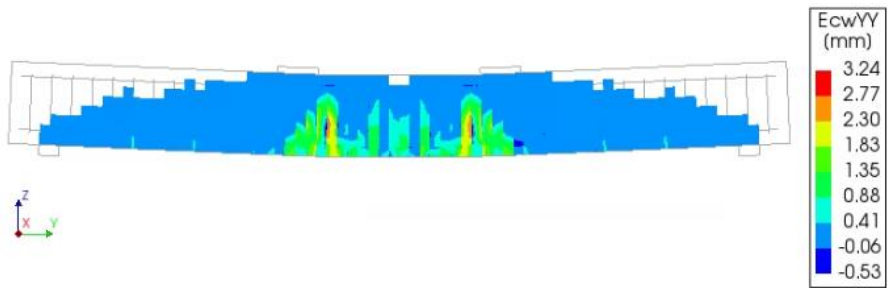
## 5.2.5 Prediction of Crack Width

The crack width of 30 MPa RC beam was predicted and the effect of concrete strength on crack widths was discussed based on prediction. Herein, RC beams with 30 MPa and 60 MPa concrete were comparatively analyzed.

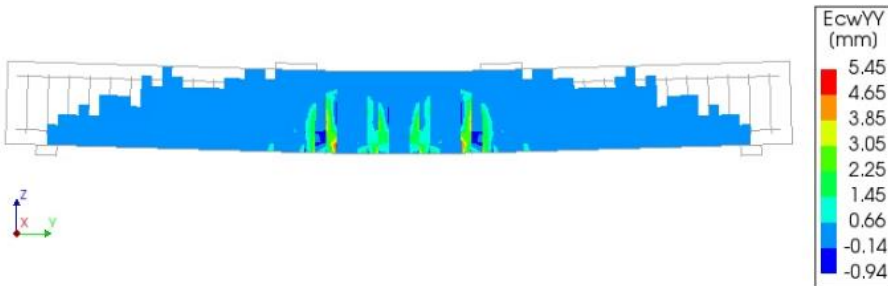
### 5.2.5.1 Crack propagation

The crack width contour of RC beams was predicted at failure, as shown in Figure 5.10. and Figure 5.11, which respectively stood for 30 MPa beams and 60 MPa RC beams. RC beams showed similar contour of crack propagation with different concrete strength, except the maximum crack width at failure. It should be noted that the maximum crack width was the local crack width at a certain point. ScTA30 showed by approximately 68% increase under freeze-thaw cycles with air-cured condition, compared to SRTA30. Considering the seawater-saturated condition under freeze-thaw cycles, ScTS30 showed further 25% increase in terms of maximum crack width, implying the increasing effect of seawater on crack width.

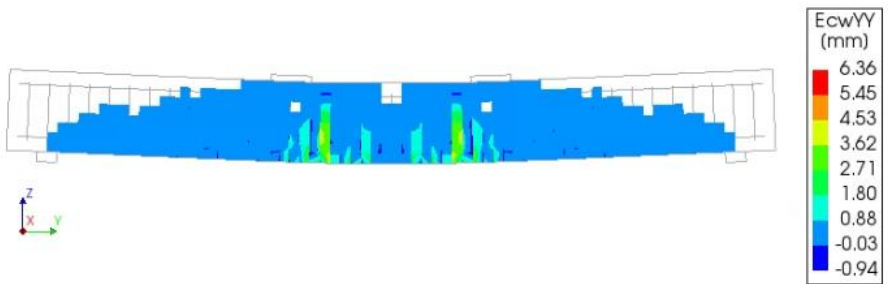
Figure. 11 showed the crack width contour of 60 MPa RC beams, and the maximum crack width showed less variation under freeze-thaw cycles with air-cured condition, but by approximately 19% increase with seawater-saturated condition which was consistent with experimental results. Seawater increased the crack width of RC beams, but less effect was found in 60 MPa RC beams contributed to the smaller porosity of concrete.



(a)

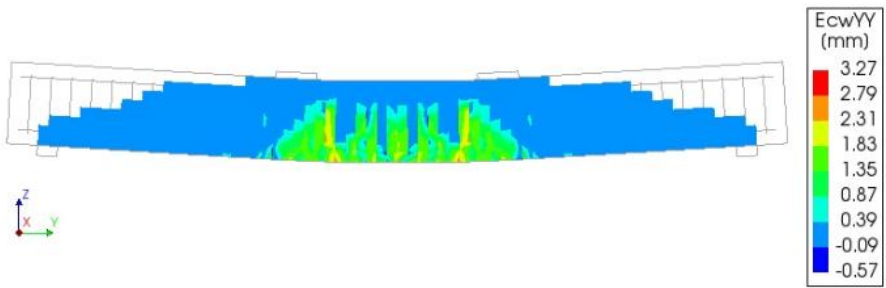


(b)

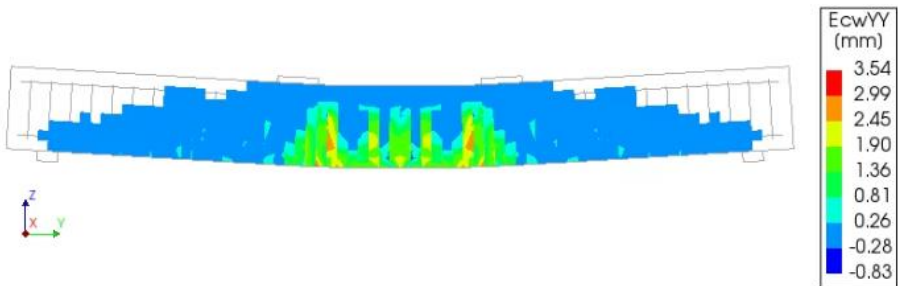


(c)

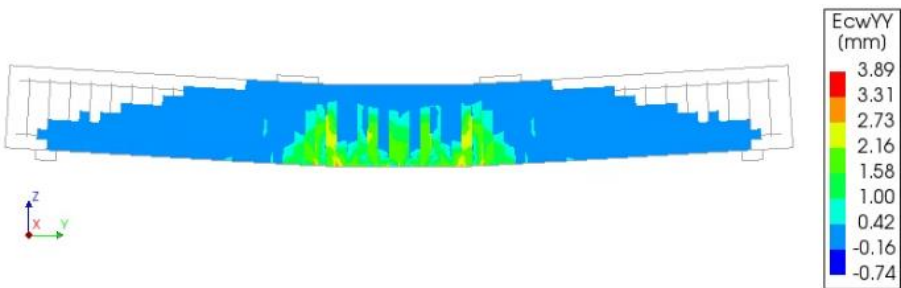
Figure 5.10 Crack width contour of 30 MPa beam in FEA: (a) SRTA30; (b) ScTA30; (c) ScTS30



(a)



(b)



(c)

Figure 5.11 Crack contour of 60 MPa beam in FEA: (a) SRTA60; (b) ScTA60;  
(c) ScTS60

### 5.2.5.2 Crack width

The crack width of 30 MPa RC beams were predicted by FEA, as shown in Figure 5.12, which were not able to measure due to the limited testing conditions. Moreover, the crack width of RC beams with 30 MPa and 60 MPa concrete strength were compared, exhibiting the effect of concrete strength on crack width. It was found that the crack width of ScTA30 slightly increased, signifying the increasing effect of freeze-thaw cycles on crack width. With seawater saturation, the crack width of ScTS30 further increased. This was possibly caused by the combined effect of freeze-thaw cycles and seawater during which the material properties of concrete decreased. The effect of temperature was reflected in FEA through the material testing data that were suffered the same freeze-thaw cycles and seawater immersion. Therefore, the decreased material properties may account for the increase in crack width.

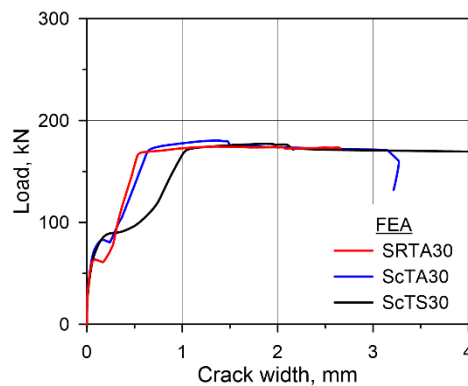


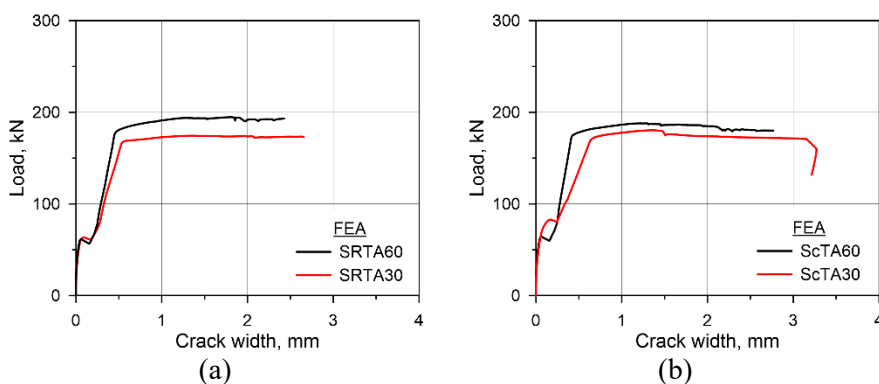
Figure 5.12 Crack width of 30 MPa beam in FEA

The predicted crack width of RC beams based on FEA were compared aiming to evaluate the effect of concrete strength on crack width, as given in Figure 5.13. Crack width only in 60 MPa RC beams were measured in flexure

tests, therefore, the comparison of crack width between 30 MPa and 60 MPa RC beams were analytically conducted. The analytical results indicated that the crack widths of SRTA30 had slight larger value in comparison to SRTA60, which revealed less effect of concrete at room temperature.

Under the freeze-thaw cycles with air-cured condition, the crack width of ScTA30 increased, in which the difference of crack width in two types of RC beam become larger. This behavior was possibly due to the greater reduction of material properties in 30 MPa concrete based on material tests result.

The crack width of ScTS30 showed greater increase compared to ScTS60 which were under the combined effect of freeze-thaw cycles and seawater saturation. Based on the material tests, the material properties of 30 MPa concrete decreased by up to 26% in terms of concrete while only less than 5% variation was found in 60 MPa. The decreased material properties would also influence the bond strength of RC beams. Therefore, the more severe cracking behavior may occur in 30 MPa RC beams.



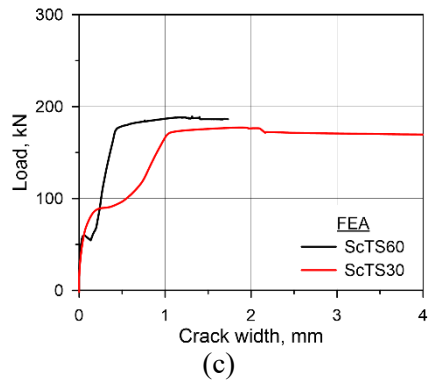


Figure 5.13 Comparison of load-crack width relation: (a) At room temperature; (b) Under freeze-thaw cycles with air-cured condition; (c) Under freeze-thaw cycles with seawater-saturation condition

### 5.3. Analytical Study on Fatigue Behavior

#### 5.3.1 Fatigue Analysis of RC beams

The fatigue life of RC beams was analyzed by three existing models, incorporating design codes and previous studies. Figure 5.14 depicted the S-N curve of steel specified in *fib* Model Code (CEB-FIP, 2010), incorporating the fatigue behavior of bars with diameter less than 40 mm. Generally, the stress range will be evaluated in accordance with a target fatigue life such as 2 million cycles or 10 million cycles. Herein, the stress range of RC beams were predicted by given fatigue life of RC beams from experiments.

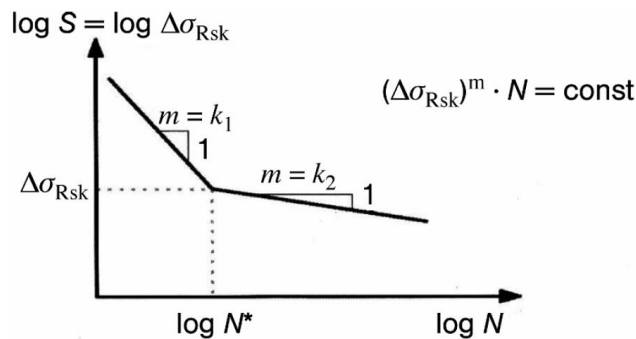


Figure 5.14 Characteristic fatigue strength curves for steel (CEB-FIP, 2010)

Equation 5.4 and 5.5 respectively stands for the prediction model proposed by Byun et al. (1997) and Helgason et al. (1976), which illustrated the relation between stress range “ $\Delta\sigma$ ” and the fatigue life “ $N$ ”.

$$\Delta\sigma = (7.825 - \log N) \cdot 100 \quad (5.4)$$

$$\Delta\sigma = (6.969 - \log N) / 0.0055 \quad (5.5)$$



The fatigue life of RC beams was analyzed based on existing prediction models as shown in Figure 5.15, and the difference of prediction results with respect to experimental results were compared, as detailed in Table 4.6. Prediction results indicated that stress range based on *fib* Model Code exhibited a conservative prediction which showed smaller stress range by given fatigue life, and thus a safe fatigue design would be conducted. Prediction by Helgason et al. (1976) presented greater prediction with some of difference greater than 10%, compared to experimental results. This can be attributed to the fact that prediction model was established based on rebar test, and the types of rebar was different from this study. Furthermore, the fatigue behavior of pure rebar and rebars embedded in RC beam can be differ since composite behavior based on bond strength will be incorporated (Byun et al. 1997). Applying the model proposed by Byun et al. (1997), stress range was predicted by less than 10%, however, the diameter of tensile rebar in RC beams was different from this study. In the experimental study by Byun et al. (1997), rebars with diameter of 16 mm were applied, while 22 mm rebars were used in this study. Therefore, prediction model with different rebar diameter may need to be compared.

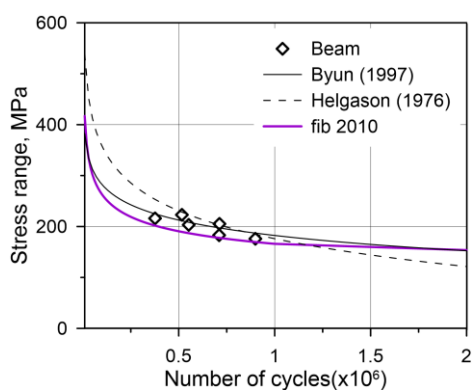


Figure 5.15 Fatigue life analysis of RC beams

Table 4.6 Comparative analysis of predicted stress range

Beam ID	Fatigue life	Stress range, MPa				Comparison		
		Test	Byun (1997)	Helgason (1976)	<i>fib</i> Model Code	(2)/ (1)	(3)/ (1)	(4)/ (1)
		(1)	(2)	(3)	(4)			
FRTA30	710,536	183	197	203	178	1.08	1.11	0.97
FcTA30	711,825	205	197	203	178	0.96	0.99	0.87
FcTS30	899,457	176	187	185	170	1.06	1.05	0.96
FRTA60	377,197	216	225	253	202	1.04	1.17	0.93
FcTA60	517,415	223	211	228	189	0.95	1.02	0.85
FcTS60	551,422	203	208	223	187	1.03	1.10	0.92

### 5.3.2 Modified Prediction Model

A modified prediction model based on testing data was established in order to investigate the difference between existing models. Nonlinear regression analyses were conducted with MATLAB program in order to establish the prediction model. The base model selected the equation of Byun et al. (1997) and Helgason et al. (1976), then the initial values were incorporated. The estimated coefficients for S-N relations were determined by conducting nonlinear regression analysis, as given in Equation 5.6.

$$\Delta\sigma=(7.560-\log N)\cdot 113 \quad (5.6)$$

With the modified prediction model, the stress range along with number of cycles was predicted, as depicted in Figure 5.16. The experimental data from previous studies incorporating rebar tests and beam tests were compared with the modified model. The modified model did not present much difference with that of existing models, showing a little effect of rebar diameter in RC beams. It can be summarized that the most of the stress range showed a larger value than predicted based on modified model, implying that RC beams would have a longer fatigue life. In a reinforced concrete, both concrete and rebar resist cyclic load in which the transmission of stress was supported by bond strength. With this manner the rebar stress in a reinforced concrete element would be reduced in comparison to the pure rebar behavior. Therefore, the S-N relation based on structural tests may need to be further developed since a safer fatigue design would possibly be achieved by considering the effect of bond strength.

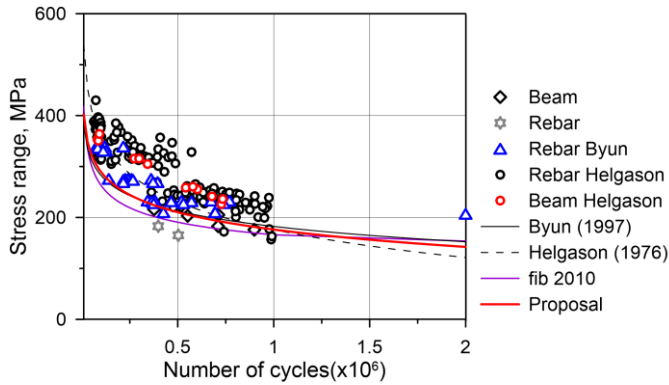


Figure 5.16 Modified prediction model of RC beams

The difference of stress range between predicted and experimental results were calculated on the basis of the following Equation 5.7. The difference of stress range from experimental results were presented using histogram, as shown in Figure 5.17. The overall prediction by *fib* Model Code exhibited a positive result in which showed 3~13% smaller stress range, compared to experimental results. Helgason et al. (1976) showed the largest fluctuation in terms of stress range prediction that was in the range of -1~17%. The modified model and Byun et al. (1997) predicted the stress range by less than 10% by given fatigue life, signifying the availability of the prediction models.

$$Difference = \frac{(Test - Prediction)}{Prediction} \quad (5.7)$$

However, two prediction models all had negative results in terms of FcTA30 and FcTA60, which can be caused by the greater stress range in experiment. Two RC beams were subjected to freeze-thaw cycles with air-cured condition, and the shrinkage strain possibly have occurred in accordance with analytical study in Chapter 4.4.2. Moreover, freeze-thaw cycles deteriorate the

bond strength of RC beams during which the faster approach to pure rebar behavior possibly occurred. In this manner, the stress range of FcTA30 and FcTA60 can be larger than RC beams at room temperature, and further accounted for the negative value compared to experimental results.

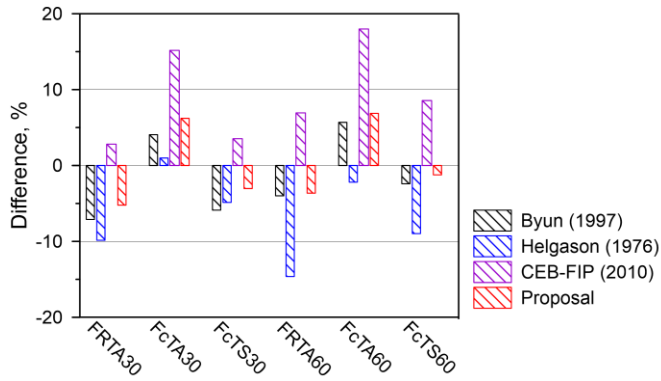


Figure 5.17 Difference of predicted stress range of RC beams

## 5.4. Concluding Remarks

In this chapter, analytical studies on flexure and fatigue behavior were conducted. Finite element analysis was applied to analyze flexure behavior in which the validity of FE model was initially verified. With the verified FE model, the effect of concrete strength on crack width of RC beams were investigated. The flexure analysis results indicated that RC beams with normal strength concrete (30 MPa) had larger crack width in comparison to the RC beams with high strength concrete (60 MPa). This phenomenon was attributed to the curtailed damage by smaller porosity of high strength concrete, leading to greater freeze-thaw resistance in reinforced high strength concrete beams. Therefore, concrete strength larger than 30 MPa was estimated to be more suitable in cold region construction, but concrete strength at higher than 60 MPa may not be necessary due to the higher cost.

The fatigue analysis for the purpose of verifying the test results were conducted. Prediction models incorporating design codes and previous studies were used to predict the stress range by given fatigue life. The *fib* Model Code had conservative predictions, and Helgason et al. (1976) predicted stress range with partial values larger than 10%. Prediction by Byun et al. (1997) exhibited rather close results with tests results by less than 10%. Considering the effect of bond strength and rebar diameter, a modified prediction model based on Helgason et al. (1976) and Byun et al. (1997) was established. Nonlinear regression analysis was utilized for the establishment of the modified prediction model. The prediction by modified prediction model showed conservative results by comparing to the testing results from previous studies. Less effect of

rebar diameter in RC beams were reflected by comparing the modified prediction model and existing model. Prediction models based on RC beam tests showed conservative results which can be attributed to the effect of bond strength, therefore, the S-N relation based on structural tests may need to be further developed for a safer fatigue design. The limited testing data were presented in this study, and extra structural testing data will be necessary in order to improve the reliability of the prediction model.

## **VI. Conclusion**

The objectives of this study were first to investigate the influence of concrete strength on the flexure and fatigue behavior of RC beams. Then, flexure behavior of RC beam subjected to combined effect of freeze-thaw cycles and seawater exposure was planned. Lastly, the fatigue behavior of RC beams under combined effect of freeze-thaw cycles and seawater exposure was investigated. The flexure behavior, which cannot be obtained from tests, were predicted by FE analysis. Besides, the fatigue life of RC beams was verified by existing models.

The primary characteristic of this study can be summarized as:

1. Literature reviews on effect of freeze-thaw cycles, seawater exposure, applied load, and its combined effect on structural behavior
2. Experimental investigation and discussions on flexure and fatigue behavior of RC beams under freeze-thaw cycles, seawater exposure
3. Analytical study on flexure and fatigue behavior of RC beams



## 6.1. Effect of Concrete Strength

Normal strength concrete (30 MPa) and high strength concrete (60 MPa) were used in RC beams in order to investigate the effect of concrete strength under freeze-thaw cycles, seawater exposure, and applied load. The following results were obtained through experiments and analytical studies.

1. RC beams all exhibited flexural failure under monotonic loading with different concrete strength. There was greater deterioration in 30 MPa concrete specimen under freeze-thaw cycles and seawater exposure, including material properties and structural behavior. Under the combined effect of freeze-thaw cycles and seawater exposure, by approximately 26% reduction in terms of concrete strength occurred in 30 MPa concrete while only less than 5% decrease of concrete strength was found in 60 MPa concrete, demonstrating the greater freeze-thaw and seawater resistance of high strength concrete.
2. Under the effect of freeze-thaw cycles and seawater exposure, 60 MPa RC beams averagely had 56% and 7% greater cracking load and ultimate load, respectively, in comparison to 30 MPa RC beams. In fatigue tests, faster damage accumulation of 30 MPa RC beams was confirmed, which was proved by 46% and 9% greater increasing ratio of central deflection and tensile strain along with number of cyclic loadings. Moreover, 30 MPa RC beams revealed wider range of crack width of RC beams, especially under seawater exposure. However, 38% shorter fatigue life was found in 60 MPa RC beam, primarily caused

by the increased bond strength which eventually resulted in greater strain range of tensile rebar.

3. The shrinkage of 60 MPa RC beams was estimated to be larger than RC beams with 30 MPa concrete according to the section analysis. The greater autogenous shrinkage of 60 MPa RC beams may account for the greater strain than 30 MPa RC beams. The reliability of analytical study (section analysis) was verified based on preliminary study in which the material testing data were adopted.
4. FE analysis for flexure tests indicated that 30 MPa RC beams had larger crack width than RC beams with 60 MPa concrete, and difference further increased considering the combined effect of freeze-thaw cycles and seawater exposure. This result was consistent with the behavior found in fatigue tests, signifying the greater freeze-thaw resistance of high strength concrete beams.

## **6.2. Effect of Freeze-thaw Cycles and Seawater**

Freeze-thaw cycles and seawater exposure were simultaneously exerted on RC beams which simulated the aggressive condition in cold regions. Both material and structural behavior of RC beams were experimentally investigated including flexure and fatigue tests. Moreover, the analytical studies were incorporated to further analyze the behavior that were hard to obtain from experiments. The results of the study through experiments and analytical studies were concluded as follows.

1. It was confirmed that concrete strength and elastic modulus decreased by freeze-thaw cycles and seawater, and it further decreased under combined effect of freeze-thaw cycles and seawater.
2. Structural behavior of RC beam decreased under freeze-thaw cycles including cracking load, ultimate load. Furthermore, freeze-thaw cycles may result in degradation of bond strength, reflected in decreased tensile strain at the same deflection level. Seawater was found to decrease the ultimate load and ductility, but increased the crack width of RC beams that could be caused by the formation of chloride crystals in concrete pores. The crack widths were also confirmed to increase by seawater in accordance analytical study on flexure behavior of RC beams.
3. Fatigue life increased in freeze-thaw cycles test possibly due to the enhanced capacity of RC beams during freezing stage. Tensile strain decreased by immersion of seawater, which was contributed to the mitigated shrinkage of concrete, and this behavior was consistent with that

from static tests. Additionally, seawater increased crack width of RC beams attributed to the formation of chloride crystals in concrete pores. A faster damage accumulation of RC beams was confirmed under combined effect of freeze-thaw cycles and seawater exposure since expansive products was reported to generate microcracks and promote damage by freeze-thaw cycles.

### **6.3. Recommendations Considering Combined Effect**

The effect of concrete strength, freeze-thaw cycles, and seawater exposure was investigated based on experiments and analytical studies. The sequent guidelines, which considered the combined effect of damages, were proposed for evaluation of structural behavior in cold regions.

1. Structural tests under aggressive environment such as extreme low temperature and seawater were usually hard to conduct. Therefore, the necessity of structural tests was also evaluated through flexure and fatigue tests. Under the environment of freeze-thaw cycles and seawater, both static and fatigue behavior of RC beams need to be considered. The ultimate capacity of RC beams can be obtained through static tests, but the behavior under repeated loading is hard to reflect only by static tests. On the contrary, fatigue tests provide the structural behavior with regards to loading cycles, introducing the damage accumulation process. Additionally, fatigue behavior structural level can be investigated and influence of aggressive environment can be better considered.
2. Freeze-thaw resistance increased as the concrete strength higher than 30 MPa, but concrete strength greater than 60 MPa may not be necessary to resist the deterioration from freeze-thaw cycles and seawater.
3. In experimental studies, freeze-thaw cycles and seawater exposure is recommended to be simultaneously considered which simulate the

actual environmental conditions. The combined effect of freeze-thaw cycles and seawater further accelerate the deterioration than the effect of freeze-thaw cycles with air-cured condition.

4. Definition of low temperatures (range) in design codes may need to be specified based on the temperature of structures, for instance, low temperature of  $-60\text{ }^{\circ}\text{C}$  is for cold regions, and  $-20\text{ }^{\circ}\text{C}$  is for the structures in residential area.  $-60\text{ }^{\circ}\text{C}$  stands for the most severe temperature on the earth and  $-20\text{ }^{\circ}\text{C}$  elaborates the temperature that major part of frost damage occurs.
5. Current fatigue design and previous studies were conducted based on material tests due to the limitation of testing conditions. With the support of experimental conditions which is possible to simulate the simultaneous effect temperature and mechanical loading, the structural behavior which are closer to the actual behavior structure can be evaluated in a certain range. The behavior that have been predicted only by material tests can be further verified through structural level tests. Besides, the bond strength which transmit the stress between concrete and reinforcing bars may influence the fatigue behavior. Stress range from structural tests was predicted to be smaller than material tests at given fatigue life, implying a safer fatigue design. Therefore, the structural tests are recommended in fatigue design of RC structure rather than only by material tests.

## 6.4. Further Study

Further studies regarding fatigue behavior were suggested in this Chapter. In this study, the effect of concrete strength and combined effect of freeze-thaw cycles and seawater were experimentally investigated. Current fatigue design is carried out based on material tests, but it was reported that fatigue strength reduces as diameter of tensile rebar decrease (Byun, 1997). Moreover, fatigue behavior of RC member presented differences considering influence of concrete strength, bond strength, and concrete cover. However, only one type of tensile rebar was used in RC beams which was deformed bars with diameter of 22 mm. Therefore, fatigue behavior of RC beams with the variable of rebar diameter may need to be investigated.

Effect of seawater on material properties and structural behavior was not fully investigated in this study due to the testing conditions. The behavior of RC beam with seawater-saturated conditions were investigated only after freeze-thaw cycles, resulting in the ambiguity of behavior before freeze-thaw cycles. Therefore, the coupling effect of freeze-thaw cycles and seawater may need to be investigated through respective tests at room and under freeze-thaw cycles. Additionally, the effect of curing age on immersion was not able to fully investigated in which the properties of concrete would differ. To better understand the effect of seawater immersion on RC beam, the curing age and behavior of saturated RC beam at room temperature are suggested to investigate.

## References

- ACI 215R-74, (1997). “Considerations for Design of Concrete Structures Subjected to Fatigue Loading.” American Concrete Institute Farmington Hills, MI.
- ACI 318-19, (2019). “Building Code Requirements for Structural Concrete and Commentary.” American Concrete Institute, Farmington Hills, MI.
- Alexander, M., (2016). “Marine concrete structures: design, durability and performance.” Woodhead Publishing.
- Amini, B., Tehrani, S.S., (2011). “Combined effects of saltwater and water flow on deterioration of concrete under freeze–thaw cycles.” *Journal of Cold Regions Engineering*, 25, 145–161.
- Andrade, C., Alonso, C., Sarria, J., (2002). “Corrosion rate evolution in concrete structures exposed to the atmosphere.” *Cement and concrete composites*, 24, 55–64.
- AS 3600-2001, (2001). “Australian standard for concrete structures.”, Australia.
- Asadi, I., Shafigh, P., Hassan, Z.F.B.A., Mahyuddin, N.B., (2018). “Thermal conductivity of concrete–A review.” *Journal of Building Engineering*, 20, 81–93.
- ASTM 370-18, (2019). “Standard test methods and definitions for mechanical testing of steel products.” ASTM International, West Conshohocken, PA.



- ASTM C39, (2014). “Test Method for Compressive Strength of Cylindrical Concrete Specimens.” ASTM International, West Conshohocken, PA.
- ASTM C666/C666M, (2015). “Standard test method for resistance of concrete to rapid freezing and thawing.” ASTM International, West Conshohocken, PA.
- AWAD, M.E.-M., Hilsdorf, H., (1971). “Strength and deformation characteristics of plain concrete subjected to high repeated and sustained loads.” University of Illinois at Urbana-Champaign.
- Banjara, N.K., Ramanjaneyulu, K., (2020). “Effect of Deficiencies on Fatigue Life of Reinforced Concrete Beams.” *ACI Structural Journal* 117, 31–44.
- Bao, J., Wang, L.J.C., (2017). “Combined effect of water and sustained compressive loading on chloride penetration into concrete.” *Construction and Building Materials*, 156, 708–718.
- Barnes, R.A., Mays, G.C., (1999). “Fatigue performance of concrete beams strengthened with CFRP plates.” *Journal of composites for construction*, 3, 63–72.
- Birnin-Yauri, U.A., Glasser, F.P., Research, C., (1998). “Friedel’s salt,  $\text{Ca}_2\text{Al}(\text{OH})_6(\text{Cl}, \text{OH}) \cdot 2\text{H}_2\text{O}$ : its solid solutions and their role in chloride binding.” *Cement and Concrete Research*, 28, 1713–1723.

- Birrcher, D.B., (2009). "Design of reinforced concrete deep beams for strength and serviceability (Doctor of Philosophy)." The University of Texas at Austin.
- Bo, D., Yang, S., Chen, S., Ye, Y., (2011). "Effect of mixed-erosion freeze-thaw cycles and persistent loading on the behavior of reinforcement concrete beams." ASCE. Journal of Cold Regions Engineering, 3, 37–52.
- Bogas, J.A., de Brito, J., Ramos, D., (2016). "Freeze–thaw resistance of concrete produced with fine recycled concrete aggregates." Journal of Cleaner Production, 115, 294–306.
- Bremner, T., Hover, K., Poston, R., Broomfield, J., Joseph, T., Price, R., Clear, K., Khan, M., Reddy, D., Clifton, J., (2001). "ACI 222R-01 protection of metals in concrete against corrosion." American Concrete Institute: Farmington Hills, MI, USA.
- Byun, K.J., Lho, B., Song, H.W., (1997). "Experimental Study on Fatigue Characteristics of Domestic Reinforcing Bars." Magazine of the Korea Concrete Institute, 9, 177–187.
- Cai, H., Liu, X., (1998). "Freeze-thaw durability of concrete: ice formation process in pores." Cement and Concrete Research, 28, 1281–1287.
- Cao, D., Ge, W., Wang, B., Tu, Y., (2015). "Study on the flexural behaviors of RC beams after freeze-thaw cycles." International Journal of Civil Engineering, 13, 92–101.

- CEB-FIP model code for Concrete Structures, (2010). “International Federation for Structural Concrete (fib).”
- CEN/TS 12390-9, (2006). “Testing hardened concrete - Part 9: Freeze-thaw resistance -Scaling.” European Committee for Standardization.
- Chai, L., Guo, L., Chen, B., Xu, Y., (2018). “Interactive effects of freeze-thaw cycle and carbonation on tensile property of ecological high ductility cementitious composites for bridge deck link slab.” *Construction and Building Materials*, 186, 773–781.
- Charalambidi, B.G., Rousakis, T.C., Karabinis, A.I., (2016). “Fatigue behavior of large-scale reinforced concrete beams strengthened in flexure with fiber-reinforced polymer laminates.” *Journal of Composites for Construction*, 20, 04016035.
- Chen, F., Gao, J., Qi, B., Shen, D., Li, L., (2017). “Degradation progress of concrete subject to combined sulfate-chloride attack under drying-wetting cycles and flexural loading.” *Construction and Building Materials*, 151, 164–171.
- Chen, W.-F., (2007). “Plasticity in reinforced concrete.” J. Ross Publishing.
- Choo, J.F., Choi, Y.-C., Kwon, S.-J., Park, K.-T., Yoo, S.-W., (2018). “Low-cycle flexural fatigue behavior of concrete beam reinforced with hybrid FRP-steel rebar.” *Advances in Civil Engineering*, 2018, 1–13.

- CIF-Test, Heine, P., Kasparek, S., Palecki, S., Auberg, R., Feldrappe, V., Siebel, E., (2004). “Test methods of frost resistance of concrete: CIF-Test: Capillary suction, internal damage and freeze thaw test—Reference method and alternative methods A and B.”
- Detwiler, R.J., Dalglish, B.J., Brady, R., (1989). “Assessing the durability of concrete in freezing and thawing.” *Materials Journal*, 86, 29–35.
- Diao, B., Sun, Y., Ye, Y., Cheng, S., (2012). “Impact of seawater corrosion and freeze-thaw cycles on the behavior of eccentrically loaded reinforced concrete columns.” *Ocean Systems Engineering*, 2, 159–171.
- Diao, B., Zhang, J., Ye, Y., Cheng, S., (2012). “Effects of freeze-thaw cycles and seawater corrosion on the behavior of reinforced air-entrained concrete beams with persistent loads.” *Journal of Cold Regions Engineering*, 27, 44–53.
- DIN 1045-2, (2014). “Concrete, reinforced and prestressed concrete structures - Part 2: Concrete - Specification, performance, production and conformity - Application rules for DIN EN 206.”
- DS 2426 - EN 206-1, (2011). “Concrete – Materials – Rules for application of EN 206-1”, Denmark.
- Duan, A., Li, Z., Zhang, W., Jin, W., (2017). “Flexural behavior of reinforced concrete beams under freeze–thaw cycles and sustained load.” *Structure and Infrastructure Engineering* 13, 1350–1358.

- European Committee for Standardization. (2004). “Eurocode 2: Design of Concrete Structures-Part 1-1: General Rules and Rules for Buildings”, Brussel, Belgium, 230.
- Flatt, R.J., (2002). “Salt damage in porous materials: how high supersaturations are generated.” *Journal of crystal growth*, 242, 435–454.
- Gautier, D.L., Bird, K.J., Charpentier, R.R., Grantz, A., Houseknecht, D.W., Klett, T.R., Moore, T.E., Pitman, J.K., Schenk, C.J., Schuenemeyer, J.H., (2009). “Assessment of undiscovered oil and gas in the Arctic.” *Science*, 324, 1175–1179.
- GOST 31384, (2017). “Protection of concrete and reinforced concrete structures against corrosion (Translated from Russian).”
- Hansson, C.M., (2011). “The impact of corrosion on society.” *Metallurgical and Materials Transactions*, 42A, 2952–2962.
- Hao, L., Liu, Y., Wang, W., Zhang, J., Zhang, Y., (2018). “Effect of salty freeze-thaw cycles on durability of thermal insulation concrete with recycled aggregates.” *Construction and Building Materials*, 189, 478–486.
- Heffernan, P., Erki, M., (2004). “Fatigue behavior of reinforced concrete beams strengthened with carbon fiber reinforced plastic laminates.” *Journal of Composites for Construction*, 8, 132–140.

- Helgason, T., Hanson, J.M., Somes, N.F., Corley, W., Hognestad, E., (1976). “Fatigue strength of high-yield reinforcing bars (National Cooperative Highway Research Program).” Transportation Research Board.
- Jang, G.-S., Yun, H.-D., Kim, S.-W., Park, W.-S., Choi, K.-B., (2009). “Flexural Behavior of Reinforced Concrete Beams Exposed to Freeze-Thawing Environments.” Journal of the Korea institute for structural maintenance and inspection, 13, 126–134.
- Ji, X., Song, Y., Liu, Y., (2008). “Effect of freeze-thaw cycles on bond strength between steel bars and concrete.” Journal of Wuhan University of Technology-Mater. Sci. Ed, 23, 584.
- Jiang, J., Yuan, Y., (2013). “Development and prediction strategy of steel corrosion rate in concrete under natural climate.” Construction and Building Materials, 44, 287–292.
- Johannesson, B., (2010). “Dimensional and ice content changes of hardened concrete at different freezing and thawing temperatures.” Cement and Concrete Composites, 32, 73–83.
- KDS 14 20 00: 2021, (2021). “Concrete Structure Design (Ultimate state design method).” Korea Concrete Institute.
- Kim, W., Lee, K.-Y., Yum, H.-S., (2003). “Tension Stiffening Effect of High-Strength Concrete in Axially Loaded Members.” Journal of the Korea Concrete Institute, 15, 915–923.

- Kosior-Kazberuk, M., Berkowski, P., (2017). "Surface scaling resistance of concrete subjected to freeze-thaw cycles and sustained load." *Procedia Engineering*, 172, 513–520.
- KS, Testing method for resistance of concrete to rapid freezing and thawing(KS F 2456), Korea Standards Association.
- Kurdowski, W., (2004). "The protective layer and decalcification of CSH in the mechanism of chloride corrosion of cement paste." *Cement and Concrete Research*, 34, 1555–1559.
- Lee, J.-H., Lee, S.-H., Kim, H.-Y., (2018). "Fatigue Strength of High Strength Reinforcing Bars Having Yield Strength of 700 MPa." *Journal of the Korea Concrete Institute*, 30, 269–279.
- Li, B., Mao, J., Nawa, T., Liu, Z., (2016). "Mesoscopic chloride ion diffusion model of marine concrete subjected to freeze-thaw cycles." *Construction and Building Materials*, 125, 337–351.
- Li, N., Long, G., Fu, Q., Wang, X., Ma, K., Xie, Y., (2019). "Effects of freeze and cyclic flexural load on mechanical evolution of filling layer self-compacting concrete." *Construction and Building Materials*, 200, 198–208.
- Li, W., Sun, W., Jiang, J., (2011). "Damage of concrete experiencing flexural fatigue load and closed freeze/thaw cycles simultaneously." *Construction and Building Materials*, 25, 2604–2610.

- Lim, C., Gowripalan, N., Sirivivatnanon, V., (2000). "Microcracking and chloride permeability of concrete under uniaxial compression." *Cement and Concrete Composites*, 22, 353–360.
- Liu, F., You, Z., Yang, X., Wang, H., (2018). "Macro-micro degradation process of fly ash concrete under alternation of freeze-thaw cycles subjected to sulfate and carbonation." *Construction and Building Materials*, 181, 369–380.
- Liu, Z., Diao, B., Zheng, X., (2015). "Effects of seawater corrosion and freeze-thaw cycles on mechanical properties of fatigue damaged reinforced concrete beams." *Advances in Materials Science and Engineering*, 2015, 1–15.
- Liu, Z., Hansen, W., (2016). "Freeze–thaw durability of high strength concrete under deicer salt exposure." *Construction and Building Materials*, 102, 478–485.
- Loo, K.Y.M., Foster, S.J., Smith, S.T., (2012). "Fatigue behavior of carbon fiber-reinforced polymer-repaired corroded reinforced concrete beams." *ACI Structural Journal*, 109, 795–803.
- Mehta, P.K., Monteiro, P.J., (2014). "Concrete: microstructure, properties, and materials." McGraw-Hill Education.
- Mirzazadeh, M.M., Noël, M., Green, M.F., (2017). "Fatigue behavior of reinforced concrete beams with temperature differentials at room and low temperature." *Journal of Structural Engineering*, 143, 04017056.



- Mirzazadeh, M.M., Noël, M., Green, M.F., (2016). “Effects of low temperature on the static behaviour of reinforced concrete beams with temperature differentials.” *Construction and Building Materials*, 112, 191–201.
- Moss, D.S., Wokingham, Birkshir (1982). “Bending fatigue of high-yield reinforcing bars in concrete.” Transport and road research laboratory, United Kingdom.
- Mu, R., Miao, C., Luo, X., Sun, W., (2002). “Interaction between loading, freeze–thaw cycles, and chloride salt attack of concrete with and without steel fiber reinforcement.” *Cement and Concrete Research*, 32, 1061–1066.
- Murdock, J.W., (1965). “A critical review of research on fatigue of plain concrete.” University of Illinois bulletin 62.
- Muthumani, A., Fay, L., Akin, M., Wang, S., Gong, J., Shi, X., (2014). “Correlating lab and field tests for evaluation of deicing and anti-icing chemicals: A review of potential approaches.” *Cold Regions Science and Technology*, 97, 21–32.
- Neville, A.M., (1995). “Properties of concrete.” Longman London.
- NS-EN 206: 2013+ NA: 2020, (2020). “Concrete–Specification, performance, production and conformity.” Norwegian Standards.
- NZS 3101-1, (2006). “Concrete structures standard. The design of concrete structures.” New Zealand Standard. Wellington, New Zealand.

- Papakonstantinou, C.G., Petrou, M.F., Harries, K.A., (2001). "Fatigue behavior of RC beams strengthened with GFRP sheets." *Journal of Composites for Construction*, 5, 246–253.
- Parvez, A., Foster, S.J., (2015). "Fatigue behavior of steel-fiber-reinforced concrete beams." *Journal of Structural Engineering*, 141, 04014117.
- Petersen, L., Lohaus, L., Polak, M.A., (2007). "Influence of freezing-and-thawing damage on behavior of reinforced concrete elements." *ACI Materials Journal*, 104, 369.
- Qiao, C., Suraneni, P., Weiss, J., Materials, B., (2018). "Damage in cement pastes exposed to NaCl solutions." *Construction and Building Materials*, 171, 120–127.
- Qiao, Y., Sun, W., Jiang, J., (2015). "Damage process of concrete subjected to combined fatigue load and freeze/thaw cycles." *Construction and Building Materials*, 93, 806–811.
- Scherer, G.W., (2004). "Stress from crystallization of salt." *Cement and concrete research*, 34, 1613–1624.
- Sereda, P., Litvan, G., (1980). "Durability of building materials and components." *American Society for Testing and Materials*.
- Shafigh, P., Asadi, I., Mahyuddin, N.B., (2018). "Concrete as a thermal mass material for building applications-A review." *Journal of Building Engineering*, 19, 14–25.

- Shang, H., Song, Y., Ou, J., (2009). "Behavior of air-entrained concrete after freeze-thaw cycles." *Acta Mechanica Solida Sinica*, 22, 261–266.
- Shang, H.S., Song, Y., (2006). "Experimental study of strength and deformation of plain concrete under biaxial compression after freezing and thawing cycles." *Cement and Concrete Research*, 36, 1857–1864.
- Shi, X., Liu, Y., Mooney, M., Berry, M., Hubbard, B., Nguyen, T.A., (2010). "Laboratory investigation and neural networks modeling of deicer ingress into Portland cement concrete and its corrosion implications." *Corrosion Reviews*, 28, 105–154.
- Shi, X., Veneziano, D., Xie, N., Gong, J., (2013). "Use of chloride-based ice control products for sustainable winter maintenance: A balanced perspective." *Cold Regions Science and Technology*, 86, 104–112.
- Sicat, E., Gong, F., Zhang, D., Ueda, T., (2013). "Change of the coefficient of thermal expansion of mortar due to damage by freeze thaw cycles." *Journal of Advanced Concrete Technology*, 11, 333–346.
- Söylev, T.A., Richardson, M.G., (2008). "Corrosion inhibitors for steel in concrete: State-of-the-art report." *Construction and Building Materials*, 22, 609–622.
- Sun, L.-F., Jiang, K., Zhu, X., Xu, L., (2020). "An alternating experimental study on the combined effect of freeze-thaw and chloride penetration in concrete." *Construction and Building Materials*, 252, 119025.

- Sun, W., Zhang, Y., Yan, H., Mu, R., (1999). "Damage and damage resistance of high strength concrete under the action of load and freeze-thaw cycles." *Cement and Concrete Research*, 29, 1519–1523.
- Suryavanshi, A.K., Scantlebury, J.D., Lyon, S.B., (1996). "Mechanism of Friedel's salt formation in cements rich in tri-calcium aluminate." *Cement and concrete research*, 26, 717–727.
- Thaulow, N., Sahu, S., (2004). "Mechanism of concrete deterioration due to salt crystallization." *Materials Characterization*, 53, 123–127.
- Thorenfeldt, E., Tomaszewicz, A., and Jensen, J. J. (1987). "Mechanical properties of high strength concrete and application in design." *Proceedings of international symposium on utilization of high strength concrete*, Stavanger, Norway, 149-159.
- Vecchio, F., (1982). "The response of reinforced concrete to in-plane shear and normal stresses." Dept. of Civil Engineering, Univ. of Toronto.
- Vecchio, F.J., Collins, M.P., (1986). "The modified compression-field theory for reinforced concrete elements subjected to shear." *ACI Journal*, 83, 219–231.
- Waagaard, K., (1977). "Fatigue of offshore concrete structures-design and experimental investigations." Presented at the Offshore Technology Conference, Offshore Technology Conference, 341–350.

- Wang, R., Zhang, Q., Li, Y., (2022). “Deterioration of concrete under the combined effects of freeze–thaw cycles and other actions: A review.”, *Construction and Building Materials*, 319, 126045.
- Wang, Y., Gong, F., Zhang, D., Ueda, T., (2016). “Estimation of ice content in mortar based on electrical measurements under freeze-thaw cycle.” *Journal of Advanced Concrete Technology*, 14, 35–46.
- Wang, Y., Li, J., Ueda, T., Zhang, D., Deng, J., (2021). “Meso-scale mechanical deterioration of mortar subjected to freeze thaw cycles and sodium chloride attack.” *Cement and Concrete Composites*, 117, 103906.
- Wu, J., Diao, B., Xu, J., Zhang, R., Zhang, W., (2020). “Effects of the reinforcement ratio and chloride corrosion on the fatigue behavior of RC beams.” *International Journal of Fatigue*, 131, 105299.
- Xiao, Q.H., Cao, Z.Y., Guan, X., Li, Q., Liu, X.L., (2019). “Damage to recycled concrete with different aggregate substitution rates from the combined action of freeze-thaw cycles and sulfate attack.” *Construction and Building Materials*, 221, 74–83.
- Xie, J., Huang, P., Guo, Y., (2012). “Fatigue behavior of reinforced concrete beams strengthened with prestressed fiber reinforced polymer.” *Construction and Building Materials*, 27, 149–157.
- Yang, X., Shen, A., Guo, Y., Zhou, S., He, T., *Materials*, B., (2018). “Deterioration mechanism of interface transition zone of concrete

- pavement under fatigue load and freeze-thaw combined in cold climatic areas.” *Construction and Building Materials*, 160, 588–597.
- Yuan, Y., Zhao, R., Li, R., Wang, Y., Cheng, Z., Li, F., Ma, Z.J., (2020). “Frost resistance of fiber-reinforced blended slag and Class F fly ash-based geopolymer concrete under the combined effect of freeze-thaw cycling and axial compressive loading.” *Construction and Building Materials*, 250, 118831.
- Yun, S.-H., Kim, J.-S., Yum, H.-S., Kim, W., (1998). “Tension Stiffening Effect of High Strength Concrete.” in: *Proceedings of the Korea Concrete Institute Conference*. Korea Concrete Institute, 495–500.
- Zhang, S., Wu, B., (2019). “Effects of salt solution on the mechanical behavior of concrete beams externally strengthened with AFRP.” *Construction and Building Materials*, 229, 117044.
- Zhang, W., Pi, Y., Kong, W., Zhang, Y., Wu, P., Zeng, W., Yang, F., (2020). “Influence of damage degree on the degradation of concrete under freezing-thawing cycles.” *Construction and Building Materials*, 260, 119903.
- Zhao, P., Xu, G., Wang, Q., Wen, C., (2021). “Impact of sustained load on damage characteristics of reinforced concrete beams under the combined action of salt freeze-thaw cycles and corrosion.” *Construction and Building Materials*, 273, 121744.

## **Appendix A**

### **Results of unconfined compression test for cylinder specimens**

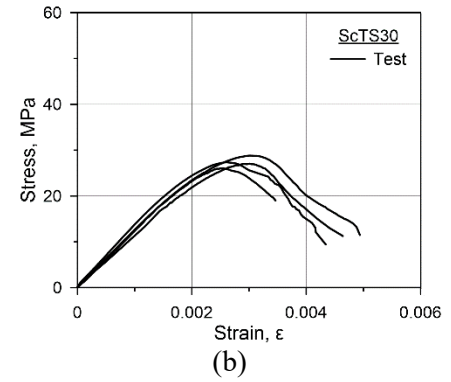
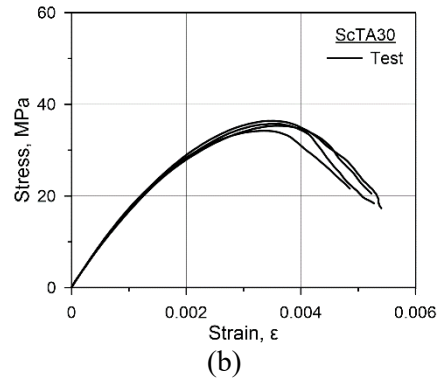
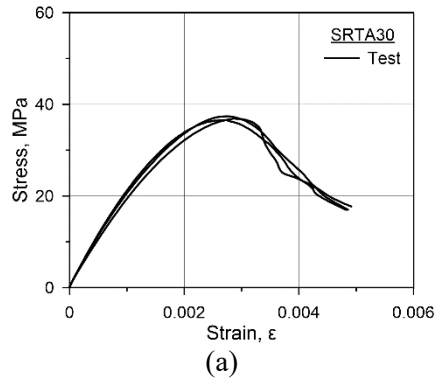


Figure A.1 Stress-strain curve for concrete cylinder of RC beams: (a) SRTA30; (b) ScTA30; (c) ScTS30



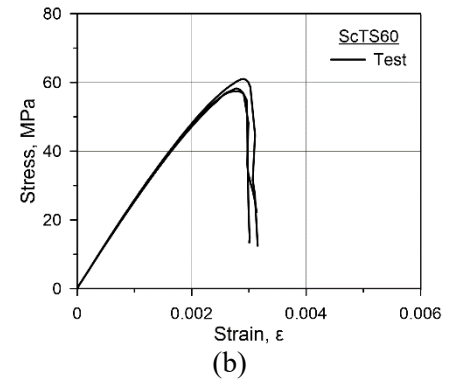
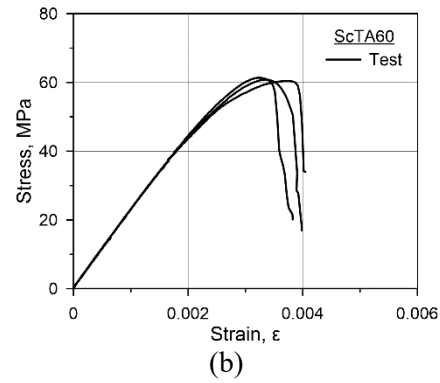
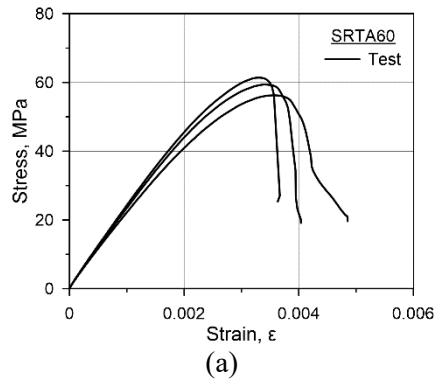


Figure A.2 Stress-strain curve for concrete cylinder of RC beams: (a) SRTA60; (b) ScTA60; (c) ScTS60

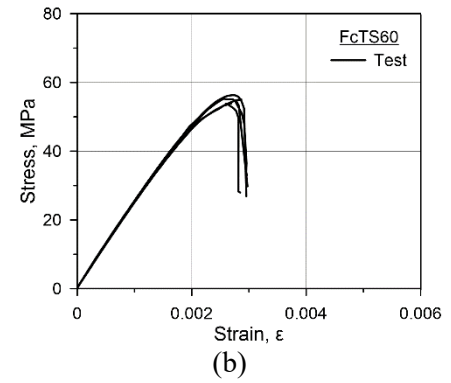
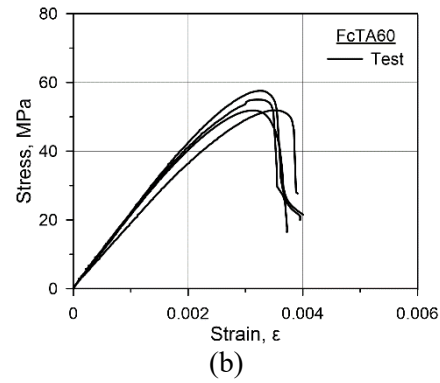
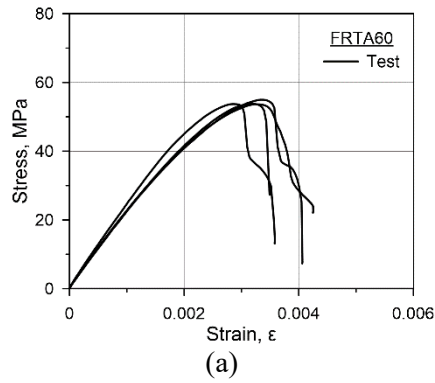
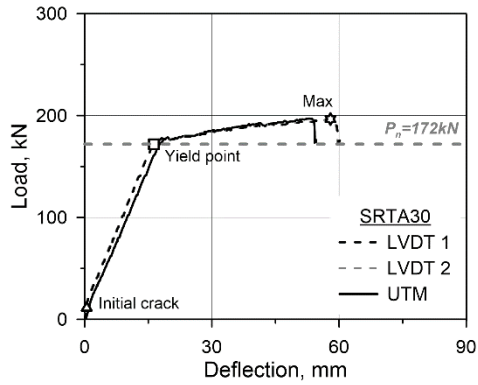


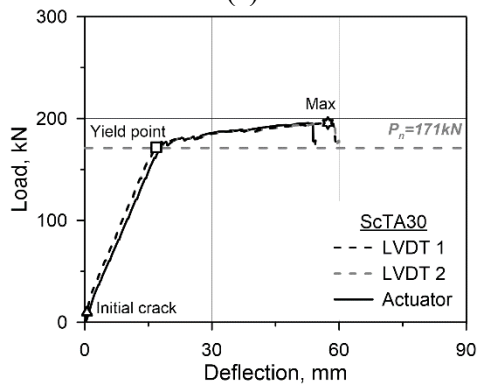
Figure A.3 Stress-strain curve for concrete cylinder of RC beams: (a) FRTA60; (b) FcTA60; (c) FcTS60

## **Appendix B**

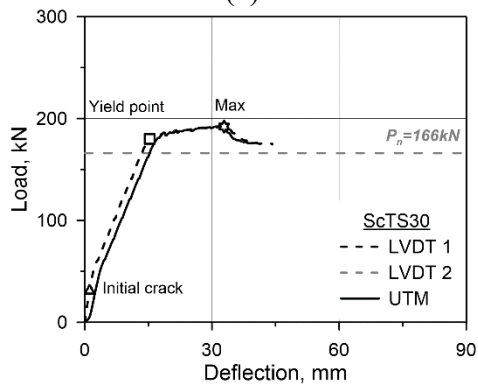
### **Static tests result of RC beams**



(a)



(b)



(c)

Figure B.1 Load-deflection curve of 30 MPa RC beams: (a) SRTA30; (b) ScTA30; (c) ScTS30

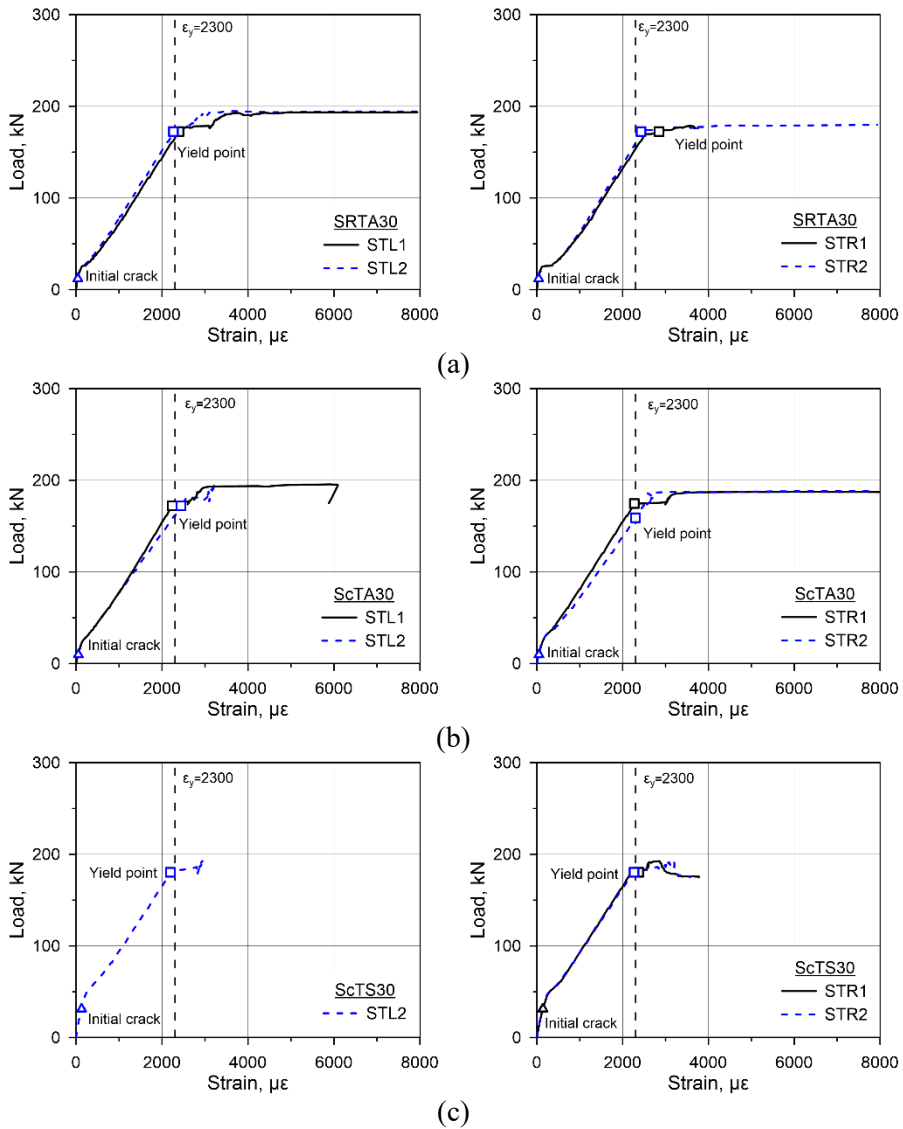


Figure B.2 Load-tensile strain curve of 30 MPa RC beams: (a) SRTA30; (b) ScTA30; (c) ScTS30

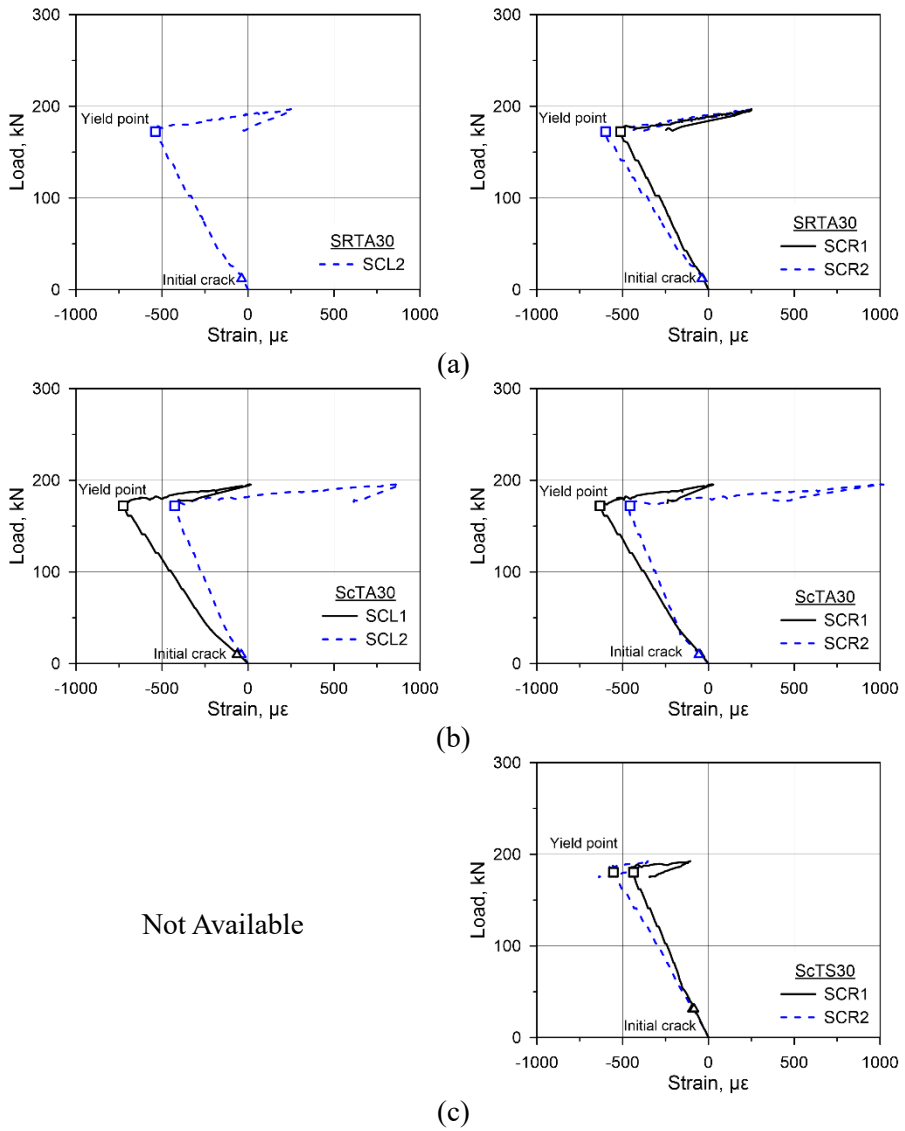
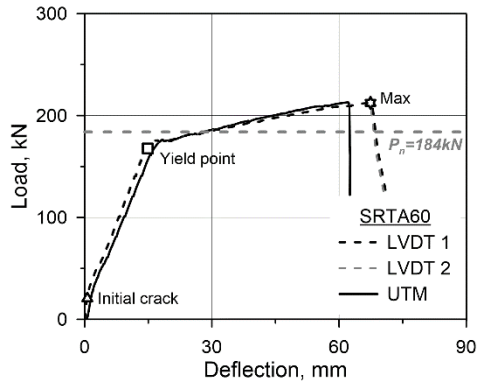
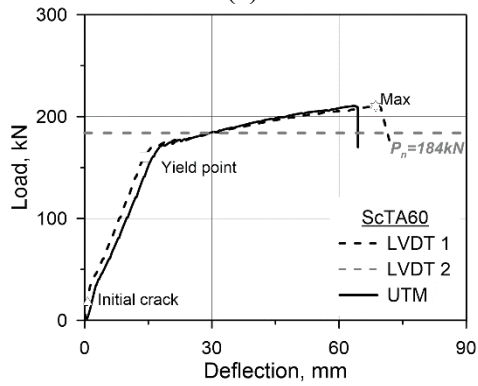


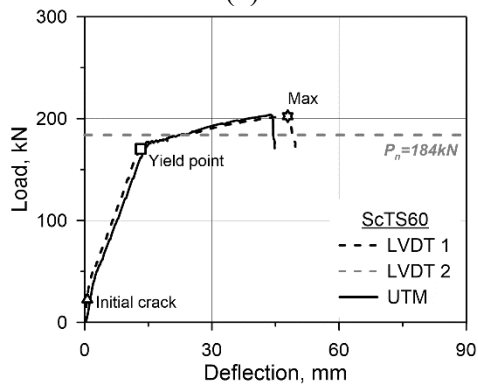
Figure B.3 Load-compressive strain curve of 30 MPa RC beams: (a) SRTA30; (b) ScTA30; (c) ScTS30



(a)



(b)



(c)

Figure B.4 Load-deflection curve of 60 MPa RC beams: (a) SRTA60; (b) ScTA60; (c) ScTS60

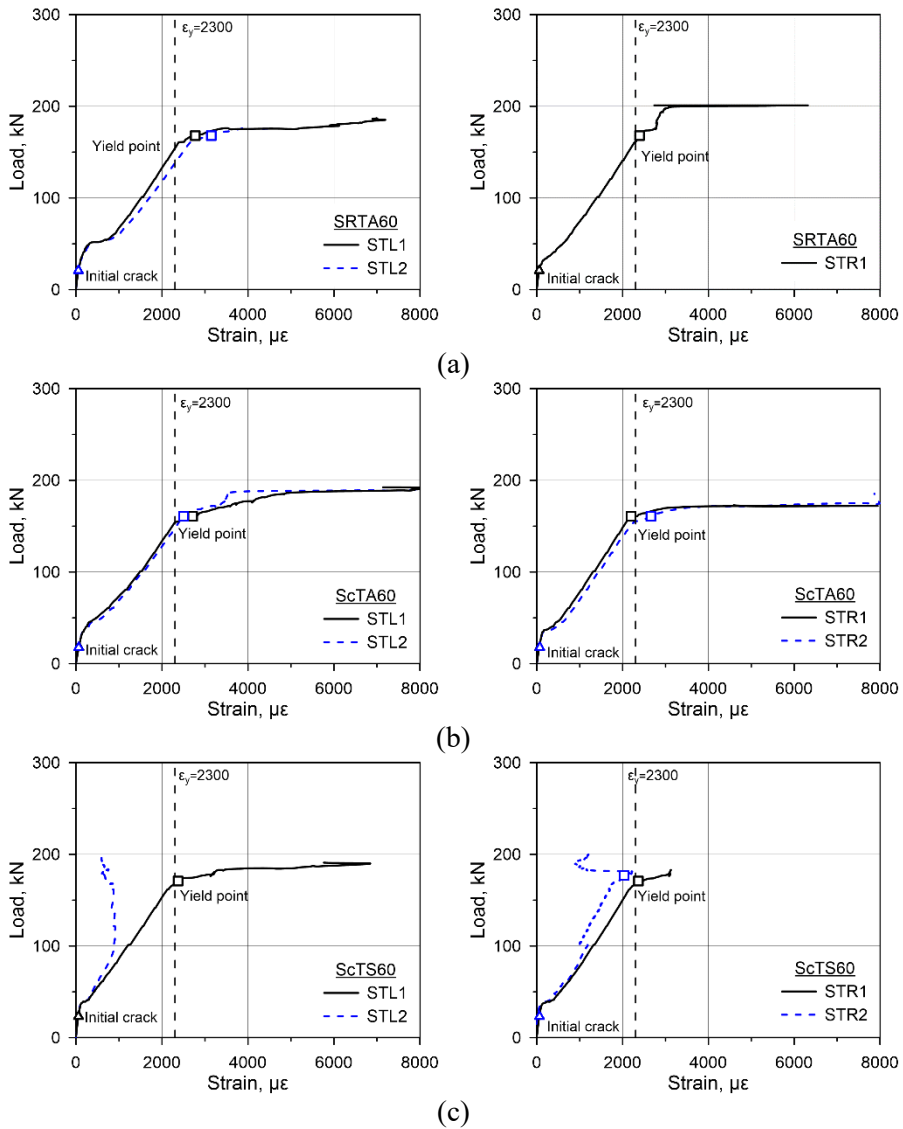


Figure B.5 Load-tensile strain curve of 60 MPa RC beams: (a) SRTA60; (b) ScTA60; (c) ScTS60



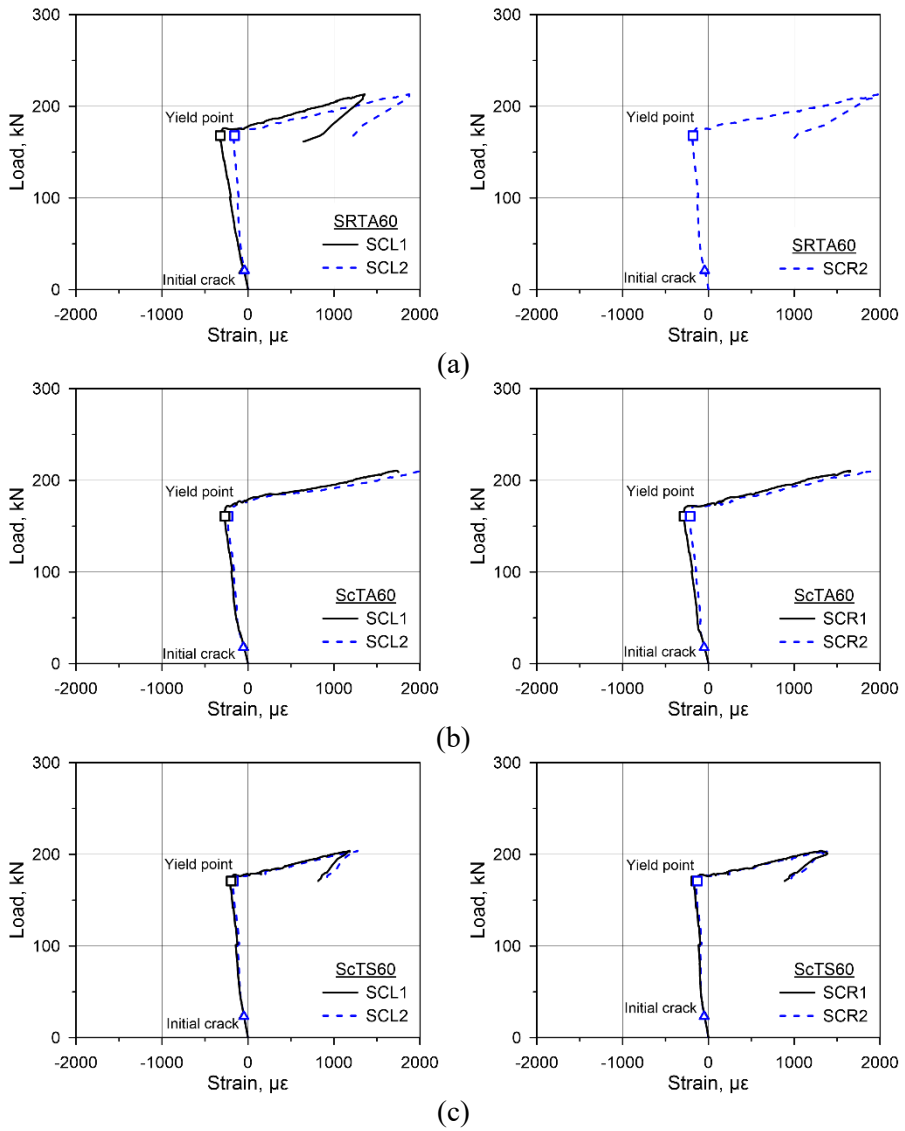


Figure B.6 Load-compressive strain curve of 60 MPa RC beams: (a) SRTA60;  
(b) ScTA60; (c) ScTS60

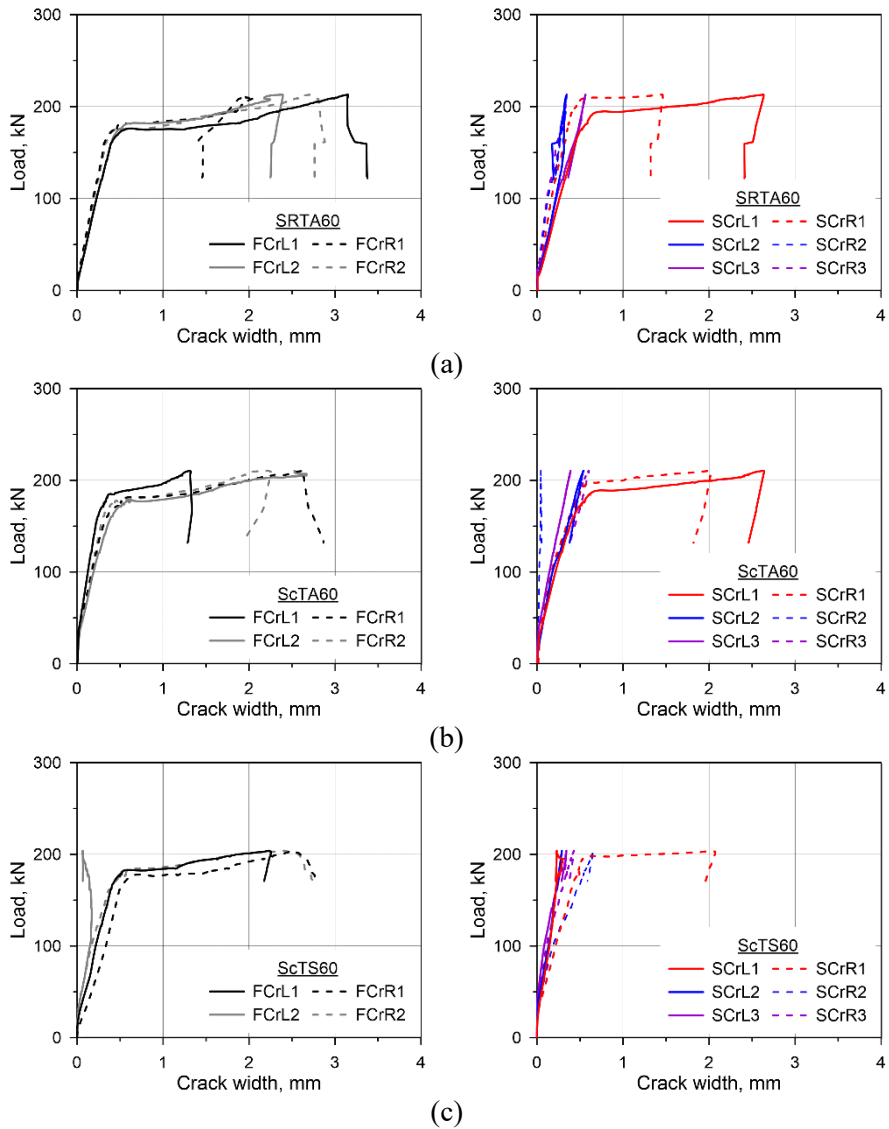
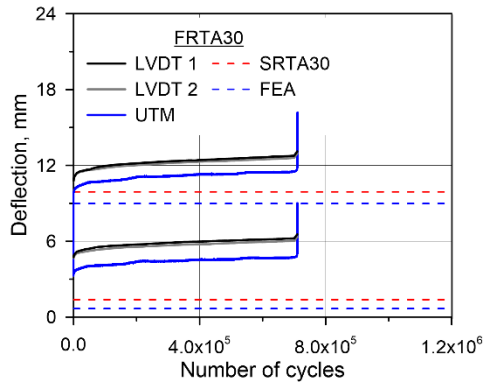


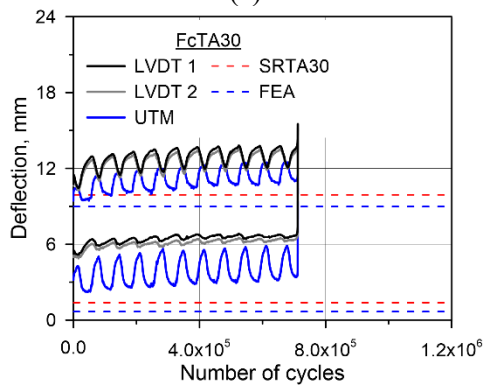
Figure B.7 Load-crack width curve of 60 MPa RC beams: (a) SRTA60; (b) ScTA60; (c) ScTS60

## **Appendix C**

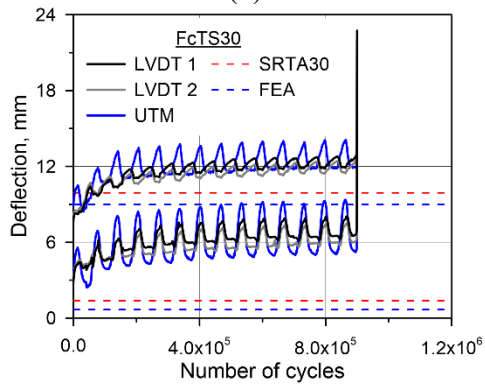
### **Fatigue tests result of RC beams**



(a)



(b)



(c)

Figure C.1 Deflection-N curve of 30 MPa RC beams: (a) FRTA30; (b) FcTA30; (c) FcTS30

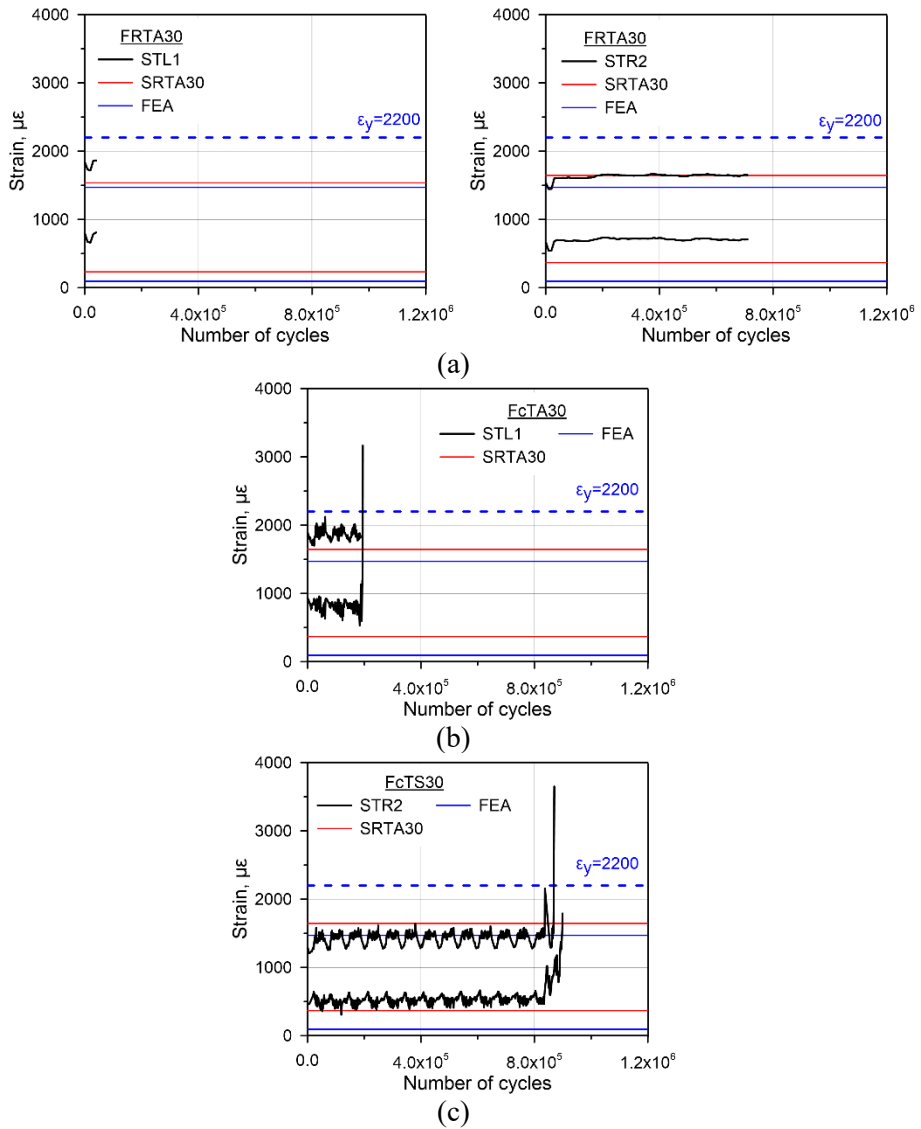


Figure C.2 Tensile strain-N curve of 30 MPa RC beams: (a) FRTA30; (b) FcTA30; (c) FcTS30

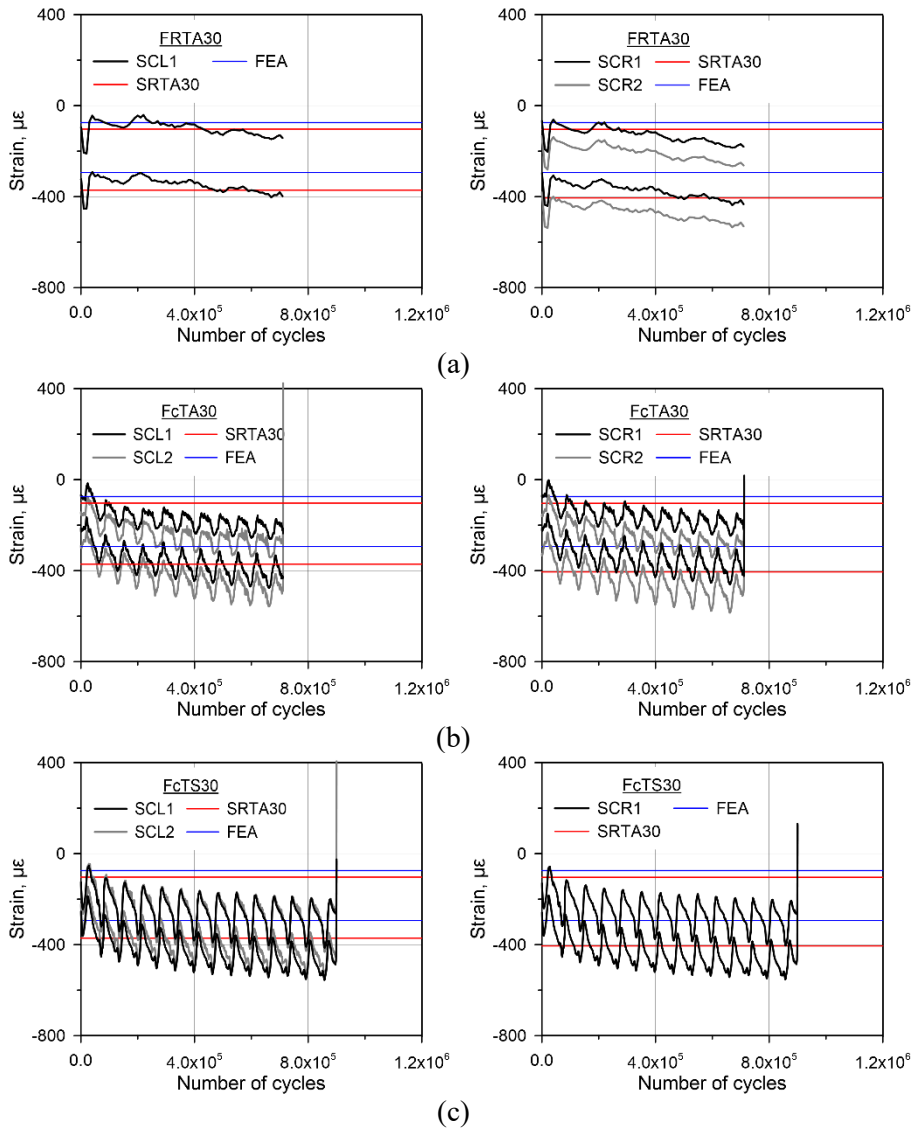
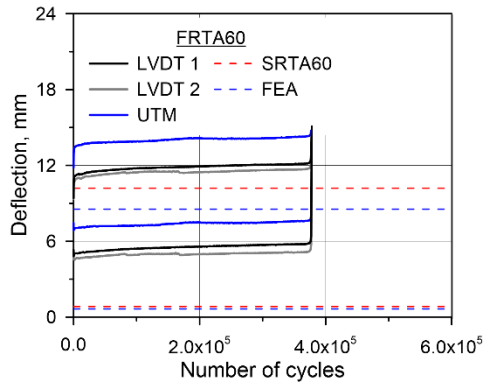
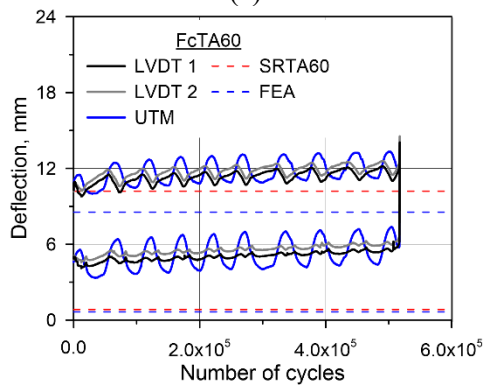


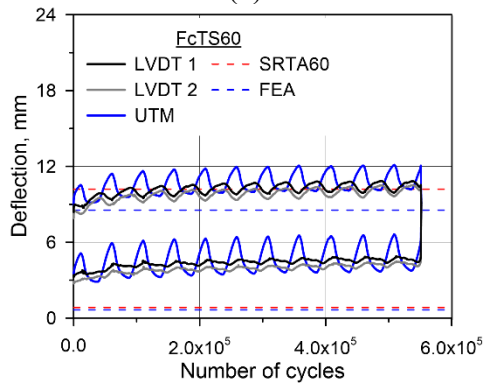
Figure C.3 Compressive strain-N curve of 30 MPa RC beams: (a) FRTA30;  
 (b) FcTA30; (c) FcTS30



(a)



(b)



(c)

Figure C.4 Deflection-N curve of 60 MPa RC beams: (a) FRTA60; (b) FcTA60; (c) FcTS60

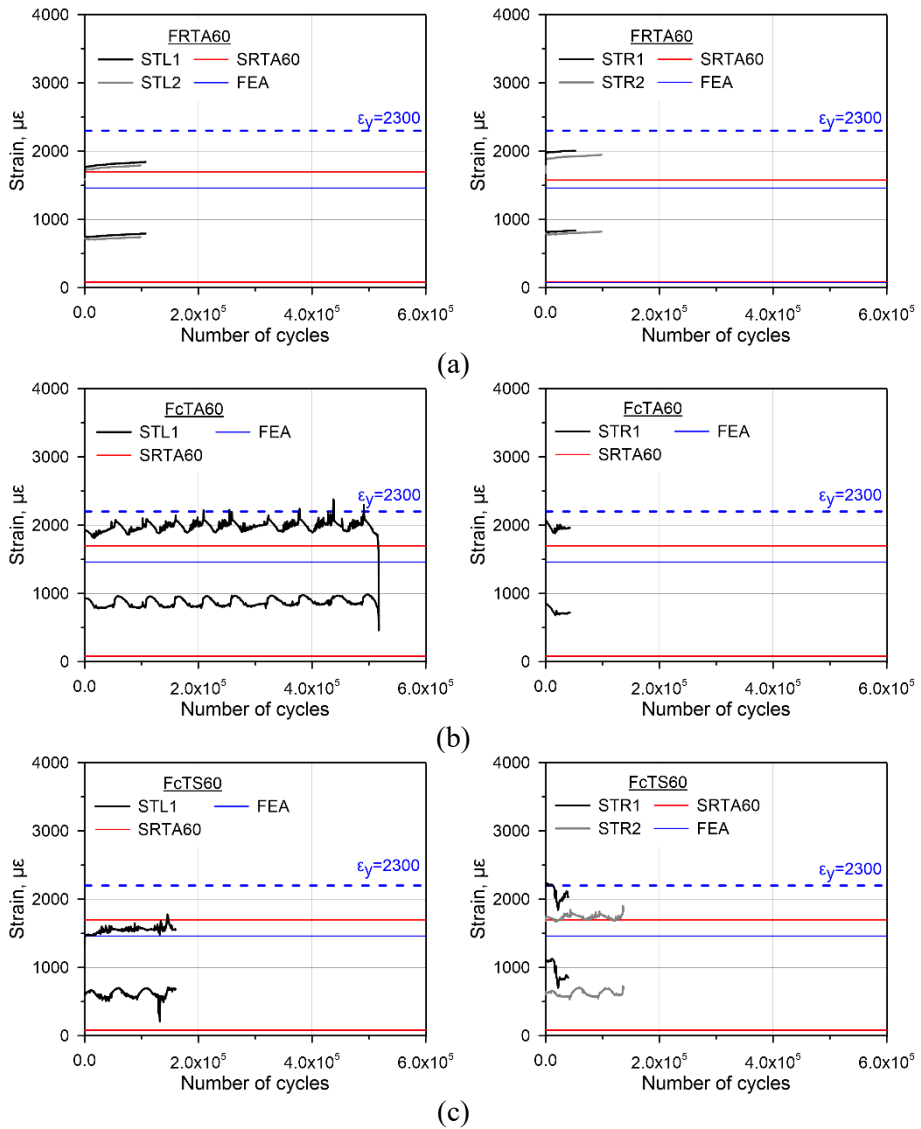


Figure C.5 Tensile strain-N curve of 60 MPa RC beams: (a) FRTA60; (b) FcTA60; (c) FcTS60



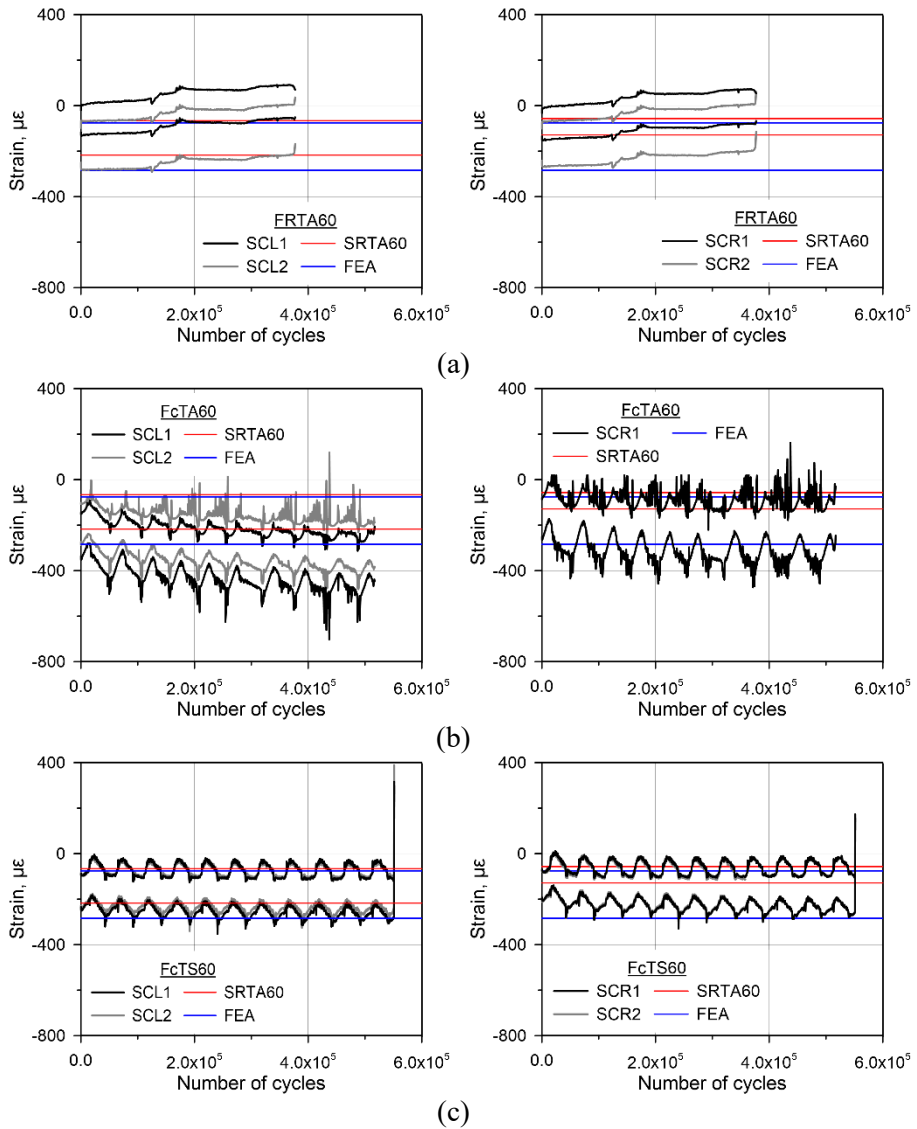


Figure C.6 Compressive strain-N curve of 60 MPa RC beams: (a) FRTA60; (b) FcTA60; (c) FcTS60

## 국문초록

# 동결융해 및 해수의 복합열화를 고려한 RC 보 정적 및 피로 거동

## 안 준 용

극한지에 건설된 콘크리트 인프라 구조물은 동결융해, 해수 및 외부 하중을 포함하여 여러가지의 환경적 손상에 취약한 상태이다. 선행연구에서는 동결융해와 해수 환경은 구조물의 열화를 증가하는 것을 제시하였지만 실제 구조물 환경을 고려하여 손상 요소에 대한 고려는 독립적으로 이루어져있다. 설계기준에서는 노출등급에 따라 구조물을 분류하고 있고 콘크리트의 최소 압축강도와 공기량을 규정하여 열악한 부식 환경에서 구조물 성능을 확보하고 있다. 동결융해, 해수 및 외부하중을 고려하여 사용 수명 기간 내에 콘크리트 구조물의 사용성 보장을 위하여 실험적 및 해석적 연구가 필요하다.

본 연구의 목적은 우선 콘크리트 강도가 RC 보의 정적 휨 성능 및 피로 성능에 미치는 영향을 파악하고, 따라서 동결융해 및 해수의 복합열화에 따른 RC 보의 정적 휨 및 피로 성능을 파악하는 것이다. 실제 구조물의 환경 조건을 모사한 실험적 연구는 아래와 같은 절차로 수행되었다.

우선 극한지 환경을 배경으로 동결융해, 해수 및 외부하중 관련 선행연구를 분석하였고 따라서 손상 요소에 따른 노출 등급과 최소 콘크리트 물성을 규정한 현행 설계 기준에 대하여 비교 분석하였다. 이를 바탕으로 설계기준에서 제시한 최소 콘크리트강도를 반영하여 콘크리트 강도에 따른 구조적 거동을 파악하였다.

총 12 개의 RC 보 시편을 제작하여 콘크리트 강도, 동결융해 및 해수가 RC 보의 구조적 거동에 미치는 영향을 실험적으로 파악하였다. 계측 장비의 허용 온도 범위를 고려하여 구조 실험에 앞서 저온 환경 계측 방안을 수립하였다. 온도 환경에 따른 RC 보 최대하중, 피로수명, 처짐, 철근 변형률, 균열 등의 구조적 거동을 측정하였다. 실험 결과를 통하여 일반 강도 콘크리트는 동결융해 및 해수 포화 시 고강도 콘크리트에 비하여 더 큰 열화를 나타낸 것을 확인하였다. 동결융해와 해수는 콘크리트의 재료특성 및 RC 보의 구조적 성능을 감소시켰고, 동결융해와 해수의 복합 효과는 RC 보의 열화를 가속하는 현상을 확인하였고 고강도 콘크리트(60 MPa)를 적용한 RC 보는 일반 콘크리트 강도(30 MPa)를 적용한 실험체에 비해 높은 동결융해 저항 성능을 보였다. 실험적으로 검증이 어려운 거동에 대하여 유한요소해석, 단면해석, 회귀분석을 포함한 해석적 연구를 통하여 추가적인 연구를 수행하였다.

동결융해 저항성능은 콘크리트 강도 증가에 따라 증가하는 것을 확인하였지만 60 MPa 이상의 강도를 사용하여 구조물 설계에 적용하는 것은 권장하지 않는다. 동결융해 및 해수의 영향을 받는

콘크리트 구조물의 성능을 평가하기 위해 정적 휨 및 피로 시험을 전부 수행하는 것이 타당할 것으로 판단되고 구조물의 노출 환경을 고려하여 동결융해와 해수의 영향은 실험적으로 동시에 고려되어야 할 것으로 판단된다. 마지막으로, 설계기준에서 저온의 정의에 대하여 구조물의 심부 온도를 바탕으로 규정할 것을 권장한다.

**주요어:** 극한지, 콘크리트구조, 동결융해, 해수 노출, 복합 효과,  
콘크리트강도, 정적 휨 거동, 피로 거동

**학 번:** 2016-28243